ISSN (1230-0322)
2025, Vol. 75, No. 3

Food

Polish Journal of Food and Nutrition Sciences

formerly Acta Alimentaria Polonica

Published
by Institute of Animal Reproduction and Food Research of the Polish Academy of Sciences, Olsztyn

Published since 1957 as
Roczniki Chemii i Technologii Żywności and Acta Alimentaria Polonica (1975–1991)

SCOPE: The Journal covers fundamental and applied research in food area and nutrition sciences with a stress on interdisciplinary studies in the areas of food, nutrition and related subjects.

POLICY: Editors select submitted manuscripts in relation to their relevance to the scope. Reviewers are selected from the Advisory Board and from Polish and international scientific centres. Identity of reviewers is kept confidential.

AUTHORSHIP FORMS referring to Authorship Responsibility, Conflict of Interest and Financial Disclosure, Copyright Transfer and Acknowledgement, and Ethical Approval of Studies are required for all authors.

FREQUENCY: Quarterly – one volume in four issues (March, June, September, December).

COVERED by Web of Science, Current Contents/Agriculture, Biology & Environmental Sciences, Journal Citation Reports and Science Citation Index Expanded, BIOSIS (Biological Abstracts), SCOPUS, FSTA (formerly: Food Science and Technology Abstracts), CAS (Chemical Abstracts), AGRICOLA, AGRO-LIBREX data base, EBSCO, FOODLINE, Leatherhead FOOD RA data base FROSTI, AGRIS, Biblioteka Nauki ICM, Biblioteka Narodowa – POLONA, and any www browser; ProQuest: The Summon, Bacteriology Abstracts, Immunology Abstracts.

EDITORIAL AND BUSINESS CORRESPONDENCE: Submit contributions (see Instructions to Authors) and address all communications regarding subscriptions, changes of address, etc. to:

CORRESPONDENCE TO: Ms. Joanna Molga
Polish Journal of Food and Nutrition Sciences
Institute of Animal Reproduction and Food Research
of Polish Academy of Sciences
ul. Trylińskiego 18, 10-683 Olsztyn, Poland
e-mail: pjfns@pan.olsztyn.pl; http://journal.pan.olsztyn.pl

Polish Journal of Food and Nutrition Sciences

ADVISORY BOARD OF PJFNS 2023–2026

Contents

ORIGINAL PAPERS

Subscription
2025 – Since 2025, PJFNS will be published only on-line. Past issues can be ordered as previously. One volume, four issues per volume. Annual subscription rates are: Poland 150 PLN, all other countries 80 EUR.
Prices are subject to exchange rate fluctuation. Subscription payments should be made by direct bank transfer to Bank Gospodarki Żywnościowej, Olsztyn, Poland, account No 17203000451110000000452110 SWIFT code: GOPZPLWOLA with corresponding banks preferably. Subscription and advertising offices at the Institute of Animal Reproduction and Food Research of Polish Academy of Sciences, ul. Trylińskiego 18, 10-683 Olsztyn, Poland, tel./fax (48 89) 5003245, e-mail: pjfns@pan.olsztyn.pl; http://journal.pan.olsztyn.pl

Wersja pierwotna (referencyjna) kwartalnika PJFNS: wersja on-line (eISSN 2083-6007)
Ark. wyd. 19, Ark. druk. 16
Skład: ITEM

ORIGINAL ARTICLE
http://journal.pan.olsztyn.pl

Polish Journal of Food and Nutrition Sciences
2025, Vol. 75, No. 3, 193–207
DOI: 10.31883/pjfns/207619
ISSN 1230-0322, e-ISSN 2083-6007

Pasta Fortified with Wild Garlic (*Allium ursinum* L.) as a Functional Food Rich in Phenolic Compounds

Cristina A. Rosan[1], Mariana F. Bei[1], Alin C. Teusdea[1], Traian O. Costea[2], Simona D. Cavalu[3], Daniela Domocos[3], Simona I. Vicas[1]*

[1]Department of Food Engineering, Faculty of Environmental Protection, University of Oradea, 26 Gen Magheru St, 410048 Oradea, Romania
[2]Advanced Materials Research Infrastructure SMARTMAT, University of Oradea, 1 University St, 410087 Oradea, Romania
[3]Faculty of Medicine and Pharmacy, University of Oradea, P-ta 1 Decembrie 10, 410087 Oradea, Romania

In this study, fortified pasta was produced using *Allium ursinum* L. in three forms: powder (5%, 10%, and 15% of the wheat flour weight); blanched and chopped leaves, used to replace 30%, 60%, and 90% (*w/w*) of the mixing liquid, while keeping the flour content constant; and water residue after blanching and chopping (replacing 30%, 60%, and 90%, *w/w,* of the mixing liquid). This approach aimed to identify the optimal formulation for a novel functional pasta with improved bioactive properties. Before and after cooking, each pasta variant was evaluated based on the total phenolic and total flavonoid contents, the antioxidant capacity, and colour parameters, while sensory analysis was conducted only after cooking. All the formulations exhibited acceptable cooking characteristics, with variations noted based on the type and quantity of wild garlic leaf formulation included. Optimum cooking time decreased from 320 s (control) to 180 s for pasta enriched with the highest level of wild garlic leaf powder. The cooking loss in pasta enriched with leaf powder and blanched leaves was found to be higher than in the control, ranging from 3.23% to 6.00%. In terms of colour analysis, these formulations significantly reduced *L** parameter, regardless the enrichment level, in both raw and cooked pasta. Enrichment with leaf powder and blanched and chopped leaves resulted in a higher total phenolic content and improved antioxidant capacity of the pasta samples. Pasta enriched with chopped leaves received the highest sensory scores, followed by pasta containing wild garlic powder, both at a medium level. The study reveals that wild garlic leaves can be utilized as a functional ingredient in pasta production, resulting in innovative, high-quality pasta.

Keywords: antioxidant capacity, blanching, chromatic parameters, cooking quality, enriched pasta, wild garlic leaves

ABBREVIATIONS

ANOVA, analysis of variance; CL, cooking loss; DPPH radical, 2,2-diphenyl-1-picrylhydrazyl radical; FRAP, ferric-reducing antioxidant power; GAE, gallic acid equivalents; HT, hydration test; IPO, International Pasta Organisation; OCT, optimum cooking time; QE, quercetin equivalents; Sa, arithmetic mean height; SI, swelling index; TE, Trolox equivalent; TFC, total flavonoid content; TPC, total phenolic content; TPTZ, 2,4,6-tri(2-pyridyl)-1,3,5-triazine; WA, water absorption.

INTRODUCTION

Since pasta can be prepared and cooked in so many different ways, it is a popular and affordable ingredient in kitchens around the world. The pasta is defined as a cooked, extruded, and dried food made primarily of water and durum wheat semolina, being regarded as an essential food in the human diet worldwide, along with bread and cereal-based products [Cappelli & Cini, 2021; Muresan *et al.*, 2017]. Pasta consumption ranks second globally after bread consumption due to its nutritional qualities, ease

***Corresponding Author:**
E-mail: **svicas@uoradea.ro** (Prof. S.I. Vicas)

Submitted: 20 February 2025
Accepted: 27 June 2025
Published on-line: 24 July 2025

of preparation, affordability, and commercial availability [Dziki, 2021]. In 2022, the International Pasta Organization (IPO) released a report showing that 16.9 million tons of pasta were produced worldwide, with the following percentages: European Union – 32.8%, the rest of Europe – 17.9%, Central and South America – 17.7%, Africa – 13.8%, North America – 12.9%, Middle East – 3.5%, Asia – 1.4%, and Australia – 0.3% [IPO, 2024]. In terms of pasta consumption *per* capita, the top 5 pasta consuming countries are Italy (23.2 kg), Tunisia (17 kg), Venezuela (13.6 kg), Greece (12.2 kg), and Peru (9.9 kg). Pasta is divided into eight families: spaghetti, tubular pasta, shell pasta, ribbon pasta, short pasta, micropasta, ravioli (filled pasta), and dumplings (pseudo-pasta) [Alexander, 2000]. This classification has been further expanded to include whole-wheat, natural, enriched, flavoured, and fortified pasta forms [Hastaoğlu *et al.*, 2023]. Pasta in some countries (Italy, Greece, and France) must be produced exclusively of durum wheat semolina [Dimitrios, 2024], while pasta in other nations is manufactured with common wheat flour.

As a result of growing demand for high-quality foods and functional foods, intense research is conducted on pasta enriched with additional, natural ingredients, in order to increase its nutritional value and bioactive potential [Dziki, 2021; Sissons, 2022]. The focus is on developing fortified products enriched with plants rich in dietary fibre and antioxidants, including fruits and vegetables, or by-products from the processing of plant and animal raw materials. These ingredients may have a positive effect on human health, although, on the other hand, they affect the technological qualities of pasta, not always in a favourable way. Among the plant materials, powdered leaves are often used as a partial substitute for wheat flour in the pasta production, for example, Bouacida *et al*. [2017] used arugula (*Eruca vesicaria* (L.) Cav.) and spinach (*Spinacia oleraceae* L.) leaf flour at three different levels of wheat semolina substitution (5%, 10% and 20%, *w/w*) and found that pasta with leaf flours had a higher dietary fibre content compared to the control formulation, and that 10% (*w/w*) substitution produced good cooking quality pasta with cooking loss ≤ 8% after 14 days of storage and a high overall acceptability score by consumers. The nutritional and nutraceutical potential of wheat pasta supplemented with powdered parsley leaves (replacing 1–4% of wheat flour, *w/w*) was evaluated by Sęczyk *et al.* [2016]. The findings demonstrated that, in comparison to the control sample, pasta produced with 4% parsley leaf in flour had a 146% higher ABTS cation radical scavenging activity and a 67% higher total phenolic content.

Wild garlic (*Allium ursinum* L.) leaves can also be used as an ingredient to enrich pasta due to their nutritional properties and bioactive compound profile. The sulphur compounds (including cysteine-sulfoxides, thiosulphinates and (poly)sulfides [Kovačević *et al.*, 2023; Sobolewska *et al.*, 2015; Vidović *et al.*, 2021] as well as phenolic compounds including phenolic acids and flavonoids (mainly kaempferol derivatives) [Oszmiański *et al.*, 2013; Parvu *et al.*, 2010; Wu *et al.*, 2009;] were determined in wild garlic. The leaves of *A. ursinum* are also high in pigments, particularly carotenoids and chlorophylls, as well as vitamin C [Bernaś *et al.*, 2024] and iron, the content of which can reach 230.34 mg/kg [Piątkowska *et al.*, 2015]. Owing to their phytochemical composition, *A. ursinum* leaves exhibit antioxidant and antimicrobial properties, cytotoxic potential, and cardioprotective effects [Sobolewska *et al.*, 2015].

So far, wild garlic leaves in three different forms (powder, extract, and encapsulated extract) have been used in pasta production by Filipčev *et al.* [2023], who assessed how the cooking process affected the pasta's bioactive compound content, antioxidant capacity, colour and texture, as well as cooking and sensory qualities. In our previous study, pasta enriched with a fixed amount of blanched and chopped wild garlic leaves was prepared, and the effect of different content of eggs in the pasta recipe on cooking properties, nutrition composition, phenolic content and antioxidant capacity of products was analysed [Rosan *et al.*, 2024]. However, to the best of our knowledge, pasta enriched with different amounts of blanched leaves has not been studied so far, and no comparisons have been made between pasta enriched with different forms of wild garlic leaves. In this study, pasta was doubly fortified with egg and *Allium ursinum* L. to enhance its nutritional and functional properties. Therefore, the aim of this study was to show how incorporation of various forms of wild garlic at different levels affects the quality indicators, bioactive compound content, antioxidant capacity, colour, microstructure and sensory characteristics of egg pasta. To achieve this, we developed three types of pasta: one with wild garlic powder as a partial flour substitute, one fortified with blanched and chopped wild garlic leaves, and one based on the recovery of the water residue after blanching and chopping the wild garlic leaves.

MATERIALS AND METHODS

Preparation of wild garlic leaf formulations

The leaves of wild garlic (*A. ursinum*) were collected in May 2024 at a site located in the forest near Băile Felix, Bihor County, northwest Romania (46°59'04.0"N 21°58'31.5"E). The plant was identified and recognized by experts from the Faculty of Medicine and Pharmacy of the University of Oradea, Romania. A specimen of the plant, bearing the code UOP 05718, is kept in the herbarium registered at the New York Botanical Garden.

The leaves of wild garlic were sorted, washed and drained to remove excess water. A part of the fresh leaves (3.5 kg) was put into the oven (model CLN 53, Nitech Pol Eko, Wodzisław, Poland) and dried at 30°C until their mass remained constant. Then, the leaves were ground into a fine powder and sieved through a sieve with mesh size of 1 mm to form *A. ursinum* powder (AUP). The low drying temperature was selected to maintain both the distinctive flavour of wild garlic and the particular green hue of the leaves. For the blanching treatment, 3 kg of wild garlic leaves were placed in a stainless-steel vessel, and hot water at 80°C was poured over them at a water-to-leaf ratio of approximately 5:1 (*w/w*). The leaves were gently stirred in the hot water for 2 min to ensure even blanching. After treatment, the leaves were transferred to a fine-mesh sieve and allowed to drain for 5 min to remove excess water. The drained and finely chopped *A. ursinum* leaves (AUL) and the resulting

water residue (AUW) after blanching and chopping (by-product) were used in the pasta formulations.

Pasta production

White superior wheat flour 000-type, commercially available (M.P. Băneasa-Moară S.A. Buftea, România), was used for the pasta production. The nutritional value of the flour was as follows (*per* 100 g): 10 g of protein, 0.9 g of fat, 76 g of carbohydrates, and 0.10 g of dietary fibre. In addition, the pasta preparation involved the use of different wild garlic formulations, eggs, water, and kitchen salt. By using three different formulations from *A. ursinum* leaves (leaf powder, blanched and chopped leaves, and water by-product of leaf blanching and chopping) at three different substitution levels (low (L), medium (M), and high (H)), ten different types of pasta were finally obtained, including the control pasta (CTRL), in which no kind of *A. ursinum* formulation was employed. *A. ursinum* leaf powder was used to replace 5%, 10% and 15% (*w/w*) of wheat flour in the pasta recipe and the resulting pasta was designated as AUP_L, AUP_M, and AUP_H, respectively. In the AUL_L, AUL_M, and AUL_H pasta recipes, the mixing liquid (water + eggs) was replaced by blanched and chopped wild garlic leaves at low (30%, *w/w*), medium (60%, *w/w*), and high (90%, *w/w*) levels, respectively, while maintaining a constant wheat flour content of 250 g. The levels of substitution by AUL were selected based on preliminary tests aimed at maintaining dough processability and pasta structure while achieving visible differences in composition. Leaf moisture was taken into account in adjusting water to maintain dough consistency. A by-product obtained from *A. ursinum* leaf blanching and chopping was used to replace water in the final pasta formulation; AUW_L, AUW_M, and AUW_H pasta was produced with 30%, 60%, and 90% (*w/w*) substitution of the mixing liquid by AUW, respectively. The ingredients for the control pasta were: wheat flour, egg, salt, and water. The coding of the pasta samples and the ingredients used are summarised in **Table 1**. Each of the ten pasta types was produced in triplicate. In total, 30 batches of pasta were made for this study.

The ingredients for each type of dough were mixed, and dough was kneaded by hand for 10 min, allowed to rest for 1 h, shaped to 3 mm thickness and separated into 7 mm wide strips with a Grünberg GR 155 cutting machine purchased from eMAG, Romania. The resulting raw pasta was dried at 30°C until its weight remained constant and was used for future analyses. A portion of each dried raw pasta was cooked in water for optimum cooking time (determined as described below). The cooked pasta was dried at 30°C for analyses of total phenolic content, total flavonoid content and antioxidant capacity.

Cooking properties determinations

Determination of the optimum cooking time

Determination was performed using AACC International approved method no. 66-50.01 [AACC, 2010]. After adding 25 g of raw dried pasta to 300 mL of boiling water, the mixture was brought to a boiling point. During cooking, pasta samples were taken at 30-s intervals and their texture was assessed by

Table 1. The ingredients of pasta enriched with *Allium ursinum* L. leaf powder (AUP), blanched and chopped leaves (AUL), and water by-product of leaf blanching and chopping (AUW).

Ingredient	Control	AUP_L	AUP_M	AUP_H	AUL_L	AUL_M	AUL_H	AUW_L	AUW_M	AUW_H
Wheat flour (g)	250	237.5	225	212.5	250	250	250	250	250	250
Egg (g)	10	10	10	10	10	10	10	10	10	10
A. ursinum leaf powder (g)	–	12.5	25	37.5	–		–	–	–	–
Blanched and chopped *A. ursinum* leaves (g)	–	–	–	–	30	60	90	–	–	–
Water by-product (g)	–	–	–	–	–	-	–	30	60	90
Water (g)	90	90	90	90	60	30	–	60	30	–
Salt (g)	0.5	0.5	0.5	0.5	0.5	0.5	0.5	0.5	0.5	0.5

squeezing them between two transparent glass slides. The optimum cooking time (OCT) was considered to be the time needed for the white core of the pasta to disappear in this test. The measurements were performed in triplicate.

Determination of cooking loss

Ten g of the dry pasta were cooked in 100 mL of water until the OCT had been reached. After cooking, water was refilled to its initial volume, and 25 mL of cooking water were dried to a constant weight at 105°C [Chetrariu & Dabija, 2021]. From the weighed residue, the solid content of the cooking water was determined and cooking loss (CL, %) was calculated as g of solids lost into the cooking water *per* 100 g of pasta.

Swelling index determination

Pasta cooked as described above for CL determination, was drained for a few minutes, weighed ($w_{cooked\ pasta}$), and then dried in an oven at 105°C until reaching a constant weight ($w_{dry\ pasta}$). The swelling index (SI) was calculated using Equation (1) [Gopalakrishnan *et al.*, 2011]:

$$SI\ (g/g) = \frac{W_{cooked\ pasta} - W_{dry\ pasta}}{W_{dry\ pasta}} \quad (1)$$

Determination of water absorption of pasta

The water absorption (WA) of pasta during cooking was determined by measuring the weight of the pasta before cooking ($w_{before\ cooking}$) and after cooking at the optimum cooking time ($w_{after\ cooking}$). The WA was calculated using Equation (2) [Chetrariu & Dabija, 2021]:

$$WA\ (\%) = \frac{W_{after\ cooking} - W_{before\ cooking}}{W_{after\ cooking}} \times 100 \quad (2)$$

Hydration test

Five g of the pasta ($w_{raw\ pasta}$) were kept at 25°C in a glass vessel with 100 mL of water. After incubation periods of 5, 10, 15, 30, 60, 90, and 180 min, the samples were taken out and drained for 1 min before being weighed ($w_{hydrated\ pasta}$). The hydration of pasta was calculated according Equation (3) [Chetrariu & Dabija, 2021]:

$$Hydration\ (\%) = \frac{W_{hydrated\ pasta} - W_{raw\ pasta}}{W_{raw\ pasta}} \times 100 \quad (3)$$

The samples were analysed in triplicate, and the curves of pasta hydration *vs*. time of hydration were plotted.

Determination of total phenolic content and total flavonoid content

The pasta was extracted using the method suggested by Filipčev *et al*. [2023]. Briefly, 1 g of raw and cooked dried pasta (previously ground) were combined with 2.5 mL of a mixture of ethanol and water (4:1, *v/v*). After 15 min of sonication at 40°C, the suspension was centrifuged for 10 min at 1,000×*g* using an NF 200 centrifuge (Nüve, Ankara, Turkey). The supernatant was used for the analyses outlined below.

The total phenolic content (TPC) was determined using the Folin-Ciocalteu reagent [Singleton *et al.*, 1999]. Briefly, 100 µL of the pasta extract were mixed with 1,700 µL of distilled water and 200 µL of freshly diluted Folin-Ciocalteu reagent (1:10, *v/v*), and shaken vigorously. Thereafter, 1,000 µL of a 7.5% Na_2CO_3 solution were added, and the mixture was kept for 2 h at room temperature in the dark. The absorbance was measured at a wavelength of 765 nm using a Shimadzu 1240 mini-UV-Vis spectrophotometer (Kyoto, Japan). Gallic acid solutions in a concentration range of 0.1–0.5 mg/mL were used for the calibration curve. A regression equation of the resulting curve was y=25.42x+0.010 with a coefficient of determination (R^2) of 0.9933. The results were reported as mg of gallic acid equivalents (GAE) *per* g of pasta dry weight (dw).

The total flavonoid content (TFC) of the pasta was determined using the aluminium chloride colorimetric method according to the procedure described by Marinelli *et al.* [2015] with some modifications. In brief, 1 mL of extract was transferred to a 10 mL volumetric flask, which already contained 4 mL of distilled water. Subsequently, 300 µL of a 5% $NaNO_2$ solution were added. After 5 min, a volume of 300 µL of a 10% $AlCl_3$ solution was introduced. Following additional 6 min, 2 µL of a 1 M NaOH solution were added. The flask volume was adjusted with distilled water, and then it was thoroughly mixed. The absorbance was recorded at a wavelength of 510 nm (Shimadzu 1240 mini-UV-Vis spectrophotometer) in comparison to a blank sample. The total flavonoid content was calculated using quercetin as a standard. The calibration curve was plotted using a concentration range of quercetin solutions (0.1–0.5 mg/mL), resulting in the regression equation: y=1.27x+0.090 (R^2=0.9988). The results were expressed as mg of quercetin equivalents (QE) *per* g of pasta dw.

Antioxidant capacity determination

The 2,2-diphenyl-1-picrylhydrazyl (DPPH) radical scavenging capacity of pasta was determined according to the method of Brand-Williams *et al.* [1995]. To this end, 100 µL of the extract were combined with 2,800 µL of a freshly prepared 80 µM DPPH radical solution. The mixture was then incubated in darkness at room temperature for exactly 30 min. The measurement of absorbance was conducted at a wavelength of 517 nm, and the results were quantified as µmol Trolox equivalents (TE) *per* g of pasta dw based on the calibration curve (y=962.19x+1.2931, R^2=0.9977) made with different concentration of Trolox (0.05–1.00 mM).

The ferric-reducing antioxidant power (FRAP) assay was based on the work of Benzie & Strain [1996], with some modifications [Vicas *et al.*, 2009]. The stock solutions were prepared: a 300 mM acetate buffer with a pH of 3.6, a 20 mM solution of $FeCl_3$×6 H_2O, and a 10 mM solution of 2,4,6-tri(2-pyridyl)-1,3,5--triazine (TPTZ) in 40 mM HCl. The FRAP solution was prepared by combining acetate buffer, $FeCl_3$×6 H_2O solution, and a TPTZ

solution in a volumetric ratio of 10:1:1. Pasta extract (100 µL) was mixed with 500 µL of the FRAP solution and 2 mL of distilled water. The mixture was left to react for 1 h in a dark environment. The absorbance was recorded at 595 nm, using a Shimadzu 1240 mini-UV-Vis spectrophotometer. The results were quantified as µmol TE *per* g of pasta dw (calibration curve regression equation: y=14.32x+0.019, R^2=0.9978).

Chromatic analysis

Pasta samples (raw and cooked) were scanned at a resolution of 600 dpi with a CanoScan 9000F scanner (Canon Inc., Tokyo, Japan). This optical image resolution generated 0.0423 mm *per* pixel and a two-dimensional definition of 1,791 µ^2. Background noise and additive noise were eliminated from the scanned image prior to processing the data in order to prevent image distortion that could produce inaccurate results. These issues have been resolved by using algorithms for contour reduction and Gaussian noise reduction. The chromatic parameters of the CIELab space, including L^* (lightness), a^* (greenness/redness), and b^* (blueness/yellowness), were examined. Moreover, total colour difference (ΔE) between each wild garlic enriched pasta (with L^*, a^* and b^* values) and the control pasta (with L_0^*, a_0^*, and b_0^* values) was calculated using Equation (4):

$$\Delta E = \sqrt{(L^* - L_0^*)^2 + (a^* - a_0^*)^2 + (b^* - b_0^*)^2} \quad (4)$$

Determination of surface roughness parameter and microstructure characteristics

The surface of raw pasta samples was visualized using a laser scanning confocal microscope (KEYENCE, model XYZ123, Keyence Corporation, Osaka, Japan). The system was operated using KEYENCE VK_X3100 software, while the images were captured at different magnifications: 250×; 1,250×; and 3,750×, and three distinct areas were considered during scanning. Arithmetical mean height (Sa) was employed as a characteristic surface roughness parameter, representing, as an absolute value, the difference in height of each point compared to the arithmetical mean of the surface.

Sensory evaluation of cooked pasta

A preliminary consumer test was carried out to evaluate the acceptability of the cooked pasta samples. The panel consisted of 21 participants (6 males and 15 females), aged between 19 and 55 years, all of whom had prior experience with sensory evaluation techniques.The hedonic test was applied utilizing a linear hedonic scale of nine points, where 1 represents "extremely unpleasant" and 9 denotes "extremely pleasant." This analysis focused on various sensory attributes, including appearance, form, texture, colour, stickiness, aroma, taste, and chewiness. The overall quality score for each sample was determined by calculating the mean of the individual scores given by the participants, divided by the total number of participants.

Dried pasta samples were cooked at OCT and served to the evaluators separately on white plates at ambient temperature. The results provide indicative insights into consumer perception and should be considered preliminary due to the limited and non-representative consumer panel size.

Statistical analysis

Each type of pasta was produced in triplicate, and results were expressed as mean and standard deviation (SD). Data for each parameter included in the study were analysed using one-way analysis of variance (ANOVA) followed by completed post-hoc multiple pairwise comparisons of means *via* Tukey's test. Differences among pasta variants were considered significant at $p<0.05$.

RESULTS AND DISCUSSION

This section discusses the impact of wild garlic fortification on the culinary properties, polyphenol content, colour parameters, antioxidant characteristics, and sensory attributes of pasta. Three formulations from wild garlic leaves as a pasta ingredient were used in the study: dried leaf powder, blanched and chopped leaves, and blanching residue. Enriching pasta by replacing wheat flour with dried plant material in the powder form is a common practice [Bianchi *et al*., 2021]. In turn, the thermal treatment applied to the leaves was performed in order to improve their texture for subsequent processing. The thermal treatment results in cellular turgor loss, leading to cell membrane destruction, while simultaneously inducing alterations in the polymers of the cell wall, particularly the pectic compounds [Einhorn-Stoll *et al*., 2007]. The blanching concurrently releases nutrients (minerals, vitamins, carbohydrates, proteins) from plant tissues into the water [Xiao *et al*., 2017]. To recover some of the nutrients lost during leaf processing, a third set of pasta was prepared using the water by-product remaining after leaf blanching and chopping.

Influence of formulations from wild garlic leaves on the cooking properties of pasta

The cooking properties, including OCT, SI, CL, WA, of pasta enriched at three different levels with wild garlic leaf powder, blanched and chopped leaves, and water by-product of leaf blanching and chopping were examined compared to the control sample (without wild garlic), and the results are shown in **Table 2**. Furthermore, the HT results are presented in **Figure 1**. Since each replicate for OCT determination produced identical values within each paste group (SD=0.00), statistical significance could not be established. However, differences between samples compared to the control were observed. The AUP pasta variants exhibited a visible reduction in OCT compared to the control, which depended on the amount of the powder used in pasta recipe. The increased substitution of wheat flour by wild garlic leaf powder led to a lesser reduction in OCT. In contrast, there was a minor difference among the AUL pasta types, with the observed decrease being lesser when compared to the control. In the third set of pasta samples (these with AUW), the OCT was almost identical to the control. The decrease in OCT of AUP and AUL pasta samples might be due to changes in the wheat protein structure caused by compounds found in wild garlic leaves, like phenolics

Table 2. Cooking properties of pasta enriched with *Allium ursinum* L. leaf powder (AUP), blanched and chopped leaves (AUL), and water by-product of leaf blanching and chopping (AUW).

Pasta	OCT(s)	WA (%)	SI (g/g)	CL (%)
CTRL	320±0.00	182±7^{ab}	3.06±0.03^{a}	3.47±0.42^{cd}
AUP_L	300±0.00	178±8^{ab}	2.35±0.02^{bc}	4.27±0.72^{b}
AUP_M	210±0.00	165±14^{ab}	2.29±0.28^{bc}	5.47±0.31^{a}
AUP_H	180±0.00	148±23^{b}	1.98±0.32^{c}	6.00±0.10^{a}
AUL_L	270±0.00	198±32^{a}	2.56±0.36^{b}	3.23±0.35^{d}
AUL_M	240±0.00	180±18^{ab}	2.27±0.17^{bc}	3.93±0.15^{bc}
AUL_H	240±0.00	194±12^{a}	2.60±0.07^{b}	3.97±0.06^{bc}
AUW_L	330±0.00	189±36^{a}	2.45±0.37^{b}	3.53±0.06^{cd}
AUW_M	330±0.00	174±6^{ab}	2.20±0.04^{bc}	3.23±0.45^{d}
AUW_H	330±0.00	179±1^{ab}	2.22±0.03^{bc}	3.73±0.15^{bcd}

Results are expressed as mean ± standard deviation (n=3). Different letters in the same column correspond to significant differences (p<0.05). OCT, optimum cooking time; WA, water absorption; SI, swelling index; CL, cooking loss. Pasta coding: CTRL, control without wild garlic; AUP_L, AUP_M and AUP_H, pasta produced with 5%, 10% and 15% (*w/w*) substitution of wheat flour by AUP, respectively; AUL_L, AUL_M and AUL_H, pasta produced with 30%, 60% and 90% (*w/w*) substitution of mixing liquid by AUL, respectively; AUW_L, AUW_M and AUW_H, pasta produced with 30%, 70% and 90% (*w/w*) substitution of mixing liquid by AUW, respectively.

and dietary fiber. Bustos *et al.* [2019] achieved similar results when they incorporated dried berry fruits in pasta recipe. This resulted in a decrease in OCT compared to the control sample; however, the level of substitution had no impact on OCT.

As the level of mixing liquid substitution by wild garlic powder increased, the water absorption in the AUP pasta set slightly decreased, but without statistically significant differences (p≥0.05) (**Table 2**). Moreover, the incorporation of different wild garlic formulations into the pasta at low and medium levels had an insignificant (p≥0.05) impact on WA. Significant differences (p<0.05) were found only between pasta with the highest substitution level (AUP_H and AUL_H pasta). In our previous study, the addition of wild garlic leaves into pasta led to a significant increase in WA compared to the control samples with different egg quantities [Rosan *et al*., 2024]. On the other hand, SI varied significantly between control pasta (3.06 g/g) and all enriched pasta samples for which it ranged from 1.98 to 2.60 g/g (**Table 2**). The SI of the AUP pasta set showed a decreasing trend with increasing the amount of wild garlic leaf powder in pasta recipe, although the differences between the samples were not statistically significant (p≥0.05). The acceptability of pasta quality was determined by its ability to absorb water (150–200 g/100 g of pasta) and achieve an SI of approximately 1.8 [Bustos *et al.*, 2019]. That estimation did not take into account pasta containing additional non-starch ingredients, which could potentially impact both of those parameters, as well as the microstructure of the pasta [Del Nobile *et al.*, 2005].

When wild garlic leaf powder was used in the pasta production, CL increased significantly (p<0.05) compared to the control, and this increase was directly proportional to the increase in the level of substitution by AUP (**Table 2**). When compared to the control, CL did not exhibit statistically significant changes (p≥0.05) in the other two pasta sets (AUL and AUW). The literature indicates that pasta with a cooking loss of up to 8% is considered acceptable [Bianchi *et al.*, 2021]. The pasta produced in our study conformed to this requirement.

The hydration test involves immersing dried pasta in water at a constant temperature of 25°C and recording its weight at various points in time. This test provides significant insights into the quality of the pasta [Chetrariu & Dabija, 2021; Rosan *et al.*, 2024]. In our study, the hydration test revealed that all pasta samples enriched with AUP and AUL exhibited higher hydration compared to the control (**Figure 1**). This effect was influenced by both the form of wild garlic incorporated and the level of substitution. In the case of AUP pasta, a rapid increase in hydration was observed during the first 30 min, followed by a plateau phase, and a slight decrease at 180 min (**Figure 1A**). This result can probably be attributed to the fine particle size and a high surface area of wild garlic powder, which promoted water absorption. For AUL pasta (**Figure 1B**), the plateau occurred later, at around 60 min, possibly due to the physical barrier effect of the wild garlic leaf fragments, which delays water penetration. In contrast, AUW pasta showed a hydration pattern comparable to that of the control (**Figure 1C**). Chetrariu & Dabija [2021] did not explicitly report hydration values of HT; they demonstrated that spelt pasta enriched with spent grain showed altered water absorption behaviour, evidenced by changes in texture and moisture distribution, that aligns with increased hydration rates commonly associated with fiber-rich additive matrices. In another study [Schettino *et al.*, 2021], pasta containing fermented spent grain (fBSG-p) exhibited the fastest water absorption, reaching equilibrium before the other samples (native spent grain pasta and control

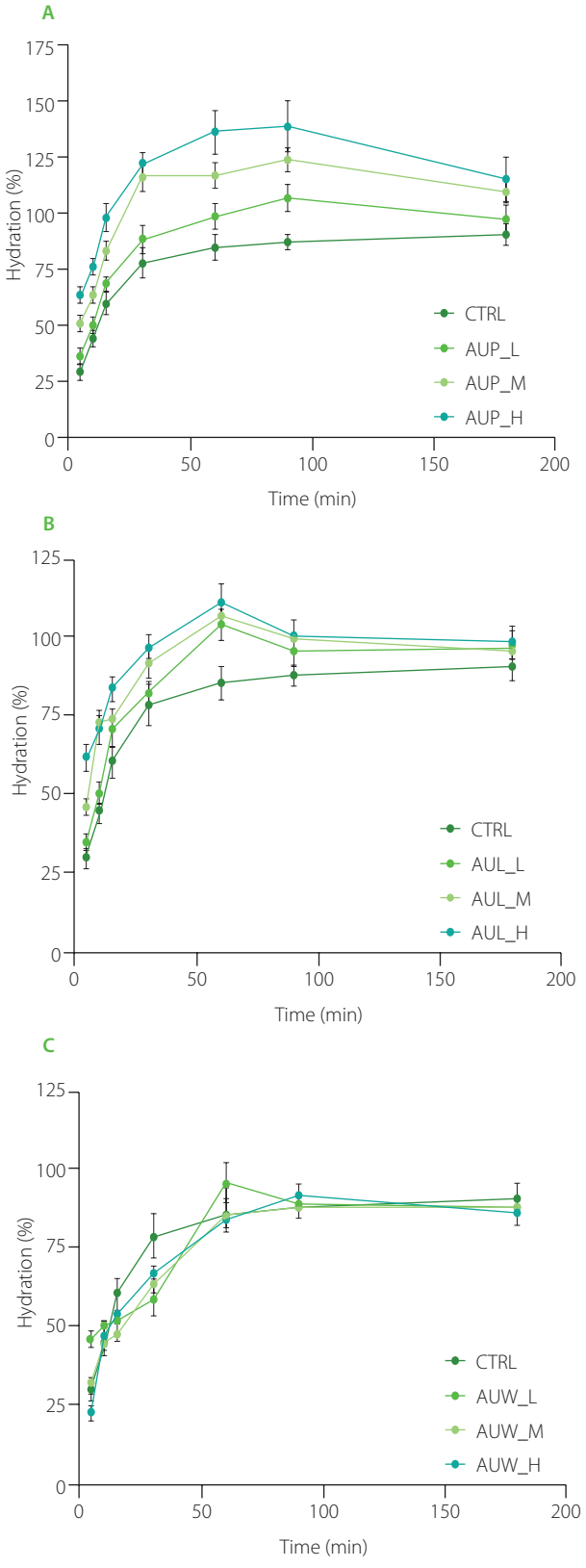

Figure 1. Results of a hydration test of pasta enriched with *Allium ursinum* L. leaf powder (AUP) (**A**), blanched and chopped leaves (AUL) (**B**), and water by-product of leaf blanching and chopping (AUW) (**C**) at 25°C over a period of 180 min. Pasta coding: CTRL, control without wild garlic; AUP_L, AUP_M and AUP_H, pasta produced with 5%, 10% and 15% (*w/w*) substitution of wheat flour by AUP, respectively; AUL_L, AUL_M and AUL_H, pasta produced with 30%, 60% and 90% (*w/w*) substitution of mixing liquid by AUL, respectively; AUW_L, AUW_M and AUW_H, pasta produced with 30%, 70% and 90% (*w/w*) substitution of mixing liquid by AUW, respectively.

pasta). The accelerated hydration observed with fBSG-p is likely due to its more porous microstructure and a higher soluble fiber content resulting from bioprocessing, which facilitates improved water penetration and retention.

Total phenolic content, total flavonoid content, and antioxidant capacity of pasta enriched with formulations from wild garlic leaves

TPC and TFC determined in both the raw and cooked forms of the pasta enriched with *A. ursinum* leaf powder, blanched and chopped leaves and by-product of leaf blanching and chopping, as well as the control pasta are presented in **Table 3**. Raw pasta enriched with wild garlic leaf powder showed a significantly higher ($p<0.05$) TPC than the CTRL, and the difference was depended on the amount of AUP used in pasta production. While the differences between AUL samples were statistically insignificant ($p\geq0.05$), in the case of the second set of raw pasta containing blanched and chopped leaves of *A. ursinum*, noticeably increased TPC was observed compared to the CTRL. When considering raw pasta with by-product, regardless of the amount of AUW used in its production, no significant differences ($p\geq0.05$) were found in the total phenolic content of the enriched and control pasta. When compared to the other raw pasta variants, the pasta enriched with AUP had the highest TPC, ranging from 2.48 to 3.72 mg GAE/g dw. The total flavonoid content of raw pasta samples followed the same trends as the total phenolic content. The highest TFC was determined in the AUP_H pastas – 0.31 mg QE/g dw. The increase in TPC and TFC of pasta enriched with AUP and AUL was expected due to the high phenolic content of wild garlic leaves [Cinkmanis *et al.*, 2022; Kovačević *et al.*, 2023; Tóth *et al.*, 2018]. Tóth *et al.* [2018] and Lachowicz *et al.* [2017] reported that the TPC of wild garlic leaves was dependent on the maturity stage of the plant and was the highest in June, *i.e.*, 827 and 470 mg GAE/kg of fresh weight, respectively. In turn, Kovačević *et al.* [2023] reported that TPC of *A. ursinum* leaves collected from different locations in Croatia ranged from 9.96 to 11.2 mg GAE/g dw. According to literature, the phenolic compounds occurring in wild garlic leaves include mainly kaempferol derivatives [Oszmiański *et al.*, 2013] followed by *p*-coumaric and ferulic acids [Parvu *et al.*, 2010]. Another study demonstrated that, gallic acid, ferulic acid, caffeic acid, chlorogenic acid, and synaptic acid were the main phenolic acids in wild garlic leaves, while the main flavonoids identified in bear's garlic leaves were rutin, catechin hydrate, and epicatechin [Cinkmanis *et al.*, 2022].

Two methods were used to evaluate the antioxidant capacity of the pasta, and respective results are shown in **Table 3**. While the FRAP method refers to the reduction of Fe^{+3} ions to Fe^{+2} within the TPTZ complex [Benzie & Strain, 1996], the DPPH assay demonstrates the ability to scavenge the DPPH radical [Brand-Williams *et al.*, 1995]. The highest DPPH radical scavenging capacity and ferric-reducing antioxidant power were demonstrated by the raw AUP_H pasta with values of 19.09 and 6.26 µmol TE/g dw, respectively. Compared to the control,

Tabel 3. Total phenolic content (TPC), total flavonoid content (TFC), and antioxidant capacity of raw and cooked pasta enriched with *Allium ursinum* L. leaf powder (AUP), blanched and chopped leaves (AUL), and water by-product of leaf blanching and chopping (AUW).

Pasta treatment	Pasta	TPC (mg GAE/g dw)	TFC (mg QE/g dw)	DPPH$^{\bullet}$ scavenging capacity (µmol TE/g dw)	FRAP (µmol TE/g dw)
Raw pasta	CTRL	1.25±0.06^{gh}	0.12±0.00^{e}	0.00±0.00^{e}	0.73±0.12^{jk}
	AUP_L	2.48±0.13^{c}	0.17±0.02^{d}	15.58±0.09^{c}	2.23±0.16^{de}
	AUP_M	3.26±0.10^{b}	0.26±0.04^{b}	17.43±0.11^{b}	4.36±0.05^{b}
	AUP_H	3.72±0.05^{a}	0.31±0.04^{a}	19.09±0.13^{a}	6.26±0.07^{a}
	AUL_L	1.52±0.08^{ef}	0.13±0.02^{e}	0.04±0.00 ^{e}	1.36±0.01^{gh}
	AUL_M	1.58±0.06^{e}	0.19±0.02^{cd}	0.04±0.01^{e}	1.54±0.07^{f}
	AUL_H	1.63±0.06^{e}	0.21±0.01^{c}	0.05±0.01^{e}	2.12±0.04^{e}
	AUW_L	1.25±0.01^{h}	0.08±0.02^{f}	0.01±0.00^{e}	0.61±0.08^{klm}
	AUW_M	1.39±0.06^{fgh}	0.09±0.01^{f}	0.01±0.00^{e}	0.64±0.05^{klm}
	AUW_H	1.40±0.12^{fg}	0.09±0.00^{f}	0.02±0.00^{e}	0.77±0.14^{j}
Cooked pasta	CTRL	0.43±0.01^{m}	0.04±0.00^{g}	0.01±0.00^{e}	0.39±0.02^{n}
	AUP_L	0.90±0.04^{i}	0.07±0.00^{f}	0.33±0.01^{d}	1.28±0.07^{h}
	AUP_M	1.34±0.15^{gh}	0.12±0.00^{e}	0.35±0.00^{d}	2.32±0.05^{d}
	AUP_H	1.81±0.05^{d}	0.19±0.00^{cd}	0.38±0.01^{d}	3.36±0.10^{c}
	AUL_L	0.63± 0.01^{kl}	0.04±0.00^{g}	0.02±0.00^{e}	0.58±0.02^{lm}
	AUL_M	0.91±0.15^{i}	0.04±0.00^{g}	0.05±0.00^{e}	1.00±0.01^{i}
	AUL_H	0.87±0.12^{ij}	0.07±0.00^{f}	0.07±0.01^{e}	1.47±0.02^{fg}
	AUW_L	0.76±0.05^{jk}	0.01±0.00^{h}	0.01±0.00^{e}	0.52±0.00^{m}
	AUW_M	0.58±0.03^{l}	0.02±0.00^{gh}	0.02±0.00^{e}	0.57±0.00^{lm}
	AUW_H	0.62±0.00^{kl}	0.03±0.00^{gh}	0.02±0.00^{e}	0.68±0.01^{jkl}

Results are expressed as mean ± standard deviation (n=3). Different letters in superscript in the same column of both, raw and cooked pasta, correspond to significant differences (p<0.05). FRAP, ferric-reducing antioxidant power; GAE, gallic acid equivalent; QE, quercetin equivalent; TE, Trolox equivalent; dw, dry weight. Pasta coding: CTRL, control without wild garlic; AUP_L, AUP_M and AUP_H, pasta produced with 5%, 10% and 15% (*w/w*) substitution of wheat flour by AUP, respectively; AUL_L, AUL_M and AUL_H, pasta produced with 30%, 60% and 90% (*w/w*) substitution of mixing liquid by AUL respectively; AUW_L, AUW_M and AUW_H, pasta produced with 30%, 70% and 90% (*w/w*) substitution of mixing liquid by AUW, respectively.

all raw AUP pasta samples showed significantly (p<0.05) higher antioxidant capacity in both assays, and raw AUL pasta was characterised by significantly (p<0.05) higher FRAP. Enhancing the antioxidant capacity of pasta is a key objective in the development of functional food products through ingredient supplementation. Filipčev *et al*. [2023] demonstrated that the incorporation of wild garlic leaves, both as powder and extract, resulted in a significant increase in the antioxidant capacity of pasta, as assessed by the DPPH assay. This enhancement was attributed primarily to the presence of phenolic compounds. In turn, fortification of pasta with egg, in combination with chopped wild garlic leaves, led to improved antioxidant capacity measured by the FRAP assay [Rosan *et al*., 2024]. This effect was found to be dose-dependent with respect to the amount of egg incorporated.

Regarding the effect of cooking on the TPC of pasta, all cooked pasta had significantly (p<0.05) lower TPC than their raw counterparts (**Table 3**). The degree of reduction depended on the pasta formulation. The sample with the highest content of wild garlic leaf powder (AUP_H) exhibited the lowest reduction (51.28%), followed by AUP_M (58.76%) and AUP_L (63.83%). In the other two pasta variants (pasta with AUL and AUW), reductions in TPC were also depended on the amount of wild garlic formulation used. Among the three pasta variants, the AUL_M pasta showed the minimum loss of TPC of 42.48%. A possible reason may have been the more difficult removal of phenolics from blanched wild garlic leaves during the cooking process. The total flavonoid contents of the pasta, as in the case of TPC, indicated a loss of these compounds during cooking depended on the amount of wild garlic leaf formulation used

in the recipe. For the AUP variants, the maximum amount of leaf powder (AUP_H) led to a TFC reduction of 37.97%, while AUP_M and AUP_L showed TFC reduction of 53.68% and 61.39%, respectively. Our findings are consistent with the research conducted by Filipčev *et al.* [2023] who used three different pasta formulations, which included wild garlic (powder, extract, and encapsulated extract) and found that cooked pasta had a lower TPC compared to raw pasta, with differences depending on the matrix. The most notable decrease in TPC was reported in the pasta formulation that included encapsulated wild garlic at moderate and high supplementation levels. Our previous study showed that the loss of phenolic compounds during cooking of pasta enriched with wild garlic leaves was influenced by the content of other dough ingredients, like eggs – wild garlic leaf enriched pasta with the highest egg content had the lowest TPC reduction [Rosan *et al.*, 2024].

Cooking reduced not only the TPC and TFC of pasta, but also the antioxidant capacity of most pasta samples (**Table 3**). This finding did not apply to the antioxidant capacity of pasta of the AUW variants determined in both assays and pasta of the AUL variants in DPPH assay, for which the results before and after cooking did not differ significantly ($p \geq 0.05$). The pasta fortified with powdered *A. ursinum* leaves showed a 98% reduction in DPPH radical scavenging capacity and 42–46% reduction in FRAP. However, greater FRAP reduction (57%) was observed in the samples with a low content of blanched and chopped *A. ursinum* leaves (AUL_L). The changes observed in the antioxidant capacity of pasta enhanced with wild garlic are in line with findings from previous research indicating a reduction in antioxidant capacity after thermal processing. In our previous study [Rosan *et al.*, 2024], we observed a significant reduction in antioxidant capacity (between 20 and 30%), as determined by the FRAP assay, in pasta fortified with wild garlic leaves and egg. This effect was attributed to the loss of phenolics in the cooking water and/or thermal degradation of bioactive compounds. Verardo *et al.* [2011] found that 11.6% of the various phenolic compounds in cooked buckwheat spaghetti were released into the cooking water, while the pasta-making process resulted in a loss of 45.9% of the total phenolic compounds originally present in the raw materials used for the production of buckwheat spaghetti. According to Bustos *et al.* [2019], in berry-enriched pasta, heating partially destroyed the phenolics and reduced antioxidant capacity, while preserving the functional properties of the product. However, some studies indicated that cooking pasta in certain instances resulted in a noticeable increase of antioxidant capacity, attributed to the release of bound antioxidant compounds from the food matrix [Podio *et al.*, 2019]. Such results were also seen in durum wheat pasta that had been enhanced with debran fractions; cooking increased the antioxidant activity *in vitro* [Fares *et al.*, 2010].

The effects of varying drying temperatures (40, 50, and 60°C) on the total phenolic content and antioxidant activity in dried leaves of *Allium ursinum* L. subsp. *ucrainicum* were examined by Lukinac & Jukić [2022]. They demonstrated that higher drying temperatures led to a significant decrease in TPC and antioxidant activity determined in the DPPH assay as temperature increased. In order to maintain the quality and nutritional value of dried *A. ursinum* leaves, our drying temperature of both leaves and fortified pasta was 30°C.

Colour of pasta enriched with formulations from wild garlic leaves

An essential quality for coloured pastas is their colour stability. The results of measurements of the colour parameters made in raw and cooked pasta enriched with wild garlic leaf formulations are displayed in **Table 4**. When *A. ursinum* formulations were used, the colour of pastas changed from the light yellow of the control pasta (CTRL) to a green hue of the wild garlic leaves, and the colour intensity being dependent on the type of wild garlic formulation. The raw pasta fortified with powdered *A. ursinum* leaves (AUP) showed the highest total colour difference compared to CTRL (46.2–52.1), but this difference did not change significantly ($p<0.05$) with the increasing substitution level of what flour by powder in pasta recipe. The ΔE for raw pasta enriched with blanched and chopped wild garlic leaves (AUL) ranged from 13.6 to 26.5, which was significantly ($p<0.05$) lower than the value for AUP pasta. Finally, the raw pasta produced with by-product of leaf blanching and chopping (AUW) showed the smallest difference compared to the control. The colour difference was also calculated between the cooked enriched pasta and the corresponding cooked control. Minor alterations were noted for the AUW pasta, whereas the sample AUP_H showed the highest ΔE (43.1). Moreover, ΔE for cooked AUP and AUL pasta was found to be lower compared to their corresponding raw pasta, indicating a reduced overall colour difference.

In the case of the raw and cooked control pasta, the colour parameter L^* was 89.9 and 74.2, respectively (**Table 4**). Regardless of the level of substitution of wheat flour by wild garlic leaf powder, the L^* values of raw and cooked pasta were lower ($p<0.05$) compared to the respective controls. The pasta with blanched and chopped wild garlic leaves (AUL) also showed low L^* values, but not as significant as AUP. When compared to the raw pasta, the L^* values significantly decreased ($p<0.05$) after cooking. According to Filipčev *et al.* [2023], dark pasta had by L^* values below 55. Regardless of the substitution level and form of enrichment, the parameter a^* had negative values for all pasta samples (**Table 4**). This indicated the green colour of pasta caused by the green hue of the wild garlic leaves. The substitution of wheat flour by AUP lowered the a^* value of raw and cooked pasta much more than AUL. Regarding the b^* value, which indicates blueness/yellowness, the AUP pasta variants had the lowest values, while the AUW pasta variants had the highest values, and an increase compared to the control pasta was observed in the case of raw pasta samples. Filipčev *et al.* [2023] reported L^* values of 72.46 and 72.59, respectively, for raw and cooked pasta produced from durum wheat semolina, which, similarly to our study, decreased significantly compared

Table 4. Parameters of colour of raw and cooked pasta enriched with *Allium ursinum* L. leaf powder (AUP), blanched and chopped leaves (AUL), and water by-product of leaf blanching and chopping (AUW).

Pasta treatment	Pasta	*L**	*a**	*b**	*ΔE*
Raw pasta	CTRL	89.9±7.2^{a}	−8.0±0.8^{ab}	−14.0±6.4^{i}	–
	AUP_L	63.1±4.9^{fg}	−27.4±3.5^{f}	26.3±4.0^{a}	52.0±2.2^{a}
	AUP_M	59.5±3.6^{g}	−23.3±4.8^{ef}	17.2±4.0^{c}	46.2±3.8^{a}
	AUP_H	58.0±2.9^{g}	−23.2±4.3^{ef}	15.9±2.8^{c}	46.3±1.1^{a}
	AUL_L	79.5±3.7^{bcde}	−11.7±4.8^{abc}	−5.9±0.6^{gh}	13.6±4.5^{cd}
	AUL_M	71.8±7.3^{def}	−17.2±7.8^{cde}	3.0±0.4^{d}	26.5±4.1^{b}
	AUL_H	74.3±4.4^{de}	−15.4±5.8^{bcd}	−1.2±0.2^{defg}	21.5±1.0^{b}
	AUW_L	88.7±3.2^{ab}	−7.0±0.5^{a}	−14.0±3.9^{i}	1.6±3.8^{e}
	AUW_M	87.4±2.3^{abc}	−8.5±0.6^{ab}	−6.8±0.5^{gh}	7.7±0.8^{d}
	AUW_H	80.9±2.1^{abcd}	−8.7±0.8^{ab}	2.0±0.3^{de}	18.4±1.3^{cd}
Cooked pasta	CTRL	74.2±3.1^{de}	−8.7±0.6^{ab}	−6.9±0.7^{gh}	–
	AUP_L	57.7±6.8^{g}	−21.4±4.1^{def}	28.9±6.4^{a}	41.4±4.1^{a}
	AUP_M	46.9±7.1^{h}	−22.8±5.3^{def}	23.8±1.6^{ab}	43.5±3.7^{a}
	AUP_H	40.7±4.4^{h}	−16.4±3.4^{cde}	19.1±9.0^{bc}	43.1±4.3^{a}
	AUL_L	69.8±7.3^{ef}	−15.3±2.9^{bcd}	−14.8±2.1^{i}	11.2±2.4^{cd}
	AUL_M	62.3±4.9^{fg}	−16.9±5.4^{cde}	−7.8±0.3^{h}	14.6±1.4^{bc}
	AUL_H	59.2±6.6^{g}	−16.5±7.7^{cde}	−4.2±0.4^{efgh}	17.2±1.0^{b}
	AUW_L	75.6±7.9^{de}	−6.6±0.6^{a}	−4.6±0.7^{fgh}	3.4±1.4^{d}
	AUW_M	74.3±5.7^{de}	−7.9±0.8^{ab}	−2.6±0.6^{defgh}	4.3±0.9^{d}
	AUW_H	77.9±7.7^{cde}	−6.5±0.6^{a}	1.4±0.6^{def}	9.3±2.1^{cd}

Results are expressed as mean ± standard deviation (n=3). Different letters in the same column of both, raw and cooked pasta, correspond to significant differences (p<0.05). *L**, lightness; *a**, greenness/redness; *b**, blueness/yellowness; *ΔE*, total colour difference compared to control. Pasta coding: CTRL, control without wild garlic; AUP_L, AUP_M and AUP_H, pasta produced with 5%, 10% and 15% (*w/w*) substitution of wheat flour by AUP, respectively; AUL_L, AUL_M and AUL_H, pasta produced with 30%, 60% and 90% (*w/w*) substitution of mixing liquid by AUL, respectively; AUW_L, AUW_M and AUW_H, pasta produced with 30%, 70% and 90% (*w/w*) substitution of mixing liquid by AUW, respectively.

to pasta enriched with wild garlic powder, extract, and encapsulated extract. At the same time, *a** values considerably increased in the samples supplemented with extract in both forms, but decreased in the samples supplemented with powder. Considering pasta enriched with other leafy plant materials, Drabińska *et al*. [2022] found lower *L** and *a** values and a higher *b** value of raw (fresh and dried at different temperatures) pasta enriched with broccoli leaf powder compared to control pasta without powder incorporation, which is consistent with our findings regarding pasta samples with AUP and AUL. However, Wang *et al.* [2021] reported a decrease in *L**, *a**, and *b** values when pasta was fortified with spinach juice, puree, and pomace. Additionally, the lightness, greenness, and yellowness of the spinach pasta were much diminished throughout the cooking process. In turn, Teterycz *et al.* [2020] produced pasta with partial replacement of semolina with legume flours of different colours and demonstrated a decrease in the lightness, unchanged redness, and an increase in yellowness of cooked pasta when green pea flour was used.

Confocal microscopy images and surface roughness parameter of raw pasta enriched with formulations from wild garlic leaves

The results of laser microscopy analysis of raw pasta fortified with various *A. ursinum* formulations are displayed in **Figure 2**. Using laser confocal microscopy and profile analysis, the arithmetic mean height (Sa), the parameter of surface roughness, was calculated and shown in **Figure 2** along with the corresponding surface image. The surface roughness analysis of pasta showed that the Sa was influenced by the level of substitution of wheat

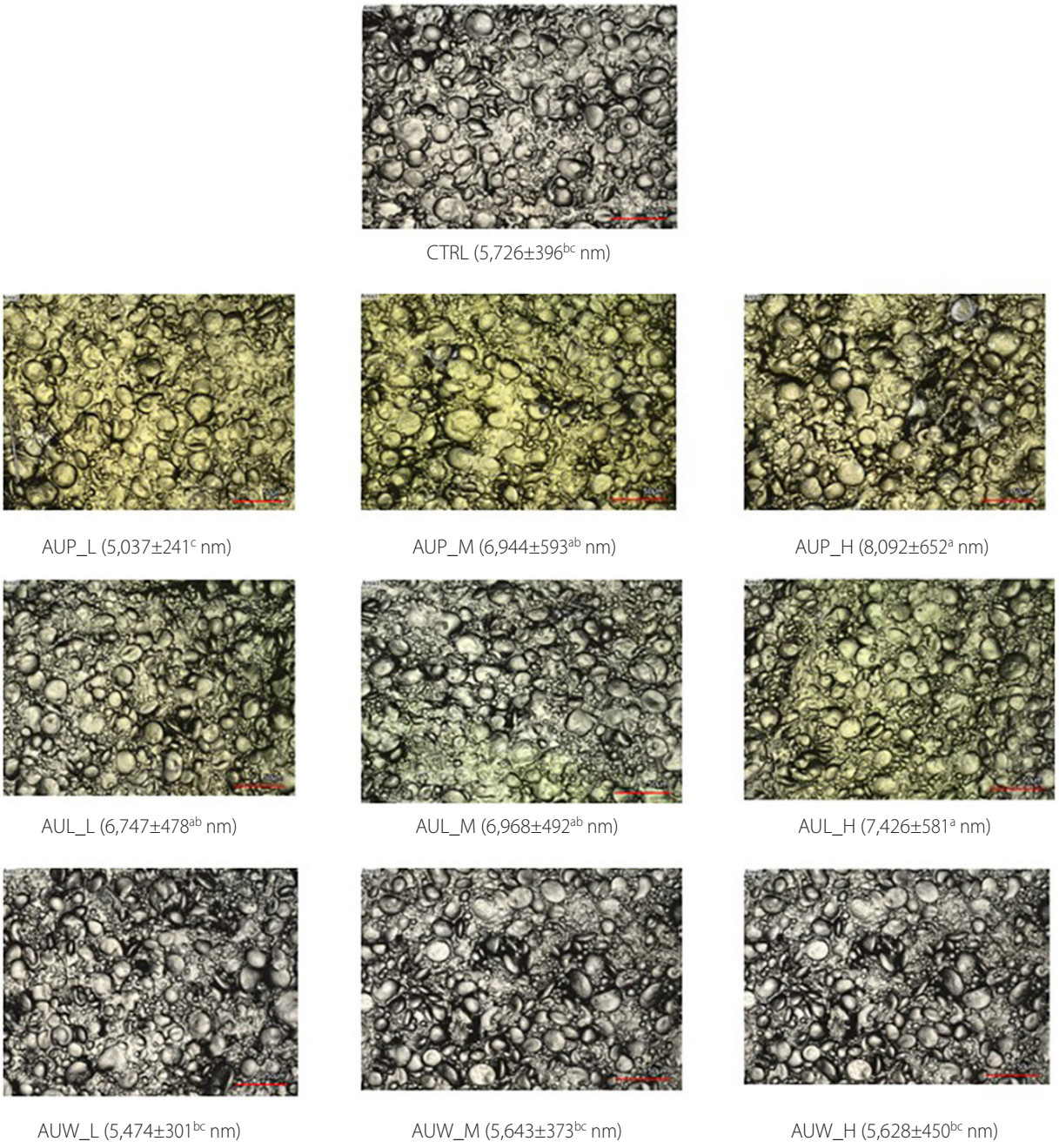

Figure 2. Confocal microscopy images and arithmetical mean height (shown in parentheses as mean ± standard deviation, n=3, and marked with different superscript letters for values that are significantly different, p<0.05) as a roughness parameter of raw pasta enriched with *Allium ursinum* L. leaf powder (AUP), blanched and chopped leaves (AUL), and water by-product of leaf blanching and chopping (AUW). Pasta coding: CTRL, control without wild garlic; AUP_L, AUP_M and AUP_H, pasta produced with 5%, 10% and 15% (*w/w*) substitution of wheat flour by AUP, respectively; AUL_L, AUL_M and AUL_H, pasta produced with 30%, 60% and 90% (*w/w*) substitution of mixing liquid by AUL, respectively; AUW_L, AUW_M and AUW_H, pasta produced with 30%, 70% and 90% (*w/w*) substitution of mixing liquid by AUW, respectively.

flour by *A. ursinum* leaf powder and was significantly (p<0.05) higher for AUP_M and AUP_H samples when compared to control pasta. Potentially large amounts of *A. ursinum* powder that remained embedded or partially exposed on the dough's surface could cause microtextures and irregularities. Powder particles may have caused the dough to become less uniform during extrusion, resulting in a rougher surface texture. Pasta with blanched and chopped leaves, as opposed to CTRL, contained larger, irregularly shaped particles that made the mixture rougher. During the extrusion and drying processes, the fibrous structure of the leaves could result in additional irregularities. The uneven distribution of the leaves in the dough also affected the roughness of the AUL pasta. Because it was evenly incorporated into the dough, using different amounts of wild garlic by-product (AUW) in pasta production proved to have no effect on the surface roughness of the dough when compared to the control.

A recent study examined changes in dried pasta during cooking, focusing on surface morphology [Ohmura *et al.*, 2023].

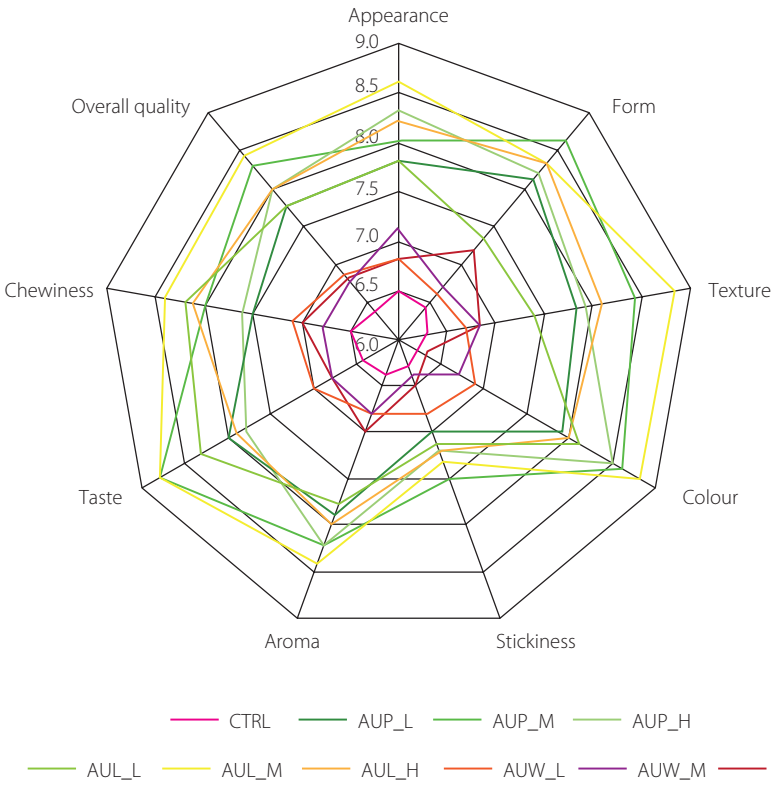

Figure 3. The sensory evaluation of cooked pasta enriched with *Allium ursinum* L. leaf powder (AUP), blanched and chopped leaves (AUL), and water by-product of leaf blanching and chopping (AUW). Pasta coding: CTRL, control without wild garlic; AUP_L, AUP_M and AUP_H, pasta produced with 5%, 10% and 15% (*w/w*) substitution of wheat flour by AUP, respectively; AUL_L, AUL_M and AUL_H, pasta produced with 30%, 60% and 90% (*w/w*) substitution of mixing liquid by AUL, respectively; AUW_L, AUW_M and AUW_H, pasta produced with 30%, 70% and 90% (*w/w*) substitution of mixing liquid by AUW, respectively.

The results did not indicate significant variations in light microscopy images. However, surface roughness measurements showed higher scores in the high-temperature dried pasta compared to the low-temperature dried pasta. As the drying temperature increased, the roughness parameters decreased, showing notable differences between the two types of cooked pasta. Using laser microscopy, it was demonstrated that, as the drying temperature increased, the variation in pasta height decreased, meaning that the surface roughness of cooked pasta (dried at high temperatures) was minimal. Cooked pasta (dried at low temperatures) showed superior surface roughness compared to other pastas, correlating with the results of cooking loss and fluorescence microscopy. The explanation was related to the fact that the more disrupted gluten network of the pasta led to a greater degree of starch granule swelling, thereby causing increased release of gluten from the outer periphery of boiled pasta. Such increases in the release of starch granules and gluten may be accountable for greater degree of surface roughness of pasta after boiling, which is also consistent with our findings.

Due to the presence of high molecular weight starch polymers that are naturally resistant to digestion and the protein matrix around gelatinized starch granules, formed during the boiling process, pasta consumption provides a source of slowly digestible carbohydrates with a moderate glycaemic index [Bustos *et al.*, 2015]. However, Colonna *et al.* [1990] noted that the starch granules were not completely enveloped by the gluten matrix and exhibited enough porosity to facilitate the diffusion of α-amylase.

Sensory scores of cooked pasta enriched with formulations from wild garlic leaves

The results obtained from the sensory evaluation of the pasta samples are presented in **Figure 3**. The scores varied, not only between the different samples but also among the evaluated sensory attributes. The attributes that mainly differentiated the pasta samples were appearance, colour, taste, and texture, which showed the greatest variability in panelist scores. Differences in visual and structural uniformity (especially due to deformation and curling in the samples with a high content of blanched and chopped wild garlic leaves) significantly affected the appearance and texture ratings. Although most sensory attributes remained constant or above 8.0, stickiness was also a differentiating factor, scoring lower (7.0–7.5) across all formulations. These elements contributed to the overall differentiation in consumer acceptability. A sensory difference was noted between the pasta samples fortified with wild garlic powder or blanched and chopped leaves and those supplemented with wild garlic by-products. Among the evaluated variants, pasta enriched with a medium level of blanched and chopped leaves (AUL_M) received the highest overall sensory score, averaging 8.43 points, followed closely by the sample with a medium content of wild garlic powder (AUP_M), with an average of 8.26 points. The classification used in this study is based on the nine-point hedonic

scale, originally developed by Peryam & Pilgrim [1957]. According with this scale, scores 8 and 9 correspond to the highest levels of consumer acceptance, interpreted as "very pleasant" and "extremely pleasant". This classification is further supported by the Society of Sensory Professionals (https://www.sensorysociety.org) which confirms these score descriptors and their use in sensory research protocols. Pasta produced with low and high contents of wild garlic powder or chopped leaves (AUP_L, AUL_H, AUP_H, AUL_L) received scores ranging between 7.75 and 7.98, placing them in the "pleasant" to "moderately pleasant" range. In contrast, the samples formulated with wild garlic by-products (AUW_L, AUW_M, AUW_H) scored between 6.76 and 6.84, which was comparable to the control sample (CTRL), which had an average score of 6.38, corresponding to a "neutral" to "slightly pleasant" sensory perception.

The study conducted by Filipčev *et al*. [2023] revealed that the addition of wild garlic powder in amounts of 5%, 7%, and 9% was favorably accepted by panelists, with the resulting pasta types ranking highly in sensory evaluations. Likewise, in our previous study, where different egg concentrations in the pasta dough were used along with an established amount of 20 g of chopped wild garlic leaves, consumers appreciated the presence of wild garlic in this form in pasta [Rosan *et al*., 2024].

CONCLUSIONS

This study investigated the effects of using wild garlic leaves in different forms (powder, blanched and chopped leaves, and by-products from leaf blanching and chopping) in pasta production at three levels (low, medium, and high). Our investigation included an in-depth assessment and comparison of cooking properties, contents of total phenolics and flavonoids, antioxidant capacity, colour, surface roughness and preliminary sensory analysis of the wild garlic-based pasta variants. All pasta formulations evaluated had satisfactory cooking qualities, though there were differences based on the type and quantity of wild garlic used. Every formulation with leaf powder and with blanched and chopped leaves significantly increased the total phenolic and total flavonoid contents and antioxidant capacity of the pasta, and higher levels of incorporation resulted in higher contents of bioactive ingredients. Despite a lower total phenolic content and antioxidant capacity of pasta with the by-product of leaf blanching and chopping compared to the other enriched pasta variants, its potential for food waste valorisation remains considerable. The colour parameters of pasta with wild garlic leaf formulations showed significant changes before and after cooking, reflecting the impact of wild garlic enrichment on the pasta's visual properties. Surface roughness analysis indicated that the medium and high levels of substitution of wheat flour by *A. ursinum* leaf powder in pasta significantly increased roughness compared to the control. Blanched and chopped leaves introduced larger, irregular particles, thereby intensifying the roughness. Although the highest substitution level by wild garlic leaf powder and blanched and chopped leaves enhanced phenolic content and antioxidant capacity, it did not yield the highest sensory scores. The pasta variants with a medium content of wild garlic blanched and chopped leaves and leaf powder were the most appreciated.

Although the present study has shown the potential of wild garlic-enriched pasta as a functional food, further research is needed to ascertain the post-consumption bioavailability of phenolic compounds. The health benefits of these compounds could be better understood if this research was done *in vivo* or using models of simulated digestion. *A. ursinum*-enriched pasta recipes for commercial use may also be improved by full consumer acceptance studies that concentrate on sensory requirements. Additionally, it is crucial to assess the long-term stability and antioxidant capacity of pasta. By-products from blanching and chopping of wild garlic leaves have shown encouraging results, which highlights the importance of considering sustainability while aiming to create functional foods that are friendly to the environment.

ACKNOWLEDGEMENTS

The authors acknowledge the support of the Technology Transfer Center CTT-UO, project code SMIS 140830, funded through the Regional Operational Programme 2014–2020. The laser confocal microscope used in this study was acquired within this project.

RESEARCH FUNDING

The APC was supported by University of Oradea. Authors received no external funds for the study.

CONFLICT OF INTERESTS

The authors declare that they have no conflict of interests.

ORICD IDs

M.F. Bei https://orcid.org/0000-0001-6732-5959
S.D. Cavalu https://orcid.org/0000-0001-7810-8925
T.O. Costea https://orcid.org/0000-0002-3206-2340
D. Domocos https://orcid.org/0000-0002-8114-6997
C.A. Rosan https://orcid.org/0000-0002-0581-7461
A.C. Teusdea https://orcid.org/0000-0002-3570-7271
S.I. Vicas https://orcid.org/0000-0001-9562-4809

REFERENCES

1. AACC (2010). *Approved Methods of Analysis* (11th ed). 66-50.01 Pasta and noodle cooking quality-firmness. American Association of Cereal Chemists. Cereals and Grains Association, St. Paul, MN, U.S.A.
2. Alexander, D. (2000). The geography of Italian pasta. *The Professional Geographer*, *52*(3), 553–566. https://doi.org/10.1111/0033-0124.00246
3. Benzie, I.F., Strain, J.J. (1996). The ferric reducing ability of plasma (FRAP) as a measure of "antioxidant power": The FRAP assay. *Analytical Biochemistry*, *239*(1), 70–76. https://doi.org/10.1006/abio.1996.0292
4. Bernaś, E., Słupski, J., Gębczyński, P., Ražná, K., Žiarovská, J. (2023). Chemical composition and genome pattern as a means of identifying the origin of preserved wild garlic (*Allium ursinum* L.) in Poland. *Agriculture*, *14*(1), art. no. 20. https://doi.org/10.3390/agriculture14010020
5. Bianchi, F., Tolve, R., Rainero, G., Bordiga, M., Brennan, C.S., Simonato, B. (2021). Technological, nutritional and sensory properties of pasta fortified with agro-industrial by-products: a review. *International Journal of Food Science & Technology*, *56*(9), 4356–4366. https://doi.org/10.1111/ijfs.15168
6. Bouacida, S., Ben Amira, A., Ben Haj Koubaier, H., Blecker, C., Bouzouita, N. (2017). Chemical composition, cooking quality, texture and consumer acceptance of pasta with *Eruca vesicaria* leaves. *International Journal of Food Science & Technology*, *52*(10), 2248–2255. https://doi.org/10.1111/ijfs.13504

7. Brand-Williams, W., Cuvelier, M.E., Berset, C. (1995). Use of a free radical method to evaluate antioxidant activity. *LWT – Food Science and Technology*, *28*(1), 25–30. **https://doi.org/10.1016/S0023-6438(95)80008-5**
8. Bustos, M.C., Paesani, C., Quiroga, F., León, A.E. (2019). Technological and sensorial quality of berry-enriched pasta. *Cereal Chemistry*, *96*(5), 967–976. **https://doi.org/10.1002/cche.10201**
9. Bustos, M.C., Perez, G.T., Leon, A.E. (2015). Structure and quality of pasta enriched with functional ingredients. *RSC Advances*, *5*(39), 30780–30792. **https://doi.org/10.1039/C4RA11857J**
10. Cappelli, A., Cini, E. (2021). Challenges and opportunities in wheat flour, pasta, bread, and bakery product production chains: A systematic review of innovations and improvement strategies to increase sustainability, productivity, and product quality. *Sustainability*, *13*(5), art. no. 2608. **https://doi.org/10.3390/su13052608**
11. Chetrariu, A., Dabija, A. (2021). Quality characteristics of spelt pasta enriched with spent grain. *Agronomy*, *11*(9), art. no. 1824. **https://doi.org/10.3390/agronomy11091824**
12. Cinkmanis, I., Augšpole, I., Sivicka, I., Vucāne, S. (2022). Evaluation of the phenolic profile of bear's garlic (*Allium Ursinum* L.) leaves. *Proceedings of the Latvian Academy of Sciences. Section B. Natural, Exact, and Applied Sciences*, *76*(4), 512–516. **https://doi.org/10.2478/prolas-2022-0079**
13. Colonna, P., Barry, J.-L., Cloarec, D., Bornet, F., Gouilloud, S., Galmiche, J.-P. (1990). Enzymic susceptibility of starch from pasta. *Journal of Cereal Science*, *11*(1), 59–70. **https://doi.org/10.1016/S0733-5210(09)80181-1**
14. Del Nobile, M.A., Baiano, A., Conte, A., Mocci, G. (2005). Influence of protein content on spaghetti cooking quality. *Journal of Cereal Science*, *41*(3), 347–356. **https://doi.org/10.1016/j.jcs.2004.12.003**
15. Dimitrios, A. (2024). Durum wheat: Uses, quality characteristics, and applied tests. In R. Wanyera M. Wamalwa (Eds.), *Wheat Research and Utilization*. IntechOpen. **https://doi.org/10.5772/intechopen.110613**
16. Drabińska, N., Nogueira, M., Ciska, E., Jeleń, H.H. (2022). Effect of drying and broccoli leaves incorporation on the nutritional quality of durum wheat pasta. *Polish Journal of Food and Nutrition Sciences*, *72*(3), 273-285. **https://doi.org/10.31883/pjfns/152070**
17. Dziki, D. (2021). Current trends in enrichment of wheat pasta: quality, nutritional value and antioxidant properties. *Processes*, *9*(8), art. no. 1280. **https://doi.org/10.3390/pr9081280**
18. Einhorn-Stoll, U., Kunzek, H., Dongowski, G. (2007). Thermal analysis of chemically and mechanically modified pectins. *Food Hydrocolloids*, *21*(7), 1101–1112. **https://doi.org/10.1016/j.foodhyd.2006.08.004**
19. Fares, C., Platani, C., Baiano, A., Menga, V. (2010). Effect of processing and cooking on phenolic acid profile and antioxidant capacity of durum wheat pasta enriched with debranning fractions of wheat. *Food Chemistry*, *119*(3), 1023–1029. **https://doi.org/10.1016/j.foodchem.2009.08.006**
20. Filipčev, B., Kojić, J., Miljanić, J., Šimurina, O., Stupar, A., Škrobot, D., Travičić, V., Pojić, M. (2023). Wild garlic (*Allium ursinum*) preparations in the design of novel functional pasta. *Foods*, *12*(24), art. no. 4376. **https://doi.org/10.3390/foods12244376**
21. Gopalakrishnan, J., Menon, R., Padmaja, G., Sajeev, M.S., Moorthy, S.N. (2011). Nutritional and functional characteristics of protein-fortified pasta from sweet potato. *Food and Nutrition Sciences*, *2*(9), 944–955. **https://doi.org/10.4236/fns.2011.29129**
22. Greve, L.C., Shackel, K.A., Ahmadi, H., McArdle, R.N., Gohlke, J.R., Labavitch, J.M. (1994). Impact of heating on carrot firmness: Contribution of cellular turgor. *Journal of Agricultural and Food Chemistry*, *42*(12), 2896–2899. **https://doi.org/10.1021/jf00048a047**
23. Hastaoğlu, E., Kelek, Z., Çapar, D. (2023). Investigations of the possibilities of developing gluten-free pasta containing hemp pulp flour and rice flour. *Turkish Journal of Agriculture - Food Science and Technology*, *11*(11), 2080–2088 (in Turkish, English abstract). **https://doi.org/10.24925/turjaf.v11i11.2080-2088.6240**
24. IPO, International Pasta Organisation (2024). Report: World pasta day 2024: A billion plates of pasta in 10 years to feed the planet. *International Pasta Organisation*. (**https://internationalpasta.org/news/world-pasta-day-2024-a-billion-plates-of-pasta-in-10-years-to-feed-the-planet/**, accessed on 21 February 2025).
25. Kovačević, T.K., Major, N., Sivec, M., Horvat, D., Krpan, M., Hruškar, M., Ban, D., Išić, N., Goreta Ban, S. (2023). Phenolic content, amino acids, volatile compounds, antioxidant capacity, and their relationship in wild garlic (*A. ursinum* L.). *Foods*, *12*(11), art. no. 2110. **https://doi.org/10.3390/foods12112110**
26. Lachowicz, S., Kolniak-Ostek, J., Oszmiański, J., Wiśniewski, R. (2017). Comparison of phenolic content and antioxidant capacity of bear garlic (*Allium ursinum* L.) in different maturity stages: Phenolics and antioxidants in bear garlic. *Journal of Food Processing and Preservation*, *41*, art. no. e12921. **https://doi.org/10.1111/jfpp.12921**
27. Lukinac, J., Jukić, M. (2022). Influence of drying temperature on the organoleptic properties, antioxidant activity and polyphenol content in dried leaves of *Allium ursinum* L. subsp. ucrainicum. *Ukrainian Food Journal*, *11*(1), 9–26. **https://doi.org/10.24263/2304-974X-2022-11-1-4**
28. Marinelli, V., Padalino, L., Nardiello, D., Del Nobile, M.A., Conte, A. (2015). New approach to enrich pasta with polyphenols from grape marc. *Journal of Chemistry*, *2015*, art. no. 734578. **https://doi.org/10.1155/2015/734578**
29. Muresan, C.C., Farcas, A., Man, S., Suharoschi, R., Vlaic, R.A. (2017). Obtaining a functional product through the exploitation of mushroom flour in pasta. *Bulletin of University of Agricultural Sciences and Veterinary Medicine Cluj-Napoca. Food Science and Technology*, *74*(1), 17-22. **https://doi.org/10.15835/buasvmcn-fst:12641**
30. Ohmura, M., Matsumiya, K., Maeda, T., Fujita, A., Hayashi, Y., Matsumura, Y. (2023). Effect of drying profiles on surface structure changes of durum wheat pasta during the boiling process. *LWT – Food Science and Technology*, *173*, art. no. 114175. **https://doi.org/10.1016/j.lwt.2022.114175**
31. Oszmiański, J., Kolniak-Ostek, J., Wojdyło, A. (2013). Characterization and content of flavonol derivatives of *Allium ursinum* L. plant. *Journal of Agricultural and Food Chemistry*, *61*(1), 176–184. **https://doi.org/10.1021/jf304268e**
32. Parvu, M., Toiu, A., Vlase, L., Parvu, A.E. (2010). Determination of some polyphenolic compounds from *Allium* species by HPLC-UV-MS. *Natural Product Research*, *24*(14), 1318–1324. **https://doi.org/10.1080/14786410903309484**
33. Peryam, D.R., Pilgrim, F.J. (1957). Hedonic scale method of measuring food preferences. Food Technology, *11*, Suppl., 9–14.
34. Piątkowska, E., Kopeć, A., Leszczyńska, T. (2015). Basic chemical composition, content of micro- and macroelements and antioxidant activity of different varieties of garlic's leaves Polish origin. *Żywność. Nauka. Technologia. Jakość*, *1*(98), 181–192. **https://doi.org/10.15193/zntj/2015/98/014**
35. Podio, N.S., Baroni, M.V., Pérez, G.T., Wunderlin, D.A. (2019). Assessment of bioactive compounds and their *in vitro* bioaccessibility in whole-wheat flour pasta. *Food Chemistry*, *293*, 408–417. **https://doi.org/10.1016/j.foodchem.2019.04.117**
36. Rosan, C.A., Bei, M.F., Tocai (Moțoc), A.C., Gitea, M.A., Vicas, S.I. (2024). Effects of *Allium ursinum* L. leaves and egg amount on quality attributes, polyphenol content, and antioxidant capacity of pasta. *Applied Sciences*, *14*(7), art. no. 7517. **https://doi.org/10.3390/app14177517**
37. Schettino, R., Verni, M., Acin-Albiac, M., Vincentini, O., Krona, A., Knaapila, A., Cagno, R.D., Gobbetti, M., Rizzello, C.G., Coda, R. (2021). Bioprocessed brewers' spent grain improves nutritional and antioxidant properties of pasta. *Antioxidants*, *10*(5), art. no. 742. **https://doi.org/10.3390/antiox10050742**
38. Sęczyk, Ł., Świeca, M., Gawlik-Dziki, U., Luty, M., Czyż, J. (2016). Effect of fortification with parsley (*Petroselinum crispum* Mill.) leaves on the nutraceutical and nutritional quality of wheat pasta. *Food Chemistry*, *190*, 419–428. **https://doi.org/10.1016/j.foodchem.2015.05.110**
39. Singleton, V.L., Orthofer, R., Lamuela-Raventós, R.M. (1999). [14] Analysis of total phenols and other oxidation substrates and antioxidants by means of folin-ciocalteu reagent. *Methods in Enzymology*, *299*, 152–178. **https://doi.org/10.1016/S0076-6879(99)99017-1**
40. Sissons, M. (2022). Development of novel pasta products with evidence based impacts on health – A review. *Foods*, *11*(1), art. no. 123. **https://doi.org/10.3390/foods11010123**
41. Sobolewska, D., Podolak, I., Makowska-Wąs, J. (2015). *Allium ursinum*: Botanical, phytochemical and pharmacological overview. *Phytochemistry Reviews*, *14*, 81–97. **https://doi.org/10.1007/s11101-013-9334-0**
42. Teterycz, D., Sobota, A., Zarzycki, P., Latoch, A. (2020). Legume flour as a natural colouring component in pasta production. *Journal of Food Science and Technology*, *57*, 301–309. **https://doi.org/10.1007/s13197-019-04061-5**
43. Tóth, T., Kovarovič, J., Bystrická, J., Vollmannová, A., Musilová, J., Lenková, M. (2018). The content of polyphenols and antioxidant activity in leaves and flowers of wild garlic (*Allium ursinum* L.). *Acta Alimentaria*, *47*(2), 252–258. **https://doi.org/10.1556/066.2018.47.2.15**
44. Verardo, V., Arráez-Román, D., Segura-Carretero, A., Marconi, E., Fernández-Gutiérrez, A., Caboni, M.F. (2011). Determination of free and bound phenolic compounds in buckwheat spaghetti by RP-HPLC-ESI-TOF-MS: Effect of ther-

mal processing from farm to fork. *Journal of Agricultural and Food Chemistry, 59*(14), 7700–7707.
https://doi.org/10.1021/jf201069k

45. Vicas, S., Prokisch, J., Rugina, O.D., Socaciu, C. (2009). Hydrophilic and lipophilic antioxidant activities of mistletoe (*Viscum album*) as determined by FRAP method. *Notulae Botanicae Horti Agrobotanici Cluj-Napoca*, *37*(2), 112–116.
https://doi.org/10.15835/nbha3723244
46. Vidović, S., Tomšik, A., Vladić, J., Jokić, S., Aladić, K., Pastor, K., Jerković, I. (2021). Supercritical carbon dioxide extraction of *Allium ursinum*: Impact of temperature and pressure on the extracts chemical profile. *Chemistry Biodiversity, 18*(4), art. no. e2100058.
https://doi.org/10.1002/cbdv.202100058
47. Wang, J., Brennan, M.A., Brennan, C.S., Serventi, L. (2021). Effect of vegetable juice, puree, and pomace on chemical and technological quality of fresh pasta. *Foods*, *10*(8), art. no. 1931.
https://doi.org/10.3390/foods10081931
48. Wu, H., Dushenkov, S., Ho, C.-T., Sang, S. (2009). Novel acetylated flavonoid glycosides from the leaves of *Allium ursinum*. *Food Chemistry, 115*(2), 592–595.
https://doi.org/10.1016/j.foodchem.2008.12.058
49. Xiao, H.-W., Pan, Z., Deng, L.-Z., El-Mashad, H.M., Yang, X.-H., Mujumdar, A.S., Gao, Z.-J., Zhang, Q. (2017). Recent developments and trends in thermal blanching – A comprehensive review. *Information Processing in Agriculture*, *4*(2), 101–127.
https://doi.org/10.1016/j.inpa.2017.02.001

ORIGINAL ARTICLE
http://journal.pan.olsztyn.pl

Polish Journal of Food and Nutrition Sciences
2025, Vol. 75, No. 3, 208–220
DOI: 10.31883/pjfns/208020
ISSN 1230-0322, e-ISSN 2083-6007

Effect of Medicinal Mushroom Powders on the Gluten Structure in the Wheat and Semolina Doughs

Agnieszka Nawrocka[1], Aldona Sobota[2], Konrad Kłosok[1], Renata Welc-Stanowska[1, 3], Agata Sumara[4], Emilia Fornal[4]

[1]Laboratory of Assessment of Grain Materials Quality, Institute of Agrophysics, Polish Academy of Sciences, Doświadczalna 4, 20-290 Lublin, Poland
[2]Department of Engineering and Cereals Technology, University of Life Sciences in Lublin, Skromna 8, 20-704, Lublin, Poland
[3]Department of Plant Physiology and Biophysics, Institute of Biological Sciences, Maria Curie-Skłodowska University, Akademicka 19, 20-033 Lublin, Poland
[4]Department of Bioanalytics, Medical University of Lublin, ul. Jaczewskiego 8, 20-090 Lublin, Poland

Wheat flour and durum semolina were enriched with powders from four medicinal mushrooms during dough mixing. Wheat flour and durum semolina were substituted with chaga, *Cordyceps sinensis*, reishi and lion's mane powders at 3%, 6%, 9%, and 12% (*w/w*). Changes in the gluten secondary structure and water populations of the dough samples were determined by means of Fourier transform infrared spectroscopy (FT-IR). As a result of mushroom powder incorporation, the formation of additional pseudo-β-sheets (aggregated structures) was observed in wheat flour doughs, whereas aggregates and additional α-helices were formed in the durum semolina doughs. Structural differences observed between dough materials can be due to the gluten index and particle size. Generally, chaga, reishi and lion's mane powders caused an increase in the content of α-helices and a decrease in the content of pseudo-β-sheets, parallel-β-sheets and antiparallel-β-sheets. *C. sinensis* powder induced the formation of pseudo-β-sheets from α-helices, β-turns and antiparallel-β-sheets. The content of the mushroom powders in wheat flour and durum semolina doughs slightly affected the changes observed in the secondary structure of gluten. Amounts of particular water populations did not change or changed slightly in the presence of medicinal mushroom powders, which was presumably due to complex chemical composition of the mushroom powders. Analysis of the FT-IR spectra showed that the type of the observed structural changes depended on the material type the dough was prepared from as well as chemical composition of the mushroom powder.

Keywords: infrared spectroscopy, mushroom polyphenolic profile, semolina dough, water populations, wheat dough

INTRODUCTION

Medicinal mushrooms, like chaga (*Inonotus obliquus* (Ach. Ex Pers.) Pilat), *Cordyceps sinensis* (*Ophiocordyceps sinensis* (Berk.) G.H. Sung, J.M. Sung, Hywel-Jones and Spatafora), reishi (*Ganoderma lucidum* (Curtis) P. Karst), and lion's mane (*Hericium erinaceus* (Bull.) Pers.), have been well-known and applied in the Chinese medicine from centuries. Recently, they have been increasingly used as food additives because they are regarded as a source of bioactive compounds, such as polysaccharides (*e.g.*, β-D-glucans), phenolic compounds, triterpenoids, active peptides, and sterols [Cateni *et al*., 2022; Łysakowska *et al*., 2023; Sousa *et al*., 2023] which show anticancer, antioxidant, antidiabetic, and immunomodulatory properties [Reis *et al*., 2017; Song *et al*., 2020]. However, the chemical composition of individual mushrooms depends on the fungus strain, cultivation conditions, degree of maturity, and anatomical part of the mushroom the additive was sourced from [Barros *et al*., 2007; Cateni *et al*., 2022].

***Corresponding Author:**
e-mail: **a.nawrocka@ipan.lublin.pl** (Prof. A. Nawrocka)

Submitted: 27 March 2025
Accepted: 1 June 2025
Published on-line: 29 July 2025

Recently, food products enriched with health-promoting additives have become increasingly popular among consumers due to their growing interest in foods with properties that prevent and/or cure various ailments. Wheat products, like bakery products and pasta, are still regarded as staple foods in the Western diet. For this reason, they can serve as good carriers of health-promoting bioactive compounds of medicinal mushrooms. Two of the medicinal mushroom species, reishi and shitake, have been used the most often as food additives [Łysakowska *et al*., 2023]. Mushroom addition to food products positively affects their chemical composition by increasing the contents of protein, total and insoluble dietary fibre, phenolic compounds, and micro- and macroelements [Reis *et al*., 2017]. On the other hand, the mushroom enriched-food products show a worse taste, texture, flavour, and appearance. Whether the changes observed in the technological quality of the product are positive or negative depends on the amount and type of powdered mushroom added, especially in the case of wheat bread and pasta [Lu *et al*., 2016; 2018]. If less than 5% of wheat flour is replaced by powdered mushroom, then usually no negative changes are observed in the quality of wheat bread dough [Lu *et al*., 2018]. If the wheat flour substitution with the mushroom powder is greater than 5%, then a product with deteriorated technological quality is obtained. Reduction in the technological and sensory quality of a wheat bread and pasta was observed as a result of the bread enrichment with white button, shitake and porcini mushrooms [Lu *et al*., 2016; 2018], reishi mushroom [Łysakowska *et al*., 2024], and lion's mane [Łysakowska *et al*., 2025a; Ulziijargal *et al*., 2013]. However, the addition of some mushrooms may improve the sensory quality of wheat products, like wheat bread made of wheat flour replaced by 5% and 10% of king trumpet mushroom (*Pleurotus eryngii*) powder [Gaglio *et al*., 2019], and biscuits with 10–20% of oyster mushroom (*Pleutorus ostreatus*) [Baltacioglu *et al*., 2021].

Reduction in the wheat product quality is partially related to the competition for water between the gluten network and mushroom dietary fibre during dough mixing. The smaller amount of water available to the gluten network during this process affects its structure and the types of water populations present in the network [Nawrocka *et al*., 2017]. Hence, the aim of this research was to determine how powders from four medicinal mushrooms, differing in the chemical composition, influenced the secondary structure and water populations of the gluten proteins in doughs. The changes were determined for dough samples prepared from wheat flour and durum semolina substituted with mushroom powders (3–12%, *w/w*) by means of the Fourier transform infrared spectroscopy.

MATERIALS AND METHODS

Materials and chemicals

Wheat flour type 750 was produced by Polskie Młyny (Warsaw, Poland), while semolina (a durum wheat milling product) was produced by Julia Malom (Kunszallas, Hungary). The ash content of the raw materials was determined according to the AACC method 08-01, while the wet gluten content, dry gluten content, gluten index, and gluten water binding capacity were determined according to the AACC method 38-12.02 [AACC, 2010]. The average particle size was analysed using the method described by Kasprzak & Rzedzicki [2012].

Farinographic measurements of durum semolina were conducted using a Farinograph-E (Brabender, model 8110142, Duisburg, Germany) according to the AACC method 54-21 [AACC, 2010], and respective results are provided in **Table 1**. Farinographic parameters of wheat flour type 750 were consistent with the results published by Łysakowska *et al*. [2025a], as the same raw material was used in both studies.

The medicinal mushrooms: chaga (*Inonotus obliques* (Ach. Ex Pers.) Pilat), *Cordyceps sinensis* (*Ophiocordyceps sinensis* (Berk.) G.H. Sung, J.M. Sung, Hywel-Jones and Spatafora), reishi (*Ganoderma lucidum* (Curtis) P. Karst), and lion's mane (*Hericium erinaceus* (Bull.) Pers.) in the powdered form were purchased from NatVita (Mirków, Poland). The same *C. sinensis*, reishi and lion's mane powders were used in previous studies, in which the dietary fibre, fat and protein contents were determined: *C. sinensis* – 48.1 g/100 g d.m., 5.6 g/100 g d.m., 33.7 g/100 g d.m., respectively [Łysakowska *et al*., 2025b]; reishi – 72.8%, 0.99%, 15.5%, respectively [Łysakowska *et al*., 2024]; and lion's mane – 54.4%, 1.92%, 21.2%, respectively [Łysakowska *et al*., 2025a].

Acetonitrile and methanol (both liquid chromatography – mass spectrometry (LC-MS) grade) were obtained from Thermo Fisher Scientific (Waltham, MA, USA). Formic acid (LC-MS grade), deuterium oxide (D_2O) and sodium chloride were purchased from Merck KGaA (Darmstadt, Germany). MilliQ water was obtained using a purification system (Millipore DirectQ3-UV, Merck KGaA, Darmstadt, Germany). Extracts were filtered through a 0.20 µm, 4 mm titan syringe filter (Thermo Fisher Scientific). Double-distilled water was used to prepare wheat flour and semolina doughs.

Preparation of the phenolic extracts from mushroom powders

Phenolic extracts from mushroom powders were prepared using a method described by Sivam *et al*. [2013]. Briefly, each

Table 1. Quality parameters of wheat flour and semolina used in the study.

Quality parameter	Wheat flour type 750*	Durum semolina
Ash (g/100 g)	0.74±0.02	0.96±0.02
Wet gluten (%)	27.5±1.0	28.7±0.1
Dry gluten (%)	10.2±0.1	10.2±0.2
Gluten index (%)	99.0±0.3	57.0±2.1
Gluten water binding capacity (%)	17.3±0.1	18.5±0.1
Average particle size (mm)	0.12±0.01	0.27±0.02
Water absorption (%)	57.9±1.1	56.7±1.4
Dough development time (min)	2.30±0.12	5.12±1.17
Dough stability (min)	6.05±0.15	12.49±1.10
Dough softening (FU)	55±1	35±4

*Chemical composition and farinographic parameters of wheat flour were taken from Łysakowska *et al.* [2025a].

of the mushroom powders (4 g) was compacted in a stainless-steel extraction cell of 22 mL. The extraction process was carried out three times with 95% methanol in an accelerated solvent extraction (ASE) extractor (ASE 350, Dionex Corporation, Sunnyvale, CA, USA). The following extraction conditions were set in the extractor: pressure – 1,500 psi, extraction temperature – 42°C, cycle time – 10 min, and static volume – 60%.

Determination of the phenolic profile of the medicinal mushrooms

The phenolic profile of mushroom extracts was determined using a liquid chromatograph (1290 Infinity, Agilent Technologies, Santa Clara, CA, USA) coupled to a quadrupole time-of-flight mass spectrometer (6550 iFunnel Q-TOF LC/MS, Agilent Technologies). LC separation was performed using an Agilent RRHD C18 Extend analytical column (2.1×100 mm, 1.8 µm) thermostated at 45°C. To this end, 1 µL of the diluted extract was injected onto the column and elution was carried out with a mobile phase consisting of solvent A – 0.1% (*v/v*) formic acid in water and solvent B – 0.1% (*v/v*) formic acid in acetonitrile, used in a gradient system (0–25 min, 3–95% B; 25–30 min, 95% B). The mobile phase flow rate was 0.4 mL/min. An Agilent Jet Stream Technology ion source (electrospray ionization, ESI) operated in the positive ion mode. It utilised nitrogen at 225°C with the flow rate of 12 L/min. Nebulizer pressure was 50 psi. Sheath gas temperature and flow rate were 275°C and 12 L/min, respectively. The voltage of capillary, nozzle and fragmentor was set at 3,500; 1,000; and 275 V, respectively. Ions were acquired in the MS scan mode at a rate of 1.2 spectra/s, and in the targeted MS/MS mode at a rate of 8 spectra/s for MS spectra and 4 spectra/s for MS/MS spectra. The MS/MS spectra were collected at a collision energy of 10 and 20 eV. Reference ions *m/z* 121.0509 and *m/z* 922.0098 were used for internal mass calibration. Agilent Mass Hunter Data Acquisition software (B.09.00) and Agilent Mass Hunter Qualitative software (B.10.00) were used for instrument control and data processing, respectively.

Liquid chromatography quadrupole time-of-flight mass spectrometry data processing

A literature review was conducted on the analysed mushroom species, based on which a list of compounds with previously confirmed presence by other researchers was compiled [Friedman, 2015; Hwang *et al.*, 2016; Kim, 2020; Kolniak-Ostek *et al.*, 2022; Tang *et al.*, 2022; Wang *et al.*, 2021]. The results obtained from the MS-level analysis were screened by extracting ions (extracted ion chromatogram, EIC) corresponding to the masses of the compounds on the established list and isotopic pattern. The ions that showed a match were then subjected to fragmentation, and the resulting fragment spectra were compared with reference spectra in the following databases: METLIN Metabolite Personal Compound Database and Library (https://metlin.scripps.edu/, Agilent Technologies, Santa Clara, CA, USA) [Guijas *et al.*, 2018; Smith *et al.*, 2005], Human Metabolome Database (HMDB) (https://www.hmdb.ca/) [Wishart *et al.*, 2002; 2007], and the Reference Metabolome Database of Plants (https://www.biosino.org/RefMetaDB/) [Shi *et al.*, 2024].

Moreover, the ions with the highest intensity were selected from the base peak chromatogram (BPC) and subjected to fragmentation. The resulting fragment spectra were searched for matches against the reference spectra in the aforementioned databases.

Preparation of doughs enriched with mushroom powders

The wheat flour and durum semolina doughs without (controls) and with mushroom powders were prepared in a Farinograph E equipped with a 50 g-mixer (Brabender, Germany) according to a standard ICC 115/1 method of the International Association for Cereal Science and Technology [1992]. Water content was determined using the Farinograph E for wheat flour and durum semolina samples separately by adding water until the dough consistency was 500 FU. The amount of water added was different for wheat flour and durum semolina. The doughs enriched with mushroom powders were prepared using the same amount of water as in the control samples. The time of dough mixing was 20 min. Wheat flour or semolina was substituted by the medicinal mushroom powders in the amounts of 3%, 6%, 9%, and 12% (*w/w*). The dough samples (control as well as doughs enriched with mushroom powder) were prepared in triplicate.

Preparation of dough samples for Fourier transform infrared spectroscopy measurements

The wheat flour/semolina dough samples after mixing process (averaged from three replicates) were freeze-dried for 24 h and pulverised. Before Fourier transform infrared spectroscopy (FT-IR) measurements, approximately 0.5 g of the powdered dough samples were put in an exicator and moisturised by a 10% (*v/v*) aqueous solution of deuterium oxide to eliminate water oscillations from the amide I band [Nawrocka *et al.*, 2017].

Fourier transform infrared spectroscopy measurements and analysis of structural changes

The FT-IR spectra were recorded using a Nicolet 6700 FT-IR spectrometer (Thermo Scientific, Madison, WI, USA) equipped with a diamond attenuated total reflection (ATR) attachment. Spectra collection and data manipulation were carried out according to Nawrocka *et al*. [2017]. For each dough sample, five FT-IR spectra were collected and averaged before calculation of difference spectra. The difference spectra were calculated by subtraction of the control sample spectrum from the spectrum of a dough sample enriched with the mushroom powders. The average difference spectra were analysed to provide qualitative information about changes in the gluten secondary structure. The spectra were processed using ORIGIN software (v.2019b PRO, OriginLab Corporation, USA). Changes in the gluten secondary structure determined by the analysis of difference spectra in the amide I (1,570–1,720 cm^{-1}) and amide III (1,200–1,340 cm^{-1}) bands were determined according to Yang *et al*. [2015] and Stani *et al*. [2020], respectively. In other words, positive and negative bands present in the difference spectrum were assigned to the particular secondary structures.

RESULTS AND DISCUSSION

Profile of phenolic compounds of the medicinal mushroom powders

Phenolic compounds, especially those characterized by strong antioxidative properties, are very important for the consumers and bakery industry. Nowadays, consumers are very interested in purchasing food products that have positive impact on their health. Phenolics are considered to have a positive effect on human health. However, they can have a negative effect on the production process of wheat bread, *e.g.*, cause dough breakdown if

Table 2. Retention times (R_t), measured mass-to-charge ratio (*m/z*) of molecular ions in positive electrospray ionization mode, *m/z* of fragment ions (MS/MS ions), collision energy (CE), compound formula, corresponding theoretical *m/z*, and accuracy of phenolic compounds identified in the *Inotutus obliquus* (chaga, Ch), *Ophiocordyceps sinensis* (*Cordyceps sinensis*, C), *Ganoderma lucidum* (reishi, R), and *Hericium erinaceus* (lion's mane, LM).

R_t (min)	Measured *m/z*	MS/MS ions (*m/z*)	CE (eV)	Compound formula	Theoretical *m/z*	Diff (ppm)	Compound	Mushroom
2.7	139.0391	65.0389 93.0335 111.0441	20	$C_7H_6O_3$	139.039	–1.93	3,4-Dihydroxybenzaldehyde	Ch
3.6	199.0603	140.0463 155.0696 116.9758 123.0436	10	$C_9H_{10}O_5$	199.0601	–1.14	Syringic acid	Ch
3.8	227.0912	155.0701 181.0493 73.0283 140.0463	10	$C_{11}H_{14}O_5$	227.0915	–1.7	Ficusol	Ch
4.7	183.0646	123.0437 95.0490 155.0701 140.0462	10	$C_9H_{10}O_4$	183.0652	–2.61	Methyl isovanillate	R, Ch
5.0	225.0756	207.0647 175.0386 147.0435 119.0486	10	$C_{11}H_{12}O_5$	225.0757	–0.55	Sinapic acid	R
6.1	369.1181	207.0652 175.0387 147.0436 119.0489	20	$C_{17}H_{20}O_9$	369.1180	–0.24	Cnidioside A	C, R, Ch, LM
6.3	273.1123	137.0592 123.0440 163.0755 147.0438	10	$C_{16}H_{16}O_4$	237.1121	–0.62	Neovestitol	R
7.0	255.0651	199.0748 137.0229 227.698 181.0641	20	$C_{15}H_{10}O_4$	255.0652	0.41	Daidzein	C, LM
7.4	285.0756	270.0515 225.0539 229.0853 242.0569	20	$C_{16}H_{12}O_5$	285.0757	0.68	Glycitein	C, LM
8.5	271.0601	153.0181 215.0699 243.0648 253.0491	20	$C_{15}H_{10}O_5$	271.0601	0.04	Genistein	C, LM
9.7	195.1018	135.0801 163.0747 107.0850 91.0543	20	$C_{11}H_{14}O_3$	195.1016	–1.21	Zingerone	R, Ch
20.7	301.0703	286.0466 168.0053 255.1471	20	$C_{16}H_{12}O_6$	301.0707	0.43	Tectorigenin	C
24.6	269.0806	254.0568 213.0894 237.0540 226.0615	20	$C_{16}H_{12}O_4$	269.0808	0.75	Formononetin	C
26.5	275.0915	201.0907 229.0844 177.0541	20	$C_{15}H_{14}O_5$	275.0914	–0.32	10-Deoxygerfelin	LM

too much of this type of compound is used [Krekora *et al*., 2020]. For these reasons, the phenolic profile of the food additives used should be determined.

Phenolic compounds identified in the studied mushrooms are listed in **Table 2**. Chaga powder contained 3,4-dihydroxybenzaldehyde, syringic acid, ficusol, methyl isovanillate, cnidioside A, and zingerone. Analysis of the *C. sinensis* extract showed the presence of daidzein, genistein, glycitein, cnidioside A, tectorigenin, and formononetin. In turn, methyl isovanillate, sinapic acid, cnidioside A, neovestitol, and zingerone were found in the reishi extract. Whereas lion's mane extract also contained daidzein, glycitein, genistein, cnidioside A, and 10-deoxygerfelin. 3,4-Dihydroxybenzaldehyde in the chaga powder was also detected by Hwang *et al*. [2016], whereas sinapic acid and vanillin were also found in reishi mushrooms by Szydłowska-Tutaj *et al*. [2023].

Changes in the secondary structure of gluten (analysis of the amide I and amide III bands)

Deconvoluted amide I bands of FT-IR spectra determined for both control samples (wheat flour (WF) dough and durum semolina (DS) dough) are shown in **Figure 1**. Gluten from semolina dough contained more β-sheets and less α-helices compared with the gluten from wheat dough. Both samples did not contain β-turns and random coils. A study by Nawrocka *et al*. [2023] concerning the secondary structure of gluten washed out from wheat bread dough showed that dough contained a small amount of β-turns in addition to β-sheets and α-helices. However, analysis of gluten extracted from wheat wholemeal demonstrated the presence of secondary structures similar to gluten washed out from wheat bread dough, but contents of these structures differed significantly [Nawrocka, 2014]. Studies of Both *et al*. [2019], Nawrocka [2014], and Nawrocka *et al*. [2023] indicated that gluten secondary structure may vary depending on the type of material gluten was extracted from.

Difference spectra in the amide III bands ascribed to changes in the secondary structure of the gluten network obtained from wheat (WF) and semolina (DS) doughs modified with chaga powder are shown in **Figure 2**. The difference spectra in the amide I band were not calculated for doughs modified with this mushroom because subtraction of the deuterium oxide spectrum caused the amide I band to disappear from the FT-IR spectra of the chaga-enriched samples. Analysis of the amide III bands showed that chaga induced a decrease in the β-sheet content in both WF and DS observed as the negative band at *ca*. 1,235 cm^{-1}. According to Nawrocka *et al*. [2018a], this band can be assigned to β-sheets connected by intermolecular H bonds, which are formed between gluten polypeptide chains and are indicative of aggregation. These bonds are regarded as those responsible for the formation of a gluten network during dough mixing. The decrease in the content of β-sheets linked by intermolecular H bonds can be due to the inability to extract gluten from dough samples and a lack of the amide I band in the FT-IR spectrum after deuterium oxide spectrum subtraction. However, a negative band located at *ca*. 1,235 cm^{-1} was also observed in our previous study [Nawrocka *et al*., 2020], investigating the effect of non-moisturized dietary fibre preparations on the gluten network in the model dough. The disappearance of these β-sheet structures was due to the dehydration of the gluten network by the dietary fibre preparations and aggregation of the gluten polypeptide chains. In the case of chaga-enriched dough, the gluten network dehydration could play a lesser role because of the inability of the gluten extraction from the WF and DS doughs, despite the high dietary fibre content (*ca*. 68%) of the chaga mushroom [Lu *et al*., 2021]. Moreover, the spectra of the WF-chaga samples showed negative and positive bands assigned to random coils and α-helices, respectively (**Figure 2A**). In the case of DS dough, the difference spectra contained three positive bands assigned to random coils, β-turns and α-helices (**Figure 2B**). The level of WF substitution with chaga powder

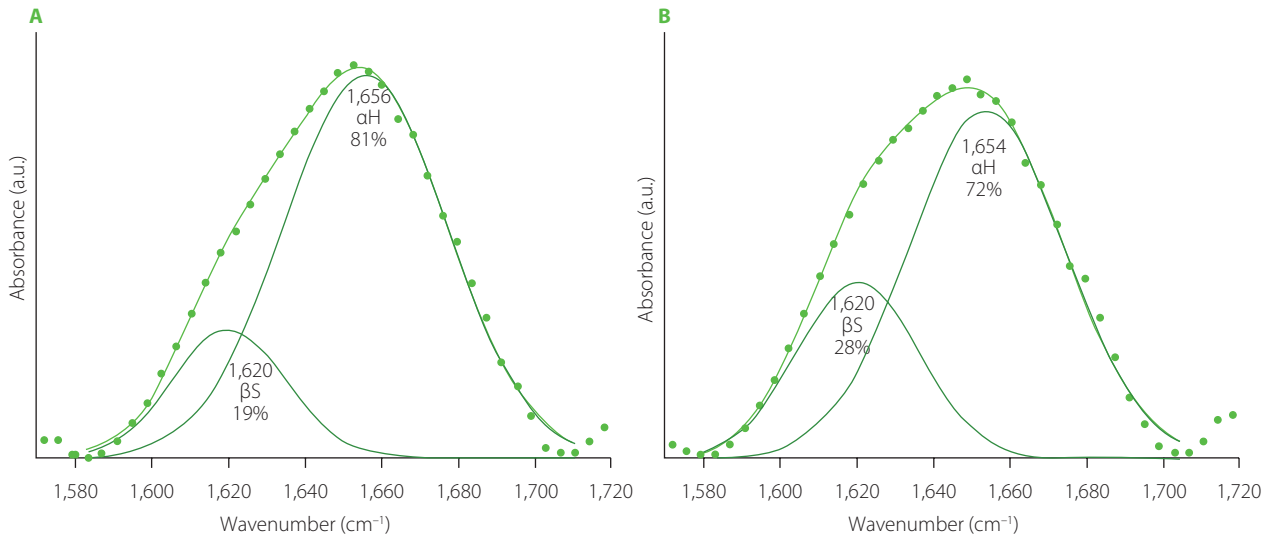

Figure 1. Deconvoluted amide I band of Fourier transform infrared spectra of the gluten network present in the wheat dough (**A**) and semolina dough (**B**). αH, α-helix; βS, β-sheet.

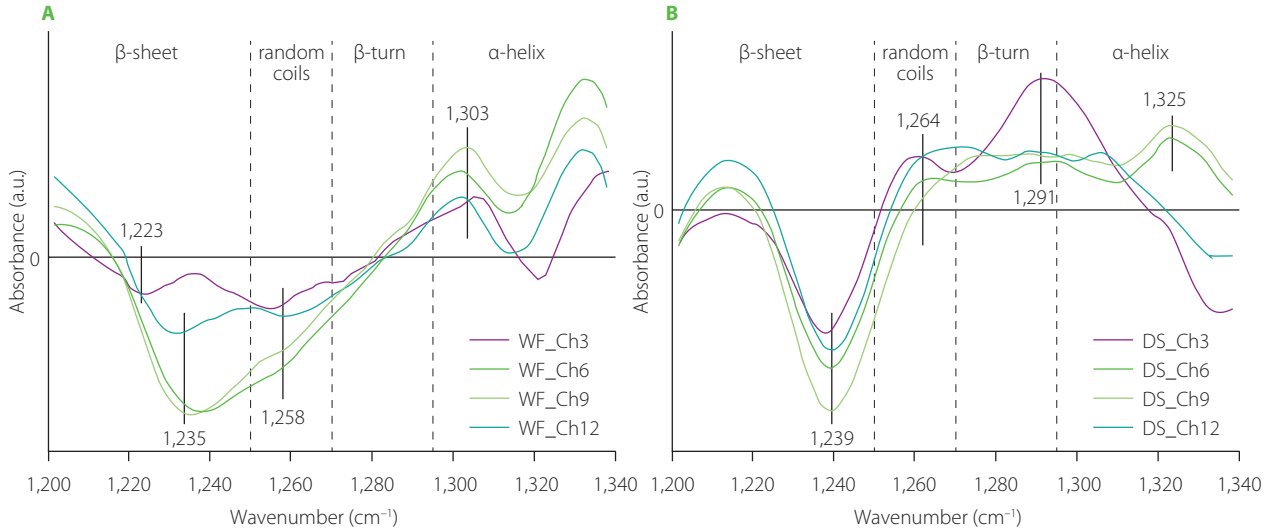

Figure 2. Fourier transform infrared difference spectra in the amide III band of the doughs from wheat flour (WF) (**A**) and durum semolina (DS) (**B**) substituted with 3–12% (*w/w*) chaga mushroom powder (Ch3–Ch12, respectively).

in the dough production had a slight effect on the spectral regions assigned to random coils and α-helices. Noticeable changes were observed in the β-sheet spectral region (**Figure 2A**). In the case of 3% (*w/w*) substitution with chaga powder, a negative band was located at *ca*. 1,223 cm^{-1}. According to Nawrocka *et al*. [2018a], this band can be connected with type II of H bonds that may be formed between gluten polypeptide chains and fibre polysaccharides present in the mushroom powder. The higher content of chaga powder in wheat dough caused the shift of the above-mentioned band to *ca*. 1,235 cm^{-1}. This band can be assigned to type I of H bonds [Nawrocka *et al*., 2018a]. The appearance of this negative band at higher levels of WF substitution with chaga powder may suggest that a certain amount of type I of the H bonds was not formed between gluten polypeptide chains in the presence of mushroom polysaccharides. Hence, the mechanical properties of the gluten network developed were modified. This change can be observed as a reduction in the quality parameters of the dough and bread [Łysakowska *et al*., 2025a]. The negative band at *ca*. 1,235 cm^{-1} was also observed in the dough samples modified with reishi and lion's mane powders, which is discussed below. In the case of DS samples, the level of semolina substitution with chaga powder affected slightly the gluten secondary structure (**Figure 2B**). This effect was observed as an increase and a decrease in the intensity of the positive and negative peaks assigned mainly to α-helices and β-sheets. The present study results indicate that particular compounds of the chaga powder interacted less with the gluten network in the DS dough compared with WF dough, which may be due to a different particle size of WF and DS (**Table 1**), since the DS particles were twice as large as those of WF.

Effects of *C. sinensis* mushroom on the gluten network in the WF and DS doughs are presented in **Figure 3**. Analysis of the difference spectra in the amide I and amide III bands showed that *C. sinensis* incorporation led to an increase in the content of β-sheets with intermolecular hydrogen bonds. The band assigned to such structures was observed at *ca*. 1,619–1,625 cm^{-1} (pseudo-β-sheets) in the amide I band, whereas the amide III band contained a band at *ca*. 1,227–1,236 cm^{-1}. Additionally, a decrease was observed in the content of β-turns and α-helices. The decrease in the content of β-turns may suggest that particular compounds of the *C. sinensis* powder may interact with amino acids present in the β-turns because β-turns are usually located at the edge of the protein complex. Moreover, β-turns can also participate in the formation of pseudo-β-sheets [Nawrocka *et al*., 2015]. Positive bands assigned to pseudo-β-sheets in the amide I band and β-sheets with intermolecular H bonds in the amide III bands were observed simultaneously as a result of wheat dough supplementation with paprika, pitted pepper and tomato pomace [Nawrocka *et al*., 2023]. The pomace contained on average 25% protein and 50% dietary fibre. Similar protein and dietary fibre contents were determined for *C. sinensis* mushroom (33% and 48%, respectively) [Łysakowska *et al*., 2025b]. The difference spectra showed that the contents of α-helices and β-turns decreased considerably (negative bands) in both types of doughs (**Figure 3C** and **D**). In turn, the content of random coils increased in the DS samples (positive bands) and decreased in the WF samples (negative bands). However, the maximum of the band assigned to random coils in the DS doughs was located closely to the edge of the β-sheet spectral region (at *ca*. 1,254 cm^{-1}). Additionally, the FT-IR spectra were registered with resolution of 4 cm^{-1}. For these reasons, this band may be partially related to β-sheet structures. The amount of the *C. sinensis* powder slightly affected the gluten secondary structure. The only structures in which noticeable changes were observed, such as an increase in the intensity of the band characteristic for this structure, were pseudo-β-sheets with a band at *ca*. 1,619 cm^{-1} for DS doughs (**Figure 3B**) and β-sheets with type I of H bonds with a band at *ca*. 1,236 cm^{-1} (**Figure 3C**). The presence of these bands may indicate that the compounds of the mushroom powder (*e.g*., polysaccharides, phenolic

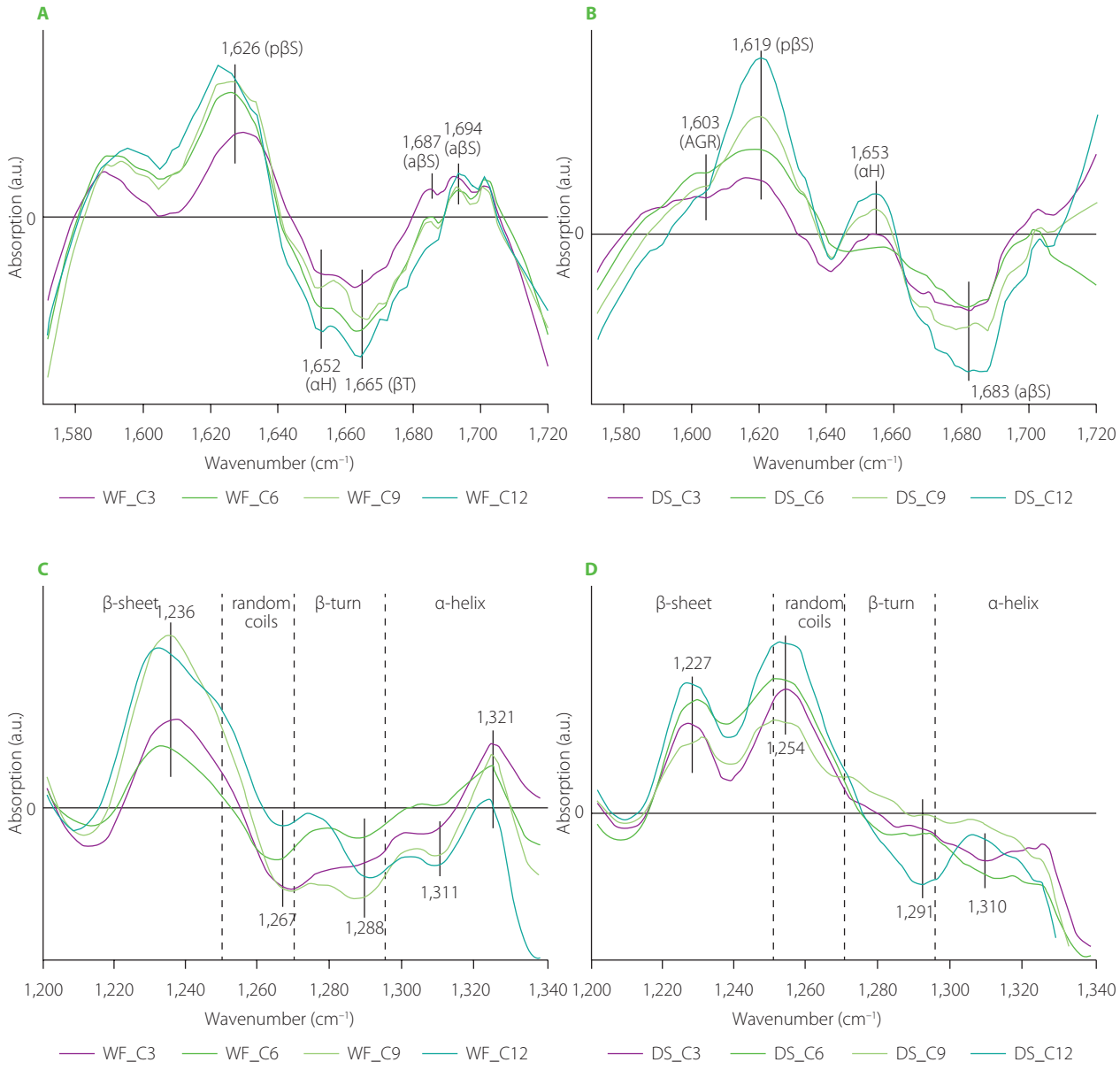

Figure 3. Fourier transform infrared difference spectra in the amide I band (**A** and **B**), and amide III band (**C** and **D**) of the doughs from wheat flour (WF) and durum semolina (DS) substituted with 3–12% (*w/w*) *Cordyceps sinensis* powder (C3–C12, respectively). AGR, aggregates; pβS, pseudo-β-sheets; αH, α-helices; βT, β-turns; aβS, antiparallel-β-sheets.

compounds) did not interact chemically with the gluten network. On the other hand, their presence induced the formation of additional hydrogen bonds between the polypeptide chains of gluten proteins during dough mixing.

The difference spectra concerning changes in the gluten structure in the doughs as a result of partial substitution of WF and DS with reishi mushroom powder are depicted in **Figure 4**. They showed that compounds of the reishi powder interacted differently with WF and DS. In the case of the WF gluten network, positive bands assigned to pseudo-β-sheets and α-helices were observed simultaneously with negative bands connected with β-turns and antiparallel-β-sheets in the amide I band. Analysis of the amide III band showed disappearance of β-sheets with intermolecular H bonds (1,234 cm^{-1}) and an increase in the content of α-helices (1,309 cm^{-1}). The decrease in the content of β-structures can be due to a reduction in gluten elasticity and, consequently, a decrease in the bread loaf volume [Łysakowska *et al.*, 2024]. The presence of the reishi powder, and especially a high content of its total dietary fibre, strengthen the gluten network, while simultaneously diminishing the retention of air bubbles by the gluten network. The DS gluten network was modified differently by the reishi mushroom powder than the WF gluten network (**Figure 4A-D**). Amide I band showed one positive band at 1,607 cm^{-1} that can be assigned to aggregates and/or hydrated/extended β-sheets [Feeney *et al.*, 2003]. The negative bands located at 1,636; 1,673 and 1,686 cm^{-1} may be ascribed to β-sheets, β-turns and antiparallel-β-sheets, respectively [Secundo & Guerrieri, 2005]. The amount of the reishi powder added to the dough had a small effect on the gluten secondary structure. The band shape and peak locations in both amide

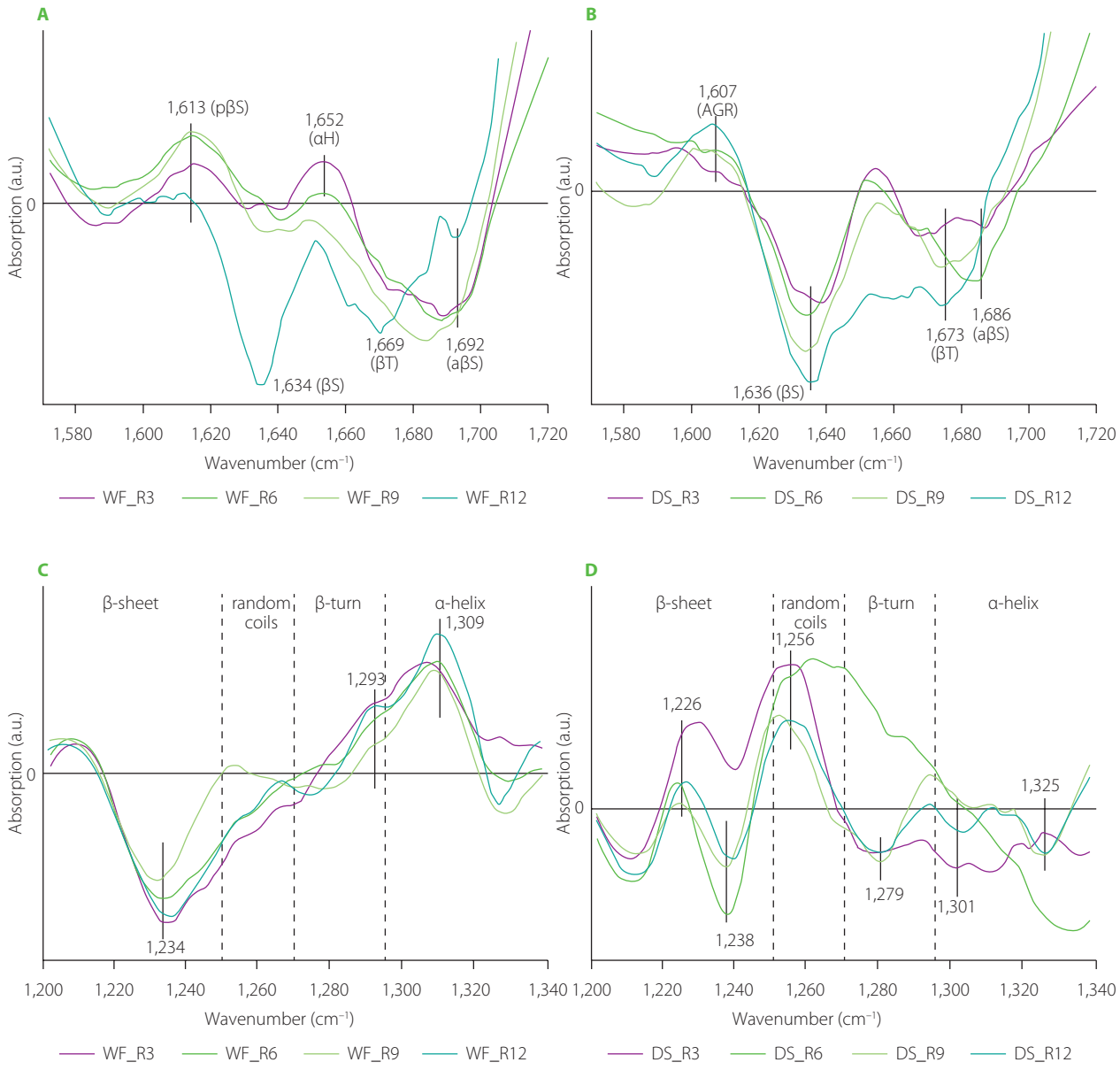

Figure 4. Fourier transform infrared difference spectra in the amide I band (**A** and **B**), and amide III band (**C** and **D**) of the doughs from wheat flour (WF) and durum semolina (DS) substituted with 3–12% (*w/w*) reishi powder (R3–R12, respectively). AGR, aggregates; pβS, pseudo-β-sheets; βS, parallel-β-sheets; αH, α-helices; βT, β-turns; aβS, antiparallel-β-sheets.

bands of the gluten modified with reishi (samples WF and DS) were similar to those modified by chaga. The similar structural changes can be related to the similar content of dietary fibre in both mushrooms, which was high and approximated 70%. Simultaneously, both mushrooms differed significantly in their protein and fat contents [Lu *et al.*, 2021; Łysakowska *et al.*, 2024]. According to Rumińska *et al.* [2020], a similar content of dietary fibre (*ca.* 70%) was determined in oil pomace obtained from hemp and milk thistle seeds. Similar changes in the secondary structure were observed only in the case of gluten modified by milk thistle. The observed differences in the secondary structure can be due to the high amount of unsaturated fatty acids in the hemp pomace compared to milk thistle pomace.

Figure 5 depicts difference spectra concerning structural changes in the gluten structure caused by addition of lion's mane mushroom powder to the WF and DS doughs. In the WF samples, substitution of WF with the lion's mane powder induced the appearance of pseudo-β-sheet (*ca.* 1,619 cm^{-1}) and α-helices (*ca.* 1,658 cm^{-1}) with the simultaneous disappearance of antiparallel-β-sheets (*ca.* 1,688 cm^{-1}). Additionally, two negative bands at 1,631 and 1,642 cm^{-1} were observed for gluten modified with the lion's mane powder at two highest substitution levels. These bands can be assigned to β-sheets and H-bonded β-turns or/and random coils [Secundo & Guerrieri, 2005]. The spectra of DS doughs showed one positive band connected with α-helices. The other parts of difference spectra, assigned to β-structures, were negative. Analysis of the amide III band showed an increase in the contents of β-turns and α-helices at the expense of β-sheets and random coils in the WF samples. The use of the lion's mane powder in a dough recipe exerted

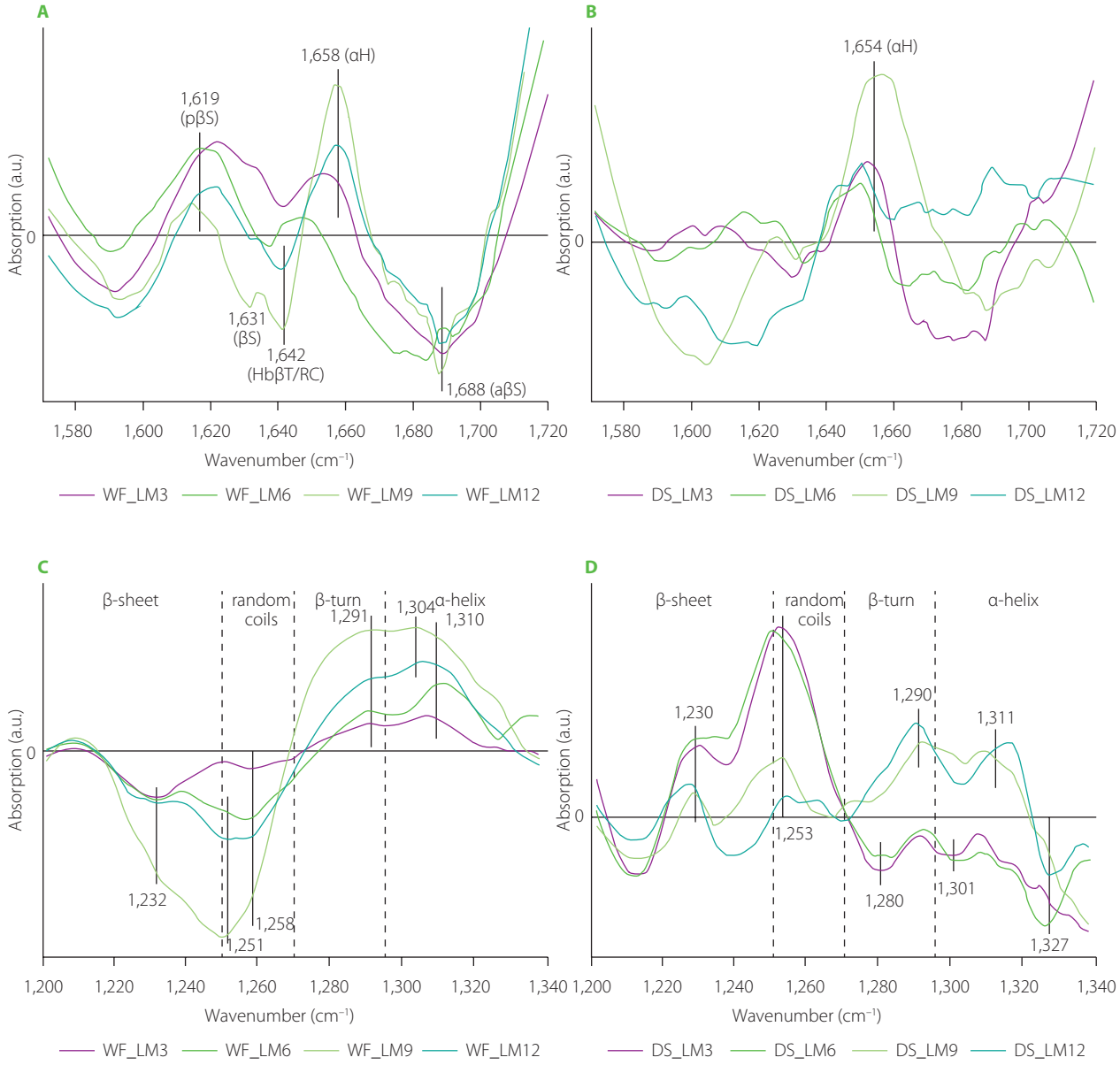

Figure 5. Fourier transform infrared difference spectra in the amide I band (**A** and **B**), and amide III band (**C** and **D**) of the doughs from wheat flour (WF) and durum semolina (DS) substituted with 3–12% (*w/w*) lion's mane powder (LM3–LM12, respectively). pβS, pseudo-β-sheets; βS, parallel-β-sheets; HbβT, hydrogen bonded β-turns; RC, random coils; αH, α-helices; aβS, antiparallel-β-sheets.

a different effect on the gluten structure in the DS samples. Doughs obtained by DS substitution with 3% and 6% (*w/w*) of lion's mane powder were characterized by positive bands in the spectral regions assigned to β-sheets and random coils. In turn, the highest content of lion's mane powder induced an increase in the content of β-turns and α-helices and a considerable decrease in the contents of β-sheet and random coils. Decreasing the number of β-sheets and β-turns can cause a decrease in the elasticity of the gluten network and, consequently, hinder proper growth and gas retention during dough fermentation. This can be visible as a decrease in the technological parameters describing wheat bread quality, such as specific bread volume, porosity, or crust hardness. A decrease in the specific bread volume and crust hardness has been observed by Łysakowska *et al.* [2025a], who studied the effect of WF substitution with lion's mane powder in the amounts of 3%–12% (*w/w*) on bread dough and bread quality. Similar results in terms of specific bread volume have been determined for bread with 5% (*w/w*) of lion's mane powder in its recipe. However, none of the textural parameters of bread (hardness, springiness, cohesiveness, gumminess, chewiness, resilience) changed upon the lion's mane addition [Ulziijargal *et al.*, 2013]. Additionally, the structural changes observed in the present study can be related to the chemical composition of the mushrooms' powder. Lion's mane and *C. sinensis* powders share a similar chemical composition in terms of fibre and protein contents [Łysakowska *et al.*, 2025a, b]. Hence, they should trigger similar structural changes, as it was observed in the case of reishi- and chaga-enriched doughs. However, similar changes in the gluten secondary structure were observed only in the amide III band of the DS spectra

(**Figures 3D** and **5D**). The addition of *C. sinensis* and lion's mane to dough formula caused the formation of β-sheets with hydrogen bonds of type II (positive band at *ca*. 1,235 cm^{-1}). According to Nawrocka *et al*. [2018a], H bonds of this type can be formed between gluten polypeptide chains and fibre polysaccharides and/or polypeptide chains of proteins present in the mushrooms powders. In the case of chaga and reishi, the spectral region assigned to β-sheets (1,200–1,250 cm^{-1}) included a negative band at *ca*. 1,238 cm^{-1}. The band at 1,238 cm^{-1} can be connected with hydrogen bonds of type I, which are formed between gluten polypeptide chains in the dough [Nawrocka *et al*., 2018a]. Moreover, a significant increase in the intensity of band assigned to random coils (1,250–1,270 cm^{-1}) was observed for doughs enriched with *C. sinensis*, reishi and lion's mane (**Figures 3D**, **4D**, **5D**). These analyses suggest that the structural changes observed in the β-sheet spectral region can be due to the presence of dietary fibre and proteins in the mushroom powders. In turn, the changes in the random coil region may be attributed to a high content of proteins in the studied powders. Reishi and lion's mane contain *ca*. 15% protein, while the fibre content is *ca*. 70% for chaga and reishi, and *ca*. 50% for *C. sinensis* and lion's mane [Lu *et al*., 2021; Łysakowska *et al*., 2024; 2025a]. Generally, analysis of the difference spectra showed that the changes observed in the secondary structure of the gluten depended on the type of the material used for dough preparation, *i.e*., wheat flour or durum semolina, as well as species of medicinal mushroom and its chemical composition. The difference spectra in the amide I band for WF samples had a positive band assigned to pseudo-β-sheets, whereas DS spectra contained positive bands connected with aggregates or α-helices. In the case of amide III band, WF spectra showed negative bands in the spectral regions connected with β-sheets and random coils, and positive bands in the regions of β-turns and α-helices. DS spectra showed opposite orientation of these spectral regions. The structural differences observed between WF and DS can be due to their physicochemical parameters, such as gluten index and particle size (**Table 1**). Finding a correlation between the chemical composition of the tested mushrooms and the structural changes observed in gluten is, however, very difficult because both the dough and the mushroom powder are complex matrices. Therefore, determining the mechanism of interaction between two such matrices is very difficult. However, previous studies addressing the rheological properties of dough and the technological properties of bread showed a significant reduction in the quality of dough, bread and pasta as a result of mushroom addition. In the case of bread dough, it was observed an increase in water absorption and dough stability and a decrease in the dough softening and dough extensibility. These farinographic changes were observed in the wheat bread as a decrease in the crumb porosity, loaf volume and springiness [Lu *et al*., 2018; Łysakowska *et al*., 2024; 2025a; Ulziijargal *et al*., 2013]. In turn, pasta enriched with edible mushroom powders showed an increase in the cooking loss and a decrease in the water absorption index [Lu *et al*., 2016]. The increase in the cooking loss of the pasta can be attributed to a loss of the gluten network continuity that may be related to the competition for water between mushroom powder rich in dietary fibre and gluten network [Tudorica *et al*., 2002].

Changes in OH stretching region (water populations)

The gluten network in dough may contain water in different forms, such as water molecules linked to the gluten network by strong and weak hydrogen bonds, small hydrogen bonded water clusters, water molecules participating in hydrogen bonds through two hydrogen atoms from one molecule, and unbound water molecules ("free water"). Changes in the particular water forms can be determined by analyzing OH stretching region in the FT-IR spectrum (2,500–4,000 cm^{-1}) [Bock & Damodaran, 2013].

Spectra concerning changes in the water populations in dough caused by the addition of the medicinal mushroom powders to dough formula are depicted in **Figure 6**. Almost all spectra showed one positive band at *ca*. 3,040 cm^{-1} assigned to strong hydrogen bonds formed between gluten network and water molecules [Bock & Damodaran, 2013]. Additionally, three negative bands were observed at *ca*. 3,250; 3,390; and 3,600 cm^{-1} which can be assigned to water molecules involved in the formation of two hydrogen bonds [Cotugno *et al*., 2001], small hydrogen bonded water clusters [Bock & Damodaran, 2013], and free water molecules [Cotugno *et al*., 2001]. Only in the case of WF_C3 and WF_C6 samples (**Figure 6C**) was a positive band observed at *ca*. 3,276 cm^{-1}. This band can be ascribed to hydrogen-bonded-associated chains of water molecules in bulk water [Jain *et al*., 1989]. Analysis of the spectra indicated that WF and DS substitution with the mushroom powders did not affect or slightly affected water populations in the dough samples, presumably due to the fact that powders had high contents of proteins, fats, phenolics *etc*., which also might have interacted with the gluten network. Hence, the observed structural changes in the gluten network may be partially related to the competition for water between gluten and mushroom dietary fibre. Similarly to the present study, research into the effect of oil pomace on the gluten structure in the bread dough showed slight changes in the water populations [Rumińska *et al*., 2020]. On the contrary, great changes in water populations were observed after the use of dietary fibre preparations as additives to bread wheat dough [Nawrocka *et al*., 2017; 2020] or fibre polysaccharides [Nawrocka *et al*., 2018b]. The differences in the water populations observed between the present study and studies concerning dietary fibre preparations can be related to the chemical composition of the additives used. For example, dietary fibre preparations, which differ in the ratio of insoluble dietary fibre (IDF) and soluble dietary fibre (SDF), may trigger changes in the intensity of the bands assigned to particular water populations. Such differences were observed for model bread dough modified with chokeberry and flax dietary fibre preparations (IDF/SDF ≅ 14 and 2 for chokeberry and flax, respectively) [Nawrocka *et al*., 2015; 2017]. Similar differences in the intensity of the bands assigned to water populations were observed upon model dough enrichment with four fibre polysaccharides

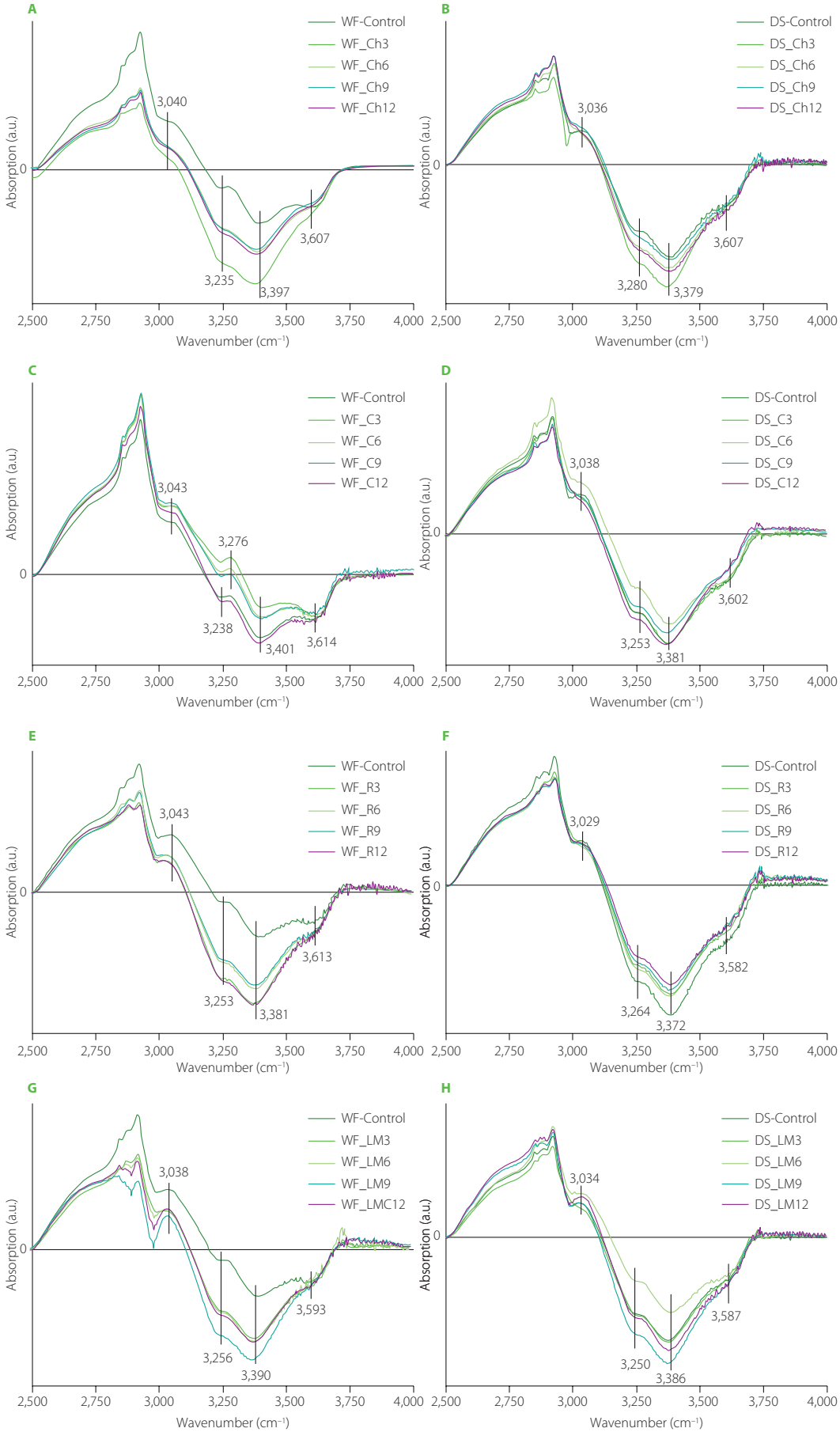

Figure 6. Fourier transform infrared difference spectra in the OH stretching region of the doughs from wheat flour (WF) and durum semolina (DS) substituted with 3–12% (*w/w*) chaga (Ch3–Ch12) (**A–B**), *Cordyceps sinensis* (C3–C12) (**C–D**), reishi (R3–R12) (**E–F**), and lion's mane (LM3–LM12) (**G–H**) powders. WF-Control and DS-Control, wheat flour and durum semolina doughs unmodified with lion's mane mushroom powder.

(microcrystalline cellulose, inulin, apple, and citrus pectin), which differed in their water holding capacity [Nawrocka *et al.*, 2018a, b]. Moreover, some additives may contain considerable amount of fat like oil pomace. In this case, analysis of the spectral region of water populations showed a slight effect of these additives on these populations [Rumińska *et al.*, 2020].

CONCLUSIONS

Fourier transform infrared spectroscopy was deployed to determine structural changes in the gluten network induced by powders from four medicinal mushroom. Additionally, the changes were studied in two types of doughs prepared from wheat flour and durum semolina. Analysis of the FT-IR spectra showed that the type of the observed structural changes depended on material type used to prepare the dough as well as species of medicinal mushroom and its chemical composition. As a result of mushroom powder addition, the formation of additional pseudo-β-sheets (aggregated structures) was observed in wheat flour doughs, whereas aggregates and additional α-helices were formed in the durum semolina doughs. The structural differences observed between dough materials can be related to the gluten index and particle size. Amounts of particular water populations did not change or changed slightly in the presence of medicinal mushroom powders, presumably due to the complex chemical composition of the powders, which contain not only large amounts of dietary fibre but also protein, fat, phenolics, minerals, *etc*. Analysis of the phenolic profile showed that the mushroom powders contained antioxidants, known from their positive effects on the human organism, such as syringic acid, sinapic acid, genistein, and daidzein. The compounds other than dietary fibre also interact with a gluten network during dough mixing. Hence, the structural changes observed in the gluten network may be partially related to the competition for water between gluten and mushroom dietary fibre.

RESEARCH FUNDING

The authors received no financial support for the research, authorship, and/or publication of this article.

CONFLICT OF INTERESTS

The authors declare that they have no conflict of interests.

ORICD IDs

E. Fornal **https://orcid.org/0000-0002-0503-0706**
K. Kłosok **https://orcid.org/0000-0001-7712-0041**
A. Nawrocka **https://orcid.org/0000-0001-8618-2092**
A. Sobota **https://orcid.org/0000-0001-6526-6764**
A. Sumara **https://orcid.org/0000-0001-8677-7379**
R. Welc-Stanowska **https://orcid.org/0000-0003-0784-898X**

REFERENCES

1. AACC (2010). *Approved Methods of Analysis* (11th Ed.). American Association of Cereal Chemists. Cereals and Grains Association, St. Paul, MN, USA.
2. Baltacioglu, C., Baltacioglu, H., Seyhan, R., Ugur, O., Avcu, O. (2021). Investigation of the effect of oyster mushroom (*Pleurotus ostreatus*) powder on biscuit production and effect on quality criteria by Fourier transform infrared spectroscopy. *Journal of Food Processing and Preservation, 45*, art. no. e15174. **https://doi.org/10.1111/jfpp.15174**
3. Barros, L., Baptista, P., Estevinho, L.M., Ferreira, I.C.F.R. (2007). Effect of fruiting body maturity stage on chemical composition and antimicrobial activity of *Lactarius* sp. mushrooms. *Journal of Agricultural and Food Chemistry, 55*(21), 8766-8771. **https://doi.org/10.1021/jf071435**
4. Bock, J.E., Damodaran, S. (2013). Bran-induced changes in water structure and gluten conformation in model gluten dough studied by Fourier transform infrared spectroscopy. *Food Hydrocolloids, 31*(2), 146-155. **https://doi.org/10.1016/j.foodhyd.2012.10.014**
5. Both, J., Esteres, V.P., Santetti, G.S., Bressiani, J., Oro, T., Gomez., M., Friedrich, M.T., Gutkoski, L.C. (2019). Phenolic compounds and free sulfhydryl groups in whole grain wheat flour modified by xylanase. *Journal of the Science of Food and Agriculture, 99*(12), 5392-5400. **https://doi.org/10.1002/jsfa.9799**
6. Cateni, F., Gargano, M.L., Procida, G., Venturella, G., Cirlincione, F., Ferraro, V. (2022). Mycochemicals in wild and cultivated mushrooms: Nutrition and health. *Phytochemistry Reviews, 21*, 339-383. **https://doi.org/10.1007/s11101-021-09748-2**
7. Cotugno, S., Larobina, D., Mensitieri, G., Musto, P., Ragosta, G. (2001). A novel spectroscopic approach to investigate transport processes in polymers: The case of water epoxy system. *Polymer, 42*(15), 6431-6438. **https://doi.org/10.1016/S0032-3861(01)00096-9**
8. Feeney, K.A., Wellner, N., Gilbert, S.M., Halford, H.G., Tatham, A.S., Shewry, P.R., Belton, P.S. (2003). Molecular structures and interactions of repetitive peptides based on wheat glutenin subunits depend on chain length. *Biopolymers, 72*(2), 123-131. **https://doi.org/10.1002/bip.10298**
9. Friedman, M. (2015). Chemistry, nutrition, and health-promoting properties of *Hericium erinaceus* (lion's mane) mushroom fruiting bodies and mycelia and their bioactive compounds. *Journal of Agricultural and Food Chemistry, 63*(32), 7108-7123. **https://doi.org/10.1021/acs.jafc.5b02914**
10. Gaglio, R., Guarcello, R., Venturella, G., Palazzolo, E., Francesca, N., Moschetti, G., Settanni, L., Saporita, P., Gargano, M.L. (2019). Microbiological, chemical and sensory aspects of bread supplemented with different percentages of the culinary mushroom *Pleutorus eryngii* in powder form. *International Journal of Food Science and Technology, 54*(4), 1197-1205. **https://doi.org/10.1111/ijfs.13997**
11. Guijas, C., Montenegro-Burke, J.R., Domingo-Almenara, X., Palermo, A., Warth, B., Hermann, G., Koellensperger, G., Huan, T., Uritboonthai, W., Aisporna, A.E., Wolan, D.W., Spilker, M.E., Benton, H.P., Siuzdak, G. (2018). METLIN: A technology platform for identifying knowns and unknowns. *Analytical Chemistry, 90*(5), 3156–3164. **https://doi.org/10.1021/acs.analchem.7b04424**
12. Hwang, B.S., Lee, I.-K., Yun, B.-S. (2016). Phenolic compounds from the fungus *Inonotus obliquus* and their antioxidant properties. *The Journal of Antibiotics, 69*, 108-110. **https://doi.org/10.1038/ja.2015.83**
13. ICC Standard No. 115/1 (1992). *Method for Using the Brabender Farinograph*, International Association for Cereal Science and Technology.
14. Jain, T.K., Varshney, M., Maitra, A. (1989). Structural studies of aerosol OT reverse micellar aggregates by FT-IR spectroscopy. *Journal of Physical Chemistry, 93*(21), 7409-7416. **https://doi.org/10.1021/j100358a032**
15. Kasprzak, M., Rzedzicki, Z. (2012). Application of grasspea wholemeal in the technology of white bread production. *Polish Journal of Food and Nutrition Sciences, 62*(4), 207-213. **https://doi.org/10.2478/v10222-012-0056-6**
16. Kim, S. (2020). Antioxidant compounds for the inhibition of enzymatic browning by polyphenol oxidases in the fruiting body extract of the edible mushroom *Hericium erinaceus*. *Foods, 9*(7), art. no. 951. **https://doi.org/10.3390/foods9070951**
17. Kolniak-Ostek, J., Oszmiański, J., Szyjka, A., Moreira, H., Barg, E. (2022). Anticancer and antioxidant activities in *Ganoderma lucidum* wild mushrooms in Poland, as well as their phenolic and triterpenoid compounds. *International Journal of Molecular Sciences, 23*(16), art. no. 9359. **https://doi.org/10.3390/ijms23169359**
18. Krekora, M., Szymańska-Chargot, M., Niewiadomski, Z., Miś, A., Nawrocka, A. (2020). Effect of cinnamic acid and its derivatives on structure of gluten proteins – A study on model dough with application of FT-Raman spectroscopy. *Food Hydrocolloids, 107*, art. no. 105935. **https://doi.org/10.1016/j.foodhyd.2020.105935**
19. Lu, X., Brennan, M.A., Serventi, L., Mason, S., Brennan, C. (2016). How the inclusion of mushroom powder can affect the physicochemical characteristics of pasta. *International Journal of Food Science and Technology, 51*(11), 2433--2439. **https://doi.org/10.1111/ijfs.13246**

20. Lu, X., Brennan, M.A., Serventi, L., Brennan, C.S. (2018). Incorporation of mushroom powder into bread dough - effects on dough rheology and bread properties. *Cereal Chemistry, 95(3),* 418-427. **https://doi.org/10.1002/cche.10043**
21. Lu, Y., Jia, Y., Xue, Z., Li, N., Liu, J., Chen, H. (2021). Recent developments in *Inonotus obliquus* (Chaga mushroom) polysaccharides: Isolation, structural characteristics, biological activities and application. *Polymers, 13*(9), art. no. 1441. **https://doi.org/10.3390/polym13091441**
22. Łysakowska, P., Sobota, A., Wirkijowska, A. (2023). Medicinal mushrooms: Their bioactive components, nutritional value and application in functional food production – a review. *Molecules, 28*(14), art. no. 5393. **https://doi.org/10.3390/molecules28145393**
23. Łysakowska, P., Sobota, A., Wirkijowska, A., Zarzycki, P., Blicharz-Kania, A. (2024). The impact of *Ganoderma lucidum* (Curtis) P. Karst. supplementation on the technological, chemical, and quality parameters of wheat bread. *Foods, 13*(19), art. no. 3101. **https://doi.org/10.3390/foods13193101**
24. Łysakowska, P., Sobota, A., Wirkijowska, A., Ivanisova, E. (2025a). Lion's Mane (Hericium erinaceus (Bull.) Pers.) as a functional component for wheat bread production: influence on physicochemical, antioxidant, and sensory properties. *International Agrophysics, 39*(1), 13-28. **https://doi.org/10.31545/intagr/194613**
25. Łysakowska, P., Sobota, A., Zarzycki, P. (2025b). Evaluation of the physicochemical, antioxidant and sensory properties of wheat bread with partial substitution of wheat flour with *Cordyceps sinensis* powder. *Polish Journal of Food and Nutrition Sciences, 75*(2), 170-183. **https://doi.org/10.31883/pjfns/205435**
26. Nawrocka, A. (2014). Conformational changes in wheat gluten after using Ag-nanoparticles. *International Agrophysics, 28*, 311-328. **https://doi.org/10.2478/intag-2014-0021**
27. Nawrocka, A., Szymańska-Chargot, M., Miś, A., Ptaszyńska, A.A., Kowalski, R., Waśko, P., Gruszecki, W.I. (2015). Influence of dietary fibre on gluten proteins structure – a study on model flour with application of FT-Raman spectroscopy. *Journal of Raman Spectroscopy, 46*(3), 309-316. **https://doi.org/10.1002/jrs.4648**
28. Nawrocka, A., Miś, A., Niewiadomski, Z. (2017). Dehydration of gluten matrix as a result of dietary fibre addition – A study on model flour with application of FT-IR spectroscopy. *Journal of Cereal Science, 74*, 86-94. **https://doi.org/10.1016/j.jcs.2017.02.001**
29. Nawrocka, A., Krekora, M., Niewiadomski, Z., Miś, A. (2018a). Characteristics of the chemical processes induced by celluloses in the model and gluten dough with application of FTIR spectroscopy. *Food Hydrocolloids, 85*, 176-184. **https://doi.org/10.1016/j.foodhyd.2018.07.020**
30. Nawrocka, A., Krekora, M., Niewiadomski, Z., Miś, A. (2018b). FTIR studies of gluten matrix dehydration after fibre polysaccharide addition. *Food Chemistry, 252*, 198-206. **https://doi.org/10.1016/j.foodchem.2018.01.110**
31. Nawrocka, A., Krekora, M., Niewiadomski, Z., Szymańska-Chargot, M., Krawęcka, A., Sobota, A., Miś, A. (2020). Effect of moisturizing pre-treatment of dietary fibre preparations on formation of gluten network during model dough mixing – A study with application of FT-IR and FT-Raman spectroscopy. *LWT – Food Science and Technology, 121*, art. no. 108959. **https://doi.org/10.1016/j.lwt.2019.108959**
32. Nawrocka, A., Zarzycki, P., Kłosok, K., Welc, R., Wirkijowska, A., Teterycz, D. (2023). Effect of dietary fibre waste originating from food production on the gluten structure in common wheat dough. *International Agrophysics, 37*(1), 101-109. **https://doi.org/10.31545/intagr/159236**
33. Reis, F.S., Martins, A., Vasconcelos, M.H., Morales, P., Ferreira, I.C.F.R. (2017). Functional foods based on extracts or compounds derived from mushrooms. *Trends in Food Science & Technology, 66*, 48-62. **https://doi.org/10.1016/j.tifs.2017.05.010**
34. Rumińska, W., Szymańska-Chargot, M., Wiącek, D., Sobota, A., Markiewicz, K.H., Wilczewska, A.Z., Miś, A., Nawrocka, A. (2020). FT-Raman and FT-IR studies of the gluten structure as a result of model dough supplementation with chosen oil pomaces. *Journal of Cereal Science, 93*, art. no. 102961. **https://doi.org/10.1016/j.jcs.2020.102961**
35. Secundo, F., Guerrieri, N. (2005). ATR-FTIR study on interactions between gliadins and dextrins and their effects on proteins secondary structure. *Journal of Agricultural and Food Chemistry, 53*(5), 1757-1764. **https://doi.org/10.1021/jf049061x**
36. Shi, H., Wu, X., Zhu, Y., Jiang, T., Wang, Z., Li, X., Liu, J., Zhang, Y., Chen, F., Gao, J., Xu, X., Zhang, G., Xiao, N., Feng, X., Zhang, P., Wu, Y., Li, A., Chen, P., Li, X. (2024). RefMetaPlant: a reference metabolome database for plants across five major phyla. *Nucleic Acids Research, 52(D1)*, D1614–D1628. **https://doi.org/10.1093/nar/gkad980**
37. Sivam, A.S., Sun-Waterhouse, D., Perera, C.O., Waterhouse, G.I.N. (2013). Application of FT-IR and Raman spectroscopy for the study of biopolymers in breads fortified with fibre and polyphenols. *Food Research International, 50*(2), 574-585. **https://doi.org/10.1016/j.foodres.2011.03.039**
38. Smith, C.A., O'Maille, G., Want, E.J., Qin, C., Trauger, S.A., Brandon, T.R., Custodio, D.E., Abagyan, R., Siuzdak, G. (2005). METLIN: A metabolite mass spectral database. *Therapeutic Drug Monitoring, 27(6)*, 747-751. **https://doi.org/10.1097/01.ftd.0000179845.53213.39**
39. Song, T., Zhang, Z., Liu, S., Chen, J., Cai, W. (2020). Effect of cultured substrates on the chemical composition and biological activities of lingzhi or reishi medicinal mushrooms, *Ganoderma lucidum* (*Agaricomycetes*). *International Journal of Medicinal Mushrooms, 22*(12), 1183-1190. **https://doi.org/10.1615/IntJMedMushrooms.2020037133**
40. Sousa, A.S., Araujo-Rodrigues, H., Pintado, M.E. (2023). The health-promoting potential of edible mushroom proteins. *Current Pharmaceutical Design, 29*(11), 804-823. **https://doi.org/10.2174/1381612829666221223103756**
41. Stani, C., Vaccari, L., Mitri, E., Birarda, G. (2020). FTIR investigation of the secondary structure of type I collagen: New insight into the amide III band. *Spectrochimica Acta A: Molecular and Biomolecular Spectroscopy, 229*, art. no. 118006. **https://doi.org/10.1016/j.saa.2019.118006**
42. Szydłowska-Tutaj, M., Szymanowska, U., Tutaj, K., Domagała, D., Złotek, U. (2023). The addition of Reishi and Lion's Mane mushroom powder to pasta influences the content of bioactive compounds and the antioxidant, potential anti-inflammatory, and anticancer properties of pasta. *Antioxidants, 12*(3), art. no. 738. **https://doi.org/10.3390/antiox12030738**
43. Tang, Z., Lin, W., Yang, J., Feng, S., Qin, Y., Xiao, Y., Chen, H., Liu, Y., Chen, H., Bu, T., Li, Q., Yao, H., Ding, C. (2022). Ultrasound-assisted extraction of *Cordyceps cicadae* polyphenols: Optimization, LC-MS characterization, antioxidant and DNA damage protection activity evaluation. *Arabian Journal of Chemistry, 15*, art. no. 103953. **https://doi.org/10.1016/j.arabjc.2022.103953**
44. Tudorica, C.M., Kuri, V., Brennan, C.S. (2002). Nutritional and physicochemical characteristics of dietary fibre enriched pasta. *Journal of Agricultural and Food Chemistry, 50*(2), 347-356. **https://doi.org/10.1021/jf0106953**
45. Ulziijargal, E., Yang, J.-H., Lin, L.-Y., Chen, C.-P., Mau, J.-L. (2013). Quality of bread supplemented with mushroom mycelia. *Food Chemistry, 138*(1), 70-76. **https://doi.org/10.1016/j.foodchem.2012.10.051**
46. Wang, Y., Ouyang, F., Teng, C., Qu, J. (2021). Optimization for the extraction of polyphenols from *Inonotus obliquus* and its antioxidation activity. *Preparative Biochemistry and Biotechnology, 51*(9), 852-859. **https://doi.org/10.1080/10826068.2020.1864642**
47. Wishart, D.S., Tzur, D., Knox, C., Eisner, R., Guo, A.C., Young, N., Cheng, D., Jewell, K., Arndt, D., Sawhney, S., Fung, C., Nikolai, L., Lewis, M., Coutouly, M.A., Forsythe, I., Tang, P., Shrivastava, S., Jeroncic, K., Stothard, P., Amegbey, G., Block, D., Hau, D.D., Wagner, J., Miniaci, J., Clements, M., Gebremedhin, M., Guo, N., Zhang, Y., Duggan, G.E., MacInnis, G.D., Weljie, A.M., Dowlatabadi, R., Bamforth, F., Clive, D., Greiner, R., Li, L., Marrie, T., Sykes, B.D., Vogel, H.J., Querengesser, L. (2007). HMDB: the Human Metabolome Database. *Nucleic Acids Research, 35*(suppl_1), D521-D526. **https://doi.org/10.1093/nar/gkl923**
48. Wishart, D.S., Guo, A., Oler, E., Wang, F., Anjum, A., Peters, H., Dizon, R., Sayeeda, Z., Tian, S., Lee, B.L., Berjanskii, M., Mah, R., Yamamoto, M., Jovel, J., Torres-Calzada, C., Hiebert-Giesbrecht, M., Lui, V.W., Varshavi, D., Varshavi, D., Allen, D., Arndt, D., Khetarpal, N., Sivakumaran, A., Harford, K., Sanford, S., Yee, K., Cao, X., Budinski, Z., Liigand, J., Zhang, L., Zheng, J., Mandal, R., Karu, N., Dambrova, M., Schiöth, H.B., Greiner, R., Gautam, V. (2022). HMDB 5.0: the Human Metabolome Database for 2022. *Nucleic Acids Research, 50(D1)*, D622-D631. **https://doi.org/10.1093/nar/gkab1062**
49. Yang, H., Yang, S., Kong, J., Dong, A., Yu, S. (2015). Obtaining information about protein secondary structures in aqueous solution using Fourier transform IR spectroscopy. *Nature Protocols, 10*(3), 382-396. **https://doi.org/10.1038/nprot.2015.024**

ORIGINAL ARTICLE
http://journal.pan.olsztyn.pl

Polish Journal of Food and Nutrition Sciences
2025, Vol. 75, No. 3, 221–233
DOI: 10.31883/pjfns/208279
ISSN 1230-0322, e-ISSN 2083-6007

Application of Ultrasound in Convective Drying of Fermented, Frozen-Thawed, and Osmotically Dehydrated Beetroot Slices

Konrad W. Nowak[1]*, Izabela Miszczak[2], Bartosz Pszczółkowski[1], Wojciech Rejmer[1], Magdalena Zielińska[3]

[1]Department of Materials and Machines Technology, Faculty of Technical Sciences, University of Warmia and Mazury in Olsztyn, ul. Oczapowskiego 11, 10-718 Olsztyn, Poland
[2]Department of Plant Food Chemistry and Processing, Faculty of Food Sciences, University of Warmia and Mazury in Olsztyn, Plac Cieszyński 1, 10-726 Olsztyn, Poland
[3]Department of Electrical and Power Engineering, Faculty of Technical Sciences, University of Warmia and Mazury in Olsztyn, ul. Oczapowskiego 11, 10-718 Olsztyn, Poland

The aim of the study was to assess the benefits of using high-power ultrasound (HPU) during convective drying of raw beetroot slices and beetroot slices subjected to fermentation, pulsed vacuum osmotic dehydration, and freezing-thawing (in selected combinations). Beetroot slices were dried at a temperature of 80°C. The HPU treatment (200 W) was applied in 5-min cycles with 10-min intervals in between. The dried products were assessed for color, microstructure, total phenolic content, antioxidant capacity, and sugar content. Additionally, a Fourier-transform infrared spectroscopy analysis was performed. The HPU treatment during convective drying exerted the most beneficial effect on raw beetroot slices by shortening drying time by 23.5% and decreasing energy consumption by 18.4%. The above treatment also shortened the drying time of fermented and osmotically dehydrated beetroot slices by 17.6%, increased the total phenolic content of product by 17.1%, and increased the ferric reducing antioxidant power by 13.7%. In addition, the ferric reducing antioxidant power of fermented beetroot slices dried with HPU assistance increased by 12.2% compared to sample dried without HPU. In the remaining cases, HPU-assisted drying did not lead to significant improvements in the evaluated parameters. All analyzed treatments decreased the intensity of red color in dried beetroot slices.

Keywords: antioxidant activity, beetroot microstructure, color parameters, drying parameters, pulsed vacuum osmotic dehydration, total phenolic content

INTRODUCTION

The beetroot (*Beta vulgaris* L.) is a plant of the Chenopodiaceae family that is native to Asia and Europe [Chhikara *et al*., 2019]. Its roots are a popular vegetable rich in carotenoids, phenolics, betalains, ascorbic acid, and B-group vitamins (thiamine, riboflavin, niacin, pantothenic acid, pyridoxine, folic acid), and they also provide fiber, low-energy sugars, and inorganic nitrate [Chhikara *et al*., 2019; Clifford *et al*., 2015]. Beetroots are also a good source of minerals, including manganese, magnesium, potassium, sodium, phosphorus, iron, zinc, and copper [Mirmiran *et al*., 2020]. Due to the abundance and diversity of health-promoting compounds, beetroots have antioxidant, anti-inflammatory, anticancer, and antidiabetic properties, and they may also contribute to reducing the risk of development of cardiovascular diseases and hypertension [Chhikara *et al*., 2019; Mirmiran *et al*., 2020]. These healthy vegetables have a unique taste and can

***Corresponding Author:**
tel.: +48 895234940; e-mail: **konrad.nowak@uwm.edu.pl** (Dr. K.W. Nowak)

Submitted: 30 April 2025
Accepted: 10 July 2025
Published on-line: 25 July 2025

be consumed fresh, cooked, and fermented [Clifford *et al.*, 2015; Sawicki & Wiczkowski, 2018].

During lactic acid fermentation, lactic acid bacteria convert plant carbohydrates to lactic acid, which lowers the pH of fermented products. In turn, the lower pH inhibits the growth of some spoilage flora and pathogenic bacteria [Montet *et al.*, 2014]. Fermentation modifies the organoleptic characteristics of raw materials, including flavor and taste, and enhances the safety, nutritional value, sensory attributes, and the shelf-life of raw foods [Czyżowska *et al.*, 2020; Montet *et al.*, 2014]. Moreover, lacto-fermentation can activate, transform, and increase the availability of bioactive compounds by softening and promoting the degradation of the food matrix, which enhances the health-promoting effects of these compounds [Daliri *et al.*, 2023; Sawicki & Wiczkowski, 2018; Zhao *et al.*, 2021]. Currently, there is a growing interest in products prepared from lacto-fermented vegetables because consumers have a preference for natural food preservation methods that increase the health benefits provided by these products. Studies have shown that fermented products can prevent and support the treatment of metabolic disorders and cardiovascular diseases, improve cognitive functions, and boost immunity [Sivamaruthi *et al.*, 2018].

Unusually for fermented products, a fermented beetroot solution is more popular than fermented beetroot tissue (especially in Central and Eastern Europe) because it has anti-carcinogenic and anti-mutagenic potential, promotes the growth of beneficial gut bacteria, and reduces the risk of development of diseases related to food intolerance [Mirmiran *et al.*, 2020]. In many cases, lacto-fermented beetroot juice is considered the main product, while fermented beetroot tissue is regarded as a by-product of the fermentation process. However, fermented beetroot tissue can also be valued for its high nutritional value and health benefits. Unfortunately, these vegetables are highly susceptible to mold spoilage due to their high water content. For this reason, after lactic acid fermentation, beetroots should be subjected to additional preservation treatments, such as freezing and/or dehydration (osmotic and/or convective). These treatments can be applied to obtain fermented beetroot chips, a novel food product that may be attractive for consumers due to its health benefits and unique taste.

Freezing is an effective food preservation method, but it can also be applied as a pre-treatment technique to improve drying efficiency. During the process, plant cell walls are damaged by ice crystals growing inside cells. By shortening drying time, freezing also minimizes the need for thermal processing, thus protecting thermolabile nutrients and increasing the nutritional value of the product [Zielinska *et al.*, 2019; Zielinska & Zielinska, 2019]. In beetroots subjected to convective drying (temperature of 40°C; airflow rate of 1 m/s), the freezing pre-treatment (at −20°C) significantly shortened drying time (by 46%). However, it had no significant effect on the content of betaxanthins and betacyanins in dried beetroots but led to a significant reduction in the content of phenolic compounds and antioxidant activity compared to beetroots dried without pre-freezing [Vallespir *et al.*, 2018].

Other food drying techniques include osmotic dehydration and pulsed vacuum osmotic dehydration (PVOD) [James *et al.*, 2014]. In raw beetroots, osmotic pre-treatment (using NaCl solution) shortened drying time, decreased water activity, promoted the retention of betanin, enhanced color preservation, and increased water resorption [Kowalski & Łechtańska, 2015]. The use of a sucrose solution in osmotic dehydration and contact drying in the refractance window technique generated similar benefits, where drying time was shortened with a rise in the concentration of the solution and the temperature of osmotic dehydration [Calderón-Chiu *et al.*, 2020]. Studies have shown that the PVOD method reduces the initial amount of water in the processed material, thus shortening the subsequent drying time [Corrêa *et al.*, 2021; Pan *et al.*, 2003]. Despite the fact that the impact of PVOD on fruit drying has been extensively studied, the influence of PVOD on the drying kinetics and the physicochemical properties of fermented beetroots has not been analyzed to date. The existing research focused mainly on the impact of PVOD on the physicochemical properties of beet tissue [Staniszewska *et al.*, 2024]. However, the extent to which this processing technique affects drying kinetics and the physicochemical properties of dried fermented beetroots remain unknown.

Ultrasonic treatments can be applied both before (as a pre-treatment) and during the drying process (as ultrasound-assisted drying) to enhance and shorten convective drying of fruits and vegetables. Both techniques can accelerate the drying process [Fijałkowska *et al.*, 2015; Szadzińska *et al.*, 2020]. However, their effectiveness can be affected by some process variables, including air velocity and air temperature [Huang *et al.*, 2020]. Moreover, the effect of ultrasonic treatment on the nutritional value and technological and functional properties of foods should be evaluated separately for each product [Soria & Villamiel, 2010]. To the best of the authors' knowledge, there are currently no published studies on fermented beetroots that were additionally frozen or osmotically dehydrated and dried using airborne high-power ultrasound (HPU).

Therefore, the aim of this study was to evaluate the effects of ultrasound-assisted drying on the drying kinetics and selected nutritional and functional properties of raw, fermented, frozen, and osmotically dehydrated fermented red beetroots relative to beetroots subjected only to convective drying.

MATERIALS AND METHODS

Material

Fresh beetroots (*Beta vulgaris L.*) were obtained from a local grocery wholesaler (Olsztyn, Poland). Their initial moisture content was 5.93±0.27 g H_2O/g dry matter (DM) [AOAC, 2002]. The vegetables were ripe, free of apparent diseases, and similar in terms of freshness and size. Before the experiments, beetroots were cleaned under tap water and cut into slices with a thickness of 4±1 mm. Raw beetroot slices (R) were divided into groups and subjected to various treatments described below. The list of treatments and the codes of products obtained as a result of these treatments are presented in **Table 1**.

Table 1. Codes of beetroot products.

Product	Beetroot treatment
RC	Raw beetroots dried in hot air
RCUS	Raw beetroots dried in hot air with ultrasound
FC	Fermented beetroots dried in hot air
FCUS	Fermented beetroots dried in hot air with ultrasound
FOC	Fermented and osmotically dehydrated beetroots dried in hot air
FOCUS	Fermented and osmotically dehydrated beetroots dried in hot air with ultrasound
FFC	Fermented, frozen and thawed beetroots dried in hot air
FFCUS	Fermented, frozen and thawed beetroots dried in hot air with ultrasound
FFOC	Fermented, osmotically dehydrated, frozen, and thawed beetroots dried in hot air
FFOCUS	Fermented, osmotically dehydrated, frozen and thawed beetroots dried in hot air with ultrasound

Fermentation

Beetroot slices (5 kg) and spices, *i.e.*, peppercorns (2.5 g), allspice (5.0 g), bay leaves (4.5 g), and garlic cloves (125 g), were placed in a glass jar, and the jar was filled with a 1.8% aqueous sodium chloride (NaCl) solution. The sample-to-solution ratio was 1:1.2 (*w/v*). The jar was closed and left to ferment in darkness. Beetroots were fermented at 20°C for 7 days. A similar fermentation method was used by Staniszewska *et al.* [2024].

Osmotic dehydration

Fermented beetroot slices (F) were subjected to osmotic dehydration (O) in a vacuum dryer (DZ ZBC II, Chemland, Stargard Szczecinski, Poland) at a temperature of 20°C. The osmotic solution was an aqueous solution composed of 60% sucrose and 5% sodium chloride. Initially, the material immersed in the osmotic solution was subjected to vacuum (−0.09 MPa) for 10 min, and then dehydrated at an atmospheric pressure for up to 180 min. The material-to-solution ratio during osmotic dehydration was 1:4 (*w/v*). Osmotic dehydration parameters approximated the optimal values described in the literature [Staniszewska *et al.*, 2024].

Freezing and thawing

Fermented beetroot slices subjected to the freezing/thawing treatment (FF) were frozen at −18°C using a GT 4932 Comfort freezer (LIEBHERR, Bischofshofen, Austria). Before drying, they were thawed at room temperature for approximately 24 h.

Drying

Beetroot slices were subjected to hot air convective drying (C), both with and without high power ultrasound (HPU), in a laboratory hybrid dryer (SLH-2, PROMIS TECH, Wroclaw, Poland) at a temperature of 80°C with an air flow rate of around 1 m/s. A single layer of beetroot slices (approx. 200 g) was spread on a mesh tray mounted on a digital scale (ACZ6200, Axis sp. z o.o., Gdańsk, Poland). Airborne ultrasound (200 W) was applied during ultrasound-assisted drying experiments. During convective drying with ultrasound assistance (CUS), HPU was used continuously in the following cycles: 10 min without ultrasound and 5 min with ultrasound assistance. The mass of dried samples (±0.01 g) was monitored and registered at 5 min intervals. The convective drying treatment was continued until no further decrease in beetroot weight was observed in two subsequent measurements which meant that equilibrium moisture content was achieved. The drying kinetics curve was plotted based on the results of a single experiment for a given treatment. The moisture content of beetroot samples before and after drying was determined in a vacuum drying oven (DZ ZBC II, Chemland, Stargard Szczeciński, Poland) at 70°C and 13.3 kPa for 24 h [AOAC, 2002] and its value was calculated by dividing the water loss by the DM content. The water loss was the difference between the weight before and after drying. The drying rate was calculated as the difference between the initial and final moisture content divided by drying time and expressed as g H_2O/(g DM×min). The energy consumption was calculated by dividing the total energy consumption registered by the drier during the whole process by the water loss.

Microstructure and color analysis

The surfaces of dried beetroot slices were examined under a digital microscope with imaging software (VHX-7000, Keynes, Osaka, Japan) at 500× and 1,000× magnification. Images were acquired at 4k resolution under full illumination.

The color of raw and dried beetroot slices was measured with a spectrophotometer (MiniScan XE Plus, Hunter Associates Laboratory Inc., Reston, USA) under standard illuminant D65, 10° observer and 8° diaphragm, and was expressed in CIE $L^*a^*b^*$ space, where L^*, a^*, and b^* represent lightness, (+)redness/(−)greenness, and (+)yellowness/(−)blueness, respectively. Total color differences (ΔE) between the samples were calculated according to Equation (1) presented below, taken from the literature [Zielinska & Markowski, 2012]. Three types of total color differences were calculated: ΔE_1 – total color difference relative to raw beetroot slices (R), ΔE_2 – total color difference relative to raw beetroot slices dried by hot air (RC), and ΔE_3 – total color difference between the same samples dried with and without ultrasound. The color of beetroots was measured directly on the surface. The results were averaged over 20 measurements.

$$\Delta E = \sqrt{(\Delta L^*)^2+(\Delta a^*)^2+(\Delta b^*)^2} \quad (1)$$

Total phenolic content, antioxidant capacity, and sugar content analysis

Pulverized dried beetroot slices (approx. 0.05 g) were extracted by sonication with 1 mL of acidified 80% (*v/v*) methanol (with 0.1% HCl, *v/v*) using a VC 750 ultrasonic processor (Sonics & Materials, Newtown, CT, USA) for 30 s. Each sample was initially

vortexed for 30 s, followed by alternating cycles of sonication and vortexing to enhance the extraction efficiency. After each cycle, the mixture was centrifuged at 13,200×g for 10 min using an Eppendorf centrifuge 5424 (Eppendorf, Wesseling-Berzdorf, Germany). This process was repeated a total of five times, with 1 mL of fresh solvent added at each step to ensure thorough extraction of the analytes. The resulting supernatants were pooled and stored at –20°C until analysis, which was carried out within 24 h [Zielinska & Zielinska, 2019]. The extraction procedure was carried out in triplicate.

The total phenolic content (TPC) and the ferric reducing antioxidant power (FRAP) were determined by Singleton *et al.* [1999] and Benzie & Strain [1996] methods, respectively. In the first assay, the appropriately diluted extract (90 µL), the Folin–Ciocalteu reagent diluted with water (1:1, *v/v*), and the saturated sodium carbonate solution were mixed in a ratio of 1:1:2 (*v/v/v*) using a thermomixer (Comfort, Eppendorf). Then, the volume of the mixture was adjusted to 2 mL with water. The mixture was allowed to stand for 25 min at ambient temperature and then the absorbance was measured at 725 nm using a UV-1800 spectrophotometer (Shimadzu Corporation, Kyoto, Japan). Gallic acid was used as the standard, and the results were expressed as mg of gallic acid equivalents (GAE) *per* g of DM. For the FRAP assay, 100 µL of the diluted extract were mixed with 3 mL of a freshly prepared FRAP reagent (a mixture of 300 mM acetate buffer pH 3.6, 10 mM 2,4,6-tris(2-pyridyl)-*s*-triazine in 40 mM HCl, and 20 mM $FeCl_3 \times 6H_2O$ in a 10:1:1, *v/v/v*, ratio). After mixture incubation at 37°C for 10 min, the absorbance was measured at 593 nm. FRAP was expressed in mg Trolox equivalents (TE) *per* g of DM. The assays were performed in triplicate.

Sugar content (SC) was determined by the spectrophotometric method [Nielsen, 2017]. The sample was prepared by heating 10 g of pulverized dried beetroot slices in 300 mL of distilled water for 10 min with stirring in a SW22 Julabo shaking water bath (JULABO GmbH, Seelbach, Germany). Then, 5 mL of 5% phenol and 1.0 mL of distilled water were added to the samples, which were then stirred for 1 min. In the next step, 5.0 mL of concentrated sulfuric acid was added, and the samples were shaken for 3 min. The resulting solution was settled for 30 min, cooled with water for 20 min, and absorbance was measured at 490 nm using an LKB Ultraspec II spectrometer (Pharmacia LKB Biotechnology, Piscataway, NJ, USA). Standard solutions containing a specific amount of D-glucose (Chempur, Piekary Śląskie, Poland) were prepared for the determination of sugar content. The measurements were performed five times for each beetroot product.

Fourier-transform infrared spectroscopy analysis

For each beetroot product, Fourier-transform infrared spectroscopy (FTIR) spectra were obtained in triplicate using a Perkin Elmer Spectrum Two device (Perkin Elmer, Waltham, MA, USA) equipped with a diamond attenuated total reflectance (ATR) gear. The spectra were registered at a resolution of 1 cm^{-1} within the wavenumber range of 4,000–450 cm^{-1} at room temperature.

Statistical analysis

Differences between beetroot products were determined by one-way analysis of variance (ANOVA) with post-hoc Duncan's test (for ΔE), the non-parametric Kruskal–Wallis test (for FRAP and TPC), and the Mann–Whitney U test (for L^*, a^*, b^*, water content, and sugar content), at a confidence level of 95% (statistical significance at $p<0.05$). Calculations were performed using Statistica 13.0 software (TIBCO Software Inc., Santa Clara, CA, USA).

RESULTS AND DISCUSSION

Drying kinetics of beetroot slices

The basic parameters of beetroot slice drying, including drying time, final water content, water loss (evaporated water), drying rate, and energy consumption, are shown in **Table 2**. The use of high-power ultrasound (HPU) in a pulse mode during the convective drying exerted the greatest impact on raw beetroot slices by shortening drying time from 183 min (RC) to 140 min (RCUS), *i.e.*, by 23.5%, and reducing specific energy consumption from 102.52 kJ/g H_2O to 83.70 kJ/g H_2O, *i.e.*, by 18.4%. The drying rate increased from 0.0318 g H_2O/(g DM×min) (RC) to 0.0409 g H_2O/(g DM×min) (RCUS), which points to a 28.6% improvement in process efficiency. The drying speed was higher in the first stage of the process, as indicated in **Figure 1A**. The increase in drying rate, the decrease in drying time, and the increase in energy efficiency can be attributed to the cavitation effect which increased the porosity of the material and facilitated the migration of water from the interior to the surface [Mason *et al.*, 1996]. Szadzińska *et al.* [2020] reported a similar significant decrease in the drying time of beetroot cubes (15 mm side length) subjected to HPU-assisted drying (200 W) at a temperature of 60°C and airflow velocity of 2 m/s relative to convective drying. These authors suggested that ultrasound improved heat and mass transfer through cavitation, which led to faster evaporation of water and shortened drying time. Ultrasound also disrupted plant cell walls, which promoted water flow from the interior to the surface of the material. Szadzińska *et al.* [2020] found that energy consumption was also lower during HPU-assisted drying than convective drying of raw beetroots, although its value was significantly higher than in our case, which could be attributed to a much longer drying time resulting from lower air temperature and thicker samples.

The drying time of fermented and osmotically dehydrated beetroot slices was also significantly shortened by the HPU treatment, from 102 min (FOC) to 84 min (FOCUS), *i.e.*, by 17.6% (**Table 2**). The latter was characterized by the shortest drying time among all experiments (mainly due to the lowest initial water content), although specific energy consumption was not the lowest (87.12 kJ/g H_2O). The HPU treatment increased the drying rate by 47.3%, from 0.0131 g H_2O/(g DM×min) (FOC) to 0.0185 g H_2O/(g DM×min) (FOCUS). This observation points to the synergistic effect of ultrasound and osmotic dehydration, which indicates that this drying technique is highly promising. Cavitation probably disrupted the sugar layer on the surface of the material, which increased the material's porosity and facilitated water evaporation.

Table 2. Basic drying parameters of a 200-g batch of beetroot slices exposed to different treatments.

Product	Initial water content (g H_2O/g DM)	Final water content (g H_2O/g DM)	Drying time (min)	Water loss (g)	Dying rate (g H_2O/(g DM×min))	Energy consumption (kJ/g H_2O)
RC	5.93±0.27^b	0.12±0.02^a	183	166.3	0.0318	102.52
RCUS	5.93±0.27^b	0.21±0.01^a	140	167.4	0.0409	83.70
FC	8.80±0.69^a	0.22±0.01^a	119	171.7	0.0721	67.31
FCUS	8.80±0.69^a	0.27±0.02^a	127	175.2	0.0671	83.47
FOC	1.65±0.22^c	0.31±0.00^a	102	112.4	0.0131	94.52
FOCUS	1.65±0.22^c	0.10±0.01^a	84	106.8	0.0185	87.12
FFC	9.85±0.26^a	0.11±0.04^a	129	181.3	0.0755	67.73
FFCUS	9.85±0.26^a	0.56±0.04^a	142	170.8	0.0654	72.83
FFOC	1.78±0.04^c	0.22±0.01^a	88	114.8	0.0177	82.67
FFOCUS	1.78±0.04^c	0.17±0.01^a	94	116.4	0.0171	89.85

Results are shown as mean ± standard error. Identical letters in the same column denote the absence of significant differences ($p \geq 0.05$). R, raw; F, fermented; O, osmotically dehydrated; FF, fermented and frozen/thawed; C, convective dried; CUS, convective dried with ultrasound assistance; DM, dry matter.

In the remaining drying treatments (FCUS, FFCUS and FFOCUS), HPU did not induce a significant decrease in drying time or specific energy consumption (**Table 2**). On the contrary, in frozen fermented beetroot slices (FFC and FFCUS), the HPU treatment significantly prolonged drying time, from 129 min to 142 min (*i.e.*, by 10.1%), and decreased the drying rate from 0.0755 to 0.0654 g H_2O/(g DM×min) (*i.e.*, by 13.4%). The curve in **Figure 1C** clearly indicates that HPU-assisted drying proceeded at a much slower rate from the very beginning of the process. The drying time of FC was also prolonged compared to FCUS, from 119 min to 127 min (*i.e.*, by 6.7%). Ultrasonic vibration breaks down plant tissues and closes pores, which slows down the diffusion of water from inside the beetroot slice [Miano *et al.*, 2021]. Convective drying of fermented (FC) and fermented and frozen/thawed beetroot slices (FFC) without HPU was the least energy-consuming treatment (relative to the mass of removed water) due to the highest initial water content (8.80 and 9.85 g H_2O/g DM, respectively) and average drying time.

In all fermented products not subjected to osmotic dehydration, fermentation significantly increased the drying rate compared to the raw samples. The drying rate of fermented beetroot slices (FC) was more than twice higher relative to raw beetroot slices (RC), reaching 0.0721 g H_2O/(g DM×min) and 0.0318 g H_2O/(g DM×min), respectively (**Table 2**). This significantly higher drying rate is consistent with previous observations made for fermented plant products such as, *e.g.*, broccoli waste [Bas-Bellver *et al.*, 2023]. Fermentation significantly reduced drying time and energy consumption compared to raw beetroot slices (**Table 2**). Drying time was 119 min for FC *vs.* 183 min for RC. Energy consumption was determined at 67.31 kJ/g H_2O in FC, and it was much lower than in RC (102.52 kJ/g H_2O). During fermentation, the structure of cell walls is disrupted through degradation of polysaccharides by enzymes (mainly cellulases and glycosidases), which led to the formation of a porous microstructure, increased water vapor permeability, and significantly accelerated the drying process [Bas-Bellver *et al.*, 2023; Janiszewska-Turak *et al.*, 2022].

A comparison of FC and FFC products revealed that freezing/thawing did not shorten the drying time of fermented beetroots, whereas such an effect was reported for raw beetroots subjected to a freezing/thawing pre-treatment [Vallespir *et al.*, 2018]. The above could be attributed to the fact that the internal structure of the beetroot matrix was significantly degraded during fermentation, which enhanced water diffusion and evaporation during drying and promoted structural breakdown after additional treatment, such as freezing/thawing, which somewhat inhibits these processes.

Osmotic dehydration alone significantly reduced the drying rate of fermented beetroot slices (FOC: 0.0131 g H_2O/(g DM×min) *vs.* FC: 0.0318 g H_2O/(g DM×min)). Moreover, this treatment also significantly shortened drying time (FOC: 102 min *vs.* FC: 119 min). The decrease in the drying rate resulted from the formation of a semi-permeable sugar layer on the surface of the material, which prevented water migration. In turn, drying time was shortened because some water had been removed from the material already during osmotic dehydration, which reduced the amount of energy needed for drying. As a result, the energy consumption associated with the drying process was higher in osmotically dehydrated products (FOC: 94.52 kJ/g H_2O) than in fermented and not osmotically dehydrated beetroot slices (FC: 67.31 kJ/g H_2O), but still lower than in raw beetroot slices (RC: 102.52 kJ/g H_2O).

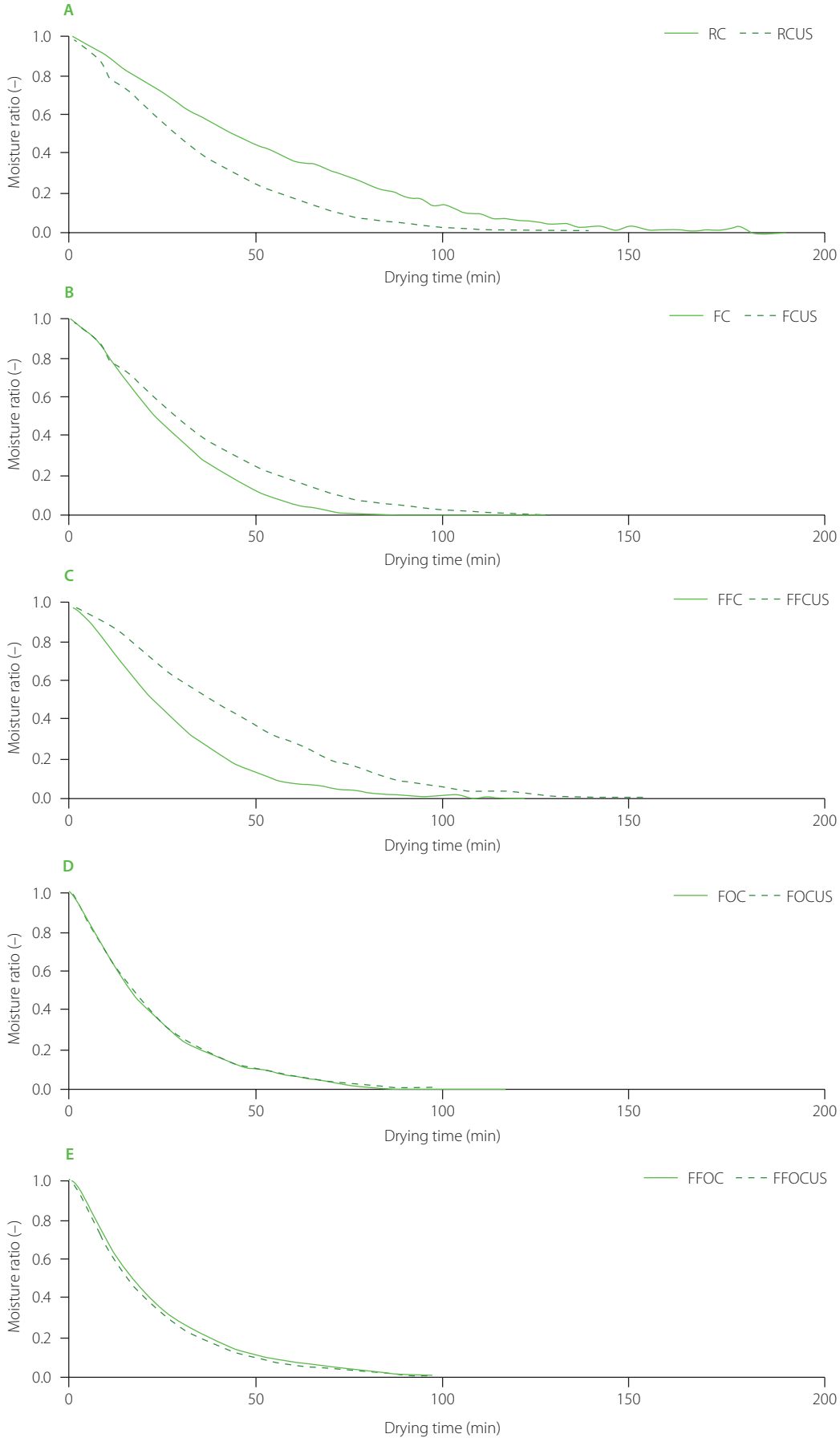

Figure 1. Drying kinetics of beetroot slices with (CUS) and without (C) ultrasound assistance: (**A**) drying of raw beetroot slices (R); (**B**) drying of fermented beetroot slices (F); (**C**) drying of fermented and frozen/thawed beetroot slices (FF); (**D**) drying of fermented and osmotically dehydrated beetroot slices (FO); (**E**) drying of fermented, frozen/thawed and osmotically dehydrated beetroot slices (FFO).

Microstructure and color of beetroot slices

The drying process with freezing and osmotic dehydration pretreatments had a significant impact on the color and structure of beetroot products (**Figure 2**, **Table 3**).

In **Figure 2**, dried raw beetroot slices (RC) present undisrupted shining cell walls. In beetroot slices dried with ultrasound (RCUS), bright zones were formed on the surface, denoting cell walls, which seems to be more ragged. The use of ultrasonic waves during convective drying led to the formation of microchannels, which slightly disrupted the structure of tissues, increased porosity and intercellular spaces [Rajewska & Mierzwa, 2017]. Ultrasound prevented sugar and water molecules from clumping and closing beetroot pores. The above improved the efficiency of water diffusion, accelerated the drying process, and improved the quality of the final product. Raw beetroot slices (RC) had an intense red-violet color and were characterized by the highest value of parameter *a** (**Table 3**). Color parameters were similar (lack of statistically significant differences for parameters *L** and *a**) in beetroots dried with ultrasound assistance (RCUS) and only *b** parameter was significantly lower and decreased from 3.1 to –0.1, which indicates a shift towards a more neutral or blue color. No significant changes were observed in parameter *L**, which indicates that lightness remained fairly constant in the analyzed samples.

No sticking effect was observed in the fermented product (FC), where sugar content decreased during the fermentation process (**Figure 2**). The use of ultrasound induced minor changes in cellular structure of FCUS product and did not contribute to the formation of a sugar layer on the surface. Fermented beetroot slices (FC) were characterized by significantly lower values

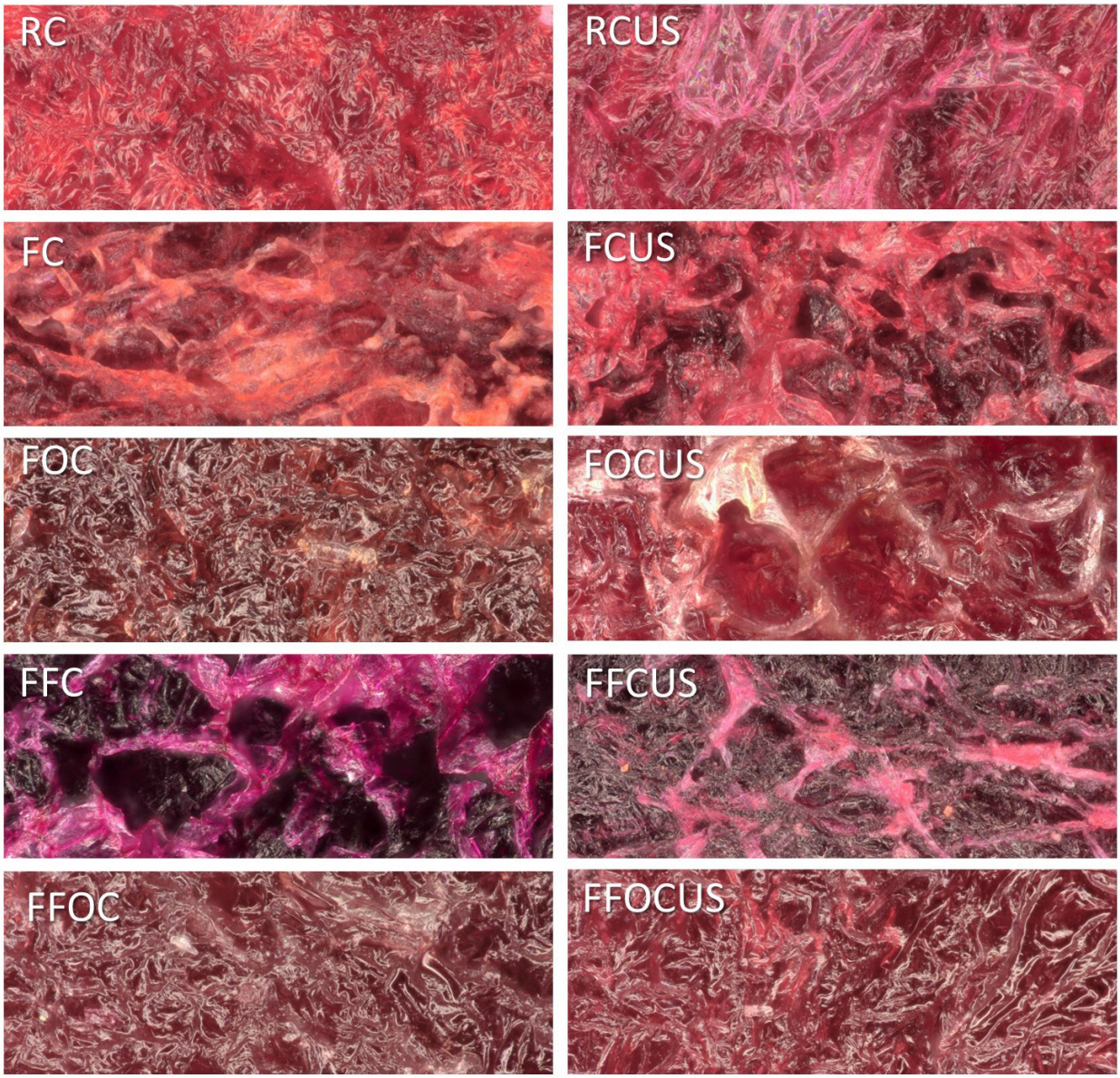

Figure 2. Microstructure of beetroot slices subjected to different treatments, 500× magnification. R, raw; F, fermented; O, osmotically dehydrated; FF, fermented and frozen/thawed; C, convective dried; CUS, convective dried with ultrasound assistance.

Table 3. Color parameters of raw beetroot slices and beetroot slices subjected to different treatments.

Product	L^*	a^*	b^*	ΔE_1	ΔE_2	ΔE_3
R	22.2±0.7	21.7±2.2	6.5±1.0	–	–	–
RC	23.8±2.5^{ab}	19.7±4.0^{a}	3.1±2.4^{b}	4.7±1.5^{c}	–	–
RCUS	24.6±1.5^{a}	18.8±2.2^{a}	−0.1±2.0^{d}	7.9±1.5^{bc}	5.5±2.9^{b}	5.5±2.9^{a}
FC	20.1±1.8^{c}	13.8±3.0^{b}	2.2±1.5^{c}	9.3±2.4^{b}	7.3±4.7^{b}	–
FCUS	17.6±2.1^{d}	10.6±3.2^{de}	−0.8±1.7^{de}	14.1±2.4^{ab}	11.8±4.9^{a}	5.9±2.2^{a}
FOC	23.9±1.5^{a}	12.3±2.1^{cd}	4.5±1.6^{a}	9.9±2.2^{b}	8.4±3.5^{ab}	–
FOCUS	23.8±1.6^{a}	13.4±2.5^{b}	4.5±1.2^{a}	8.8±2.2^{bc}	7.5±3.3^{b}	2.7±1.5^{b}
FFC	19.8±1.9^{c}	8.6±2.6^{f}	−1.4±1.4^{e}	15.5±2.4^{a}	12.7±4.8^{a}	–
FFCUS	20.1±2.0^{c}	11.6±3.1^{cde}	−1.1±1.4^{de}	10.5±2.3^{b}	9.5±4.2^{a}	4.3±1.7^{a}
FFOC	27.0±2.9^{a}	12.9±2.0^{bc}	3.7±1.4^{ab}	10.6±1.8^{b}	8.7±2.8^{ab}	–
FFOCUS	22.3±2.5^{b}	9.9±2.5^{ef}	2.9±1.3^{bc}	12.4±2.3^{ab}	10.3±4.3^{a}	6.0±3.1^{a}

The presented values are means ± standard errors. Values marked with identical letters in the same column for dried products do not differ significantly ($p \geq 0.05$). L^*, lightness; a^*, (+)redness/(–)greenness; b^*, (+)yellowness/(–)blueness; ΔE_1, total color difference relative to raw beetroot; ΔE_2, total color difference relative to raw beetroot dried by hot air (RC); ΔE_3, total color difference between the same samples dried with and without ultrasound; R, raw; F, fermented; O, osmotically dehydrated; FF, fermented and frozen/thawed; C, convective dried; CUS, convective dried with ultrasound assistance.

of parameters L^* and a^* than raw beetroots (RC), which indicates a color shift towards darker and less red (**Table 3**). Parameter a^* decreased to 13.8 and parameter L^* decreased to 20.1. The use of ultrasound in the fermented samples (FCUS) led to a further significant reduction in the values of these parameters compared to raw beetroot (RC), where L^* reached 17.6, a^* reached 10.6 and additionally b^* reached −0.8. These changes indicate a significant color shift towards darker, greener and bluer shades, which could be attributed to pigment degradation during fermentation. A similar effect (decreasing of L^* and b^* parameters) was observed for apple slices by Mierzwa & Kowalski [2016].

The freezing/thawing treatment led to the formation of ice crystals capable of damaging cell walls. In **Figure 2**, structural damage with a large number of protrusions and cracks can be clearly observed in fermented and frozen/thawed (FF) products. The frozen/thawed sample had a normal cellular structure, which indicates that tissue integrity was preserved after this treatment. The fact that these structures were clearly visible could be related to higher porosity which facilitated water migration during drying. In the FFC product dried without ultrasound, clusters of cell walls were observed on the surface, probably because sugar was released from the inside of the material during the drying process. The moisture released during thawing contributed to the formation of a uniform sugar layer. In the samples dried with ultrasound (FFCUS), this process did not occur because residual sugars were evenly distributed throughout the material under the influence of ultrasound and were reabsorbed inside the material. Due to controlled distribution of water during freezing, glossy sugar residues and a more uniform structure were observed in the FFCUS samples. Even distribution of sugars and microstructural changes indicate that the synergistic effect of ultrasound and freezing/thawing treatments contributed to an improvement in the quality of dried beetroots.

Convective drying of fermented and frozen/thawed beetroot slices (FFC and FFCUS) produced darker and more purple beetroot products compared to dried beetroot without pre-treatment (RC) (**Table 3**). Additionally, the color of all osmotically dehydrated samples (FOC, FOCUS, FFOC and FFOCUS) was lighter than in the case of just frozen and fermented beetroot slices, which may be attributed to betanin leaching (the lowest FRAP and TPC – see **Table 4**) and sugars from the osmotic solution sticking to the surface of the slices. A significant decrease in the values of parameters a^* and b^* was noted in the fermented and frozen/thawed (FFC) product relative to the RC sample, which indicates a shift towards ruby red color. After the ultrasound treatment (FFCUS), the value of a^* significantly increased to 11.6, which suggests that red color was partially restored, whereas the value of b^* remained low (−1.1), indicating the presence of blue color.

During osmotic dehydration of fermented beetroot slices, water was removed from cells along the osmotic gradient. Beetroot slices subjected to osmotic dehydration and convective drying (FOC) had a compact and less porous structure (**Figure 2**). In addition, they had a higher sugar content (**Table 4**), and drying led to the formation of a glossy sugar layer on their surface. The ultrasound treatment increased the penetration of the osmotic sugar solution, highlighting pores and cell walls in the FOCUS samples. In these samples, ultrasound promoted the diffusion of sugar molecules inside beetroot tissues and increased sugar saturation. Ultrasound-assisted drying of osmotically dehydrated beetroot slices (FOCUS) induced additional changes, including

Table 4. Total phenolic content (TPC), ferric reducing antioxidant power (FRAP), and sugar content (SC) of beetroot slices subjected to different treatments.

Product	TPC (mg GAE/g DM)	FRAP (mg TE/g DM)	SC (g/100 g DM)
RC	7.73±0.21^{c}	19.52±0.75^{b}	47.20±0.86^{a}
RCUS	9.05±0.18^{a}	24.45±0.30^{a}	44.40±1.72^{a}
FC	8.09±0.25^{b}	16.13±0.55^{d}	12.40±0.93^{c}
FCUS	8.04±0.33^{b}	18.10±0.42^{c}	10.80±0.37^{c}
FOC	1.46±0.06^{g}	2.19±0.08^{g}	31.00±0.45^{b}
FOCUS	1.71±0.08^{f}	2.49±0.03^{g}	30.40±1.63^{b}
FFC	7.26±0.27^{d}	15.27±0.60^{e}	3.80±0.37^{d}
FFCUS	5.95±0.24^{e}	12.91±0.47^{f}	2.40±0.24^{e}
FFOC	1.46±0.08^{g}	2.20±0.06^{g}	4.60±0.24^{d}
FFOCUS	1.45±0.05^{g}	2.20±0.05^{g}	4.40±0.24^{d}

The presented values are means ± standard errors. Values marked with identical letters in the same column do not differ significantly ($p \geq 0.05$). GAE, Gallic acid equivalent; TE, Trolox equivalent; DM, dry matter; R, raw; F, fermented; O, osmotically dehydrated; FF, fermented and frozen/thawed; C, convective dried; CUS, convective dried with ultrasound assistance.

increased porosity and the formation of micro-channels, which improved drying efficiency. The benefit was not as great as expected, but is somehow contrasting with results obtained by Mierzwa & Kowalski [2016], who dried previously osmotically dehydrated apple slices under HPU assistance. Drying osmotically dehydrated beetroot slices (FOC) decreased the value of parameter a^* to 12.3 and increased the value of parameter b^* to 4.5 compared to beetroot dried without pre-treatment (RC) (**Table 3**). The change in the color (ΔE_2) of osmotically dehydrated and dried beetroot slices (FOC) was similar to the values reported by Calderón-Chiu *et al.* [2020]. These authors reported that ΔE reached 8.19 in osmotically dehydrated beetroots (5-mm thick slices, temperature of 30°C, 65% sugar content) dried at 85°C using the refractance window method. The ultrasound drying of osmotically dehydrated beetroot slices (FOCUS) induced the smallest total color difference ($\Delta E_3 = 2.7$) relative to the FOC sample (**Table 3**).

The structure of FFOC and FFOCUS products was similar to that of FOC samples (**Figure 2**). Additionally, the samples that were and were not subjected to ultrasound-assisted drying had an identical structure. These results indicate that in osmotically dehydrated samples, freezing caused pores to close after the freezing/thawing cycle. In these samples, sugars were dissolved by water absorption during thawing, which promoted the formation of a compact structure and could explain the difference relative to the FOCUS product. The values of color parameters were similar in FFOC and FFOCUS products, where a^* was determined at 12.9 (FFOC) and 9.9 (FFOCUS), and b^* was determined at 3.7 (FFOC) and 2.9 (FFOCUS), which indicated that the ultrasound treatment had a negligent impact on red and yellow hues of fermented, osmotically dehydrated, and frozen beetroot slices. However, the total color difference between these products was high ($\Delta E_3 = 6.0$).

Total phenolic content, antioxidant capacity, and sugar content of dried beetroot slices

The total phenolic content, antioxidant capacity, and sugar content of dried beetroot slices differed significantly across treatments (**Table 4**). The TPC and FRAP were highest in raw beetroot slices dried with ultrasound assistance (RCUS) and lowest in osmotically dehydrated products (FOC, FOCUS, FFOC, FFOCUS). The total phenolic content ranged from 1.45 to 9.05 mg GAE/g DM, FRAP ranged from 2.19 to 24.45 mg TE/g DM, and SC ranged from 2.40 to 47.20 g/100 g DM.

Sugar content was highest in raw beetroot slices subjected to convective drying (RC) and ultrasound-assisted convective drying (RCUS). The sugar content of these products was 47.20 and 44.40 g/100 g DM, respectively. The ultrasound treatment induced a minor decrease in sugar content, but the observed difference was not significant. Ultrasound could have influenced the microscopic distribution of sugars in beetroot tissues, but the overall sugar content remained high. Ultrasound-assisted drying of raw beetroot slices led to a significant increase in TPC and FRAP of the RCUS product relative to the sample dried without ultrasound (RC) (**Table 4**). The TPC increased from 7.73 to 9.05 mg GAE/g DM, and FRAP increased from 19.52 to 24.45 mg TE/g DM. The above increase probably resulted from shorter drying times (by up to 23%) (**Table 2**), which minimized the thermal degradation of phenolic compounds. Additionally, the cavitation effect generated by ultrasound disrupted the plant matrix, which facilitated the extraction of bioactive compounds and increased the antioxidant capacity of dried beetroots. This result is consistent with the literature data concerning drying raspberries and goldenberries [Ashtiani *et al.*, 2022; Cakmak *et al.*, 2021].

Ultrasound-assisted drying of fermented beetroot slices had a minor effect on TPC which remained fairly constant in FC (8.09 mg GAE/g DM) and FCUS (8.04 mg GAE/g DM) products (**Table 4**). However, FRAP increased from 16.13 to 18.10 mg TE/g DM. The sugar content of FC and FCUS products was determined at 12.40 and 10.80 g/100 g DM, respectively, and was significantly lower than in raw beetroots. Most probably, this difference can be attributed to fermentation during which sugars were used by bacteria as a substrate for the production of lactic acid [Montet *et al.*, 2014]. Ultrasound-assisted drying had no significant effect on the sugar content of fermented beetroot slices, which suggests that the effect of fermentation outweighed the potential effect of the ultrasound treatment.

The freezing/thawing treatment before convective drying led to the degradation of phenolic compounds. As a result, TPC decreased from 8.09 mg GAE/g DM (FC) to 7.26 mg GAE/g DM (FFC), and FRAP decreased from 16.13 mg TE/g DM (FC) to 15.27 mg TE/g DM (FFC) (**Table 4**). These changes were most likely caused by freezing damage to beetroot tissues. The phase change of water from a liquid to a solid phase (ice) led to the breakdown of cell walls and the loss of bioactive compounds [Dalmau *et al.*, 2019; Vallespir *et al.*, 2019]. Ultrasound-assisted drying of frozen/

thawed beetroot slices led to a further decrease in TPC and FRAP of the FFCUS product (by 18% and 15%, respectively) compared to the FFC sample (**Table 4**). The cavitation effect generated by the ultrasound treatment resulted in a greater loss of natural juice during drying, which decreased the TPC and FRAP. The lowest sugar content was noted in fermented and frozen/thawed beetroot slices that were or were not osmotically dehydrated (FFC, FFCUS, FFOC and FFOCUS). The sugar content of these products ranged from 2.40 to 4.60 g/100 g DM. The freezing/thawing treatment led to a significant loss of sugars during thawing [Screde, 1983]. It is worth noting that the ultrasound treatment promoted a further decrease in the sugar content of FFCUS product, probably because the sugar leaching process was intensified under the influence of ultrasonic cavitation.

Convective drying of osmotically dehydrated beetroot slices led to a significant decrease in TPC and FRAP of the FOC product compared to the FC sample (**Table 4**); TPC content was reduced by 82% (from 8.09 to 1.46 mg GAE/g DM), whereas FRAP decreased by 86% (from 16.13 to 2.19 mg TE/g DM). Most probably, the observed decrease was caused by water diffusion during osmotic dehydration when water-soluble phenolics were removed from beetroot tissues into the surrounding osmotic solution. Phenolic compounds were further degraded during convective drying, and TPC and FRAP were lowest in osmotically dehydrated samples (FOC, FOCUS, FFOC, FFOCUS). The ultrasound treatment had no significant effect on TPC and FRAP during the drying of fermented, frozen/thawed, and osmotically dehydrated beetroot slices. This may be due to considerable tissue deformation during freezing/thawing and osmotic dehydration, which reduced the impact of the ultrasound treatment during drying. Similar observations were made by other authors for beetroot and celery root [Nicetin *et al.*, 2022; Staniszewska *et al.*, 2024]. In the group of fermented and dried beetroot samples, sugar content was highest in FOC and FOCUS products (31.00 and 30.40 g/100 g DM, respectively). These products had the highest sugar content because sugar was adsorbed from the osmotic solution during osmotic dehydration [Corrêa *et al.*, 2010]. This process promoted the accumulation of sugars in beetroot slices, which increased their sugar content. However, the sugar content of FFOC and FFOCUS products was several times lower because sugars were most probably removed during thawing. As a result, the final sugar content of FFOC and FFOCUS samples was determined at 4.60 and 4.40 g/100 g DM, respectively.

Fourier-transform infrared spectroscopy data of dried beetroot slices

The FTIR spectra of dried beetroot slices are shown in **Figure 3**. Different absorption bands of these spectra (3,293; 2,927; 1,736; 1,638; 1,421; 1,375; 1,330; 1,241; 1,104; 1,038; 988; 922; and 828 cm^{-1}) are associated with chemical bonds characteristic of carbohydrates, alcohols, carboxylic acids, esters, alkenes, ketones, pectins, and other organic compounds present in beetroots. The 3,293 cm^{-1} band corresponds to the stretching vibrations of the hydroxyl group (–OH) which is present in water and alcohols. In beetroots, this band may indicate the presence of carbohydrates and water. The 2,927 cm^{-1} band indicates the presence of C–H bonds related to the stretching vibrations of alkyl groups (–CH_3, –CH_2–) [Singh *et al.*, 2017; Xin *et al.*, 2020]. The 1,736 cm^{-1} band corresponds to the stretching vibrations of the carbonyl bond (C=O) in esters and carboxylic acids, and it may be associated with the presence of hemicellulose, pectins, and other organic compounds in beetroots. The 1,638 cm^{-1} band can be attributed to the stretching vibrations of C=C bonds in alkenes and C=O bonds in amides and ketones, which may correspond to organic dyes such as betanin [Aztatzi-Rugerio *et al.*, 2019]. The 1,421 cm^{-1} band corresponds to the bending vibrations of the methyl group (–CH_3) and the carboxylate group (COO–); the 1,375 cm^{-1} band is associated with the bending vibrations of the methyl group (–CH_3), whereas the 1,330 cm^{-1} band corresponds to the bending vibrations of the methoxy group (–OCH_3) and the deformation vibrations of the nitro group (NO_2). In turn, the 1,241 cm^{-1} band is attributed to the stretching vibrations of C–O bonds in esters and carboxylic acids, which may indicate the presence of pectins and other polysaccharides [Monsoor, 2005; Xin *et al.*, 2020]. The 1,104 cm^{-1} band corresponds to the stretching vibrations of C–O–C bonds in ethers and glycosidic bonds in sugars, and the 1,038 cm^{-1} band corresponds to the stretching vibrations of C–O bonds in alcohol, which may be related to the presence of carbohydrates and cellulose [Xin *et al.*, 2020]. The 988 cm^{-1} band corresponds to the stretching vibrations of C–H bonds in alkenes and the bending vibrations of the CH_2 group in carbohydrates; the 922 cm^{-1} band corresponds to the stretching vibrations of C–O–C bonds in acid anhydrides and the deformation vibrations of alkene C–H bonds, whereas the 828 cm^{-1} band corresponds to the bending vibrations of C–H bonds in alkene groups and the deformation bonds of the aromatic group [Aztatzi-Rugerio *et al.*, 2019].

These results indicate that fermentation, freezing/thawing, osmotic dehydration, and convective drying with or without ultrasound treatment significantly influenced the intensity and position of absorption bands. The highest intensity of the bands corresponding to C=C multiple bonds was observed in raw beetroot slices subjected to convective drying. These results correlate with findings of Lohumi *et al.* [2017]. The bands at 1,638; 1,105; and 1,037 cm^{-1} were associated with changes in pigment content during ultrasound-assisted drying of raw beetroot slices. The ultrasound-assisted drying of raw and frozen/thawed beetroot slices subjected to osmotic dehydration led to the loss of pigments. Fermented beetroot slices subjected to ultrasound-assisted drying were characterized by a higher pigment content because betanin was stabilized by hydrogen cations formed during the fermentation process [Atav & Yurdakul, 2016; Volia *et al.*, 2019]. Fermentation led to the degradation of sugars, which significantly reduced the intensity of the absorption bands associated with hydroxyl groups (3,293 cm^{-1}).

The freezing/thawing process led to the formation of ice crystals inside cells, which increased the risk of damage to cell walls. The FTIR spectra of fermented and frozen/thawed (FF) product revealed clear structural damage. A higher content of deposited

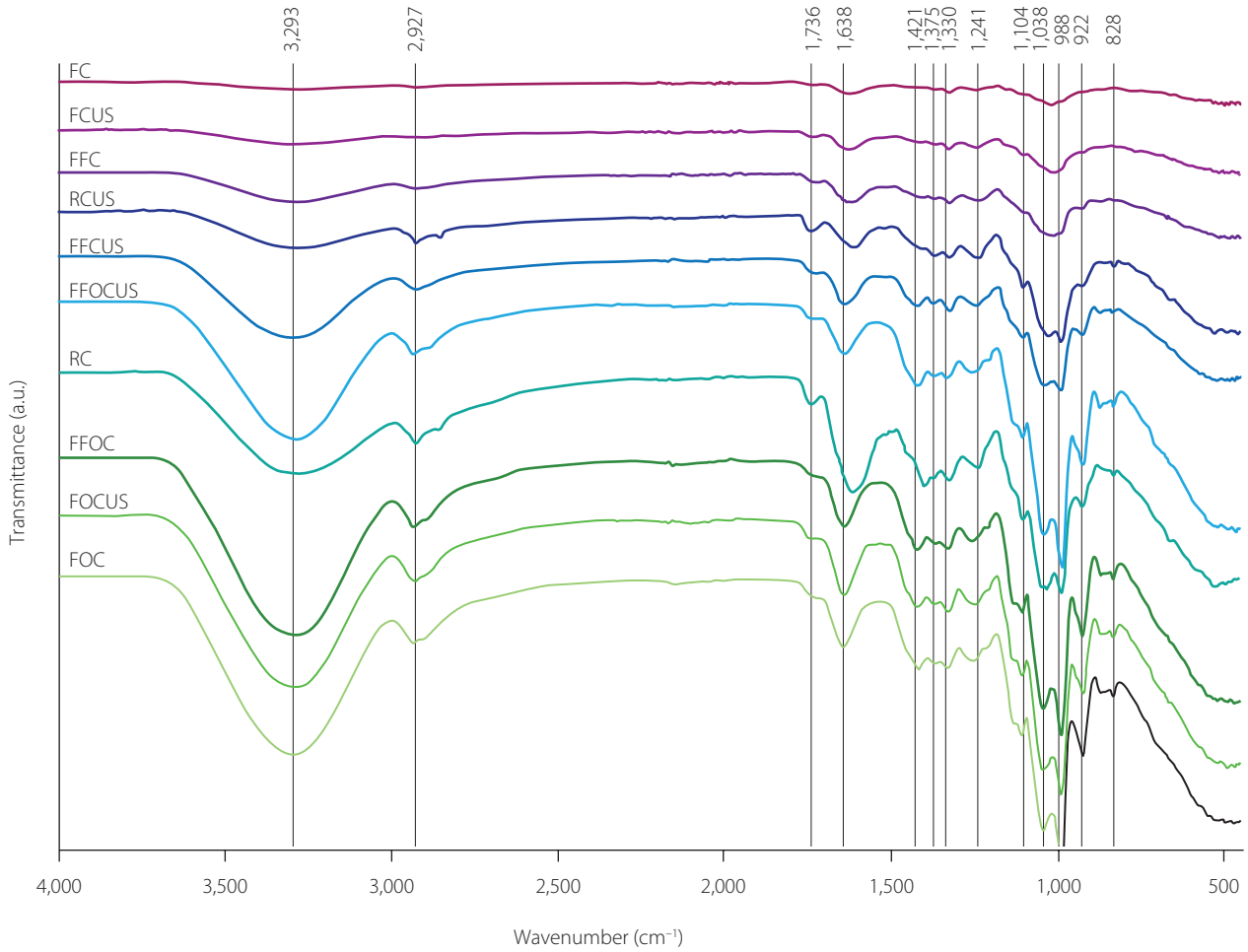

Figure 3. Fourier-transform infrared spectra of beetroot slices subjected to different treatments. R, raw; F, fermented; O, osmotically dehydrated; FF, fermented and frozen/thawed; C, convective dried; CUS, convective dried with ultrasound assistance.

water in frozen samples increased the intensity of the bands corresponding to the hydroxyl group (3,293 cm^{-1}). At the same time, the decrease in the intensity of the bands corresponding to C=C and C=O groups denoted the loss of pigments, as indicated by the lower values of parameters a^* and b^* (**Table 3**).

The absorption bands in the FTIR spectra of the osmotically dehydrated sample (FOC) had the highest intensity in the range of 3,700–2,800 cm^{-1}, which corresponds to the hydroxyl group and is associated with higher sugar content. Higher band intensity was also associated with the content of the pigment produced during osmosis. The intensity of these bands was lower in dried fermented beetroot slices, which could be attributed to the lower content of water and the breakdown of carbohydrates during lactic acid fermentation [Nizamlioglu *et al.*, 2022]. Band intensity was somewhat higher in frozen beetroot slices due to the higher content of water deposited during freezing [Zaritzky, 2010].

CONCLUSIONS

The study demonstrated that the high-power ultrasound treatment applied during convective drying exerted the most beneficial effect on raw beetroot slices by reducing drying time and energy consumption. The ultrasound treatment also significantly increased total phenolic content and the ferric reducing antioxidant power, and induced a negligible shift in color parameters toward blue (more purple than red). Considering the pretreatments, ultrasound-assisted drying shortened the drying times of fermented and osmotically dehydrated beetroot slices, increased the total phenolic content and the ferric reducing antioxidant power of this sample, and increased the ferric reducing antioxidant power of fermented beetroots. In the remaining cases (such as beetroots only fermented or fermented and frozen/thawed – both osmotically dehydrated and not), the ultrasound treatment did not induce significant beneficial changes in the drying process or the properties of the final product. Sometimes the changes were undesirable, such as significant prolongation of drying time in fermented and frozen/thawed beetroots, a decrease in total phenolic content with the associated reduction in the ferric reducing antioxidant power.

The combination of fermentation, freezing/thawing, and ultrasonication treatments led to severe structural damage, which increased porosity and promoted water migration during the drying of beetroot slices. Interestingly, osmotically dehydrated beetroots subjected to ultrasound-assisted drying had a more uniform structure with micro-channels, which increased drying efficiency. All analyzed treatments decreased the intensity

of red color in dried beetroot slices. However, in some cases changes in the color of dried beetroots (some color parameters for FOCUS, FFOCUS) were unnoticeable, which can be deemed as desired. The observed changes in the values of color parameters *L**, *a**, and *b** denote the extent to which these processes affected the appearance of the final product, which is an important consideration from the consumers' point of view.

Fermentation alone shortened the convective drying time of beetroot slices and significantly decreased the sugar content in relation to drying beetroot without additional treatments. This can be of use in the production of dietetic snacks. Additionally, osmotic dehydration of fermented beetroot slices shortened convective drying time in relation to fermentation alone, which besides the energy savings can allow modifying the taste of the mentioned dietetic beetroot snacks. Subsequent freezing-thawing of fermented and osmotically dehydrated beetroots shortened convective drying time, but slightly prolonged convective drying of fermented beetroots. The above along with the results of antioxidant capacity leads to the conclusion that the production of fermented beetroot, followed by freezing and drying, can provide an interesting dietetic product at reduced costs.

In the future, other ultrasound parameters, such as power, exposure time and frequency, should be examined to optimize the ultrasound-assisted drying of raw (RCUS), fermented and osmotically dehydrated (FOCUS) beetroots. Ultrasound-assisted drying is not recommended for processing beetroots that are fermented only or frozen/thawed and fermented.

ACKNOWLEDGEMENTS

The authors would like to thank Professor Danuta Zielińska for providing access to her laboratory.

RESEARCH FUNDING

The research described in this paper was financed by the National Science Centre in Kraków, Poland (grant No. 2020/37/B/NZ9/00687).

CONFLICT OF INTERESTS

Authors declare no conflict of interests.

ORCID IDs

I. Miszczak https://orcid.org/0000-0001-7868-3794
K.W. Nowak https://orcid.org/0000-0002-0431-4176
B. Pszczółkowski https://orcid.org/0000-0002-7985-9488
W. Rejmer https://orcid.org/0000-0002-1955-1553
M. Zielińska https://orcid.org/0000-0001-7127-4891

REFERENCES

1. AOAC (2002). *Official Methods of Analysis. Method number 934.06 – Moisture in Dried Fruits* (16th ed.). The Association of Official Analytical Chemists, Arlington, Rockville, USA.
2. Ashtiani, M.S.H., Rafiee, M., Morad, M.M., Martynenko, A. (2022). Cold plasma pretreatment improves the quality and nutritional value of ultrasound-assisted convective drying: The case of goldenberry. *Drying Technology, 40*(8), 1639-1657. https://doi.org/10.1080/07373937.2022.2050255
3. Atav, R., Yurdakul, A. (2016). Ultrasonic assisted dyeing of Angora fibre. *Fibres & Textiles in Eastern Europe, 5*(119), 137-142. https://doi.org/10.5604/12303666.1215539
4. Aztatzi-Rugerio, L., Granados-Balbuena, S.Y., Zainos-Cuapio, Y., Ocaranza-Sánchez, E., Rojas-López, M. (2019). Analysis of the degradation of betanin obtained from beetroot using Fourier transform infrared spectroscopy. *Journal of Food Science and Technology, 56*(8), 3677-3686. https://doi.org/10.1007/s13197-019-03826-2
5. Bas-Bellver, C., Barrera, C., Betoret, N., Segui, L. (2023). Impact of fermentation pretreatment on drying behaviour and antioxidant attributes of broccoli waste powdered ingredients. *Foods, 12*(19), art. no. 3526. https://doi.org/10.3390/foods12193526
6. Benzie, I.F.F., Strain, J.J. (1996). The Ferric Reducing Ability of Plasma (FRAP) as a measure of "Antioxidant Power": The FRAP assay. *Analytical Biochemistry, 239*(1), 70-76. https://doi.org/10.1006/abio.1996.0292
7. Cakmak, Z.H.T., Cakmakoglu, S.K., Avci, E., Sagdic, O., Karasu, S. (2021). Ultrasound-assisted vacuum drying as alternative drying method to increase drying rate and bioactive compounds retention of raspberry. *Journal of Food Processing and Preservation, 45*, art. no. e16044. https://doi.org/10.1111/jfpp.16044
8. Calderón-Chiu, C., Martínez-Sánchez, C.E., Rodríguez-Miranda, J., Juárez-Barrientos, J.M., Carmona-García, R., Herman-Lara, E. (2020). Evaluation of the combined effect of osmotic and Refractance Window drying on the drying kinetics, physical, and phytochemical properties of beet. *Drying Technology, 38*(12), 1663-1675. https://doi.org/10.1080/07373937.2019.1655439
9. Chhikara, N., Kushwaha, K., Sharma, P., Gat, Y., Panghal, A. (2019). Bioactive compounds of beetroot and utilization in food processing industry: A critical review. *Food Chemistry, 272*, 192-200. https://doi.org/10.1016/j.foodchem.2018.08.022
10. Clifford, T., Howatson, G., West, D.J., Stevenson, E.J. (2015). The potential benefits of red beetroot supplementation in health and disease. *Nutrients, 7*(4), 2801-2822. https://doi.org/10.3390/nu7042801
11. Corrêa, J.L.G., Lopes, F.J., de Mello Júnior, R.E., de Jesus Junqueira, J.R., de Mendonça, K.S., Macedo, L.L., Salvio, L.G.A. (2021). Drying of persimmon fruit (*Diospyros kaki* L.) pretreated by different osmotic processes. *Journal of Food Process Engineering, 44*(10), art. no. e13809. https://doi.org/10.1111/jfpe.13809
12. Corrêa, J.L.G., Pereira, L.M., Vieira, G.S., Hubinger, M.D. (2010). Mass transfer kinetics of pulsed vacuum osmotic dehydration of guavas. *Journal of Food Engineering, 96*(4), 498-504. https://doi.org/10.1016/j.jfoodeng.2009.08.032
13. Czyżowska, A., Siemianowska, K., Śniadowska, M., Nowak, A. (2020). Bioactive compounds and microbial quality of stored fermented red beetroots and red beetroot juice. *Polish Journal of Food and Nutrition Sciences, 70*(1), 35-44. https://doi.org/10.31883/pjfns/116611
14. Daliri, E.B.M., Balnionytė, T., Stankevičiūtė, J., Lastauskienė, E., Meškys, R., Burokas, A. (2023). High temperature lacto-fermentation improves antioxidant and antidiabetic potentials of Lithuanian red beetroot. *LWT – Food Science and Technology, 185*, art. no. 115122. https://doi.org/10.1016/j.lwt.2023.115122
15. Dalmau, M.E., Llabrés, P.J., Eim, V.S., Rosselló, C., Simal, S. (2019). Influence of freezing on the bioaccessibility of beetroot (*Beta vulgaris*) bioactive compounds during *in vitro* gastric digestion. *Journal of the Science of Food and Agriculture, 99*(3), 1055-1065. https://doi.org/10.1002/jsfa.9272
16. Fijałkowska, A., Nowacka, M., Witrowa-Rajchert, D. (2015). Effect of ultrasound waves on drying process and selected properties of beetroot tissue. *ŻYWNOŚĆ. Nauka. Technologia. Jakość, 2*(99), 138-149 (in Polish, English abstract). https://doi.org/10.15193/zntj/2015/99/028
17. Huang, D., Men, K., Li, D., Wen, T., Gong, Z., Sunden, B., Wu, Z. (2020). Application of ultrasound technology in the drying of food products. *Ultrasonics Sonochemistry, 63*, art. no. 104950. https://doi.org/10.1016/j.ultsonch.2019.104950
18. James, C., Purnell, G., James, S.J. (2014). A critical review of dehydrofreezing of fruits and vegetables. *Food and Bioprocess Technology, 7*, 1219-1234. https://doi.org/10.1007/s11947-014-1293-y
19. Janiszewska-Turak, E., Rybak, K., Pobiega, K., Nikodem, A., Gramza-Michałowska, A. (2022). Sustainable production and characteristics of dried fermented vegetables. *Fermentation, 8*(11), art. no. 659. https://doi.org/10.3390/fermentation8110659
20. Kowalski, S.J., Łechtańska, J.M. (2015). Drying of red beetroot after osmotic pretreatment: Kinetics and quality considerations. *Chemical and Process Engineering, 36*(3), 345-354. https://doi.org/10.1515/cpe-2015-0024
21. Lohumi, S., Joshi, R., Kandpal, L.M., Lee, H., Kim, M.S., Cho, H., Mo, C., Seo, Y.W., Rahman, A., Cho, B.K. (2017). Quantitative analysis of Sudan dye adulteration in paprika powder using FTIR spectroscopy. *Food Additives & Contaminants: Part A, 34*(5), 678-686. https://doi.org/10.1080/19440049.2017.1290828

22. Mason, T.J., Paniwnyk, L., Lorimer, J.P. (1996). The uses of ultrasound in food technology. *Ultrasonics Sonochemistry, 3*(3), S253-S260. **https://doi.org/10.1016/S1350-4177(96)00034-X**
23. Miano, A.C, Rojas, M.L., Augusto, P.E.D. (2021). Combining ultrasound, vacuum and/or ethanol as pretreatments to the convective drying of celery slices. *Ultrasonics Sonochemistry, 79*, art. no. 105779. **https://doi.org/10.1016/j.ultsonch.2021.105779**
24. Mierzwa, D., Kowalski, S.J. (2016). Ultrasound-assisted osmotic dehydration and convective drying of apples: process kinetics and quality issues. *Chemical and Process Engineering, 37*(3), 383-391. **https://doi.org/10.1515/cpe-2016-0031**
25. Mirmiran, P., Houshialsadat, Z., Gaeini, Z., Bahadoran, Z., Azizi, F. (2020). Functional properties of beetroot (*Beta vulgaris*) in management of cardiometabolic diseases. *Nutrition and Metabolism, 17*(1), art. no. 3. **https://doi.org/10.1186/s12986-019-0421-0**
26. Monsoor, M.A. (2005). Effect of drying methods on the functional properties of soy hull pectin. *Carbohydrate Polymers, 61*(3), 362-367. **https://doi.org/10.1016/j.carbpol.2005.06.009**
27. Montet, D., Ray, R.C., Zakhia-Rozi, N. (2014). Lactic acid fermentation of vegetables and fruits. In R.C. Ray, D. Montet (Eds.), *Microorganisms and Fermentation of Traditional Foods*, CRC Press, Boca Raton, FL, USA, pp. 108-140.
28. Nicetin, M., Pezo, L., Pergal, M., Loncar, B., Filipovic, V., Knezevic, V., Demir, H., Filipovic, J., Manojlovic, D. (2022). Celery root phenols content, antioxidant capacities and their correlations after osmotic dehydration in molasses. *Foods, 11*(13), art. no. 1945. **https://doi.org/10.3390/foods11131945**
29. Nielsen, S.S., (2017). Total carbohydrate by phenol-sulfuric acid method. In S.S. Nielsen (Ed.), *Food Analysis in Laboratory Manual. Food Science Text Series* (3rd editon), Springer Cham, pp. 138-141. **https://doi.org/10.1007/978-3-319-44127-6_14**
30. Nizamlioglu, N.M., Yasar, S., Bulut, Y. (2022). Chemical *versus* infrared spectroscopic measurements of quality attributes of sun or oven dried fruit leathers from apple, plum and apple-plum mixture. *LWT – Food Science and Technology, 153*, art. no. 112420. **https://doi.org/10.1016/j.lwt.2021.112420**
31. Pan, Y.K., Zhao, L.J., Zhang, Y., Chen, G., Mujumdar, A.S. (2003). Osmotic dehydration pretreatment in drying of fruits and vegetables. *Drying Technology, 21*(6), 1101-1114. **https://doi.org/10.1081/DRT-120021877**
32. Rajewska, K., Mierzwa, D. (2017). Influence of ultrasound on the microstructure of plant tissue. *Innovative Food Science & Emerging Technologies, 43*, 117-129. **https://doi.org/10.1016/j.ifset.2017.07.034**
33. Sawicki, T., Wiczkowski, W. (2018). The effects of boiling and fermentation on betalain profiles and antioxidant capacities of red beetroot products. *Food Chemistry, 259*, 292-303. **https://doi.org/10.1016/j.foodchem.2018.03.143**
34. Screde, G. (1983). Changes in sucrose, fructose and glucose content of frozen strawberries with thawing. *Journal of Food Science, 48*(4), 1094-1096. **https://doi.org/10.1111/j.1365-2621.1983.tb09168.x**
35. Singh, G., Sachdeva, R., Rai, B., Saini, G.S.S. (2017). Structure and vibrational spectroscopic study of alpha-tocopherol. *Journal of Molecular Structure, 1144*, 347-354. **https://doi.org/10.1016/j.molstruc.2017.05.037**
36. Singleton, V.L., Orthofer, R., Lamuela-Raventós, R.M. (1999). Analysis of total phenols and other oxidation substrates and antioxidants by means of Folin-Ciocalteu reagent. *Methods in Enzymology, 299*, 152-178. **https://doi.org/10.1016/S0076-6879(99)99017-1**
37. Sivamaruthi, B., Kesika, P., Prasanth, M., Chaiyasut, C. (2018). A mini review on antidiabetic properties of fermented foods. *Nutrients, 10*(12), art. no. 1973. **https://doi.org/10.3390/nu10121973**
38. Soria, A.C., Villamiel, M. (2010). Effect of ultrasound on the technological properties and bioactivity of food: a review. *Trends in Food Science & Technology, 21*(7), 323-331. **https://doi.org/10.1016/j.tifs.2010.04.003**
39. Staniszewska, I., Nowak, K.W., Zielinska, D., Konopka, I., Zielinska, M. (2024). Pulsed vacuum osmotic dehydration (PVOD) of fermented beetroot: Modeling and optimization by response surface methodology (RSM). *Food and Bioprocess Technology, 17*, 977-990. **https://doi.org/10.1007/s11947-023-03173-3**
40. Szadzińska, J., Mierzwa, D., Pawłowski, A., Musielak, G., Pashminehazar, R., Kharaghani, A. (2020). Ultrasound- and microwave-assisted intermittent drying of red beetroot. *Drying Technology, 38*(1-2), 93-107. **https://doi.org/10.1080/07373937.2019.1624565**
41. Vallespir, F., Cárcel, J.A., Marra, F., Eim, V.S., Simal, S. (2018). Improvement of mass transfer by freezing pre-treatment and ultrasound application on the convective drying of beetroot (*Beta vulgaris* L.). *Food and Bioprocess Technology, 11*, 72-83. **https://doi.org/10.1007/s11947-017-1999-8**
42. Vallespir, F., Rodríguez, Ó., Eim, V.S., Rosselló, C., Simal, S. (2019). Effects of freezing treatments before convective drying on quality parameters: Vegetables with different microstructures. *Journal of Food Engineering*, 249, 15-24. **https://doi.org/10.1016/j.jfoodeng.2019.01.006**
43. Volia, M.F., Tereshatov, E.E., Mazan, V., Folden III, C.M., Boltoeva, M. (2019). Effect of aqueous hydrochloric acid and zwitterionic betaine on the mutual solubility between a protic betainium-based ionic liquid and water. *Journal of Molecular Liquids, 276*, 296-306. **https://doi.org/10.1016/j.molliq.2018.11.136**
44. Xin, H., Yang, Y., Qi, L., Wen-Qing, H. (2020). Effect of high pressure homogenization on sugar beet pulp: Physicochemical, thermal and structural properties. *LWT – Food Science and Technology, 134*, art. no. 110177. **https://doi.org/10.1016/j.lwt.2020.110177**
45. Zaritzky, N.E. (2010). Chapter 20 – Chemical and physical deterioration of frozen foods. In L.H. Skibsted, J. Risbo, M.L. Andersen (Eds.), *Chemical Deterioration and Physical Instability of Food and Beverages*, Woodhead Publishing, Sawston, pp. 561-607. **https://doi.org/10.1533/9781845699260.3.561**
46. Zhao, Y.S., Eweys, A.S., Zhang, J.Y., Zhu, Y., Bai, J., Darwesh, O.M., Zhang, H.B., Xiao, X. (2021). Fermentation affects the antioxidant activity of plant-based food material though the release and production of bioactive components. *Antioxidants, 10*(12), art. no. 2004. **https://doi.org/10.3390/antiox10122004**
47. Zielinska, M., Markowski, M. (2012). Color characteristics of carrots: Effect of drying and rehydration. *International Journal of Food Properties, 15*(2), 450-466. **https://doi.org/10.1080/10942912.2010.489209**
48. Zielinska, M., Markowski, M., Zielinska, D. (2019). The effect of freezing on the hot air and microwave vacuum drying kinetics and texture of whole cranberries. *Drying Technology, 37*(13), 1714-1730. **https://doi.org/10.1080/07373937.2018.1543317**
49. Zielinska, M., Zielinska, D. (2019). Effects of freezing, convective and microwave–vacuum drying on the content of bioactive compounds and color of cranberries. *LWT – Food Science and Technology, 104*, 202-209. **https://doi.org/10.1016/j.lwt.2019.01.041**

ORIGINAL ARTICLE
http://journal.pan.olsztyn.pl

Polish Journal of Food and Nutrition Sciences
2025, Vol. 75, No. 3, 234–244
DOI: 10.31883/pjfns/208305
ISSN 1230-0322, e-ISSN 2083-6007

Structural Characteristics and Physicochemical Properties of Soluble Dietary Fiber Preparations from *Citrus sinensis* Peel

Huong C. Nguyen[1,2], Nhan C. Tran[1], Truc T. Tran[1]*

[1]Institute of Food and Biotechnology (IFB), Can Tho University (CTU), Campus II, 3/2 street, Ninh Kieu Ward, 94000 Can Tho City, Vietnam
[2]Faculty of Food Science and Technology (FST), Ho Chi Minh City University of Industry and Trade (HUIT), 700000 Ho Chi Minh City, Vietnam

This study evaluated the effects of acid, alkaline, cellulase-assisted, and xylanase-assisted extraction methods of orange by-products (*Citrus sinensis* peel) on the chemical composition, structure and physicochemical properties of resulting soluble dietary fiber (SDF) preparations. The highest extraction efficiency was obtained using the method with citric acid (31.37%). The pectin, hemicellulose and cellulose contents of fiber produced with this method (A-SDF) were 58.63, 7.38, and 8.42 g/100 g dry matter (dm), respectively. The method with citric acid resulted in an A-SDF with a water holding capacity of 19.17 g/g and an emulsifying capacity of 91.00%, which were superior to those obtained using alkaline and enzyme-assisted extractions. Fiber obtained by xylanase-assisted extraction had similar emulsion stability (75.77%), water swelling capacity (8.67 mL/g), and oil holding capacity (2.49 g/g) as A-SDF. Scanning electron microscopy images showed that A-SDF had a rough, porous surface favorable for hydration, while alkaline-extracted SDF (B-SDF) displayed dense, compact structures. Fourier-transform infrared spectra confirmed stronger hydroxyl and carboxyl group signals in A-SDF, suggesting its better hydrophilicity. X-ray diffraction analysis indicated the highest crystallinity index in B-SDF (41.83%), whereas fibers extracted using enzymes had more amorphous patterns, reflecting structural disruption. These findings demonstrate that acid-assisted extraction using citric acid is the most effective method for extracting soluble fiber from citrus by-products.

Keywords: acid treatment, alkali treatment, dietary fiber composition, enzyme-assisted extraction, orange by-product, orange peel

INTRODUCTION

Citrus is a major fruit crop grown worldwide, with oranges, tangerines, lemons, citron, and grapefruits accounting for 62, 17, 11, and 10% of the total citrus production in 2020, respectively [FAO, 2021]. The consumption of citrus fruits, both fresh and processed by the food industry, generates more than 54 million tons of waste annually on a global scale, with 50–60% of these unused by-products consisting mainly of peels [Teigiserova *et al*., 2021]. Citrus fruit peels are a rich source of dietary fiber and phenolic compounds, including flavonoids, which contribute to their natural antioxidant activity [Ani & Abel, 2018; Makni *et al*., 2018]. Among citrus by-products, *Citrus sinensis* (orange) peel contains 46.5% of total dietary fiber, with soluble dietary fiber (SDF) and insoluble dietary fiber (IDF) fractions accounting for 9.2% and 37.3% of peel, respectively [Núñez-Gómez *et al*., 2024]. However, the structural characteristics of dietary fiber extracted from orange peel are largely influenced by the composition of its cell wall polysaccharides, such as pectin, cellulose,

***Corresponding Author:**
tel: +84909712070; e-mail: **tttruc@ctu.edu.vn** (T.T. Truc)

Submitted: 28 March 2025
Accepted: 15 July 2025
Published on-line: 11 August 2025

hemicellulose, and lignin [de Castro *et al.*, 2024]. Both dietary fiber fractions offer distinct health benefits, such as improved digestive health, cholesterol reduction, and glycemic control [Dhingra *et al.*, 2012]. In addition to these health benefits, dietary fiber possesses desired functional properties, such as water retention, oil retention, and gel formation, making it a valuable industrial food additive for improving nutritional content and texture [Elleuch *et al.*, 2011; Tejada-Ortigoza *et al.*, 2016].

The extraction method significantly influences the structural and functional properties of the resulting dietary fiber. Acid, alkaline, and enzyme-assisted extractions, modify fiber composition and physicochemical properties, enhancing their potential applications in food formulations [Berktas & Cam, 2025; Tang *et al.*, 2024; Zhang *et al.*, 2017]. These variations are further affected by the nature of the raw material and the extraction conditions used, which ultimately determine the molecular structure, surface morphology, and degree of polymerization of the extracted SDF [Berktas & Cam, 2025; Wang *et al.*, 2015]. For instance, treating IDF through mild acid hydrolysis (*e.g.*, 0.2% sulfuric acid) can convert part of it into soluble components, thereby enhancing water-holding capacity (WHC) and water solubility (WSC) by removing starch and protein, along with microstructural changes [Qi *et al.*, 2015]. However, the efficiency of chemical extraction methods depends heavily on the food matrix and nature of the extracted polysaccharides [Wang *et al.*, 2022]. For example, fibers extracted from sugar beet have much higher WHC and WSC values than those from pea hulls when alkaline extraction methods are used [Bertin *et al.*, 1988; Weightman *et al.*, 1995]. Chemical extraction methods, such as acid or base treatment, are relatively simple and cost-effective. They can be applied to a wide range of raw materials, leading to high extraction yields and modifications of fiber structure and properties [Qi *et al.*, 2015; Tejada-Ortigoza *et al.*, 2016]. However, the major drawback of these methods is the potential destruction of food structure due to prolonged processing times and high temperatures. This can lead to the degradation of polysaccharides with functional groups such as hydroxyl and carboxyl groups, which can negatively impact the structural integrity and functional properties of the resulting dietary fiber [Berktas & Cam, 2025; Wang *et al.*, 2015].

To mitigate environmental and operational challenges, such as high temperatures and equipment corrosion, enzyme-assisted extraction has been developed as an alternative. It can increase the SDF/IDF ratio by selectively hydrolyzing insoluble polysaccharide chains (*e.g.*, cellulose and hemicellulose) into smaller, water-soluble fragments [Zhao *et al.*, 2025; Zheng & Li, 2018]. This enzymatic breakdown also exposes more hydrophilic functional groups, such as hydroxyl groups, thereby enhancing water-holding capacity and surface area [Tang *et al.*, 2024; Yoon *et al.*, 2005]. However, enzymatic methods are limited by their complexity, time consumption, high enzyme costs, and the need for precise temperature control [Elleuch *et al.*, 2011]. Despite extensive research on fiber extraction, optimizing the method to maximize yield and functionality while maintaining environmental sustainability remains a challenge. This study evaluated the effects of different extraction methods (acidic, alkaline, and enzyme-assisted) on the yield, structure, and physicochemical properties of SDF preparations from *C. sinensis* peel, with the aim of identifying the most effective approach for future practical applications in food processing.

MATERIALS AND METHODS

Chemicals and reagents

A dietary fiber analysis kit was obtained from Megazyme (Wicklow, Ireland). All chemicals used in this study, including sodium phosphate dodecahydrate ($Na_2HPO_4 \times 12H_2O$), sodium dihydrogen phosphate dihydrate ($NaH_2PO_4 \times 2H_2O$), and citric acid, were purchased from Merck (Darmstadt, Germany). Enzymes used for fiber extraction – xylanase with an activity of 100,000 U/g and cellulase with an activity of 10,000 U/g were purchased from Angel Yeast Co., Ltd (Yichang, Hubei, China). Ethanol used in all pre-treatment steps was sourced domestically from Vietnam.

Material and its preparation

The orange by-products (collected after segment separation or juice extraction) were obtained directly from VinaGreenCo One Member Co., Ltd. (My Hoa Commune, Binh Minh Town, Vinh Long Province, Vietnam). Upon receipt, the outer peels were discarded. The remaining white peels, cores, and pulp were thoroughly rinsed with running water to remove any residual fruit flesh. The components were then chopped and subjected to ethanol pre-treatment by soaking in 96% ethanol at a 1:3 (*w/v*) ratio for 30 min at 60°C, using a reflux system equipped with a 40-cm condenser and thermometer attached to a two-neck flask. Following ethanol treatment, the samples were rinsed with 70% (*v/v*) ethanol and dried at 60°C to a constant weight (moisture content approximately 4 g/100 g). The dried material was ground using an SK200 dry mill (SEKA, Tokyo, Japan), and the resulting powder was passed through an 80-mesh sieve to ensure uniform particle size [Huong *et al.*, 2024]. The final orange powder was stored in vacuum-sealed polyamide (PA) bags at room temperature (25°C) until further analyses.

Methods of soluble dietary fiber extraction

Acid extraction

The acid extraction method was adapted from Kermani *et al.* [2014] and Dong *et al.* [2020]. Ten grams of orange peel powder were mixed with a 4% citric acid solution at a solid to liquid ratio of 1:40 (g/mL) and heated at 70°C for 90 min, pH 1.9. After extraction, the mixture was centrifuged at 2,800×*g* for 10 min, and the supernatant was collected. Then, supernatant was mixed with two volumes of 96% ethanol and left undisturbed for 2 h. The resulting precipitate was filtered, and dried at 60°C to a constant weight, yielding soluble dietary fiber preparation obtained under acid conditions, referred to as A-SDF.

Alkaline extraction

The method of extraction under alkaline conditions was adapted from Wang *et al.* [2015] with slight modifications. Orange peel powder (10 g) was suspended in a 0.5% NaOH solution at a solid

to liquid ratio of 1:40 (g/mL) and heated at 60°C for 60 min. After extraction, the mixture was centrifuged at 2,800×*g* for 10 min, and from the supernatant, the SDF was precipitated by adding two volumes of 96% ethanol and left for 2 h. Then, the precipitate was filtered and dried at 60°C to a constant weight, yielding an SDF preparation obtained under alkaline conditions, denoted as B-SDF.

Enzyme-assisted extraction

Enzyme-assisted extractions of orange peel powder were carried out according to the procedure used previously by Dong *et al.* [2020]. Orange peel powder (10 g) was mixed with 500 mL of citrate buffer and hydrolyzed with cellulase (enzyme to powder ratio, E/P, of 0.2%, *w/w*) at 50°C, pH 5, for 60 min, or with xylanase (E/P of 0.2%, *w/w*) at 60°C, pH 4.5, for 90 min. The enzymes were then inactivated by heating at 90°C for 15 min. SDF was precipitated following a procedure described above for the acid extraction, yielding SDF preparations (EC-SDF and EX-SDF, respectively).

Extraction efficiency calculation

The extraction efficiency (EE, %) of acid, alkaline, and enzyme-assisted methods was calculated using Equation (1):

$$EE = (M_1/M_0) \times 100 \quad (1)$$

where: M_1 is the mass of the SDF preparation obtained after drying (g) and M_0 is the mass of the orange peel powder (g).

Determination of fiber composition

The content of IDF and SDF in SDF preparations was determined following AOAC International methods no. 991.42 and 993.19, respectively [AOAC, 2005]. Total dietary fiber was calculated as a sum of SDF and IDF. The powdered SDF preparations were mixed with phosphate buffer and hydrolyzed sequentially with α-amylase (pH 6.0) at 100°C for 15 min, protease (pH 7.5) at 60°C for 30 min, and amyloglucosidase (pH 4.5) at 60°C for 30 min to hydrolyze starch and protein. The resulting residue (IDF) was filtered and washed thoroughly with distilled water, ethanol, and acetone. The filtrate was mixed with 96% ethanol (at a liquid/ethanol ratio of 1:2, *v/v*) at room temperature (25°C) for 1 h. The resulting precipitate with SDF was further washed with ethanol and acetone to obtain the SDF fraction. Weights of both IDF and SDF residues were corrected for protein (determined as Kjeldahl nitrogen × 6.25) and ash content, as specified in the AOAC protocols. Final dietary fiber contents were calculated on a dry weight basis and expressed as g *per* 100 g of dry matter of preparation (g/100 g dm).

Determination of pectin content in SDF preparations was performed based on the method described by Carré & Haynes [1922] with slight modifications. The dried SDF preparations were treated with oxalic acid, pH 4.6 (at a solid to liquid ratio of 1:40, *w/v*) at 85°C for 1 h. The mixture was filtered through a nylon cloth to remove the residues, and pectin was precipitated by adding twice volumes of 96% ethanol. The precipitate was washed several times with 70% ethanol and dried at 50°C. An aliquot of 0.15 g (W) of this crude pectin was neutralized with 100 mL of 0.1 M NaOH. Subsequently, 50 mL of 0.1 M acetic acid was added and allowed to react for 5 min at room temperature (25°C), followed by the addition of 50 mL of 1 M $CaCl_2$. After equilibrating for 1 h at room temperature (25°C), the mixture was boiled for 5 min. The formed precipitate was filtered and washed with hot water until no chloride ions were detected (tested with a 1% $AgNO_3$ solution). The final residue was dried at 105°C and weighed. Pectin content was calculated using Equation (2) and expressed in g *per* 100 g of dry SDF preparation (g/100 g dm):

$$Pectin = W_1/W \times 0.92 \times 100 \quad (2)$$

where: W_1 is the weight of the dried calcium pectate (g), W is the weight of the SDF sample used for precipitation (g), and 0.92 is the conversion factor accounting for calcium content in the precipitate.

Cellulose content was determined according to the method of Liu *et al.* [2021] with minor modifications. One gram of dried SDF preparation (W) was mixed with 25 mL of a nitric acid–ethanol solution (1:4, *v/v*). The suspension was refluxed in a boiling water bath for 1 h, filtered, and the insoluble residue was collected. The procedure was repeated until the fibers appeared white. The residue was washed with warm distilled water to neutral pH, followed by two rinses with 96% ethanol, and dried at 105°C to a constant weight (W_1). The dried residue was then ashed at 575°C, and the ash weight was recorded (W_2). The cellulose content (g/100 g dm) was calculated using Equation (3):

$$Cellulose = (W_1 - W_2)/W \times 100 \quad (3)$$

Hemicellulose content in SDF preparations was determined by subtracting the cellulose content from the holocellulose content. The latter was determined by the method previously used by Viera *et al.* [2007]. One gram of dried SDF preparation (W) was combined with 0.75 g of sodium chlorite, 0.5 mL of glacial acetic acid, and 100 mL of distilled water in a 250-mL beaker. The mixture was stirred until the chlorite dissolved, then incubated in a water bath at 70°C for 1 h with occasional stirring. The same amounts of reagents were added every hour over the next two hours, resulting in a total digestion time of 3 h. The mixture was cooled to 10°C, filtered, and washed six times with ice-cold water. The resulting holocellulose was dried at 105°C for 6 h, and weighed (W_1). The cellulose content determined previously was recorded as W_2. The hemicellulose content (g/100 g dm) was calculated using Equation (4):

$$Hemicellulose = (W_1 - W_2)/W \times 100 \quad (4)$$

Determination of functional properties

Water solubility

The water solubility (WS) of SDF preparations was determined using the method described by Wang *et al.* [2015], with slight

modifications. One gram of dried SDF sample (W) was mixed with distilled water (5 mL) in a 15-mL centrifuge tube. The mixture was heated at 90°C for 30 min in a water bath, mixed every 5 min for 30 s, and centrifuged at 2,800×*g* for 10 min. The supernatant was collected, dried at 105°C, and weighed (W_1). The WS (g/g) was calculated using Equation (5):

$$WS = W_1/W \quad (5)$$

Water holding capacity

The water holding capacity (WHC) was determined following the method described by Dong *et al.* [2020], with minor modifications. The dried SDF preparation (W, 0.5 g) was mixed with 20 mL of distilled water in a 50-mL centrifuge tube. After equilibration at room temperature (25°C) for 24 h, the sample was centrifuged at 2,800×*g* for 10 min. The supernatant was discarded, and the weight of the hydrated residue (W_1) was recorded. The WHC (g/g) was calculated using Equation (6):

$$WHC = (W_1 - W)/W \quad (6)$$

Oil holding capacity

The oil holding capacity (OHC) was determined according to the method described by Sangnark & Noomhorm [2003] with minor modifications. The dried SDF preparation (W, 0.5 g) was mixed with soybean oil (5 mL) in a 15-mL centrifuge tube. After equilibration at 4°C for 1 h, the sample was centrifuged at 2,800×*g* for 20 min. The unbound oil was discarded, and the weight of the oil-retained residue (W_1) was recorded. The OHC (g/g) was calculated using Equation (7):

$$OHC = (W_1 - W)/W \quad (7)$$

Water swelling capacity

Water swelling capacity (WSC) was assessed using the method described by Ma & Mu [2016]. Briefly, 0.2 g of dried SDF preparation (W) was mixed with 10 mL of distilled water in a graduated 15-mL tube and equilibrated at room temperature (25°C) for 18 h. The volume of the sample before (V_1) and after (V_2) hydration was recorded. The WSC (mL/g) was calculated using Equation (8):

$$WSC = (V_2 - V_1)/W \quad (8)$$

Emulsifying capacity and emulsion stability

The emulsifying capacity (EC) was evaluated following the method of Nandi & Ghosh [2015] with slight modifications. Specifically, 0.5 g of dried SDF preparations was dispersed in 50 mL of distilled water and homogenized at 10,000 rpm for 1 min. Subsequently, 50 mL of soybean oil was added, and the mixture was homogenized again at the same speed and duration. The resulting emulsion was centrifuged at 2,800×*g* for 5 min. After centrifugation, the total volume of the system (W_v) and the volume of the emulsion layer (EL_{vi}) were recorded. The EC (%) was then calculated using Equation (9):

$$EC = (EL_{vi}/W_v) \times 100 \quad (9)$$

To determine emulsion stability (ES), the freshly prepared emulsion (from the EC determination) was heated at 80°C for 30 min, then allowed to cool to room temperature (25°C) and centrifuged at 2,800×*g* for 5 min. The volume of the remaining emulsified layer after heating (EL_{vf}) was recorded. ES was calculated as a percentage of the initial emulsion volume (EL_{vi}) using Equation (10):

$$ES = (EL_{vf}/EL_{vi}) \times 100 \quad (10)$$

Analysis of structural characteristics

The SDF preparations were analyzed for their structural characteristics using Fourier-transform infrared spectroscopy (FTIR), X-ray diffraction (XRD), and scanning electron microscopy (SEM). FTIR analysis was conducted on a Frontier NIR/MIR spectrometer (Perkin Elmer, Waltham, MA, USA) within the wavelength range of 400–4,000 cm^{-1} to identify the functional group vibrations. For sample preparation, dried powder was mixed with potassium bromide (KBr) in a 1:40 ratio by weight and compressed into 1-mm thick pellets using a hydraulic press. Each sample was scanned 20 times to ensure reliable spectral resolution.

XRD analysis was carried out using an Empyrean X-ray diffractometer (PANalytical, Almelo, Netherlands) equipped with Cu K-α radiation (λ=1.5406 Å), operating over at 40 kV and 40 mA. Diffraction patterns were recorded over a 2θ range of 5–80° at a step size of 0.02° and a counting time of 0.5 s *per* step. The primary aim of this analysis was to evaluate the crystalline *versus* amorphous nature of the extracted fiber samples. The crystallinity index (CI) was calculated based on the integrated intensities obtained from the diffractograms. Specifically, the CI (%) was determined using Equation (11) [Salem *et al*., 2023]:

$$CI = [A_c/(A_c+A_a)] \times 100 \quad (11)$$

where: A_c is the integrated area under the crystalline peaks, A_a is the integrated area under the amorphous halo or background, and (A_c+A_a) represents the total area under the XRD curve.

Peak fitting and area integration were performed using HighScore Plus software (PANalytical), allowing separation of the crystalline and amorphous contributions by deconvoluting overlapping peaks. This approach enables an accurate estimation of the relative crystallinity by quantifying the ratio of the crystalline signal to the total diffracted intensity.

For microstructural examination, SEM images were obtained using a JSM IT 200 field-emission scanning electron microscope (Jeol, Tokyo, Japan) operated at an accelerating voltage of 10 kV. Prior to imaging, the samples were affixed to double-sided conductive adhesive tape and sputter-coated with platinum to enhance conductivity and image clarity. SEM images were captured at magnifications of 100×; 1,000×; and 7,000×.

Statistical analysis

All data collected were based on the results of at least three replicates for each experiment and are expressed as mean ± standard deviation. Statistical analyses were performed using Statgraphics Centurion 16.1 software (StatPoint Technologies, Inc., Warrenton, VA, USA). Analysis of variance (ANOVA), followed by the least significant difference (LSD) test, was used to determine significant differences ($p<0.05$) between SDF preparations obtained under different conditions.

RESULTS AND DISCUSSION

Extraction efficiency and fiber composition

The extraction efficiency of orange by-products and composition of soluble dietary fiber preparations obtained using various extraction methods, including extraction under acid and alkaline conditions (resulting in A-SDF and B-SDF, respectively, and enzyme-assisted extraction with cellulase and xylanase (resulting in EC-SDF and EX-SDF, respectively), is shown in **Table 1**. The EE varied significantly ($p<0.05$) depending on the extraction method. The highest EE was achieved with chemical extraction methods: 31.37% with acid extraction and 24.18% with alkaline extraction. This was followed by the cellulose-assisted method (16.88%), while the lowest extraction efficiency was obtained using the xylanase-assisted method (13.88%). The significantly higher EE of A-SDF method suggests that citric acid extraction was more effective at solubilizing orange by-product matter than enzymatic treatments. Citric acid may facilitate the breakdown of the plant matrix and improve fiber solubilization, as observed in previous studies [Maran *et al*., 2017]. Enzymatic methods resulted in the lowest EE, possibly due to the selective hydrolysis of specific fiber components, leading to reduced overall recovery [Canela-Xandri *et al.*, 2018]. For instance, cellulase acts on β-1,4 glycosidic bonds, whereas xylanase breaks the bonds between hemicellulose and cellulose, leading to a lower extraction efficiency but a higher SDF content due to the breakdown of cellulose and hemicellulose into soluble fibers [Song *et al*., 2021; Zhao *et al*., 2025; Zheng & Li, 2018].

For total dietary fiber (TDF), significant differences ($p<0.05$) were observed among the preparations obtained by different extraction methods (**Table 1**). EC-SDF exhibited the highest TDF content (66.81 g/100 g dm), significantly greater than all the other samples. EX-SDF showed a higher TDF content (66.58 g/100 g dm) compared to A-SDF and B-SDF, whose TDF contents were 66.09 and 66.17 g/100 g dm, respectively. These findings suggest that enzymatic treatments, particularly those with cellulase and xylanase, enhanced the total fiber recovery compared to acid and alkaline extractions. Moreover, there were substantial differences in the content of IDF and SDF fractions. B-SDF and EX-SDF had the highest IDF content (25.13 and 22.10 g/100 g dm, respectively), whereas EC-SDF had the highest SDF content (50.11 g/100 g dm), followed by A-SDF (48.24 g/100 g dm). This indicated that cellulase treatment effectively converted IDF into SDF, which is consistent with the findings of Zheng & Li [2018]. In terms of specific fiber components, EX-SDF exhibited the highest cellulose content (11.73 g/100 g dm), indicating that xylanase-assisted extraction preserved the cellulose structure while degrading hemicellulose. B-SDF had the highest hemicellulose content (7.58 g/100 g dm), suggesting that alkaline treatment effectively preserved hemicellulose. Notably, EC-SDF had the highest pectin content (61.22 g/100 g dm), followed by A-SDF and B-SDF (58.31–58.63 g/100 g dm). The EX-SDF pectin content was the lowest (56.24 g/100 g dm). The higher pectin content in EC-SDF supported the role of cellulase in selectively breaking down cellulose while preserving pectin. In turn, a high pectin content contributes to enhanced functional properties, such as water-holding capacity and water-swelling capacity relevant to food applications [Huang *et al*., 2021]. In conclusion, extraction under acid conditions provided the highest yield and maintained a good balance between SDF and IDF of A-SDF. In turn, alkaline extraction was proved suitable for obtaining preparations for applications that require a higher IDF content. Among all methods, cellulase treatment increased the content of SDF and pectin the most, making EC-SDF ideal for functional foods, whereas xylanase-assisted method preserved cellulose but resulted in lower EE. These findings highlight the influence of extraction method on fiber yield and composition, consistent with trends observed in other studies using enzymatic or chemical extraction techniques [Dong *et al*., 2020; Huang *et al*., 2021; Zhang *et al*., 2017; Zhao *et al*., 2025].

Table 1. Extraction efficiency of orange by-products and composition of soluble dietary fiber (SDF) preparations obtained by different methods.

Preparation	Extraction efficiency (%)	TDF (g/100 g dm)	IDF (g/100 g dm)	SDF (g/100 g dm)	Cellulose (g/100 g dm)	Hemicellulose (g/100 g dm)	Pectin (g/100 g dm)
A-SDF	31.37±0.78^{a}	66.09±0.02^{c}	17.85±0.01^{c}	48.24±0.01^{b}	8.42±0.01^{d}	7.38±0.02^{b}	58.63±0.59^{b}
B-SDF	24.18±1.68^{b}	66.17±0.04^{c}	25.13±0.01^{a}	41.03±0.03^{d}	9.97±0.01^{b}	7.58±0.02^{a}	58.31±0.50^{b}
EC-SDF	16.88±0.80^{c}	66.81±0.04^{a}	16.80±0.01^{d}	50.01±0.04^{a}	8.91±0.01^{c}	6.42±0.03^{d}	61.22±0.97^{a}
EX-SDF	13.88±0.20^{d}	66.58±0.12^{b}	22.10±0.03^{b}	44.48±0.10^{c}	11.73±0.02^{a}	6.74±0.03^{c}	56.24±0.69^{c}

Data are presented as the mean ± standard deviation. Different letters in the same column indicate statistically significant differences between preparations ($p<0.05$). A-SDF, SDF preparation obtained under acid conditions; B-SDF, SDF preparation obtained under alkaline conditions; EC-SDF, SDF preparation obtained by cellulose-assisted extraction; EX-SDF, SDF preparation obtained by xylanase-assisted extraction; dm, dry matter; IDF, insoluble dietary fiber; TDF, total dietary fiber.

Table 2. Physicochemical properties of soluble dietary fiber (SDF) preparations obtained from orange by-products using different methods.

Preparation	WS (g/g)	WHC (g/g)	OHC (g/g)	WSC (mL/g)	EC (%)	ES (%)
A-SDF	75.33±3.34^{a}	19.17±0.91^{a}	2.38±0.48^{a}	8.17±1.44^{ab}	91.00±1.00^{a}	79.40±1.15^{a}
B-SDF	50.05±0.65^{b}	4.85±0.35^{b}	1.34±0.06^{b}	4.92±0.11^{c}	59.17±0.76^{b}	53.52±0.60^{b}
EC-SDF	54.17±1.96^{b}	5.51±0.18^{b}	2.40±0.05^{a}	6.67±0.58^{b}	42.94±1.09^{c}	9.32±0.24^{c}
EX-SDF	76.20±3.12^{a}	4.55±0.36^{b}	2.49±0.44^{a}	8.67±0.44^{a}	3.00±0.95^{d}	75.77±7.21^{a}

Data are presented as mean ± standard deviation. Different letters within the same column indicate statistically significant differences between preparations (p<0.05). A-SDF, SDF preparation obtained under acid conditions; B-SDF, SDF preparation obtained under alkaline conditions; EC-SDF, SDF preparation obtained by cellulose-assisted extraction; EX-SDF, SDF preparation obtained xylanase-assisted extraction; WS, water solubility; WHC, water holding capacity; OHC, oil holding capacity; WSC, water swelling capacity; EC, emulsifying capacity; ES, emulsion stability.

Functional properties

The physicochemical properties of SDF preparation obtained from orange by-products using different extraction methods, including water solubility, water holding capacity, oil holding capacity, water swelling capacity, emulsifying capacity, and emulsifying stability, are shown in **Table 2**. A-SDF exhibited the highest WHC (19.17 g/g), which was significantly different (p<0.05) from the other samples. The WHC of B-SDF, EC-SDF, and EX-SDF ranged from 4.55 to 5.51 and the values did not differ significantly (p≥0.05) from each other. The WHC of A-SDF was higher than that reported for orange peel soluble dietary fiber extracted using steam explosion and sulfuric-acid soaking method – 5.52 g/g [Wang *et al*., 2015]. In turn, Huang *et al*. [2021] found higher WHC, compared to the value in our study for B-SDF, for untreated citrus peel (8.32 g/g) and treated under different alkaline conditions (18.26–21.32 g/g) compared to the value in our study for B-SDF. Generally, WHC is enhanced by chemical and enzymatic treatments that disrupt hydrogen bonds in cellulose and hemicellulose, de-esterify pectin, and expose hydrophilic groups, thereby increasing the fiber's water absorption capacity [Liu *et al*., 2021; Zhang *et al*., 2020].

The fiber hydrolyzed by xylanase exhibited a higher swelling capacity (8.67 mL/g), while the alkaline treatment resulted in the lowest WSC (4.92 mL/g), with a significant (p<0.05) difference observed between the samples (**Table 2**). This result was consistent with previous studies, which suggested that WSC depends on the soluble fiber content [Navarro-González *et al*., 2011], particularly due to the exposure of small-sized pectin with a large surface area, allowing for the formation of hydrogen bonds that promote water absorption and swelling [Ma & Mu, 2016; Navarro-González *et al*., 2011]. The lower WSC in the alkaline-treated samples could also be related to the disruption of the matrix structure and the breakdown of polysaccharide linkages under alkaline conditions [Jiang *et al*., 2020].

The OHC of dietary fiber is important for improving the texture and mouthfeel of food products and may also assist in retaining lipophilic nutrients during formulation [Marczak & Mendes, 2024]. Additionally, dietary fiber with high OHC has been associated with potential cholesterol-lowering effects due to its ability to bind bile acids and fats [Elleuch *et al*., 2011]. In this study, OHC ranged from 1.34 to 2.49 g/g (**Table 2**). These values were comparable to those obtained in previous studies on citrus peel-derived dietary fiber, which reported OHC ranging from 2.08 to 5.0 g/g, depending on the extraction method and fiber structure [Huang *et al*., 2021; Zhang *et al*., 2020; Zhao *et al*., 2025]. Among the tested samples, the OHC of A-SDF, EC-SDF, and EX-SDF ranged from 2.38 to 2.49 g/g and did not differ significantly (p≥0.05), suggesting that both acid and enzyme-assisted extractions were similarly effective in preserving oil-binding functionality. In contrast, B-SDF exhibited a significantly (p<0.05) lower OHC (1.34 g/g), indicating that alkaline treatment may reduce the fiber's ability to retain oil. This reduction could be attributed to structural degradation or loss of hydrophobic binding sites during alkaline hydrolysis. The relatively higher OHC observed in the acid- and enzymatic-treated fibers may be due to a more porous surface morphology and greater exposure of lipophilic groups, which facilitate oil entrapment within the fiber matrix [Dong *et al*., 2020; Zhang *et al*., 2020].

The WS of SDF preparations obtained from orange by-products ranged from 50.05 to 76.20 (g/g). While water solubility is often influenced by the soluble fiber content, no strong correlation was observed in this study. Notably, EC-SDF exhibited the highest SDF content (50.01 g/100 g dm) but showed relatively low WS (54.17 g/g). This discrepancy may be attributed to the structural characteristics of the extracted polysaccharides. Enzymatic degradation likely produced smaller molecular weight fragments, including low-methoxyl pectin, which may have altered solubility behavior and increased solution viscosity, thereby affecting dispersibility and solubility kinetics [Kermani *et al*., 2014; Song *et al*., 2021].

Emulsifying capacity refers to the ability of a substance to facilitate the dispersion of two immiscible liquid phases, while emulsion stability indicates to maintain the stability of the formed emulsion over time [Dong *et al*., 2020]. The A-SDF, B-SDF, EC-SDF, and EX-SDF preparations exhibited EC of 91.00, 59.17, 42.94, and 3.00%, and corresponding ES of 79.40, 53.52, 9.32, and 75.77%, respectively (**Table 2**). Interestingly, EX-SDF demonstrated a relatively high ES despite its extremely low EC. The intense degradation induced by xylanase likely enhanced its water swelling capacity due to increased porosity, allowing more water to be absorbed into the fiber matrix. However, the re-agglomeration of fragmented structures into

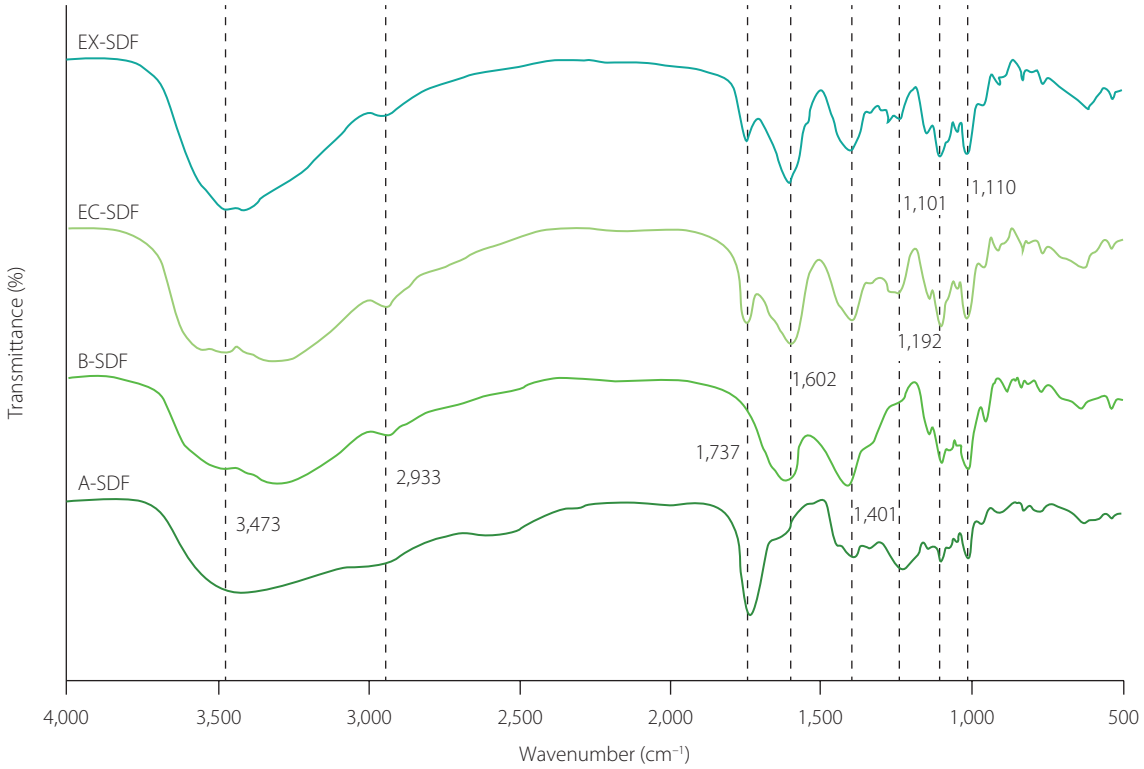

Figure 1. Fourier-transform infrared spectra of soluble dietary fiber preparations obtained from orange by-products by different methods including acid extraction (A-SDF), alkaline extraction (B-SDF), cellulose-assisted extraction (EC-SDF), and xylanase-assisted extraction (EX-SDF).

denser, more ordered forms may have reduced the available surface area, contributing to a lower water holding capacity and hindering effective contact between the oil and water phases-thereby reducing EC. SDF preparations obtained through enzyme-assisted extraction generally exhibited lower EC compared to those extracted chemically (**Table 2**). This difference could be explained by the extensive disruption of cellulose and hemicellulose during enzymatic treatment, which may impair both hydration ability and oil-binding performance, ultimately diminishing emulsifying potential [Zheng & Li, 2018]. The emulsifying behavior of SDF is influenced by multiple factors, including WHC, OHC, fiber structure, and surface characteristics [Jia *et al*., 2019; Zhang *et al*., 2017]. Among these factors, the ability of dietary fibers to retain water (WHC) and bind oil (OHC) is particularly important, as it enhances the fiber's ability to stabilize oil–water interfaces in emulsions.

Structural characteristics

Characteristic functional groups of the soluble dietary fiber preparations

The FTIR spectra revealed that all the SDF preparations exhibited similar characteristic spectra, as shown in **Figure 1**. The SDF samples exhibited strong absorption in the 3,300–3,500 cm^{-1} region, with a distinct absorption peak at 3,473 cm^{-1}, corresponding to the O–H group's hydrogen bond vibration in polysaccharides [Dong *et al.*, 2020]. Compared to A-SDF, shifts in the absorption band and a reduction in peak intensity observed in B-SDF and EC-SDF suggest the disruption of hydrogen bonds in the cellulose and hemicellulose chains [Song *et al.*, 2021]. Additionally, a slight increase in intensity may be attributed to the formation of hydrogen bonds between the hemicellulose and pectin chains [Zhang *et al.*, 2020]. All citrus fibers exhibited C–H stretching vibrations from the $–CH_2$ and $–CH_3$ groups of polysaccharides at approximately 2,933 cm^{-1} [Song *et al.*, 2021; Yan *et al.*, 2015]. Furthermore, the peak at 2,933 cm^{-1} is associated with the intermolecular hydrogen bonding of the –OH group in cellulose [Jia *et al.*, 2019]. The decreased absorption intensity at 2,933 cm^{-1} in the modified citrus fibers indicates a reduction in the polysaccharide content and disruption of hydrogen bonds between –OH groups in the cellulose structure, which could enhance the functional properties of citrus fibers. A distinct absorption peak at approximately 1,737 cm^{-1} was assigned to the C=O stretching of hemicellulose, pectin, or lignin [Zhang *et al.*, 2020], but this peak disappeared after alkaline hydrolysis [Jiang *et al.*, 2005]. The characteristic wavenumber position for the C=O vibration of the acetyl and uronic ester groups in hemicellulose, observed at approximately 1,737 cm^{-1}, was present in all samples but disappeared after alkaline hydrolysis, as the alkaline medium solubilizes both hemicellulose and lignin [Jiang *et al.*, 2005]. Peaks at 1,602 cm^{-1} and 1,401 cm^{-1}, corresponding to the aromatic benzene ring vibrations associated with the bending or stretching of aromatic hydrocarbons in lignin [Ma & Mu, 2016; Song *et al.*, 2021], were detected in all samples. The weaker signal observed for A-SDF may indicate that lignin was partially precipitated in the acidic medium. Additionally, the wavenumber ranges between 1,000 and 1,200 cm^{-1} are characteristic

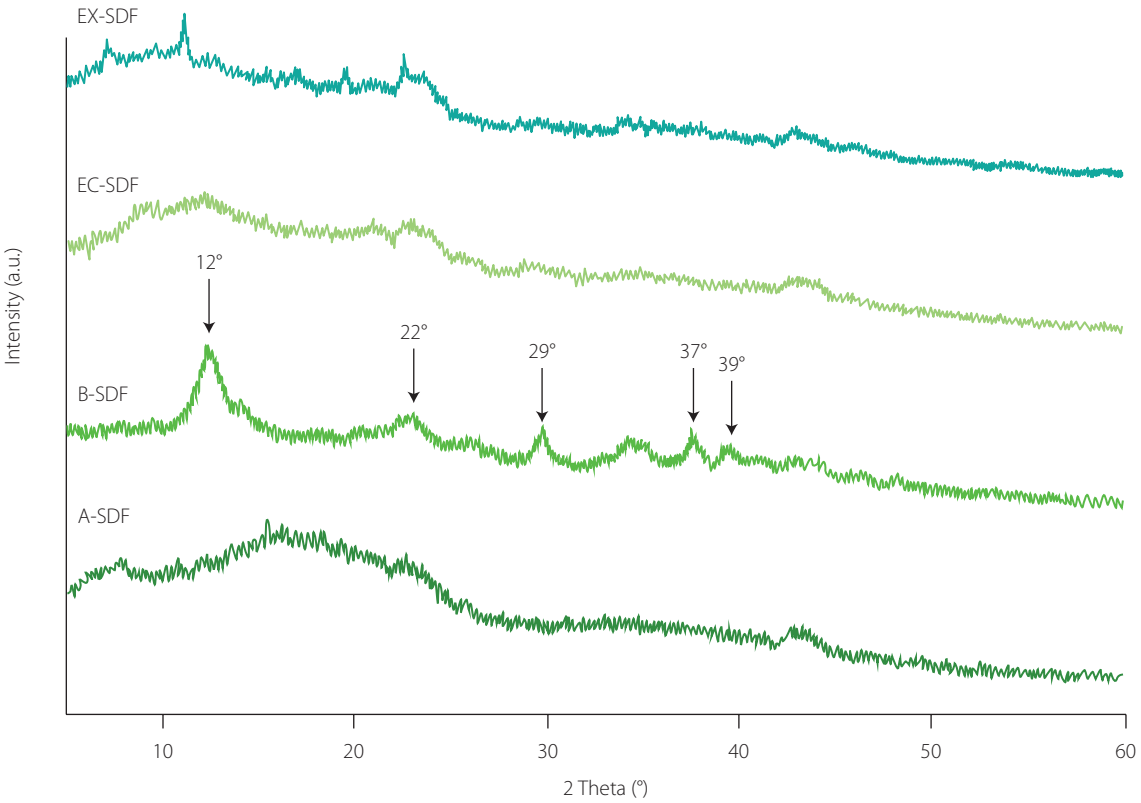

Figure 2. X-ray diffraction patterns of soluble dietary fiber preparations obtained from orange by-products by different methods including acid extraction (A-SDF), alkaline extraction (B-SDF), cellulose-assisted extraction (EC-SDF), and xylanase-assisted extraction (EX-SDF).

of the C–O and C–C stretching vibrations in the glycan core [Dong *et al.*, 2020].

Amorphous and crystal structural characteristics of soluble dietary fiber preparations using X-ray diffraction

The XRD patterns of the SDF preparations are shown in **Figure 2**, where the fibers processed by all four extraction methods exhibited similar main peaks at 12° and 22°, indicating that all samples contained type I cellulose [Song *et al.*, 2021; Zhang *et al.*, 2020]. The narrow peak positions and widths of the B-SDF and EX-SDF samples suggest that the ordered crystalline regions were not significantly disrupted by enzymatic hydrolysis with xylanase or by alkaline treatment [Jiang *et al.*, 2020]. In contrast, A-SDF and EC-SDF exhibited broader peak widths, indicating a more amorphous structure in these fibers. The crystallinity index (CI) of A-SDF, B-SDF, EC-SDF, and EX-SDF was 34.64, 41.83, 30.13, and 37.43%, respectively. The higher CI of the citrus fiber after alkaline treatment is likely due to the degradation of some amorphous components, such as pectin or lignin [Zhang *et al.*, 2020]. The lower CI determined for EC-SDF compared to the other preparations suggests that cellulase hydrolysis may have disrupted the ordered cellulose structure. This enzymatic action is known to break hydrogen bonds and degrade crystalline regions, converting them into more amorphous forms [Hassan *et al.*, 2018; Jiang *et al.*, 2020]. The decrease in (hemi)cellulose content, as was shown in **Table 1**, further demonstrates the solubilization of these components during cellulase treatment.

Microstructural characteristics of soluble dietary fiber preparations

The morphological structures of SDF preparations obtained by different methods revealed notable differences under SEM (**Figure 3**). SDF produced through acid extraction (A-SDF) displayed smaller particle with rougher and more porous surfaces. These characteristics contributed to its superior water absorption, resulting in significantly higher water-holding capacity and water swelling capacity compared to the EC-SDF, EX-SDF and B-SDF fibers (**Table 2**). The irregular shapes provide a greater surface area for interaction with water molecules. Moreover, the coarse surface may enhance emulsifying capacity (EC) by offering additional sites for interaction with oil droplets. Citric acid extraction primarily solubilizes pectin, moderately disrupting the matrix and preserving the fiber network-likely due to limited hydrolysis of polysaccharides [Maran *et al.*, 2017].

In contrast, the SDF preparation obtained with sodium hydroxide showed a highly fragmented and irregular structure (**Figure 3B**). At higher magnifications (1,000× and 7,000×), the surfaces appeared smoother and less porous, suggesting a reduction in structural integrity. Alkaline treatment resulted in intense fiber degradation, as evidenced by B-SDF significantly lower water swelling capacity (4.92 mL/g) and soluble dietary fiber content (41.03 g/100 g dm) compared to the other preparations (**Tables 1** and **2**). This reduction in functional properties is likely due to compromised fiber porosity and solubility. Furthermore, B-SDF exhibited the lowest oil-holding capacity

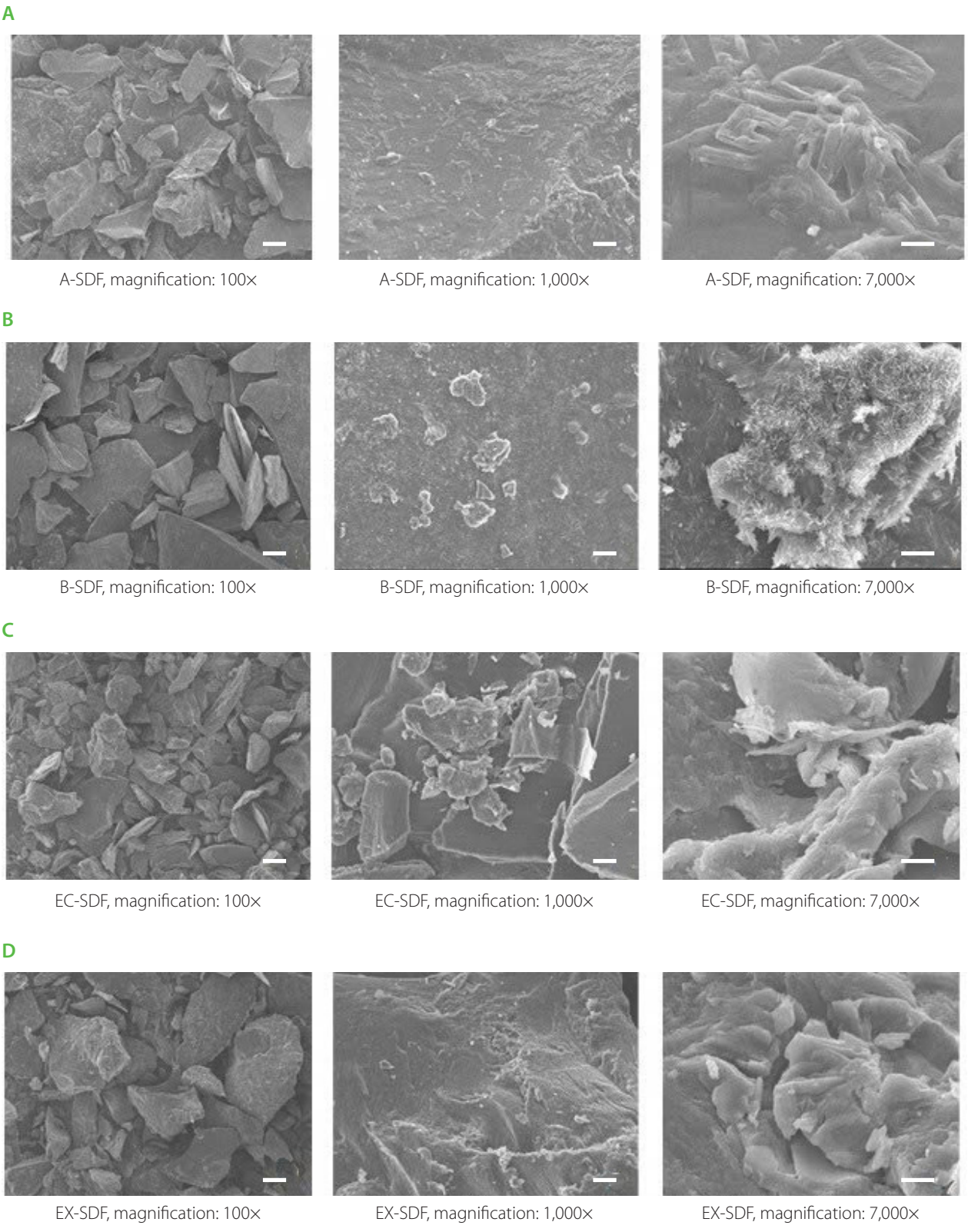

Figure 3. Scanning electron microscopy images of soluble dietary fiber preparations obtained from orange by-products by different methods including (**A**) acid extraction (A-SDF), (**B**) alkaline extraction (B-SDF), (**C**) cellulose-assisted extraction (EC-SDF), and (**D**) xylanase-assisted extraction (EX-SDF).

(1.34 g/g), which may be attributed to its smoother and more compact surface structure. Similar effects of alkaline degradation on fiber microstructure and functionality have also been reported by Ma & Mu [2016]. The SDF preparation obtained through cellulase hydrolysis exhibited a distinctly broken fibrous network, particularly evident at the 2 μm scale (**Figure 3C**). The enzymatic breakdown of cellulose resulted in enhanced surface roughness and increase porosity, which contributed to

better water absorption and water swelling capacity. Among all preparations, EX-SDF showed the most pronounced fiber disintegration. SEM images (**Figure 3D**) revealed a highly porous and irregular network formed by extensive hydrolysis, indicating the strong action of xylanase on hemicellulose. While the high porosity suggested potential for improved hydration and swelling, EX-SDF actually recorded the lowest WHC among all samples (**Table 2**). This paradox may be explained by excessive fiber breakdown and surface aggregation of small molecules, which reduce the effective surface area for water retention. Furthermore, the fragmented and disordered structure may have hindered oil binding and emulsification, due to the lack of continuous surface needed for stable interactions [Jia *et al*., 2019]. Interestingly, the fiber surface in EX-SDF also appeared denser in some regions with rounded voids, possibly resulting from the re-aggregation of degraded fragments into a more compact structure. This reorganization may have reduced water accessibility, thereby lowering the WHC of the enzyme-treated samples compared to the acid-treated ones (**Table 2**). Similarly, Song *et al*. [2021] reported that enzymatic modification can disrupt fiber structure and reduce WHC due to the breakdown of organized polysaccharide networks.

Thus, the morphological differences among SDF samples may be related to differences in their functional properties, including hydration, solubility, oil adsorption, and emulsifying behaviors. These findings align with previous reports that associate fiber porosity with water retention properties [Dong *et al*., 2020]. Based on the observed microstructural characteristics, acid extraction appears to be the most effective method for enhancing the hydration capacity of soluble dietary fiber.

CONCLUSIONS

The findings of this study demonstrate that the structural and functional properties of SDF extracted from *C. sinensis* peels vary significantly depending on the extraction method used, including acid, alkaline, and enzymatic treatments. Each method imparted distinct characteristics to the SDF preparations, highlighting their potential for tailored applications in food formulations. The choice of extraction method had a pronounced influence on fiber yield, structural morphology, and physicochemical properties. Among the approaches evaluated, the use of citric acid provided the highest extraction efficiency and superior water-holding and emulsifying properties, attributed to the increased porosity and solubility of the resulting SDF preparations. Alkaline extraction resulted in fiber with the highest crystallinity index, indicating a more ordered structure. Enzymatic treatments led to preparations with high oil holding capacity, but in general, these preparations showed variable properties depending on the enzyme used. The properties (WS, OHC, WSC, ES, CI) of the fiber produced by xylanase-assisted extraction were similar to those of fiber obtained under acidic conditions. These results underscore the specific advantages of each method depending on targeted application. The highest water-holding capacity and emulsion stability of citric acid-extracted fiber indicates its suitability for applications focused on moisture retention and emulsion stabilization. Future studies should explore the industrial-scale applications and focus on scaling up these extraction techniques and evaluating the nutritional functionalities, including especially the prebiotic potential of the resulting fiber. Ultimately, the optimized utilization of *C. sinensis* peels as a dietary fiber source offers a promising strategy for sustainable food production and agro-industrial waste valorization.

ACKNOWLEDGMENTS

This search supported by Ho Chi Minh City University of Industry and Trade, Vietnam and Institute of Food and Biotechnology of Can Tho University.

RESEARCH FUNDING

This work was financially supported by Ho Chi Minh City University of Industry and Trade under Contract no 20/HĐ-DCT dated January 17, 2025.

CONFLICTS OF INTERESTS

The authors declare no conflicts of interest.

ORCID IDs

H.C. Nguyen **https://orcid.org/0009-0001-7225-2341**
N.C. Tran **https://orcid.org/0009-0000-6755-3732**
T.T. Tran **https://orcid.org/0000-0002-5476-5098**

REFERENCES

1. Ani, P.N., Abel, H.C. (2018). Nutrient, phytochemical, and antinutrient composition of *Citrus maxima* fruit juice and peel extract. *Food Science and Nutrition*, *6*(3), 653–658. **https://doi.org/10.1002/fsn3.604**
2. AOAC International (2005). Official Methods of Analysis of AOAC International (18th ed.). Gaithersburg, MD, USA: AOAC International.
3. Berktas, S., Cam, M. (2025). Effects of acid, alkaline and enzymatic extraction methods on functional, structural and antioxidant properties of dietary fiber fractions from quince (*Cydonia oblonga* Miller). *Food Chemistry*, *464*(Part 1), art. no. 141596. **https://doi.org/10.1016/j.foodchem.2024.141596**
4. Bertin, C., Rouau, X., Thibault, J.F. (1988). Structure and properties of sugar beet fibres. *Journal of the Science of Food and Agriculture*, *44*(1), 15-29. **https://doi.org/10.1002/jsfa.2740440104**
5. Canela-Xandri, A., Balcells, M., Villorbina, G., Ángel Cubero, M., Canela-Garayoa, R. (2018). Effect of enzymatic treatments on dietary fruit fibre properties. *Biocatalysis and Biotransformation*, *36*(2), 172-179. **https://doi.org/10.1080/10242422.2017.1313836**
6. Carré, M.H., Haynes, D. (1922). The estimation of pectin as calcium pectate and the application of this method to the determination of the soluble pectin in apples. *Biochemical Journal*, *16*(1), 60-69. **https://doi.org/10.1042/bj0160060**
7. de Castro, S.C., Stanisic, D., Tasic, L. (2024). Sequential extraction of hesperidin, pectin, lignin, and cellulose from orange peels: towards valorization of agro-waste. *Biofuels, Bioproducts and Biorefining*, *18*(4), 804–817. **https://doi.org/10.1002/bbb.2606**
8. Dhingra, D., Michael, M., Rajput, H., Patil, R.T. (2012). Dietary fibre in foods: A review. *Journal of Food Science and Technology*, *49*(3), 255–266. **https://doi.org/10.1007/s13197-011-0365-5**
9. Dong, W., Wang, D., Hu, R., Long, Y., Lv, L. (2020). Chemical composition, structural and functional properties of soluble dietary fiber obtained from coffee peel using different extraction methods. *Food Research International*, *136*, art. no. 109497. **https://doi.org/10.1016/j.foodres.2020.109497**
10. Elleuch, M., Bedigian, D., Roiseux, O., Besbes, S., Blecker, C., Attia, H. (2011). Dietary fibre and fibre-rich by-products of food processing: Characterisation, technological functionality and commercial applications: A review. *Food Chemistry*, *124*(2), 411–421. **https://doi.org/10.1016/j.foodchem.2010.06.077**
11. FAO (2021). *Citrus Fruit Statistical Compendium 2020*. Food and Agriculture Organization of the United Nations: Rome, Italy.

12. Hassan, M., Berglund, L., Hassan, E., Abou-Zeid, R., Oksman, K. (2018). Effect of xylanase pretreatment of rice straw unbleached soda and neutral sulfite pulps on isolation of nanofibers and their properties. *Cellulose*, *25*(5), 2939–2953. **https://doi.org/10.1007/s10570-018-1779-2**
13. Huang, J.Y., Liao, J.S., Qi, J.R., Jiang, W.X., Yang, X.Q. (2021). Structural and physicochemical properties of pectin-rich dietary fiber prepared from citrus peel. *Food Hydrocolloids*, *110*, art. no. 106140. **https://doi.org/10.1016/j.foodhyd.2020.106140**
14. Huong, N.C., Nhan, T.C., Truc, T.T. (2024). A study on pretreatment conditions to obtain dietary fiber from sanh orange's by-products (*Citrus sinensis*). *Agriculture and Rural Development*, *1*, 23–31.
15. Jia, M., Chen, J., Liu, X., Xie, M., Nie, S., Chen, Y., Xie, J., Yu, Q. (2019). Structural characteristics and functional properties of soluble dietary fiber from defatted rice bran obtained through *Trichoderma viride*f ermentation. *Food Hydrocolloids*, *94*, 468–474. **https://doi.org/10.1016/j.foodhyd.2019.03.047**
16. Jiang, C.M., Liu, S.C., Wu, M.C., Chang, W.H., Chang, H.M. (2005). Determination of the degree of esterification of alkaline de-esterified pectins by capillary zone electrophoresis. *Food Chemistry*, *91*(3), 551-555. **https://doi.org/10.1016/j.foodchem.2004.10.003**
17. Jiang, Y., Yin, H., Zheng, Y., Wang, D., Liu, Z., Deng, Y., Zhao, Y. (2020). Structure, physicochemical and bioactive properties of dietary fibers from *Akebia trifoliate* (Thunb.) Koidz. seeds using ultrasonication/shear emulsifying/microwave-assisted enzymatic extraction. *Food Research International*, *136*, art. no. 109348. **https://doi.org/10.1016/j.foodres.2020.109348**
18. Kermani, Z., Shpigelman, A., Kyomugasho, C., Van Buggenhout, S., Ramezani, M., Van Loey, A.M., Hendrickx, M.E. (2014). The impact of extraction with a chelating agent under acidic conditions on the cell wall polymers of mango peel. *Food Chemistry*, *161*, 199–207. **https://doi.org/10.1016/j.foodchem.2014.03.131**
19. Liu, Y., Zhang, H., Yi, C., Quan, K., Lin, B. (2021). Chemical composition, structure, physicochemical and functional properties of rice bran dietary fiber modified by cellulase treatment. *Food Chemistry*, *342*, art. no. 128352. **https://doi.org/10.1016/j.foodchem.2020.128352**
20. Ma, M.M., Mu, T.H. (2016). Effects of extraction methods and particle size distribution on the structural, physicochemical, and functional properties of dietary fiber from deoiled cumin. *Food Chemistry*, *194*, 237–246. **https://doi.org/10.1016/j.foodchem.2015.07.095**
21. Makni, M., Jemai, R., Kriaa, W., Chtourou, Y., Fetoui, H. (2018). *Citrus limon* from Tunisia: Phytochemical and physicochemical properties and biological activities. *BioMed Research International*, *2018*, art. no. 625546. **https://doi.org/10.1155/2018/6251546**
22. Maran, J.P., Priya, B., Al-Dhabi, N.A., Ponmurugan, K., Moorthy, I.G., Sivarajasekar, N. (2017). Ultrasound assisted citric acid mediated pectin extraction from industrial waste of *Musa balbisiana*. *Ultrasonics Sonochemistry*, *35*(Part A), 204–209. **https://doi.org/10.1016/j.ultsonch.2016.09.019**
23. Marczak, A., Mendes, A.C. (2024). Dietary fibers: Shaping textural and functional properties of processed meats and plant-based meat alternatives. *Foods*, *13*(12), art. no. 1952. **https://doi.org/10.3390/foods13121952**
24. Nandi, I., Ghosh, M. (2015). Studies on functional and antioxidant property of dietary fibre extracted from defatted sesame husk, rice bran and flaxseed. *Bioactive Carbohydrates and Dietary Fibre*, *5*(2), 129–136. **https://doi.org/10.1016/j.bcdf.2015.03.001**
25. Navarro-González, I., García-Valverde, V., García-Alonso, J., Periago, M.J. (2011). Chemical profile, functional and antioxidant properties of tomato peel fiber. *Food Research International*, *44*(5), 1528–1535. **https://doi.org/10.1016/j.foodres.2011.04.005**
26. Núñez-Gómez, V., Jesús Periago, M., Luis Ordóñez-Díaz, J., Pereira-Caro, G., Manuel Moreno-Rojas, J., González-Barrio, R. (2024). Dietary fibre fractions rich in (poly)phenols from orange by-products and their metabolisation by *in vitro* digestion and colonic fermentation. *Food Research International*, 177, art. no. 113718. **https://doi.org/10.1016/j.foodres.2023.113718**
27. Qi, J., Yokoyama, W., Masamba, K.G., Majeed, H., Zhong, F., Li, Y. (2015). Structural and physico-chemical properties of insoluble rice bran fiber: Effect of acid–base induced modifications. *RSC Advances*, *5*(97), 79915–79923. **https://doi.org/10.1039/C5RA15408A**
28. Salem, K.S., Kasera, N.K., Rahman, M.A., Jameel, H., Habibi, Y., Eichhorn, S.J., French, A.D., Pal, L., Lucia, L.A. (2023). Comparison and assessment of methods for cellulose crystallinity determination. *Chemical Society Reviews*, *52*(18), 6417-6446. **https://doi.org/10.1039/d2cs00569g**
29. Sangnark, A., Noomhorm, A. (2003). Effect of particle sizes on functional properties of dietary fibre prepared from sugarcane bagasse. *Food Chemistry*, *80*(2), 221–229. **https://doi.org/10.1016/S0308-8146(02)00257-1**
30. Song, L.W., Qi, J.R, Liao, J.S, Yang, X.Q. (2021). Enzymatic and enzyme-physical modification of citrus fiber by xylanase and planetary ball milling treatment. *Food Hydrocolloids*, *121*, art. no. 107015. **https://doi.org/10.1016/j.foodhyd.2021.107015**
31. Tang, W., Lin, X., Walayat, N., Liu, J., Zhao, P. (2024). Dietary fiber modification: structure, physicochemical properties, bioactivities, and application – a review. *Critical Reviews in Food Science and Nutrition*, *64*(22), 7895–7915. **https://doi.org/10.1080/10408398.2023.2193651**
32. Teigiserova, D.A., Tiruta-Barna, L., Ahmadi, A., Hamelin, L., Thomsen, M. (2021). A step closer to circular bioeconomy for citrus peel waste: A review of yields and technologies for sustainable management of essential oils. *Journal of Environmental Management*, *280*, art. no. 111832. **https://doi.org/10.1016/j.jenvman.2020.111832**
33. Tejada-Ortigoza, V., Garcia-Amezquita, L.E., Serna-Saldívar, S.O., Welti-Chanes, J. (2016). Advances in the functional characterization and extraction processes of dietary fiber. *Food Engineering Reviews*, *8*(3), 251–271. **https://doi.org/10.1007/s12393-015-9134-y**
34. Viera, R.G., Rodrigues Filho, G., de Assunção, R.M., Meireles, C.D.S., Vieira, J.G., de Oliveira, G.S. (2007). Synthesis and characterization of methylcellulose from sugar cane bagasse cellulose. *Carbohydrate Polymers*, *67*(2), 182–189. **https://doi.org/10.1016/j.carbpol.2006.05.007**
35. Wang, L., Xu, H., Yuan, F., Fan, R., Gao, Y. (2015). Preparation and physicochemical properties of soluble dietary fiber from orange peel assisted by steam explosion and dilute acid soaking. *Food Chemistry*, *185*, 90-98. **https://doi.org/10.1016/j.foodchem.2015.03.112**
36. Wang, S., Fang, Y., Xu, Y., Zhu, B., Piao, J., Zhu, L., Wu, J. (2022). The effects of different extraction methods on physicochemical, functional and physiological properties of soluble and insoluble dietary fiber from *Rubus chingii* Hu. fruits. *Journal of Functional Foods*, *93*, 105081. **https://doi.org/10.1016/j.jff.2022.105081**
37. Weightman, R.M., Renard, C.M.G.C., Gallant, D.J., Thibault, J.F. (1995). Structure and properties of the polysaccharides from pea hulls – II. Modification of the composition and physico-chemical properties of pea hulls by chemical extraction of the constituent polysaccharides. *Carbohydrate Polymers*, *26*(2), 121-128. **https://doi.org/10.1016/0144-8617(94)00102-Y**
38. Yan, X., Ye, R., Chen, Y. (2015). Blasting extrusion processing: The increase of soluble dietary fiber content and extraction of soluble-fiber polysaccharides from wheat bran. *Food Chemistry*, *180*, 106–115. **https://doi.org/10.1016/j.foodchem.2015.01.127**
39. Yoon, K.Y., Cha, M., Shin, S.R., Kim, K.S. (2005). Enzymatic production of a soluble-fibre hydrolyzate from carrot pomace and its sugar composition. *Food Chemistry*, *92*(1), 151-157. **https://doi.org/10.1016/j.foodchem.2004.07.014**
40. Zhang, W., Zeng, G., Pan, Y., Chen, W., Huang, W., Chen, H., Li, Y. (2017). Properties of soluble dietary fiber-polysaccharide from papaya peel obtained through alkaline or ultrasound-assisted alkaline extraction. *Carbohydrate Polymers*, *172*, 102–112. **https://doi.org/10.1016/j.carbpol.2017.05.030**
41. Zhang, Y., Liao, J., Qi, J. (2020). Functional and structural properties of dietary fiber from citrus peel affected by the alkali combined with high-speed homogenization treatment, *LWT – Food Science and Technology*, *128*, art. no. 109397. **https://doi.org/10.1016/j.lwt.2020.109397**
42. Zhao, X., Liu, Y., Huang, X., Cui, C., Wang, W. (2025). Enhancing functionality of citrus fibers from peel and pulp pomace via combined alkaline hydrogen peroxide and xylanase modification. *Food Hydrocolloids*, *168*, art. no. 111526. **https://doi.org/10.1016/j.foodhyd.2025.111526**
43. Zheng, Y., Li, Y. (2018). Physicochemical and functional properties of coconut (*Cocos nucifera* L) cake dietary fibres: Effects of cellulase hydrolysis, acid treatment and particle size distribution. *Food Chemistry*, *257*, 135–142. **https://doi.org/10.1016/j.foodchem.2018.03.012**

ORIGINAL ARTICLE
http://journal.pan.olsztyn.pl

Polish Journal of Food and Nutrition Sciences
2025, Vol. 75, No. 3, 245–260
DOI: 10.31883/pjfns/208802
ISSN 1230-0322, e-ISSN 2083-6007

Functional Olive Oils Infused with Mediterranean Herbs Enhance Cheese Preservation and Nutritional Profile

Souha Ammar[1], Hamza Gadhoumi[2], Nejia Farhat[1], Asma Mejri[1], Salma Nait-Mohamed[1], Kamel Hessini[3], Moufida Saidani Tounsi[2], Nabil Ben Youssef[1], Fethi Ben Slama[4,5], Hedia Manai-Djebali[1]*

[1]Laboratory of Olive Biotechnology, LR15CBBC05, Biotechnology Center of Borj-Cedria, BP 901, 2050, Hammam-Lif, Tunisia
[2]Laboratory of Medicinal and Aromatic Plants, LR15CBBC06, Biotechnology Center of Borj-Cedria, BP 901, 2050, Hammam-Lif, Tunisia
[3]Department of Biology, College of Sciences, Taif University, P.O. Box 11099, Taif, 21944, Saudi Arabia
[4]Department of Nutrition, Higher School of Health Sciences and Techniques of Tunis, 4021 Tunis, Tunisia
[5]Biochemistry and Biotechnology Research Laboratory, LR01ES05, Faculty of Sciences of Tunis, 2092 Manar II, Tunis, Tunisia

The demand for functional foods has driven research into bioactive-enriched dietary products. In this study, olive oil was enriched with phenolic-rich herbs, including oregano, rosemary, basil, and thyme, using an optimized ultrasound-assisted extraction (UAE) process. The resulting infused oils were evaluated for their phenolic content, antioxidant capacity, oxidative stability, and effects on cheese preservation. Rosemary-infused oil exhibited the highest total phenolic content (556.1 mg GAE/kg) and oxidative stability in the Rancimat test (induction time of 82.25 h), while oregano- and basil-infused oils had the strongest DPPH radical scavenging capacity (IC_{50} of 2.36–2.38 mg/mL). Cheese stored in these plant-infused oils showed reduced lipid oxidation and microbial growth over 21 days. The lowest content of thiobarbituric acid reactive substances (TBARS) was recorded in the cheese immersed in rosemary- and thyme-infused oils (0.53 and 0.66 mg MDA/kg cheese, respectively); whereas the untreated cheese had TBARS value of 2.98 mg MDA/kg cheese. Microbiological analysis revealed a reduction in counts of coliforms and yeasts and molds, particularly in the cheese treated with oregano- and basil-infused oils. These results highlight the potential of bioactive-enriched olive oils as natural preservatives and functional ingredients, extending cheese shelf life while enhancing its nutritional value. This study provides a foundation for developing innovative functional foods that integrate plant-derived antioxidants and antimicrobials into widely consumed products.

Keywords: cheese, functional food, medicinal plants, oil enrichment

INTRODUCTION

The concept of functional foods, *i.e.*, foods that offer additional health benefits besides providing basic nutrients, has gained widespread attention in recent years due to the increasing consumer demand for health-promoting and disease-preventing dietary products [Deshmukh & Gutte, 2024]. Dairy products, especially cheese, are among the most widely consumed foods due to their rich nutrient profile, including proteins, calcium and vitamins [Araujo *et al*., 2024]. The incorporation of bioactive ingredients into cheese can enable the development of new functional foods, products with improved nutritional properties and adapted to contemporary dietary trends.

The traditional high-fat diet, often characterized by high levels of unhealthy fats and sugars, has been implicated in causing various health issues, including obesity, metabolic disorders, and cardiovascular diseases [Navarro *et al*., 2024]. In contrast, emerging dietary approaches emphasize a healthier high-fat paradigm, focusing on high-fat products, such as extra virgin

***Corresponding Author:**
tel.: +216 79 325 855; fax: +216 79 325 638; e-mail: **hedia_manai@yahoo.fr / Hedia.Manai@cbbc.rnrt.tn** (Dr. H. Manai-Djebali)

Submitted: 16 March 2025
Accepted: 30 July 2025
Published on-line: 13 August 2025

olive oil containing omega-3 fatty acids and natural bioactive compounds such as phenolics [Tsimihodimos & Psoma, 2024]. These compounds have been shown to elicit numerous health benefits due to anti-inflammatory, antioxidant, and cardiovascular protective effects [Gabbia, 2024]. The diet with extra virgin olive oil promotes better metabolic health, improves energy balance, and protects against the adverse effects of traditional high-fat diets [Tsimihodimos & Psoma, 2024].

Oregano (*Origanum vulgare* L.), rosemary (*Rosmarinus officinalis* L.), basil (*Ocimum basilicum* L.), and thyme (*Thymus vulgaris* L.) are aromatic herbs widely known for their high content of phenolic compounds and essential oils, which exhibit strong antioxidant, antimicrobial, and anti-inflammatory activities [Delgado *et al*., 2023; Nieto, 2020; Zhakipbekov *et al*., 2024]. These herbs have traditionally been used in Mediterranean cuisine, and their integration into food products has gained scientific attention for their ability to enhance both flavor and health benefits [Delgado *et al*., 2023]. The enrichment of olive oil with these herbs has been shown to extend its shelf life and improve its bioactive properties [Barreca *et al*., 2021; Özcan *et al*., 2022; Yfanti *et al*., 2024]. This enrichment is most often performed by maceration of herbs in oil. The additional use of advanced techniques, such as ultrasound assistance, allows for the extraction of higher levels of bioactive compounds. Ultrasound treatment is known to improve the extraction efficiency by disrupting the plant cell walls, thereby enhancing the transfer of phenolic compounds and essential oils into the olive oil matrix [Ioannis *et al*., 2024].

In the context of functional foods, combining enriched olive oil with cheese presents a novel approach to creating a product that not only provides essential nutrients but also elicits enhanced health benefits. Cheese is an excellent vehicle for delivering bioactive compounds, as its fat matrix can effectively encapsulate and preserve these compounds during storage. Additionally, the inclusion of herbs with antimicrobial properties in the olive oil may contribute to the microbial stability of cheese, extending its shelf life without the need for artificial preservatives. This is particularly relevant for fresh cheeses, which are more susceptible to microbial spoilage due to their higher moisture content [Klisović *et al*., 2022].

This study focused on enriching extra virgin olive oil with phenolic-rich Mediterranean herbs, namely oregano, rosemary, basil, and thyme, and assessing the functional properties of the resulting formulations. The enriched oils were evaluated for their phenolic content, antioxidant capacity, and key quality parameters. In the second stage of the study, these bioactive oils were used to preserve fresh cheese, with particular attention given to their ability to preserve the product's physicochemical quality and microbiological safety during 21 days of storage. By determining phenolic content, antioxidant potential, and quality of herb-infused oils, as well as tracking changes in the nutritional value and oxidative and microbial stability of cheeses, we aimed to demonstrate the functional value of herb-infused oils as natural preservatives and carriers of health-promoting compounds in dairy applications.

MATERIAL AND METHODS

Materials

Oregano (*Origanum vulgare* L.), rosemary (*Rosmarinus officinalis* L.), basil (*Ocimum basilicum* L.), and thyme (*Thymus vulgaris* L.), were commercially sourced from the Tunisian market. The plant materials were dried in an amber environment at 30 ±2°C for 24 h.

The Tunisian Chétoui variety of olive, harvested during the 2023–2024 season at the experimental station of the Centre of Biotechnology of Borj-Cédria was used to obtain olive oil.

Fresh milk for cheese production was sourced from a local farm in Soliman, Tunisia. Its physicochemical parameters determined using a Lactoscan SP milk analyzer (Milkotronic Ltd., Nova Zagora, Bulgaria) were provided by the supplier, including: lipid content (32.46±2.15 g/L), protein content (31.94±1.06 g/L), lactose content (45.80±2.76 g/L), salt content (5.66±0.53 g/L), and density (1.08±0.01 g/mL). All values were reported as mean ± standard deviation (n=3).

Preparation of plant extracts

Each plant was ground to fine powder (20 µm) using a knife mill Grindomix GM 200 (Retsch, Haan, Germany), and then 2 g of the powder was mixed with 20 mL of 80% (*v/v*) methanol solution. The resulting mixtures were subjected to ultrasound-assisted extraction using a sonication bath (Sonoxer DIGIPLUS DL 102 H, Bandelin Electronics GmbH & Co. KG, Berlin, Germany, 40 kHz frequency) for 15 min at 100% ultrasonic power corresponding to 120 W, with the temperature maintained at 40°C [Manai-Djebali *et al*., 2024]. After extraction, the samples were centrifuged at 5,000 rpm (2,795×*g*) for 15 min, and the supernatants were collected. The solvents were subsequently removed from the supernatants using a rotary evaporator (Buchi Rotavapor R-200, Flawil, Switzerland) under reduced pressure (237 mbar) at 40°C until complete evaporation was achieved. Extraction was performed in triplicate.

Determination of contents of total phenolics, total flavonoids, and condensed tannins of plants

Total phenolic content (TPC) was determined using the spectrophotometric method with the Folin-Ciocalteu reagent according to the procedure described by Habachi *et al*. [2022]. A 125 µL aliquot of dissolved extract (10 µg/mL in methanol 80%, *v/v*) was mixed with 500 µL of distilled water and 125 µL of the Folin-Ciocalteu reagent. After 3 min of agitation at 150 rpm, 1,250 µL of a 7% Na_2CO_3 solution was added, and the volume was adjusted to 3 mL with distilled water. The reaction mixture was incubated for 1.5 h in the dark at ambient temperature, and the absorbance was measured at 760 nm. TPC was expressed in mg of gallic acid equivalent (GAE) *per* g of plant dry matter (DM). Measurement was performed in triplicate.

Condensed tannins (CT) were quantified using the vanillin method [Habachi *et al*., 2022]. A volume of 25 µL of extract solution (10 µg/mL in methanol 80%, *v/v*) was mixed with 1,500 µL of a 4% vanillin solution and 750 µL of HCl, and the mixture was incubated for 15 min in the dark. Absorbance was measured at 500 nm. Tannin content was expressed in mg of catechin

equivalent (CE) *per* g of plant DM for each of the three replicates performed.

The total flavonoid content (TFC) was quantified based on the formation of a stable complex between aluminum chloride and flavonoids. Assay was carried out according to the procedure described by Habachi *et al*. [2022] in triplicate. A total of 250 µL of dissolved extract (1 mg/mL) was mixed with 75 µL of a 5% $NaNO_2$ solution and incubated for 6 min in the dark. Following the addition of 150 µL of a 10% $AlCl_3$ solution and 500 µL of a 1 M NaOH solution, the mixture was adjusted to 2.5 mL with distilled water. Absorbance was read at 510 nm, and TFC was expressed in mg of quercetin equivalent *per* g of plant DM.

Determination of composition of phenolics and other compounds in plants by high-performance liquid chromatography

The content of individual phenolic compounds and some volatile compounds of plant extracts was determined using a high-performance liquid chromatography (HPLC) system (Agilent 1260, Agilent Technologies, Santa Clara, CA, USA) equipped with a diode array detector (DAD). Chromatographic separation was performed on a Hypersil ODS-C18 column (4.6×100 mm, 0.5 µm; Agilent Technologies), maintained at 25°C. The mobile phase consisted of HPLC water with 0.2% (*v/v*) formic acid (solvent A) and acetonitrile (solvent B), delivered at a flow rate of 0.7 mL/min according to a gradient program: 35% (*v/v*) solvent B for 0–7 min, 60% (*v/v*) solvent B for 7–10 min, 80% (*v/v*) solvent B for 10–15 min, 100% solvent B for 15–26 min, and back to 35% (*v/v*) solvent B for 26–31 min. An injection volume of 10 µL was used. Individual compounds were identified by comparing their retention times and DAD spectral profiles (characteristic absorption maxima) with those of authentic standards. Quantification was performed using calibration curves constructed from authentic standards, with peak areas at 280 nm plotted against known concentrations. Results were expressed in mg *per* g of dry extract (DE).

Determination of antioxidant activity of plant extracts

Antioxidant activity was evaluated using the assay with 2,2-diphenyl-1-picrylhydrazyl (DPPH) radical [Brand-Williams *et al*., 1995]. A solution of 10 mg of DPPH radical in 120 mL of methanol was prepared. The reaction was started by mixing 500 µL of this solution with 500 µL of extract solution in 80% (*v/v*) methanol at various concentrations (10–100 µg/mL) and was continued in the dark for 30 min, followed by absorbance measurement at 517 nm. The percentage inhibition of DPPH radicals was calculated using Equation (1):

$$\text{Inhibition (\%)} = [(A_{control} - A_{sample}) / A_{control}] \times 100 \quad (1)$$

where: $A_{control}$ is the absorbance of the DPPH radical solution without the extract, and A_{sample} is the absorbance of the DPPH radical solution with the extract. The IC_{50}, defined as the concentration of extract (µg/mL) required to inhibit 50% of the DPPH radicals, was determined by interpolation of the plotted curve of % inhibition against extract concentration.

The reducing power was evaluated using the potassium ferricyanide assay according to the procedure described by Yeddes *et al*. [2019]. A volume of 1 mL of each extract solution at concentrations of 50, 100, 200, 400, and 800 µg/mL, prepared in 80% (*v/v*) methanol, was mixed with 0.2 M phosphate buffer (pH 6.6) and a 1% $K_3Fe(CN)_6$ solution in a ratio of 1:1:1 (*v/v/v*), incubated at 50°C for 20 min, and then 1 mL of a 10% trichloroacetic acid solution was added. The absorbance was read at 700 nm, and the concentration of extract producing an absorbance of 0.5 ($A_{0.5}$) was calculated using an absorbance against extract concentration curve.

Measurements were performed in triplicate.

Preparation of plant-infused oils

To prepare plant-infused oils, each dried plant material (10 g) was macerated in oil (100 mL) and the process of transferring lipid-soluble compounds from plant to oil was assisted by ultrasound using a sonication bath (Sonoxer DIGIPLUS DL 102 H, 40 kHz frequency). The sonication power of 40%, 60%, and 80%, corresponding to 48 W, 72 W, and 96 W, and maceration time of 5 min, 15 min, and 20 min were used. The temperature of the bath was maintained at 70°C [Manai-Djebali *et al*., 2024]. After the sonication process, the mixtures were centrifuged at 4,000 rpm (1,789×*g*) for 15 min to remove plant residues. The supernatant oils were collected and stored at 4°C for further analysis.

Determination of oil quality indices

Free acidity, expressed as a percentage of oleic acid, was determined by titrating an olive oil sample dissolved in a neutralized ether-ethanol mixture with sodium hydroxide. The peroxide value (PV) was measured by reacting the oil with potassium iodide, followed by titration with sodium thiosulfate. PV was expressed as milliequivalents of active oxygen (meq O_2) *per* kg of oil. Specific extinction coefficients, K_{232}, K_{264}, K_{268}, and K_{272}, indicating oil oxidation levels, were evaluated by measuring absorbance at 232 nm, 264 nm, 268 nm, and 272 nm, respectively, of a 1% (*w/v*) oil solution in cyclohexane using a 1 cm pathlength cuvette. The variation in specific extinction (ΔK) was calculated using Equation (2):

$$\Delta K = K_{268} - (K_{264} + K_{272})/2 \quad (2)$$

All these indices were determined according to the official methods of the International Olive Council [IOOC, 2024].

The bitterness index (K_{225}) was assessed *via* UV spectrophotometry by extracting the polar fraction from 1 g of olive oil dissolved in 5 mL of hexane using 5 mL of 60% (*v/v*) methanol in water. The mixture was vortexed for 2 min and centrifuged at 3,000 rpm (1,370×*g*) for 5 min. The polar fraction was collected, and its absorbance was measured at 225 nm in a 1 cm pathlength cuvette, with K_{225} reported as the absorbance value [Inarejos-Garcia *et al*., 2009]. All measurements were performed in triplicate.

Determination of pigment content in oils

To determine the content of chlorophylls and carotenoids, a 1.5 g olive oil sample was mixed with 5 mL of cyclohexane, and the absorbance was read at 470 nm (A_{470}) and 670 nm (A_{670}). The content of chlorophylls and carotenoids (mg/kg) was calculated using Equation (3) and Equation (4), respectively [Jebabli *et al*., 2020].

$$\text{Chlorophyll content} = \frac{A_{670} \times 10^6}{613 \times d \times 100} \quad (3)$$

$$\text{Carotenoid content} = \frac{A_{470} \times 10^6}{2{,}000 \times d \times 100} \quad (4)$$

where: 613 and 2,000 are the specific extinction coefficients (L/(g×cm)) for chlorophylls and carotenoids, respectively; d is the spectrophotometer cell thickness (1 cm); and 100 is a factor accounting for the dilution of the oil (1.5 g in 5 mL cyclohexane, equivalent to 300 g/L) and unit conversion to mg/kg. Both determinations were performed in triplicate.

Determination of oil phenolic compound content

Oils were extracted following the method of Jebabli *et al*. [2020]. In a 50 mL tube, 2.5 g of olive oil was dissolved in 5 mL of hexane. After agitation, 5 mL of a methanolic solution (60:40 methanol/water, *v/v*) was added, and the mixture was agitated for 2–3 min. The solution was centrifuged at 3,500 rpm (1,370×*g*) for 10 min, and the polar phase was transferred to another tube for analysis of the TPC, TFC and content of CT. The determinations were carried out according to the procedures described above, the same as those used for the analysis of phenolic compounds of plants, and results were expressed in mg GAE/kg oil, mg QE/kg oil, and mg CE/kg oil, respectively.

Determination of antioxidant activity of oils

The antioxidant activity of the olive oil samples was assessed using the DPPH assay, adapted from the method of Christodouleas *et al*. [2014] with modification. Olive oil (100 mg) was mixed with 2,000 µL of isopropanol, vigorously vortexed for 1 min to ensure homogeneity, and diluted in isopropanol to obtain a stock solution of 50 mg/mL. This stock solution was further diluted in isopropanol to achieve concentrations ranging from 2 to 50 mg/mL. A DPPH radical solution was prepared by dissolving 10 mg of DPPH in 120 mL of isopropanol, freshly prepared to ensure radical stability. Each assay tube contained 1,000 µL of the diluted oil solution and 500 µL of the DPPH solution, mixed thoroughly and incubated in the dark for 30 min at room temperature. The absorbance was measured at 517 nm using a UV-Vis spectrophotometer. The percentage inhibition of DPPH radicals was calculated using Equation (1). The IC_{50}, defined as the oil concentration (mg/mL) required to inhibit 50% of the DPPH radicals, was determined by plotting % inhibition against the oil concentration curve. Measurement was performed in triplicate.

Determination of fatty acid composition of oils

The fatty acid composition of olive oil was analyzed using gas chromatography with flame ionization detection (GC-FID) on an Agilent 7890B GC System (Agilent Technologies). Fatty acid methyl esters (FAMEs) were prepared from 0.1 g of olive oil by adding 1 mL of a methanol solution containing 2 M potassium hydroxide. The mixture was vortexed for 30 s and allowed to react at room temperature for 30 min, as *per* the International Olive Council method [IOOC, 2024]. Subsequently, 1 mL of hexane was added to extract the FAMEs, the mixture was vortexed again, and the phases were separated. The hexane layer containing the FAMEs was collected. For GC-FID analysis, an HP-INNOWax capillary column (30 m × 0.25 mm, 0.25 µm film thickness; Agilent Technologies) was used. The injector was maintained at 250°C, and the detector at 300°C. A temperature program was applied, starting at 140°C (held for 5 min), ramping at 4°C/min to 240°C (held for 10 min). Helium was used as the carrier gas at a flow rate of 1 mL/min. A 1-µL sample of the hexane extract was injected, and the FID response was monitored for peak identification based on retention times compared to standard FAMEs. Results were expressed as a percentage of total fatty acids. Analysis was performed in triplicate.

Analysis of volatile compounds of oils

Volatile compounds of the oils were extracted using headspace solid-phase micro-extraction (HS-SPME) and analyzed by gas chromatography-mass spectrometry (GC-MS) according to the method of Haddada *et al*. [2007]. A SPME unit with a divinylbenzene/carboxen/polydimethylsiloxane (DVB/CAR/PDMS) 1 cm, 50/30 µm fiber (Agilent Technologies) was used to adsorb volatile compounds from the headspace of a 20-mL vial containing 5±0.01 g of olive oil, equilibrated for 2 h at 50±2°C. After equilibrium, the SPME fiber was exposed to the headspace for 30 min to adsorb volatile compounds. The fiber was then transferred to the injection port of an Agilent 7890A/5977 GC-MS system for desorption for over 3 min. Volatile compound analysis was conducted using an HP-5MS capillary column (30 m × 0.25 mm, 0.25 µm film thickness; Agilent Technologies), with an injector temperature of 250°C and a transfer line temperature of 220°C. The temperature program ranged from 60°C to 200°C at a rate of 5°C/min. Helium was used as the carrier gas at a flow rate of 1.7 mL/min, and the injection was performed in the splitless mode. Mass spectra of detected compounds were compared to those in the Wiley Registry 9th Edition (Wiley 09) and National Institute of Standards and Technology (NIST 2011) spectral libraries using OpenLab Agilent software (Agilent Technologies). Compounds were identified based on a similarity index greater than 80% with a scan time of 1 s and a mass range of 30–500 *m/z*. Volatile compound contents were expressed as relative percentages (% of total volatile compounds), based on the integrated peak areas from the total ion chromatogram (TIC), without external calibration. Analysis was performed in triplicate.

Oil oxidative stability analysis

The Rancimat test was used to assess the oxidative stability of olive oils. It was performed using a Rancimat 679 device (Metrohm Co., Basel, Switzerland) according to the procedure approved by the International Organization for Standardization (ISO) No. 6886:2016 [ISO, 2016], with analyses conducted in duplicate. Oil (3 g) was placed into a designated cylindrical vessel. The sample was exposed to an airflow of 10 L/h and heated to 100°C. The volatile compounds released during oxidation were collected in 65 mL of distilled water. Proper glassware cleaning was essential before use: the conductivity cell and electrodes were carefully cleaned, dried at 80°C, and soaked overnight in a detergent solution before being rinsed sequentially with running water, acetone, and distilled water. Induction time was determined based on conductivity measurement and oxidative stability index (day/kg) was calculated using Equation (5):

$$\text{Oxidative stability} = (h \times 1{,}000) / (W \times 24) \quad (5)$$

where: h is induction time (h) and W is oil weight (g).

Cheese production

The production process began with milk pasteurization at 80°C for 15 min to eliminate pathogenic microorganisms and ensure the microbiological safety of the final product. Following pasteurization, the milk was cooled to 37°C and coagulated using 0.03% rennet (MAFI-MIC 15, Tunis, Tunisia), a natural coagulant, leading to the formation of a homogeneous and smooth curd. The curd was cut into small pieces to facilitate whey drainage. The fragmented curd was transferred into plastic molds and allowed to undergo spontaneous whey expulsion for 24 h at 20°C, contributing to the final texture and consistency of the cheese. Three batches were prepared for each cheese type. After complete drainage, the fresh cheese was cut into cubes of 1×1×1 cm using a stainless-steel knife, and the freshly cut cubes were immersed in olive oil or plant-infused oils. This procedure aimed to enrich the cheese with antioxidants while improving its sensory profile and shelf-life stability. The immersion process was conducted under controlled conditions (24 h at 4°C). Following immersion, the cheese samples were drained and used for analyses.

Nutritional composition analysis of cheese

The nutritional composition of the cheese was determined by analyzing its water, lipid, protein, and reducing sugar contents, along with its total energy value. Water content was determined by oven drying, where 2 g of cheese was weighed, dried at 105°C for 24 h until constant weight, and the weight loss was calculated as water content (g/100 g cheese). Lipids were determined by homogenizing 1 g of cheese with 10 mL of hexane, followed by centrifugation at 3,500 rpm (1,370×*g*) for 10 min and solvent evaporation from the extract. The lipid residue was weighed to calculate lipid content, expressed in g/100 g cheese. For protein determination, 1 g of cheese was homogenized in 10 mL of 0.1 M phosphate buffer (pH 7.0) and centrifuged at 3,500 rpm (1,370×*g*) for 10 min. Proteins in the supernatant were quantified using the Bradford assay with bovine serum albumin (BSA) as the standard, measuring absorbance at 595 nm [Bradford, 1976]. Protein content was expressed in g/100 g cheese. Reducing sugars, as a proxy for carbohydrate content, were assessed by homogenizing 1 g of cheese in 10 mL of 0.1 M phosphate buffer (pH 7.0), followed by centrifugation at 3,500 rpm (1,370×*g*) for 10 min. A 1 mL aliquot of the supernatant was mixed with 1 mL of 3,5-dinitrosalicylic acid (DNS) reagent, heated at 100°C for 5 min, cooled, and diluted to 10 mL with distilled water [Miller, 1959]. Absorbance was measured at 540 nm, and reducing sugar content was expressed as glucose equivalents in g/100 g cheese. The total energy value (kcal/100 g) was calculated using Equation (6):

$$\text{Energy value} = (\text{Protein} \times 4) + (\text{Lipids} \times 9) + (\text{Carbohydrates} \times 4) \quad (6)$$

Determination of cheese stability during storage

Oxidative stability

Lipid oxidation stability of cheese samples was assessed by measuring content of thiobarbituric acid reactive substances (TBARS) during storage at 4°C for 21 days. Samples (4 g) were collected on days 1, 7, 14, and 21 and mixed with 10 mL of a 10% (*w/v*) trichloroacetic acid (TCA) solution [Antonino *et al.*, 2025]. The mixture was vortexed for 5 min. Subsequently, 5 mL of a 0.02 M thiobarbituric acid (TBA) solution was added, and the mixture was vortexed again. The mixture was centrifuged at 14,000×*g* for 10 min. The supernatant was filtered through 0.45 µm nylon filters and incubated in a thermostat bath at 100°C for 30 min. After cooling, absorbance was measured at 532 nm. The TBARS content was quantified using a calibration curve for malondialdehyde (MDA), and results were expressed as mg MDA *per* kg of cheese. Three samples for each time point were analyzed.

Microbiological stability

Microbiological stability of cheese was evaluated over three weeks by monitoring total aerobic mesophilic bacteria, coliforms, lactic acid bacteria, yeasts, and molds. Cheese samples (1 g) were homogenized in physiological saline, serially diluted, and plated on selective media: plate count agar (30°C) for mesophilic bacteria, De Man–Rogosa–Sharpe (MRS) agar (37°C) for lactic acid bacteria, Sabouraud agar (37°C) for yeasts and molds, and violet red bile lactose (VRBL) agar (30°C) for coliforms [Garofalo *et al.*, 2024]. Colony counts were expressed as log CFU/g of cheese after incubation under optimal conditions for each microorganism.

Statistical analysis

The quantitative data on plants, olive oils and cheeses were expressed as the mean and standard deviation. Their statistical analysis was conducted using the Statistical Package for Social Sciences (SPSS) software, version 24 (IBM Corp., Armonk, NY, USA, 2016). The analysis of variance (ANOVA) was performed. The Newman-Keuls post hoc test was employed to determine

significant differences between groups. Statistical significance was established at $p<0.05$.

RESULTS AND DISCUSSION

Content of phenolics of different classes in plants

The TPC, TFC and CT content in the oregano, rosemary, basil and thyme are summarized in **Table 1**. The analyses revealed different contents of distinct classes of phenolics of these four plants. Oregano exhibited the highest TPC (9.39 mg GAE/g DM). Both, basil and oregano were the richest in flavonoids (TFC of 9.42–8.46 mg QE/g DM). On the other hand, basil had a significantly ($p<0.05$) lower CT content (1.32 mg CE/g DM) compared to the other plants (1.37–1.40 mg CE/g DM). Oregano stood out for its high phenolic content, which aligned with findings from a previous study that also highlighted a strong antioxidant potential of this plant, making it a valuable ingredient in functional food applications [Mateus *et al*., 2024]. Basil, with its elevated flavonoid levels, may provide significant anti-inflammatory, antioxidant, and antimicrobial properties, as basil flavonoids are well-known for their ability to scavenge free radicals, modulate enzyme function, and inhibit inflammatory mediators [Kamelnia *et al*., 2023]. This makes basil a promising candidate for use in health products targeting chronic inflammation and oxidative stress-related conditions. In turn, the presence of condensed tannins in plants may be responsible for their antioxidant and antimicrobial properties [Fraga-Corral *et al*., 2021]. Tannins are associated with plant defence mechanisms and could be conventionally used for food preservation. The differences in phenolic profiles among these plants underline the importance of plant species selection depending on the desired health benefits or functional properties in product formulation.

Composition of phenolics and other compounds in plant extracts determined by high-performance liquid chromatography

The studied plants exhibited distinct contents of individual phenolics and some volatile compounds (**Table 2**). Among phenolics, oregano, rosemary and basil were particularly rich in rosmarinic acid with contents of 20.25, 15.30, and 12.11 mg/g dry extract (DE), respectively. The findings were consisted with literature data that indicates rosmarinic acid and its methyl ester as main phenolic compounds of these plants [Mateus *et al*., 2024; Popescu *et al*., 2023; Yeddes *et al*., 2019]. Additionally, the rosemary extract had a high content of carnosic acid (24.53 mg/g DE) and carnosol (5.05 mg/g DE), which were absent in the other plant extracts. These volatile compounds, widely studied for their antioxidant properties, contribute to the efficacy of rosemary in various therapeutic and food applications [Habtemariam, 2023]. Caffeic acid was identified in all extracts, with the highest content determined in oregano (5.02 mg/g DE). Ferulic acid and *p*-coumaric acid were also abundant in the oregano extract, at 4.21 and 3.11 mg/g DE, respectively. Flavonoids, such as luteolin and apigenin, were detected in all plant extracts. The content of the former was significantly ($p<0.05$) higher in thyme and rosemary extracts (2.20–2.56 mg/g DE) than in the remaining plants, while the content of the latter in oregano, rosemary and basil extracts (0.79–0.94 mg/g DE) significantly ($p<0.05$) exceeded its content in the thyme extract. The thyme extract stood out due to its high content of thymol (25.51 mg/g DE) and carvacrol (15.21 mg/g DE), two its well-known volatile compounds with antimicrobial and antioxidant activities [Nieto, 2020]. Rosemary and thyme extracts were also rich in chlorogenic acid, whereas the basil extract lacked this compound. The basil extract contained significant amounts of chicoric acid (7.17 mg/g DE), which was absent in the other plants analyzed. In contrast, a previous study by Popescu *et al*. [2023] reported a lower chicoric acid content of 1.30 mg/g in basil extract dry weight, possibly due to differences in extraction methods, basil cultivars, or growing conditions.

Antioxidant activity of plant extracts

The results in **Table 1** highlight the antioxidant activity of rosemary, thyme, basil, and oregano extracts, evaluated as DPPH radical scavenging activity and reducing power. Rosemary and thyme extracts demonstrated the highest DPPH radical scavenging activity with an IC_{50} value of 15.2–15.6 µg/mL, followed by basil (20.3 µg/mL) and oregano (25.0 µg/mL). The rosemary extract had also the highest reducing power with an $A_{0.5}$ value

Table 1. Content of phenolics of different classes in plants and antioxidant activity of plant extracts.

Content/antioxidant activity	Oregano	Rosemary	Basil	Thyme
Total phenolic content (mg GAE/g DM)	9.39 ± 1.63^{a}	6.78 ± 0.04^{c}	6.00 ± 1.47^{d}	7.34 ± 1.92^{b}
Total flavonoid content (mg QE/g DM)	8.46 ± 1.27^{a}	6.15 ± 0.30^{b}	9.42 ± 2.09^{a}	6.22 ± 1.83^{b}
Condensed tannin content (mg CE/g DM)	1.38 ± 0.05^{a}	1.40 ± 0.17^{a}	1.32 ± 0.10^{b}	1.37 ± 0.03^{a}
DPPH assay (IC_{50}, µg/mL)	25.0 ± 1.2^{a}	15.2 ± 1.3^{c}	20.3 ± 1.5^{b}	15.6 ± 1.8^{c}
Reducing power ($A_{0.5}$, µg/mL)	415 ± 11^{a}	301 ± 12^{c}	341 ± 22^{b}	328 ± 10^{b}

Values are expressed as mean ± standard deviation from three replicates. Significant differences between plants are indicated by different superscripts ($p<0.05$). GAE, gallic acid equivalent; QE, quercetin equivalent; CE, catechin equivalent; DM, dry matter; IC_{50}, concentration of extract required to inhibit 50% of DPPH radicals; $A_{0.5}$, concentration of extract required to achieve an absorbance of 0.5 in the reducing power assay.

Table 2. Content of individual phenolic compounds and some volatile compounds in plants (mg/g dry extract) determined by high-performance liquid chromatography.

Compound	Oregano	Rosemary	Basil	Thyme
Rosmarinic acid	20.25±1.50^{a}	15.30±0.41^{b}	12.11±0.30^{c}	0.51±0.08^{d}
Carnosic acid	–	24.53±1.99	–	–
Carnosol	–	5.05±1.03	–	–
Caffeic acid	5.02±0.25^{a}	4.10±0.38^{b}	3.22±0.20^{c}	3.12±0.20^{c}
Ferulic acid	4.21±0.31^{a}	2.55±0.26^{b}	2.29±0.55^{b}	1.56±0.10^{c}
p-Coumaric acid	3.11±0.25^{a}	1.22±0.10^{b}	1.01±0.09^{b}	1.33±0.05^{b}
Chlorogenic acid	1.51±0.19^{b}	2.10±0.30^{a}	–	2.31±0.96^{a}
Luteolin	1.33±0.10^{b}	2.20±0.20^{a}	1.54±0.19^{b}	2.56±0.22^{a}
Apigenin	0.79±0.11^{a}	0.94±0.01^{a}	0.81±0.15^{a}	0.63±0.01^{b}
Vanillic acid	0.94±0.01^{a}	0.83±0.01^{a}	0.55±0.11^{b}	–
Protocatechuic acid	0.87±0.01^{a}	–	1.01±0.09^{a}	–
Thymol	–	–	–	25.51±0.72
Carvacrol	–	–	–	15.21±0.41
Chicoric acid	–	–	7.17±0.37	–

Values are expressed as mean ± standard deviation from three replicates. Significant differences between plants are indicated by different superscripts (p<0.05).

of 301 µg/mL. Reducing power of thyme and basil extracts did not differ significantly (p≥0.05) from each other (328–341 µg/mL), but was higher than that of the oregano extract (415 µg/mL). These results are consistent with other reports showing rosemary's exceptional antioxidant properties, which have been linked to its high phenolic content, particularly rosmarinic acid as well as phenolic diterpenes [Yeddes *et al.*, 2019]. Moreover, antioxidant efficacy of thyme extract is supported by its high content of thymol and carvacrol, compounds that, in addition to phenolics, contribute significantly to its reducing power and antiradical activity [Nieto, 2020].

Optimization of olive oil enrichment

The preliminary study aimed to evaluate the impact of sonication power and maceration time on the enrichment of oils with various plant materials. The study was conducted by varying the sonication power at 40%, 60%, and 80%, and applying different maceration times (5, 15, and 20 min), with a fixed plant-to-oil ratio of 1:10 (*w/v*). The results, expressed as IC_{50} values of DPPH assay, are presented in **Table 3**. Optimal antioxidant activity was consistently achieved at 40% sonication power and 15 min of maceration, as evidenced by the lowest IC_{50} values across all plant-infused oils. Specifically, rosemary-infused oil exhibited the highest antioxidant capacity with an IC_{50} of 0.42 mg/mL, followed by thyme (1.31 mg/mL), basil (1.51 mg/mL), and oregano (2.72 mg/mL) at these conditions. These values were significantly

Table 3. DPPH radical scavenging activity (IC_{50}, mg/mL) of olive oils enriched with oregano, rosemary, basil, and thyme *via* ultrasound-assisted extraction at different sonication powers and process times.

Oil/Maceration time	40% Power	60% Power	80% Power
Olive oil + oregano, 5 min	6.71±0.34^{aB}	4.31±0.22^{bB}	6.65±0.33^{aB}
Olive oil + oregano, 15 min	2.72±0.14^{bC}	7.70±0.29^{aA}	7.54±0.38^{aA}
Olive oil + oregano, 20 min	8.03±0.40^{aA}	7.62±0.38^{bA}	6.23±0.31^{cB}
Olive oil + rosemary, 5 min	2.42±0.12^{aA}	1.91±0.10^{bB}	1.87±0.09^{bB}
Olive oil + rosemary, 15 min	0.42±0.02^{cC}	1.63±0.08^{bC}	2.16±0.11^{aA}
Olive oil + rosemary, 20 min	1.86±0.11^{bB}	4.84±0.24^{aA}	1.89±0.09^{bB}
Olive oil + basil, 5 min	7.12±0.16^{cA}	9.59±0.48^{aA}	7.66±0.38^{bA}
Olive oil + basil, 15 min	1.51±0.08^{cC}	7.53±0.48^{aB}	6.37±0.32^{bB}
Olive oil + basil, 20 min	5.01±0.55^{bB}	5.50±0.28^{bC}	6.43±0.62^{aB}
Olive oil + thyme, 5 min	3.47±0.17^{bB}	1.61±0.08^{cB}	4.32±0.22^{aA}
Olive oil + thyme, 15 min	1.31±0.07^{cC}	2.08±0.10^{bA}	3.33±0.19^{aB}
Olive oil + thyme, 20 min	3.60±0.18^{bA}	2.16±0.11^{cA}	4.42±0.12^{aA}

Values are expressed as mean ± standard deviation from three replicates. Lowercase letters (a–c) indicate significant differences between sonication powers for the same plant and time (p<0.05). Uppercase letters (A–C) indicate significant differences between times for the same plant and sonication power (p<0.05). IC_{50}, oil concentration required to inhibit 50% of the DPPH radicals.

lower (p<0.05) than those at 60% and 80% power for the same plants and time, suggesting that moderate sonication power enhances the extraction of bioactive compounds.

These results align with the findings of Ben Hamouda *et al*. [2025], who demonstrated that UAE conditions, such as sonication power, duration, and solute/solvent ratio, significantly affected the antioxidant activity of carob extracts. Sonication power, for instance, enhances extraction efficiency by increasing cavitation, which disrupts cell walls and releases bioactive compounds. A power of 320 W yielded a total phenolic content of 16.68 mg GAE/g from *Rubus alceifolius* leaves [Tran *et al*., 2023]. The duration of sonication also played a critical role; longer times, such as 37.20 min for *Corchorus olitorius* leaves, yielded 13.92 mg GAE/g [Biswas *et al*., 2023].

Pigment content and quality indices of olive oils

The analysis of the chemical composition of pure olive oil and olive oils infused with various plants revealed notable differences in carotenoid and chlorophyll contents (**Table 4**). Carotenoid content was significantly (p<0.05) higher in thyme and oregano oils (5.30–5.46 mg/kg) than in the other oils, potentially enhancing their antioxidant properties, while olive oil showed the lowest carotenoid content (2.58 mg/kg). Chlorophyll content was significant in oregano, basil and thyme oils (17.04–17.64 mg/kg), which may contribute to their vibrant green color and perceived freshness. Olive oil contained more than three times less chlorophylls (5.19 mg/kg). This transfer of carotenoids and chlorophylls from herbs to oil during maceration is consistent with the findings of Karacabey *et al*. [2016], who reported that it was dependent on process conditions, particularly temperature; as at higher temperatures, oil viscosity decreases and mass diffusion increases.

Among oil quality indices, the specific extinction coefficient (K_{232}) varied according to the plant added (**Table 4**); with the rosemary oil exhibiting the highest value (3.28). The bitterness index was significantly (p<0.05) lower in basil, rosemary and thyme oils (0.10–0.13) than oregano oil (0.17), indicating a milder flavor profile, while olive oil displayed a higher level of bitterness (0.23). Moisture content remained consistently low across all samples, ensuring oil stability. The peroxide values indicate the extent of lipid oxidation, reflecting the level of primary oxidation products in oils [Zhang *et al*., 2021]. All plant-infused oils had lower peroxide values than olive oil, with rosemary oil showing a favorable level (11.00 meq O_2/kg oil), suggesting good preservation potential of plant antioxidants. Free acidity levels vary among the oils, with values within the limit of the IOOC (0.8) [IOOC, 2019], which could impact flavor and shelf life. Overall, these findings highlight the importance of plant selection and enrichment methods in maximizing the beneficial properties of infused oils, contributing to their potential applications in food and health industries.

Phenolic contents and antioxidant capacity of olive oils

The total phenolic content of olive oil was significantly enhanced through infusion with oregano, rosemary, basil, and thyme (**Table 4**). In particular, the rosemary-infused oil showed the highest TPC (556.1 mg GAE/kg), followed by oregano and thyme (529.8–534.4 mg GAE/kg), and basil oil (511.7 mg GAE/kg). This

Table 4. Chemical composition and quality parameters of olive oil and plant-infused olive oils.

Parameter	Olive oil + oregano	Olive oil + rosemary	Olive oil + basil	Olive oil + thyme	Olive oil
K_{232}	2.77±0.08^{bc}	3.28±0.17^{a}	2.83±0.08^{b}	3.07±0.09^{b}	2.38±0.08^{c}
ΔK	0.0012±0.0008^{c}	0.0025±0.0005^{b}	0.0014±0.0001^{c}	0.0015±0.0006^{c}	0.0037±0.0007^{a}
Carotenoid content (mg/kg oil)	5.30±0.18^{a}	4.59±0.06^{b}	3.82±0.07^{c}	5.46±0.15^{a}	2.58±0.05^{d}
Chlorophyll content (mg/kg oil)	17.31±0.60^{a}	10.15±0.19^{b}	17.64±0.28^{a}	17.04±0.40^{a}	5.19±0.10^{c}
Bitterness index	0.17±0.01^{a}	0.11±0.01^{b}	0.10±0.01^{b}	0.13±0.01^{b}	0.23±0.01^{a}
Moisture (%)	0.30±0.01^{a}	0.30±0.01^{a}	0.24±0.01^{b}	0.24±0.01^{b}	0.18±0.01^{c}
Peroxide value (meq O_2/kg oil)	11.50±0.10^{c}	11.00±0.10^{d}	13.75±0.10^{b}	12.00±0.10^{c}	14.50±0.01^{a}
Free acidity (%)	0.43±0.01^{b}	0.69±0.01^{a}	0.44±0.01^{b}	0.65±0.01^{a}	0.34±0.01^{b}
Total phenolic content (mg GAE/kg oil)	534.4±2.8^{b}	556.1±20.4^{a}	511.7±5.1^{c}	529.8±5.3^{b}	318.6±12.0^{d}
Total flavonoid content (mg QE/kg oil)	464.7±2.1^{b}	484.9±6.6^{a}	337.2±8.7^{c}	337.9±3.0^{c}	233.6±6.4^{d}
Condensed tannin content (mg CE/kg oil)	53.83±1.33^{b}	56.80±1.18^{a}	57.05±1.73^{a}	52.22±1.09^{b}	52.54±2.01^{b}
DPPH assay (IC_{50}, mg/mL)	2.36±0.18^{d}	3.18±0.11^{b}	2.38±0.14^{d}	2.58±0.09^{c}	7.85±0.19^{a}

Values are expressed as mean ± standard deviation from three replicates. Significant differences between oils are indicated by different superscripts (p<0.05). K_{232}, specific extinction coefficient; ΔK, variation in specific extinction coefficients, GAE, gallic acid equivalent; QE, quercetin equivalent; CE, catechin equivalent; IC_{50}, oil concentration required to inhibit 50% of the DPPH radicals.

was a substantial increase compared to the control olive oil (318.6 mg GAE/kg), highlighting the effective transfer of phenolics from the herbs into the oil. The total flavonoid content followed a similar trend, with the rosemary- and oregano-infused oils showing the highest values (484.9 and 464.7 mg QE/g kg, respectively). The higher TPC and TFC in these infused oils aligns with previous studies that emphasize the role of phenolic compounds from herbs like rosemary, oregano, sage, and wild nettle in enhancing oil antioxidant properties [Karacabey *et al*., 2016; Manai-Djebali *et al*., 2024 ; Yfanti *et al*., 2024]. Condensed tannin content of rosemary and basil oils was also elevated compared to olive oil, contributing to the bitterness and oxidative stability of the oils, although the increase was less pronounced than TPC and TFC (**Table 4**). In the case of oregano and thyme oils, CT content did not even differ significantly ($p \geq 0.05$) from that in olive oil.

The DPPH radical scavenging activity results highlighted significant differences in antioxidant capacity between the herb-infused olive oils and the control (**Table 4**). Oregano- and basil-infused oils exhibited the most potent antioxidant effect with an IC_{50} of 2.36–2.38 mg/mL, followed closely by thyme (2.58 mg/mL). This indicated that these herbs substantially enhance the radical-scavenging capacity of the olive oil, likely due to the high content of phenolic compounds known for their ability to donate hydrogen atoms and neutralize free radicals. Interestingly, the rosemary-infused oil, despite having the highest total phenolic content (556.1 mg GAE/Kg), exhibited a higher IC_{50} (3.18 mg/mL) compared to the other herb-infused oils. This apparent discrepancy may be attributed to the nature of the phenolic compounds present in rosemary. While rosemary is known to contain potent antioxidants, such as rosmarinic acid and carnosic acid [Yeddes *et al*., 2019], the efficiency of these compounds in DPPH assays might vary due to their specific molecular structure, particularly their steric hindrance and redox potential [Chiorcea-Paquim *et al*., 2020]. Moreover, the mechanism of action of rosemary compounds as antioxidants may involve both radical scavenging and metal chelation, which might not be fully captured by the DPPH assay alone, as noted in previous reports [Liu *et al*., 2024]. In contrast, the virgin olive oil exhibited a significantly higher IC_{50} (7.85 mg/mL), underscoring the limited radical-scavenging capacity of olive oil on its own, despite its natural phenolic content, such as hydroxytyrosol, oleuropein and its derivatives [Jukić Špika *et al*., 2022]. This reinforces the efficacy of using herb infusion to enhance the antioxidant properties of olive oil.

Fatty acid composition of olive oils

The fatty acid composition of the pure olive oil and plant-infused olive oils is shown in **Table 5**. For the content of most fatty acids, no significant ($p \geq 0.05$) differences were found between the oils (except C18:2, C20:0 and C22:1). The predominant fatty acid across all samples was oleic acid (C18:1), with values ranging from 68.51 to 69.03% total fatty acids. This aligns well with the typical composition of extra virgin olive oil, where oleic acid generally accounts for 55–83% of the total fatty acids [IOOC, 2021]. The presence of this monounsaturated fatty acid is a key factor contributing to olive oil's health benefits, including cardiovascular protection and anti-inflammatory effects [Marcelino *et al*., 2019]. Palmitic acid (C16:0), the major saturated fatty acid in olive oil, showed a similar content across the samples (12.56 to 12.79% total fatty acids), which was in line with the established values of 7.5–20% total fatty acids in olive oils [IOOC, 2021]. Linoleic acid (C18:2), a polyunsaturated fatty acid, was another critical

Table 5. Fatty acid composition (% total fatty acids) of olive oil and plant-infused olive oils.

Fatty acid	Olive oil + oregano	Olive oil + rosemary	Olive oil + basil	Olive oil + thyme	Olive oil
C14:0	0.09±0.10^{a}	0.00±0.00^{a}	0.00±0.00^{a}	0.00±0.00^{a}	0.02±0.01^{a}
C16:0	12.64±0.01^{a}	12.56±0.01^{a}	12.79±0.04^{a}	12.69±0.01^{a}	12.66±0.03^{a}
C16:1	0.59±0.01^{a}	0.58±0.01^{a}	0.55±0.01^{a}	0.57±0.03^{a}	0.57±0.02^{a}
C18:0	0.00±0.00^{a}	0.01±0.01^{a}	0.01±0.01^{a}	0.00±0.00^{a}	0.01±0.01^{a}
C18:1	68.77±0.05^{a}	69.03±0.01^{a}	68.51±0.02^{a}	68.85±0.05^{a}	68.86±0.11^{a}
C18:2	15.89±0.01^{b}	15.85±0.01^{b}	16.17±0.01^{a}	15.94±0.01^{b}	15.87±0.02^{b}
C18:3	0.01±0.05^{a}	0.01±0.01^{a}	0.02±0.01^{a}	0.00±0.01^{a}	0.02±0.01^{a}
C20:0	0.81±0.06^{a}	0.69±0.01^{b}	0.76±0.03^{a}	0.70±0.01^{ab}	0.74±0.05^{a}
C20:1	0.95±0.03^{a}	0.98±0.01^{a}	0.90±0.02^{a}	0.94±0.02^{a}	0.96±0.03^{a}
C22:0	0.01±0.01^{a}	0.01±0.01^{a}	0.01±0.01^{a}	0.01±0.01^{a}	0.01±0.01^{a}
C22:1	0.14±0.01^{a}	0.01±0.01^{b}	0.01±0.02^{b}	0.01±0.01^{b}	0.02±0.01^{b}
C24:0	0.01±0.01^{a}	0.01±0.01^{a}	0.02±0.01^{a}	0.01±0.01^{a}	0.02±0.01^{a}

Values are expressed as mean ± standard deviation from three replicates. Significant differences between oils are indicated by different superscripts ($p<0.05$).

compound, with levels ranging from 15.85 to 16.17% total fatty acids in the infused oils in our study, again within the typical range (3.5–21%) for olive oils [Tsimihodimos & Psoma, 2024]. The minor fatty acids, such as palmitoleic acid (C16:1) and stearic acid (C18:0), remained consistent with the known fatty acid profiles of extra virgin olive oils [IOOC, 2021], further supporting the conclusion that the infusion process with oregano, rosemary, basil, and thyme does not significantly alter the fatty acid composition. This stability in fatty acid profile indicates that the enrichment with aromatic herbs mainly affects the phenolic composition and antioxidant properties of the oils, rather than altering their lipid structure. This observation is critical, as it suggests that the health-promoting properties associated with the fatty acids in olive oil are preserved, while additional benefits may arise from the enhanced phenolic content contributed by the herbs.

Volatile compounds in olive oils

The volatile compound profiles of olive oils infused with various aromatic plants (rosemary, oregano, basil, thyme) and non-infused olive oil are shown in **Table 6**. Each infused oil exhibited a unique composition, underscoring the predominance of specific volatile compounds. The rosemary-infused oil was dominated by camphor (28.11% of total volatile compounds), 1,8-cineole (32.44%), and α-pinene (17.00%), reflecting its terpene-rich profile. The oregano-infused oil was characterized by high levels of *p*-cymene (32.12%), thymol (18.45%), α-pinene (15.45%), and carvacrol (14.85%). The basil-infused oil stood out with exceptional concentrations of methyl chavicol (52.34%), linalool (17.35%), and limonene (13.98%), indicating its sweet and aromatic profile. The thyme-infused oil showed a high content of carvacrol (74.01%), along with notable levels of terpinene (5.34%) and thymol (5.33%), emphasizing its intense aromatic properties. In contrast, the non-infused olive oil was dominated by hexanal (62.35%) and octanal (13.28%), which are characteristic of non-infused vegetable oils, giving it a simpler, herbaceous profile.

The analysis of volatile compounds in plant-infused olive oils highlights distinct chemical profiles, crucial for their biological activities. Each infused oil contained specific bioactive compounds, including terpenes and volatile phenols, which may contribute to their antioxidant, antimicrobial, and anti-inflammatory properties. Rosemary essential oil, rich in camphor, 1,8-cineole, and α-pinene, exhibited strong radical-scavenging

Table 6. Volatile compound contents (% total volatile compounds) in olive oil and plant-infused olive oils.

Volatile compound	Olive oil + rosemary	Olive oil + oregano	Olive oil + basil	Olive oil + thyme	Olive oil
α-Pinene	17.00±0.51^{a}	15.45±0.07^{b}	5.02±0.03^{c}	1.85±0.06^{d}	0.82±0.02^{e}
p-Cymene	1.35±0.22^{b}	32.12±0.36^{a}	–	1.15±0.24^{b}	0.35±0.22^{c}
Limonene	0.35±0.03^{d}	1.40±0.55^{b}	13.98±2.99^{a}	0.98±0.03^{c}	–
Terpinene	0.25±0.01^{c}	12.89±0.18^{a}	0.18±0.01^{c}	5.34±0.16^{b}	–
Hexanal	–	–	–	–	62.35±0.01^{a}
Octanal	–	–	–	–	13.28±0.01^{a}
1,8-Cineole	32.44±0.42^{a}	5.98±0.03^{b}	1.54±0.05^{d}	2.35±0.07^{c}	-–
Linalool	3.52±0.02^{b}	0.24±0.01^{c}	17.35±0.52^{a}	0.30±0.01^{c}	0.08±0.01^{d}
Citral	–	0.61±0.01^{b}	0.96±0.02^{a}	0.00±0.01^{c}	0.00±0.01^{c}
(*E*)-2-Hexenal	–	–	–	–	15.12±0.01^{a}
2-Pentylfuran	–	–	–	–	6.01±0.01^{a}
Borneol	7.23±1.02^{a}	2.36±0.17^{b}	0.30±0.01^{c}	0.12±0.01^{d}	–
Bornyl acetate	4.35±0.13^{a}	1.45±0.04^{b}	–	0.98±0.03^{c}	–
Camphor	28.11±0.45^{a}	–	0.13±0.01^{bc}	–	–
Methyl chavicol	–	–	52.34±0.37^{a}	–	–
Eugenol	–	–	3.45±0.31^{a}	–	–
Thymol	0.12±0.01^{c}	18.45±0.55^{b}	0.07±0.01^{c}	5.33±0.01^{b}	–
Carvacrol	–	14.85±0.45^{b}	0.01±0.01^{c}	74.01±2.22^{a}	–

Values are expressed as mean ± standard deviation from three replicates. Significant differences between oils are indicated by different superscripts (p<0.05).

Table 7. Oxidative stability of olive oil and plant-infused olive oils in the Rancimat test.

Oil	Induction time (h)	Oxidative stability index (day/kg)
Olive oil + oregano	34.42±0.02^{c}	409.8±0.3^{c}
Olive oil + rosemary	82.25±1.23^{a}	978.8±15.4^{a}
Olive oil + basil	30.89±0.50^{d}	367.8±6.0^{d}
Olive oil + thyme	51.48±0.17^{b}	612.9±2.1^{b}
Olive oil	34.44±0.59^{c}	410.0±7.1^{c}

Values are expressed as mean ± standard deviation from three replicates. Significant differences between oils are indicated by different superscripts (p<0.05).

activity and anti-inflammatory potential [Becer *et al*., 2023]. Thymol and carvacrol, the main volatile compounds of the thyme-infused oil in our study, demonstrate remarkable antimicrobial activity, effectively inhibiting pathogenic microorganisms [Mączka *et al*., 2023]. In turn, methyl chavicol and linalool, the main compounds of basil essential oil, are primarily associated with antioxidant and antimicrobial effects, respectively [Zhakipbekov *et al*., 2024]. Finally, the oregano-infused oil was rich in *p*-cymene, a compound also known for its superior antimicrobial and antioxidant properties [Balahbib *et al*., 2021].

Oxidative stability of olive oils in Rancimat test

The induction times of oxidation of pure olive oil and plant-infused olive oils measured in the Rancimat test are presented in **Table 7**. The infusion with aromatic plants significantly influenced olive oil oxidative stability. The rosemary-infused oil exhibited the best oxidation stability, with an induction time of 82.25 h, which was 2.4 times higher than for the control oil (34.44 h). The thyme-infused oil also showed a notable improvement, with an induction time of 51.48 h. Although the stability of the thyme-infused oil was significantly (p<0.05) lower than that of the rosemary-infused oil, it was still superior to the control oil. In terms of oxidative stability index (expressed in day/kg), the rosemary-infused oil recorded a value of 978.8 day/kg compared to 410.0 day/kg for the control oil, indicating a significant reduction in oxidation. In contrast, infusion of olive oils with basil and oregano did not yield significant benefits, with induction times of 30.89 h and 34.42 h, respectively, both close to the control oil. The oxidative stability index for these oils was also low, with 367.8 day/kg for basil and 409.8 day/kg for oregano. In a previous study, essential oils from plants such as sage, oregano, rosemary, and thyme were reported to effectively protect the oleic acid of olive oil oxidized by irradiation at 360 nm for 32 h [Barreca *et al*., 2021]. In turn, Özcan *et al*. [2022] studied the effect of thyme, rosemary, and sage essential oils and extracts from these plants on the oxidative stability of olive oil during storage and found that the rosemary extract contributed to maintaining oil quality by stabilizing free fatty acid level.

Nutritional composition of cheeses

The nutritional composition of fresh cheeses stored in different infused olive oils (rosemary, oregano, basil, thyme), as well as in pure olive oil, compared to a control fresh cheese not immersed in oil is shown in **Table 8**. The cheeses stored in olive oil exhibited relatively homogeneous protein content, around 10 g/100 g, compared to 22.56 g/100 g determined in the control cheese, suggesting a dilution effect due to oil absorption. In contrast, the lipid content was significantly higher in the cheeses stored in oils, reaching approximately 48–49 g/100 g, compared to 21.63 g/100 g determined in the control cheese, indicating substantial lipid uptake from the oil. This lipid absorption results in a higher energy value for the cheeses preserved in oils (approximately 479–496 kcal/100 g), while the control cheese, with its lower lipid content, had a lower caloric value (293.2 kcal/100 g). The carbohydrate content remained low across all samples (1.41–2.06 g/100 g), contributing negligibly to total energy. Additionally, the water content was lower in the cheeses immersed in oil (approximately 37–40 g/100 g) compared to the control cheese (52.15 g/100 g).

Oxidative stability of cheeses during storage

The TBARS values of cheeses demonstrated that their immersion in plant-infused olive oils significantly affected their oxidative stability over time (**Table 9**). On day 1, the TBARS values

Table 8. Nutritional composition of the untreated fresh cheese and cheeses treated with olive oils.

Cheese	Proteins (g/100 g)	Lipids (g/100 g)	Carbohydrates (g/100 g)	Water (g/100 g)	Energy value (kcal/100 g)
Cheese + rosemary-infused oil	10.51±0.53^{b}	48.55±2.43^{a}	1.99±0.10^{a}	38.36±1.92^{b}	487.2±12.7^{a}
Cheese + oregano-infused oil	10.56±0.53^{b}	48.23±2.41^{a}	2.01±0.10^{a}	38.66±1.93^{b}	484.4±12.6^{a}
Cheese + basil-infused oil	10.76±0.54^{b}	49.55±2.48^{a}	1.86±0.09^{a}	37.19±1.86^{b}	496.4±12.9^{a}
Cheese + thyme-infused oil	9.99±0.50^{b}	48.09±2.40^{a}	1.55±0.08^{ab}	40.12±2.01^{b}	479.0±12.5^{a}
Cheese + pure olive oil	10.64±0.53^{b}	49.06±2.45^{a}	1.41±0.07^{b}	38.69±1.93^{b}	489.7±12.7^{a}
Untreated fresh cheese	22.56±1.13^{a}	21.63±1.08^{b}	2.06±0.10^{a}	52.15±2.61^{a}	293.2±7.6^{b}

Values are expressed as mean ± standard deviation from three replicates. Significant differences between cheeses are indicated by different superscripts (p<0.05).

Table 9. Content of thiobarbituric acid reactive substances of the untreated fresh cheese and cheeses treated with olive oils (mg MDA/kg cheese) over storage time.

Cheese	Day 1	Day 7	Day 14	Day 21
Cheese + rosemary-infused oil	0.41 ± 0.04^{bA}	0.40 ± 0.02^{bC}	0.42 ± 0.02^{bE}	0.53 ± 0.02^{aE}
Cheese + oregano-infused oil	0.41 ± 0.02^{cA}	0.41 ± 0.01^{cC}	0.63 ± 0.03^{bC}	0.86 ± 0.09^{aC}
Cheese + basil-infused oil	0.42 ± 0.02^{cA}	0.43 ± 0.03^{cC}	0.66 ± 0.02^{bC}	0.86 ± 0.07^{aC}
Cheese + thyme-infused oil	0.44 ± 0.03^{cA}	0.41 ± 0.01^{cC}	0.52 ± 0.01^{bD}	0.66 ± 0.05^{aD}
Cheese + pure olive oil	0.40 ± 0.03^{dA}	0.49 ± 0.02^{cB}	0.83 ± 0.03^{bB}	1.06 ± 0.02^{aB}
Untreated fresh cheese	0.45 ± 0.02^{dA}	0.65 ± 0.05^{cA}	1.97 ± 0.05^{bA}	2.98 ± 0.12^{aA}

Values are expressed as mean ± standard deviation (n=3). Lowercase letters (a–d) indicate significant differences between time points within the same sample. Uppercase letters (A–E) indicate significant differences between treatments at the same time point (p<0.05). MDA, malondialdehyde equivalent.

for all cheeses ranged between 0.40 and 0.45 mg MDA/kg and did not differ significantly (p≥0.05) from each other. After 7 days, TBARS values increased significantly (p<0.05) only for the untreated control cheese to 0.65 mg MDA/kg and for the cheese preserved in non-enriched oil to 0.49 mg MDA/kg. For the cheeses treated with the plant-infused oils, TBARS values did not differ significantly (p≥0.05) and were in the range of 0.40–0.43 mg MDA/kg. By day 14, the cheese immersed in the rosemary-infused oil showed the best oxidative stability, with a TBARS value of 0.42 mg MDA/kg. The thyme-infused oil yield a slightly higher result (0.52 mg MDA/kg cheese) followed by oregano- and basil-infused oils with a similar effect (0.63–0.66 mg MDA/kg cheese). The untreated cheese and the cheese treated with pure olive oil exhibited much higher TBARS values (1.97 and 0.83 mg MDA/kg, respectively), reaffirming the protective effect of plant-infused oils. On day 21, the rosemary-infused oil maintained its superior effectiveness yielding a TBARS value of 0.53 mg MDA/kg cheese, closely followed by the thyme-infused oil (0.66 mg MDA/kg cheese). In contrast, the cheeses treated with basil- and oregano-infused oils displayed higher TBARS values (0.86 mg MDA/kg), suggesting that rosemary and thyme ensured more stable preservation. The cheese immersed in non-infused olive oil (1.06 mg MDA/kg) and the untreated cheese (2.98 mg MDA/kg) showed significantly higher oxidation levels, confirming the notable protective effect of plant-infused oils.

The application of herb-infused oils for cheese preservation, as explored in this study, addresses challenges observed in previous research on oil-cheese interactions. Klisović *et al.* [2022] found that the immersion of semi-hard, hard, and soft whey cheeses in extra virgin olive oil (EVOO) for two months accelerated hydrolytic and oxidative degradation, with phenolic content reductions of 85.0–93.5% and increases in oxidation indicators (*e.g.*, K_{232}) and trans-oleic fatty acid beyond EVOO quality limits, driven by fat migration and cheese composition (moisture, proteins). Similarly, Popescu *et al.* [2023] demonstrated that microencapsulated basil extract at 0.6–0.9% (*w/w*) in cream cheese inhibited post-fermentation, improved water retention, and enhanced textural properties, extending shelf life by 7 days at 4°C, despite the challenges of direct plant extract use due to sensory impacts.

Microbiological stability of cheeses

The microbiological stability study revealed significant differences in bacterial, fungal, and coliform counts across various cheese samples over 21 days (**Figure 1**). Lactic acid bacteria decreased significantly in cheeses treated with the plant-infused oils (oregano, rosemary, basil, and thyme), while the untreated fresh cheese showed no significant variation. This suggests that the plant-infused oils alter the microbial environment. The total aerobic mesophilic flora increased in the untreated cheese during storage from 5.27 to 7.94 log CFU/g. In turn, the cheeses treated with herb-infused oils, particularly rosemary and basil, showed significantly reduced microbial proliferation (p<0.05), with the total aerobic mesophilic flora counts of 4.64 log CFU/g (rosemary) and 4.58 log CFU/g (basil) at day 7, and 4.53 log CFU/g (rosemary) and 4.49 log CFU/g (basil) at day 14 (**Figure 1B**). Yeast and mold counts (**Figure 1C**) followed a similar trend, with the untreated cheese displaying continuous fungal growth, reaching 7.75 log CFU/g on day 21. In contrast, the cheeses treated with the herb-infused oils showed reduced counts, with oregano at 5.27 log CFU/g (day 7) and 5.14 log CFU/g (day 14), rosemary at 5.43 log CFU/g (day 7) and 5.32 log CFU/g (day 14), and basil at 5.06 log CFU/g (day 7) and 4.49 log CFU/g (day 14), compared to the untreated cheese. Total and thermotolerant coliform counts (**Figure 1D**) in the untreated fresh cheese increased from 5.15 log CFU/g on day 1 to 6.86 log CFU/g on day 21 at 4°C, while in the cheese stored in the non-enriched olive oil their count reached 6.07 log CFU/g by day 21. In contrast, the cheeses treated with the herb-infused oils showed significantly lower coliform counts (p<0.05), with basil (4.73 log CFU/g on day 7, 4.90 log CFU/g on day 21), oregano (4.85 log CFU/g on day 7, 4.92 log CFU/g on day 21), thyme (4.90 log CFU/g on day 7, 5.04 log CFU/g on day 21), and rosemary (4.88 log CFU/g on day 7, 5.04 log CFU/g on day 21) demonstrating pronounced reductions, particularly on days 7 and 14. These findings highlight

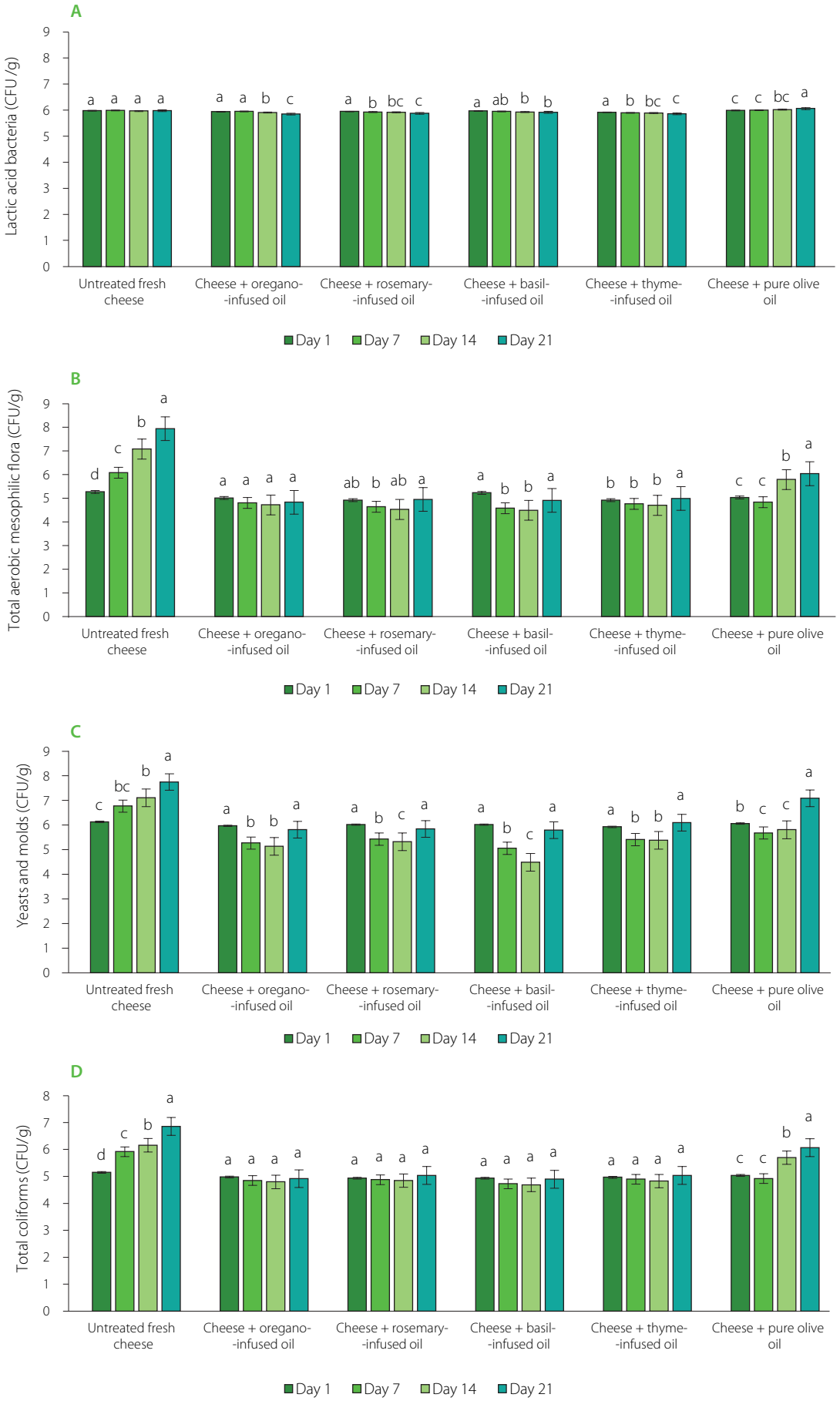

Figure 1. Counts of lactic acid bacteria (**A**), total aerobic mesophilic flora (**B**), yeasts and molds (**C**), and total coliforms (**D**) of the untreated cheese and cheeses treated with plant-infused oils during 21 days of storage. Results are presented as mean and standard deviation following three repetitions. For each cheese, significant differences between time points are indicated by different letters ($p<0.05$).

the antimicrobial and antifungal potential of the plant-infused oils, particularly oregano and basil, in improving cheese microbiological stability and shelf life.

Factors controlling microbial growth in cheese include water activity, salt concentration, redox potential, pH, temperature, and possibly bacteriocin production by certain microorganisms. These "hurdles" may not be significant individually, but together they effectively inhibit microbial growth [Hayaloglu, 2016]. Microbiological monitoring over four time points revealed significant differences between control and cheeses treated with plant-infused oils, they inhibited coliforms, molds, and yeasts during the first two weeks, extending shelf life. The control cheese developed surface mold after two weeks, whereas the flavored cheeses remained stable beyond this period. Inhibition of undesirable microbes, including yeasts and molds, was observed as early as in the first week. The total aerobic mesophilic flora is a key hygiene indicator in cheese. The cheeses stored in the plant-infused oils had microbial loads below the French regulatory limit of 5 log CFU/mL [Benyahia *et al*., 2021]. The total aerobic mesophilic flora levels decreased during the first two weeks, likely due to salting and water loss, limiting microbial growth [Hamama, 1989]. Unlike our findings, Rhiat *et al*. [2011] reported the total absence of coliforms, though their presence does not always indicate fecal contamination, as some originate from dairy equipment residues. Enriched olive oil helped preserve cheese organoleptic properties and extended shelf life. According to Mason & Wasserman [1987], bioactive compounds in the oil interfere with microbial membrane proteins, such as adenosine triphosphatase, either by direct interaction with hydrophobic protein regions or by disrupting proton translocation across the membrane, thereby preventing adenosine diphosphate (ADP) phosphorylation.

CONCLUSIONS

The findings of this study underscore the efficacy of ultrasound-assisted extraction in enhancing the functional properties of olive oil through the infusion of phenolic-rich herbs such as oregano, rosemary, basil, and thyme. The plant-infused olive oils exhibited significantly improved antioxidant capacity, and the basil-infused oil showed the strongest DPPH radical scavenging potential. The most effective improvement in the oxidative stability of olive oil was achieved by rosemary. When applied for fresh cheese immersion, these plant-infused oils significantly reduced lipid oxidation and microbial proliferation during storage. Among the formulations, rosemary- and thyme-infused oils provided superior protection against oxidation, while oregano- and basil-infused oils exhibited strong antimicrobial effects, leading to an extended shelf life. These results position bioactive-infused olive oils as promising alternatives to synthetic preservatives in the dairy industry. Beyond their preservative role, these enriched oils contribute to the development of innovative functional foods that align with consumer demands for natural, health-promoting dietary options. Their ability to enhance the nutritional profile of cheese while improving storage stability offers potential applications in artisanal and industrial dairy production. Future research should explore consumer sensory acceptance, large-scale processing feasibility, and the potential synergistic effects of combining different bioactive compounds. This study lays the groundwork for further innovations in the field of functional foods, with implications for both food preservation and human health.

ACKNOWLEDGEMENTS

The authors extend their appreciation to Taif University, Saudi Arabia, for supporting this work (project number TU-DSPP-2024-115).

RESEARCH FUNDING

This research was funded by Taif University, Saudi Arabia, Project No. TU-DSPP-2024-115 and by Tunisian Ministry of Higher Education and Scientific Research (LR15CBBC06).

CONFLICT OF INTERESTS

The authors declare no conflicts of interest.

ORCID IDs

N. Ben Youssef https://orcid.org/0000-0001-8706-2244
N. Farhat https://orcid.org/0000-0001-7769-0095
H. Gadhoumi https://orcid.org/0000-0002-9293-9191
K. Hessini https://orcid.org/0000-0002-8929-9234
H. Manai-Djebali https://orcid.org/0000-0001-5703-0460
A. Mejri https://orcid.org/0000-0002-8172-5163
S. Nait-Mohamed https://orcid.org/0000-0002-2996-1724
M. Saidani Tounsi https://orcid.org/0000-0003-1548-1655

REFERENCES

1. Antonino, C., Natrella, G., Caponio, G.R., Zago, L., Difonzo, G., Faccia, M. (2025). Reuse of UHT milk close to expiring and almond okara in the production of fresh cheese. *Food Frontiers*, *6*(4), 2052-2064. https://doi.org/10.1002/fft2.70045
2. Araujo, H.C.S., de Jesus, M.S., Sandes, R.D.D., Leite Neta, M.T.S., Narain, N. (2024). Functional cheeses: Updates on probiotic preservation methods. *Fermentation*, *10*(1), art. no. 8. https://doi.org/10.3390/fermentation10010008
3. Balahbib, A., El Omari, N., El Hachlafi, N., Lakhdar, F., El Menyiy, N., Salhi, N., Mrabti, H.N., Bakrim, S., Zengin, G., Bouyahya, A. (2021). Health beneficial and pharmacological properties of p-cymene. *Food and Chemical Toxicology*, *153*, art. no. 112259. https://doi.org/10.1016/j.fct.2021.112259
4. Barreca, S., La Bella, S., Maggio, A., Licata, M., Buscemi, S., Leto, C., Pace, A., Tuttolomondo, T. (2021). Flavouring extra-virgin olive oil with aromatic and medicinal plants essential oils stabilizes oleic acid composition during photo-oxidative stress. *Agriculture*, *11*(3), art. no. 266. https://doi.org/10.3390/agriculture11030266
5. Becer, E., Altundağ, E.M., Güran, M., Seda Vatansever, H., Ustürk, S., Hanoğlu, D.Y., Hüsnü Can Başer, K. (2023). Composition and antibacterial, anti-inflammatory, antioxidant, and anticancer activities of *Rosmarinus officinalis* L. essential oil. *South African Journal of Botany, 160*, 437-445. https://doi.org/10.1016/j.sajb.2023.07.028
6. Ben Hamouda, G., Bettaieb Rebey, I., Zar Kalai, F., Hammami, M., Ksouri, R. (2025). Enhancing antioxidant yield from carob (*Ceratonia siliqua* L.): evaluating the efficacy of maceration and ultrasound-assisted methods. *International Journal of Environmental Health Research*, *35*(7), 1793–1805. https://doi.org/10.1080/09603123.2024.2407456
7. Benyahia, F.A., Zitoun, O.A., Meghzili, B., Foufou, E., Zidoune, M.N. (2021). Use of *Pergularia tomentosa* plant enzymatic coagulant system in fresh cheese-making. *Food and Nutrition Sciences*, *12*(11), 1028–1040. https://doi.org/10.4236/fns.2021.1211076
8. Biswas, A., Dey, S., Xiao, A., Deng, Y., Birhanie, Z.M., Roy, R., Akhter, D., Liu, L., Li, D. (2023). Ultrasound-assisted extraction (UAE) of antioxidant phenolics from *Corchorus olitorius* leaves: a response surface optimization. *Chemical and Biological Technologies in Agriculture*, *10*(1), art. no. 64. https://doi.org/10.1186/s40538-023-00443-2
9. Bradford, M.M. (1976) A rapid and sensitive method for the quantitation of microgram quantities of protein utilizing the principle of protein-dye binding. *Analytical Biochemistry*, *72*(1-2), 248-254. https://doi.org/10.1016/0003-2697(76)90527-3

10. Brand-Williams, W., Cuvelier, M.E., Berset, C. (1995). Use of a free radical method to evaluate antioxidant activity. *LWT – Food Science and Technology*, *28*(1), 25-30. **https://doi.org/10.1016/S0023-6438(95)80008-5**
11. Chiorcea-Paquim, A.-M., Enache, T.A., De Souza Gil, E., Oliveira-Brett, A.M. (2020). Natural phenolic antioxidants electrochemistry: Towards a new food science methodology. *Comprehensive Reviews in Food Science and Food Safety*, *19*(4), 1680–1726. **https://doi.org/10.1111/1541-4337.12566**
12. Christodouleas, D.C., Fotakis, C., Nikokavoura, A., Papadopoulos, K., Calokerinos, A.C. (2014). Modified DPPH and ABTS assays to assess the antioxidant profile of untreated oils. *Food Analytical Methods*, *8*(5), 1294–1302. **https://doi.org/10.1007/s12161-014-0005-6**
13. Delgado, A., Gonçalves, S., Romano, A. (2023). Mediterranean diet: The role of phenolic compounds from aromatic plant foods. *Foods*, *12*(4), art. no. 840. **https://doi.org/10.3390/foods12040840**
14. Deshmukh, V., Gutte, R.K. (2024). Sustainable Health and Functional Foods. In W. Leal Filho, T. Dibbern, S.R. de Maya, M.-C. Alarcón-del-Amo, L.M. Rives (Eds.), *The Contribution of Universities Towards Education for Sustainable Development* (1st ed.), Springer Cham, pp. 439–451. **https://doi.org/10.1007/978-3-031-49853-4_25**
15. Fraga-Corral, M., Otero, P., Echave, J., Garcia-Oliveira, P., Carpena, M., Jarboui, A., Nuñez-Estevez, B., Simal-Gandara, J., Prieto, M.A. (2021). By-products of agri-food industry as tannin-rich sources: A review of tannins' biological activities and their potential for valorization. *Foods*, *10*(1), art. no. 137. **https://doi.org/10.3390/foods10010137**
16. Gabbia, D. (2024). Beneficial effects of tyrosol and oleocanthal from extra virgin olive oil on liver health: Insights into their mechanisms of action. *Biology*, *13*(10), art. no. 760. **https://doi.org/10.3390/biology13100760**
17. Garofalo, G., Taspinar, T., Busetta, G., Mastrangelo, S., Portolano, B., Sardina, M.T., Gaglio, R., Erten, H., Settanni, L. (2024). Description of Ewiss cheese, a new ewe milk cheese processed by Swiss cheese manufacturing techniques: Microbiological, physicochemical, and sensory aspects. *Journal of Dairy Science*, *107*(9), 6614–6628. **https://doi.org/10.3168/jds.2024-24711**
18. Habachi, E., Rebey, I.B., Dakhlaoui, S., Hammami, M., Sawsen, S., Msaada, K., Merah, O., Bourgou, S. (2022). *Arbutus unedo*: Innovative source of antioxidant, anti-inflammatory and anti-tyrosinase phenolics for novel cosmeceuticals. *Cosmetics*, *9*(6), art. no. 143. **https://doi.org/10.3390/cosmetics9060143**
19. Habtemariam, S. (2023). Anti-inflammatory therapeutic mechanisms of natural products: insight from rosemary diterpenes, carnosic acid and carnosol. *Biomedicines*, *11*(2), art. no. 545. **https://doi.org/10.3390/biomedicines11020545**
20. Haddada, F.M., Manai, H., Daoud, D., Fernandez, X., Lizzani-Cuvelier, L., Zarrouk, M. (2007). Profiles of volatile compounds from some monovarietal Tunisian virgin olive oils. Comparison with French PDO. *Food Chemistry*, *103*(2), 467–476. **https://doi.org/10.1016/j.foodchem.2006.08.023**
21. Hamama, A. (1989). Bacteriological quality of Moroccan fresh cheeses. In J.-L. Tisserand (Ed.), *Le lait dans la région méditerranéenne*, CIHEAM, Paris, France, pp. 223–227, (in French, English abstract).
22. Hayaloglu, A.A. (2016). Cheese: Microbiology of cheese. In *Reference Module in Food Science*. Elsevier Inc., Amsterdam, Netherlands, p. 9. **https://doi.org/10.1016/B978-0-08-100596-5.00675-2**
23. Inarejos-Garcia, A.M., Androulaki, A., Salvador, M.D., Fregapane, G., Tsimidou, M.Z. (2009). Discussion on the objective evaluation of virgin olive oil bitterness. *Food Research International*, *42*(2), 279–284. **https://doi.org/10.1016/j.foodres.2008.11.009**
24. IOOC (2021). *Trade standard applying to olive oils and olive-pomace oils.* No. COI/T.15/NC No. 3; Version 17. International Olive Council, Madrid, Spain.
25. IOOC (2019). *Trade standard applying to olive oils and olive pomace oils*. No. COI/T.15/NC No 3/Rev. 14, November 2019. International Olive Council, Madrid, Spain.
26. IOOC (2024). *Standards and methods – Chemistry and standardisation unit*. International Olive Council, Madrid, Spain.
27. ISO (2016). ISO Standard No. 6886:2016: *Animal and vegetable fats and oils — Determination of oxidative stability (accelerated oxidation test)*, International Organization for Standardization.
28. Ioannis, M., Alexandros, S., Sotirios, E., Stamatia, C., Erminta, T. (2024). Chapter 5 – Antioxidants from aromatic herbs in food preservation. In M. Pateiro (Ed.), *Natural Antioxidants to Enhance the Shelf-Life of Food*, Academic Press, pp. 103–146. **https://doi.org/10.1016/B978-0-443-15386-0.00005-9**
29. Jebabli, H., Nsir, H., Taamalli, A., Abu-Reidah, I., Álvarez-Martínez, F.J., Losada-Echeberria, M., Barrajón Catalán, E., Mhamdi, R. (2020). Industrial-scale study of the chemical composition of olive oil process-derived matrices. *Processes*, *8*(6), art. no. 701. **https://doi.org/10.3390/pr8060701**
30. Jukić Špika, M., Liber, Z., Montemurro, C., Miazzi, M.M., Ljubenkov, I., Soldo, B., Žanetić, M., Vitanović, E., Politeo, O., Škevin, D. (2022). Quantitatively unraveling hierarchy of factors impacting virgin olive oil phenolic profile and oxidative stability. *Antioxidants*, *11*(3), art. no. 594. **https://doi.org/10.3390/antiox11030594**
31. Kamelnia, E., Mohebbati, R., Kamelnia, R., El-Seedi, H.R., Boskabady, M.H. (2023). Anti-inflammatory, immunomodulatory and anti-oxidant effects of *Ocimum basilicum* L. and its main constituents: A review. *Iranian Journal of Basic Medical Sciences*, *26*(6), 617-627. **https://doi.org/10.22038/IJBMS.2023.67466.14783**
32. Karacabey, E., Özkan, G., Dalgıç, L., Sermet, S.O. (2016). Rosemary aromatization of extra virgin olive oil and process optimization including antioxidant potential and yield. *Turkish Journal of Agriculture - Food Science and Technology*, *4*(8), 628–635. **https://doi.org/10.24925/turjaf.v4i8.628-635.724**
33. Klisović, D., Koprivnjak, O., Novoselić, A., Pleadin, J., Lešić, T., Brkić Bubola, K. (2022). Compositional changes in the extra virgin olive oil used as a medium for cheese preservation. *Foods*, *11*(15), art. no. 2329. **https://doi.org/10.3390/foods11152329**
34. Liu, X.-Y., Wang, W.-Z., Yao, S.-P., Li, X.-Y., Han, R.-M., Zhang, D., Zhao, Z., Wang, Y., Zhang, J.-P. (2024). Antioxidation activity enhancement by intramolecular hydrogen bond and non-browning mechanism of active ingredients in rosemary: Carnosic acid and carnosol. *The Journal of Physical Chemistry B*, *128*(31), 7627–7638. **https://doi.org/10.1021/acs.jpcb.4c02949**
35. Mączka, W., Twardawska, M., Grabarczyk, M., Wińska, K. (2023). Carvacrol – A natural phenolic compound with antimicrobial properties. *Antibiotics*, *12*(5), art. no. 824. **https://doi.org/10.3390/antibiotics12050824**
36. Manai-Djebali, H., Yeddes, W., Hammami, M., Nait-Mohamed, S., Habachi, E., Msaada, K., Ben Youssef, N. (2024). Exploring the synergistic potential of wild nettle and olive oil: bioactive compounds, antioxidant capacity, and antibacterial properties. *International Journal of Environmental Health Research*, *34*(8), 3046–3055. **https://doi.org/10.1080/09603123.2023.2287589**
37. Marcelino, G., Hiane, P.A., Freitas, K. de C., Santana, L.F., Pott, A., Donadon, J.R., Guimarães, R. de C.A. (2019). Effects of olive oil and its minor components on cardiovascular diseases, inflammation, and gut microbiota. *Nutrients*, *11*(8), art. no. 1826. **https://doi.org/10.3390/nu11081826**
38. Mason, T.L., Wasserman, B.P. (1987). Inactivation of red beet β-glucan synthase by native and oxidized phenolic compounds. *Phytochemistry*, *26*(8), 2197–2202. **https://doi.org/10.1016/S0031-9422(00)84683-X**
39. Mateus, A.R.S., Serrano, C., Almeida, C., Soares, A., Rolim Lopes, V., Sanches-Silva, A. (2024). Beyond thymol and carvacrol: characterizing the phenolic profiles and antioxidant capacity of Portuguese oregano and thyme for food applications. *Applied Sciences*, *14*(19), art. no. 8924. **https://doi.org/10.3390/app14198924**
40. Miller, G.L. (1959) Use of dinitrosalicylic acid reagent for determination of reducing sugar. *Analytical Chemistry*, *31*(3), 426–428. **https://doi.org/10.1021/ac60147a030**
41. Navarro, M. del C., Gálvez, I., Hinchado, M.D., Otero, E., Torres-Piles, S., Francisco-Morcillo, J., de La Fuente, M., Martín-Cordero, L., Ortega, E. (2024). Immunoneuroendocrine, stress, metabolic, and behavioural responses in high-fat diet-induced obesity. *Nutrients*, *16*(14), art. no. 2209. **https://doi.org/10.3390/nu16142209**
42. Nieto, G. (2020). A review on applications and uses of *Thymus* in the food industry. *Plants*, *9*(8), art. no. 961. **https://doi.org/10.3390/plants9080961**
43. Özcan, M., AL Juhaimi, F., Uslu, N., Ghafoor, K., Babiker, E., Mohamed Ahmed, I. (2022). Use of herbal essential oil and extracts as antioxidant sources in quality stabilization of extra virgin olive oil stored in different time and packages. *Journal of Food Measurement and Characterization*, *16*, 700–713. **https://doi.org/10.1007/s11694-021-01195-z**
44. Popescu, L., Cojocari, D., Lung, I., Kacso, I., Ciorîță, A., Ghendov-Mosanu, A., Balan, G., Pintea, A., Sturza, R. (2023). Effect of microencapsulated basil extract on cream cheese quality and stability. *Molecules*, *28*(8), art. no. 3305. **https://doi.org/10.3390/molecules28083305**
45. Rhiat, M., Labioui, H., Driouich, A., Aouane, M., Chbab, Y., Driouich, A., Mennane, Z., Ouhssine, M. (2011). Comparative study of bacteriological home costs Moroccans marketed (Mahlabats) and the cheeses manufactured in the laboratory. *Afrique Science: Revue Internationale Des Sciences et Technologie*, *7*(3), 108-112 (in French, English abstract).
46. Tran, C.H., Nghiem, M.T., Dinh, A.M.T., Dang, T.T.N., Van Do, T.T., Chu, T.N., Mai, T.H., Phan, V.M. (2023). Optimization conditions of ultrasound-assisted extraction for phenolic compounds and antioxidant activity from *Rubus alceifolius* Poir leaves. *International Journal of Food Science*, *2023*(1), art. no. 7576179. **https://doi.org/10.1155/2023/7576179**

47. Tsimihodimos, V., Psoma, O. (2024). Extra virgin olive oil and metabolic diseases. *International Journal of Molecular Sciences*, *25*(15), art. no. 8117. **https://doi.org/10.3390/ijms25158117**
48. Yeddes, W., Chalghoum, A., Aidi-Wannes, W., Ksouri, R.,Saidani Tounsi, M. (2019). Effect of bioclimatic area and season on phenolics and antioxidant activities of rosemary (*Rosmarinus officinalis* L.) leaves. *Journal of Essential Oil Research*, *31*(5), 432–443. **https://doi.org/10.1080/10412905.2019.1577305**
49. Yfanti, P., Lazaridou, P., Boti, V., Douma, D., Lekka, M.E. (2024). Enrichment of olive oils with natural bioactive compounds from aromatic and medicinal herbs: Phytochemical analysis and antioxidant potential. *Molecules*, *29*(5), art. no. 1141. **https://doi.org/10.3390/molecules29051141**
50. Zhakipbekov, K., Turgumbayeva, A., Akhelova, S., Bekmuratova, K., Blinova, O., Utegenova, G., Shertaeva, K., Sadykov, N., Tastambek, K., Saginbazarova, A., Urazgaliyev, K., Tulegenova, G., Zhalimova, Z., Karasova, Z. (2024). Antimicrobial and other pharmacological properties of *Ocimum basilicum*, Lamiaceae. *Molecules*, *29*(2), art. no. 388. **https://doi.org/10.3390/molecules29020388**
51. Zhang, N., Li, Y., Wen, S., Sun, Y., Chen, J., Gao, Y., Sagymbek, A., Yu, X. (2021). Analytical methods for determining the peroxide value of edible oils: A mini-review. *Food Chemistry*, 358, art. no. 129834. **https://doi.org/10.1016/j.foodchem.2021.129834**

ORIGINAL ARTICLE
http://journal.pan.olsztyn.pl

Polish Journal of Food and Nutrition Sciences
2025, Vol. 75, No. 3, 261–273
DOI: 10.31883/pjfns/209006
ISSN 1230-0322, e-ISSN 2083-6007

Quality Differences of Longnan Green Tea Based on Physicochemical Parameters and Volatile Organic Compound Profile

Youqiong Liu[1], Hongjie Zhang[1], Junyi Ma[1]*, Shengyan Zhang[1], Xueli Chen[1], Xuancheng Li[2]

[1]College of Life Science, Northwest Normal University, Lanzhou, 730070, China
[2]Wudu Tea Technology Guidance Station, Longnan, 746000, China

This study systematically analyzed the chemical composition and profile of volatile organic compounds (VOCs) of green tea samples from three counties (Wenxian, Wudu, and Kangxian) in Longnan, Gansu Province of China, to elucidate their quality differentiation. Principal component analysis (PCA) of 14 physicochemical parameters extracted five principal components accounting for 82.25% of the total variance, indicating that most of the variance within the data set could be explained. Significant differences were found in contents of glutamic acid, tea polysaccharides, water extract, caffeine and free amino acids among the three production areas. Seventy-two VOCs were identified using headspace-gas chromatography-ion mobility spectrometry (HS-GC-IMS), and the VOCs were predominantly comprised of aldehydes, ketones, and alcohols. Wenxian green tea contained higher proportions of alcohols and aldehydes, Wudu green tea was rich in terpenes, and Kangxian green tea demonstrated a higher ketone content. Orthogonal partial least squares-discriminant analysis (OPLS-DA) effectively discriminated tea origins with robust model parameters (R^2Y=0.937, R^2X=0.719, Q^2=0.71) and identified 52 key VOCs with variable importance in projection (VIP)>1 and p<0.05 as potential geographical markers for differentiating Longnan green teas from different production areas. These findings establish a quality evaluation framework for Longnan green tea while providing technical support for geographical indication protection and targeted development of characteristic regional tea products.

Keywords: aroma compounds, *Camellia sinensis*, green tea quality, ion mobility spectrometry, partial least squares-discriminant analysis, principal component analysis

INTRODUCTION

Tea, which originated in China, is widely favored by consumers due to its distinct flavor and potential health benefits [Pan *et al.*, 2022]. The health benefits of tea are primarily attributed to its secondary metabolites, such as phenolics, caffeine, and other bioactive compounds. Green tea is classified as an unfermented tea because the processing method includes a fixed degreening step to prevent the tea from fermenting [Parvez & Wani, 2024]. The phenolic compounds in green tea remain unoxidized during processing, which effectively preserves the natural green coloration and fresh flavor characteristics of this tea variety. The quality of green tea is principally determined through the comprehensive evaluation of visual appearance, leaf base characteristics, aromatic profile, color of the tea infusion, and infusion taste characteristics [Yu *et al.*, 2020]. The aromatic complexity of green tea arises from its diverse composition of volatile organic compounds (VOCs) with specific chemical classes imparting distinct olfactory notes [Kun *et al.*, 2025]. Aldehydes contribute fresh herbaceous and floral aromas, while terpenes deliver floral-citrus and fruity nuances. Pyrazines introduce nutty and roasted

***Corresponding Author:**
tel: +86-931-7971723; e-mail: **skymjy@nwnu.edu.cn** (Prof. J.-y. Ma)

Submitted: 14 Janury 2025
Accepted: 5 August 2025
Published on-line: 20 August 2025

scent dimensions, complemented by esters and ketones that provide fruity-sweet and minty aromatic layers [Yin *et al.*, 2022]. While non-volatile compounds play a crucial role in shaping the flavor and the taste profile of green tea [Deng *et al.*, 2022; Yu *et al.*, 2014]. The principal bitter and astringent compounds in green tea can broadly be categorized into phenolics and alkaloids, exemplified by catechins, gallic acid, and caffeine [Yu *et al.*, 2014]. According to Zhang *et al*. [2020] and the references therein, caffeine, epicatechin gallate (ECG), and epigallocatechin gallate (EGCG) contribute to the bitterness of green tea, while amino acids, particularly glutamic acid (Glu), glutamine, and L-theanine, are primarily responsible for the umami taste. The sweet-tasting amino acids, such as L-alanine, L-glycine, L-serine, L-proline, L-threonine, and carbohydrates including glucose, saccharose and fructose, are also presented in green tea and tea infusions. These compounds typically impart a sweet aftertaste following the perception of bitterness or astringency. Additionally, compounds like epigallocatechin (EGC) and epicatechin (EC) can enhance the persistence of this sweet aftertaste [Zhang *et al.*, 2020].

Principal component analysis (PCA) reduces dimensions by transforming multiple indicators into several composite indicators [Shi *et al.*, 2021]. Based on this characteristic, PCA can be used to identify the key quality indicators of green tea samples so as to provide a clear understanding of how different factors contribute to overall tea quality.

Ion mobility spectrometry (IMS) represents a novel analytical technique that detects gas-phase molecules and characterizes ionic species based on their differential migration velocities through electric fields in gaseous phases [Wang *et al.*, 2020]. Requiring no sample preparation, this method operates at standard atmospheric pressure. By merging high separation capabilities of gas chromatography (GC) with the fast detection strengths of IMS, this integrated technique offers excellent resolution and sensitivity, providing a robust foundation for both qualitative and quantitative analyses of trace VOCs, particularly in the discrimination of structurally similar isomers [Vautz *et al.*, 2018]. Applications of this GC-IMS technique have expanded to various food science domains, which include quality assessment [Zheng *et al.*, 2024], production process monitoring [Chen *et al.*, 2024], VOCs differentiation [Zhu *et al.*, 2024], flavor characterization [Li *et al.*, 2024], and adulteration identification [Wu *et al.*, 2024].

Longnan is located in the southeastern part of Gansu Province, China, and is the only tea-producing region in Gansu. However, current research on the quality assessment of Longnan green tea is still limited, and its specific quality attributes and competitive advantages remain inadequately characterized. Therefore, the aim of this study was to analyze the chemical composition and identify the key VOCs of green tea from Wenxian, Wudu, and Kangxian in Longnan to establish a reference framework for optimizing and identifying the characteristic traits of Longnan green tea and fostering the development of regional specialty products. This study provides valuable information for understanding the quality variations and characteristics of green tea among these counties.

MATERIALS AND METHODS

Plant material

A total of 24 commercial green tea products of different brands and manufacturers were randomly collected from Wenxian (WX), Wudu (WD), and Kangxian (KX) in Longnan (China), including 8 samples from WX, 7 samples from WD, and 9 samples from KX. All these green tea products are listed in **Table S1** in Supplementary Materials. The products were stored at 4°C in the dark until they were analyzed.

Determination of water extract content and chemical composition of green tea

Determination of water extract content and chemical composition of Longnan green tea was conducted by Gansu Digital Herbal Inspection Center Co., Ltd (Dingxi, China). The results of these analyses were expressed in g of the determined extract/-compound *per* 100 g of tea leaves.

The water extract content was determined using the International Organization for Standardization (ISO) standard [ISO 9768: 1994]. Namely, the water-soluble substances were extracted from the tea leaves by refluxing with boiling water. Then, the content of water-soluble substances was calculated after filtration, rinsing, drying, and weighing the tea residue.

The content of tea polysaccharides (TPS) was analyzed according to an occupation standard established by the General Administration of Quality Supervision, Inspection and Quarantine of China [SN/T 4260-2015]. Weighed tea (0.5 g) was soaked with water, and anhydrous ethanol was added. After centrifugation, the residue was subjected to ultrasound-assisted extraction with boiling water. The extraction was repeated, and the combined supernatants were cooled and filtered. Then, the reaction of the extract with the phenol-sulfur reagent was performed, and absorbance was measured at 490 nm. The TPS content was calculated based on a glucose standard curve.

Gallocatechin gallate (GCG) was analyzed according to a method previously used by Wang *et al.* [2019]. The extract of green tea obtained by ultrasound-assisted extraction with 80% (*v/v*) methanol solution was separated by a Waters Alliance e2695-2998 high-performance liquid chromatography (HPLC) system with a diode array detector and an Empower 3 data workstation (Waters Corporation, Milford, MA, USA). Elution of compounds from Waters SunFire C18 column (4.6×250 mm, 5 µm) was carried out in a gradient system using acetonitrile and 0.5% (*v/v*) acetic acid as the mobile phase with a flow rate of 0.7 mL/min. The target compound was detected at 270 nm and 360 nm dual wavelength and quantified using GCG standard.

The content of EC, EGC, ECG, catechin (C), and EGCG were measured by the HPLC method according to the ISO standard [ISO 14502-2:2005]**.** Catechins were extracted from ground tea samples using 70% (*v/v*) aqueous methanol in a 70°C water bath. Separation was achieved using a Waters Alliance e2695-2998 HPLC system equipped with a Waters SunFire C18 column (4.6×250 mm, 5 µm) under gradient elution, and the target compound was detected at 278 nm. Quantification was performed directly by external standard calibration.

The L-theanine content was quantified based on the ISO standard [ISO 19563:2017]. Tea samples were extracted with boiling water. The extract was purified by polyamide column chromatography, and HPLC analysis was carried out using the same HPLC system with the same C18 column as during GCG content determination. Water and acetonitrile were used as a mobile phase, and a UV detection wavelength was 210 nm. The L-theanine identification and quantification were based on comparative data obtained from the standard.

The contents of Glu and arginine (Arg) were determined using the GB standard [GB/T 30987-2020] issued by the State Administration for Market Regulation of China and the National Standardization Administration of China. A fully automatic amino acid analyzer (L-8900, Hitachi Ltd., Tokyo, Japan) was used in our study. Tea water extract obtained at boiling temperature, was separated by the sulfonic acid type cation exchange column of the amino acid analyzer. The eluted amino acids were derivatized with ninhydrin at 135°C. The primary and secondary amine derivatization products were detected at wavelengths of 570 nm and 440 nm, respectively, through the visible light detector. The retention time was used for qualitative analysis, and the external standard working curves of Glu and Arg were used for quantitative determination.

The total content of free amino acids (FAA) was determined according to a GB standard [GB/T 8314-2013] by reaction of α-amino group of amino acids with ninhydrin at pH 8.0 and detection of a formed purple complex at 570 nm. Quantification was performed by external standard calibration using glutamic acid standards.

The content of caffeine was measured using the ISO standard [ISO 10727:2002]. Namely, the caffeine in tea was extracted with boiling water in the presence of magnesium oxide. HPLC analysis of the extract was performed using a Waters SunFire C18 column (4.6×250 mm, 5 µm), 30% (*v/v*) methanol as a mobile phase, and an ultraviolet detector set to 280 nm. The retention time was used for qualitative analysis, and the external standard working curves of caffeine were used for quantitative determination.

The crude fiber content was analyzed following the ISO standard [ISO 15598:1999]. Namely, the sample was digested with 1.25% NaOH, and the residue was then subjected to incineration and weighed. The crude fiber content was calculated based on the mass loss during the incineration process.

Analysis of volatile organic compounds

The headspace-gas chromatography-ion mobility spectrometry (HS-GC-IMS) analysis of representative tea samples was performed using an HS-10 autosampler (Shimadzu, Kyoto, Japan) coupled with a GC-2010 Pro chromatograph (Shimadzu) and an IMS module (Hanon Advanced Technology Group Co., Ltd, Shandong, China). The system was equipped with a DB-5 capillary column (30 m×0.25 mm×0.25 µm, Shimadzu). The tea samples were first crushed and then passed through 50-mesh and 10-mesh sieves, after which the intermediate particles were accurately weighed (2.000±0.005 g) and transferred into headspace bottles. These samples were incubated at 90°C for 25 min and shaken for 10 min. A pressure of 100 kPa was then applied for 1 min, followed by equilibration for another 1 min. Subsequently, 0.5 mL of the headspace gas was sampled using a 95°C heated syringe and injected into the GC injector at 105°C with a split ratio of 10:1. High-purity nitrogen (>99.999%) served as the carrier gas at a flow rate of 1.0 mL/min. The analytes were ionized in the IMS ionization chamber using a ^{3}H ionization source in a positive ion mode. The resulting ions were introduced into a drift tube with a 100 µs injection pulse width, operated at a drift voltage of 180 V and a temperature of 45°C. Each spectrum was generated from the mean of 12 scans. *n*-Ketones of C_4–C_9 (Shanghai Aladdin Scientific Corp, Shanghai, China) were used as external reference standards to determine the retention index (RI) of each compound. All VOCs were identified by comparing their RIs and drift times (DT) with those of the reference compounds listed in the proprietary GAS ^{3}H_IMS library (Hanon Advanced Technology Group Co., Ltd; version 1.4.2, updated annually) and the NIST 2020 Mass Spectral Library (National Institute of Standards and Technology, Gaithersburg, MD, USA) accessed through the VOCal software (0.4.03, Hanon Advanced Technology Group Co., Ltd). The quantification of VOCs was performed by calculating peak volumes by integrating signals across both chromatographic and ion mobility dimensions. Relative content was expressed as the percentage of each compound's peak volume relative to the total ion current of all VOCs detected in the sample.

Statistical analysis

Measurements were conducted in triplicate for water extract, chemical composition, and VOC analyses, and the results were expressed as means and standard deviations. The analysis of variance (ANOVA) with Tukey's post hoc test for normally distributed variables, and the Kruskal-Wallis test with Holm-Bonferroni correction for non-normally distributed variables were used to evaluate the differences in physicochemical parameters and VOCs among Longnan green teas from three different counties. Differences were considered statistically significant at $p<0.05$.

The 14 quality indicators of Longnan green tea were subjected to PCA to obtain the eigenvalue, variance contribution rate, and cumulative contribution rate of each component. Only components with eigenvalues greater than 1 were selected for further analysis. The score function expressions (Y_n) for principal components 1 to 5 were calculated using Equation (1):

$$Y_n = PC_1 \times z_1 + PC_2 \times z_2 + PC_3 \times z_3 + \ldots + PC_n \times z_n \quad (1)$$

where: PC_n denotes the feature vector of the corresponding matrix, z_n represents the standardized index for evaluating tea quality.

Subsequently, the comprehensive quality score (Y) of green tea was calculated using Equation (2):

$$Y = Y_1 \times \frac{E_1}{E_1 + E_2 + E_3 + E_4 + E_5} + Y_2 \times \frac{E_2}{E_1 + E_2 + E_3 + E_4 + E_5} + \\ + Y_3 \times \frac{E_3}{E_1 + E_2 + E_3 + E_4 + E_5} + Y_4 \times \frac{E_4}{E_1 + E_2 + E_3 + E_4 + E_5} + \\ + Y_5 \times \frac{E_5}{E_1 + E_2 + E_3 + E_4 + E_5} \quad (2)$$

where: E_1, E_2, E_3, E_4, and E_5 are the eigenvalues of PC_1, PC_2, PC_3, PC_4, and PC_5, respectively. The calculation steps for the comprehensive evaluation score were based on methods referenced from previous studies [Shi *et al.*, 2021].

ANOVA and PCA were carried out using SPSS (version 24.0, IBM, Armonk, NY, USA). SIMCA 14.1 (Sartorius Stedim Data Analytics AB, Umeå, Sweden) software was used to conduct orthogonal partial least squares-discriminant analysis (OPLS-DA) for determining variable importance in projection (VIP) scores. Heat map was subsequently created using Origin 2021 (Origin Lab, Northampton, MA, USA).

RESULTS AND DISCUSSION

Physicochemical parameters of green tea

Multiple components, which influence the quality of green tea, are essential to the scientific evaluation of tea taste quality. This study analyzed the variations in the contents of C, EC, ECG, EGC, EGCG, GCG, L-theanine, Glu, Arg, FAA, TPS, crude fiber, caffeine, and tea water extract among Longnan green tea samples from different counties (**Table 1**). The green tea samples from the three counties in Longnan exhibited similar contents of individual catechins and L-theanine ($p \geq 0.05$), but differed significantly in key indices such as tea water extract, Glu, TPS, FAA, and caffeine ($p < 0.05$). The mean tea water extract was significantly higher in the green tea from KX compared to WX and WD samples. The mean TPS content was markedly higher in the KX green tea than in the WX samples. Conversely, the mean content of Glu was considerably higher in the WX green tea than in WD and KX samples. Moreover, the WD green tea had significantly higher mean levels of caffeine and FAA average compared to the KX samples.

Water extracts

The tea water extracts of all green tea samples ranged from 41.88 to 46.48 g/100 g (**Table 1**). The lower means for WD and WX green tea (43.17 and 43.57 g/100 g, respectively) compared to the mean for the KX sample (45.10 g/100 g) may suggest differences in plucking or drying processes, or variations in leaf maturity at harvest, potentially leading to a lower yield of extractable compounds [Aaqil *et al.*, 2023]. In turn, the higher extractability indicating a higher content of soluble solids may suggest a potentially richer flavor and aroma profile.

Table 1. Water extract content and chemical composition (g/100 g) of Longnan green tea samples from different counties: Wenxian (WX), Wudu (WD), and Kangxian (KX).

Physicochemical indicator	WX		WD		KX	
	Min–max	Mean	Min–max	Mean	Min–max	Mean
Water extract	42.96–44.89	43.57±0.63^{b}	41.88–45.55	43.17±1.26^{b}	43.37–46.48	45.10±1.02^{a}
TPS	0.53–1.02	0.78±0.17^{b}	0.68–1.15	0.88±0.15^{ab}	0.95–1.20	1.02±0.09^{a}
C	0.21–0.48	0.28±0.09^{a}	0.16–0.38	0.27±0.08^{a}	0.12–0.33	0.23±0.08^{a}
GCG	0.26–1.77	1.11±0.49^{a}	0.27–1.89	1.21±0.61^{a}	0.44–1.50	0.83±0.39^{a}
EC	0.46–0.79	0.58±0.10^{a}	0.40–0.86	0.58±0.16^{a}	0.37–0.76	0.61±0.13^{a}
ECG	1.95–3.87	3.11±0.57^{a}	2.49–3.39	3.01±0.32^{a}	2.26–3.54	2.78±0.39^{a}
EGC	0.06–3.03	0.79±0.97^{a}	0.02–1.23	0.64±0.56^{a}	0.11–2.02	1.19±0.70^{a}
EGCG	5.24–9.66	8.34±1.64^{a}	7.62–11.22	9.38±1.26^{a}	8.63–10.84	9.54±0.63^{a}
FAA	5.45–8.61	6.87±1.00^{ab}	6.01–8.51	7.07±0.80^{a}	4.60–6.69	5.81±0.69^{b}
L-Theanine	0.74–1.71	1.27±0.37^{a}	0.48–1.60	0.93±0.38^{a}	0.62–2.65	1.09±0.69^{a}
Glu	0.23–0.58	0.43±0.11^{a}	0.24–0.52	0.38±0.11^{b}	0.22–0.41	0.30±0.06^{b}
Arg	0.10–0.57	0.28±0.17^{a}	0.05–0.59	0.20±0.18^{a}	0.05–0.31	0.16±0.08^{a}
Caffeine	3.28–4.31	3.84±0.35^{ab}	3.68–4.62	4.25±0.31^{a}	3.30–4.44	3.76±0.38^{b}
Crude fiber	6.42–8.86	7.26±0.93^{a}	7.35–9.94	8.12±1.15^{a}	7.51–9.19	8.22±0.61^{a}

The values are pooled from Longnan green tea samples in three different counties. Values in the same row with different superscript letters (a, b) indicate significant differences ($p < 0.05$)
TPS, tea polysaccharides; C, catechin; GCG, gallocatechin gallate; EC, epicatechin; ECG, epicatechin gallate; EGC, epigallocatechin; EGCG, epigallocatechin gallate; FAA, free amino acids; Glu, glutamic acid; Arg, arginine.

Tea polysaccharides

Polysaccharides in tea are known to contribute to mouthfeel, potential bioactivities, and health benefits such as antioxidant and immunomodulatory effects [Wang *et al*., 2022]. In our study, the TPS content of the WX green tea ranged from 0.53 to 1.02 g/100 g with a mean of 0.78 g/100 g. In turn, the WD green tea contained TPS in the range of 0.68–1.15 g/100 g with a mean of 0.88 g/100 g, while the KX green tea had 0.95–1.20 g/100 g with a mean of 1.02 g/100 g (**Table 1**). The TPS content in Longnan green tea was higher compared to literature data for Luzhou high-mountain green tea, for which it ranged from 0.43 to 0.53 g/100 g [Zheng *et al*., 2021]. These differences in TPS content may be influenced by raw materials and post-harvest processing techniques [Xiao *et al*., 2023]. The relatively higher TPS content in the KX green tea may enhance both its functional value and sensory attributes.

Catechins

The primary catechins in green tea include EGCG, EGC, ECG, EC and C. EGCG is usually the most abundant, followed by ECG, EGC, EC, and C in a descending order [Koch *et al.*, 2018]. Similar findings were observed in this study, where EGCG was the most abundant catechin with the content ranging from 5.24 g/100 g to 11.22 g/100 g (**Table 1**). The second with a high content was ECG (1.95–3.89 mg/100 g). The content of EGC was in a broad range from 0.02 to 3.03 g/100 g. In turn, lower contents were found for EC (0.37–0.86 mg/100 g) and C (0.12–0.48 mg/100 g). The contents of catechins in tea are influenced by multiple factors, such as the variety of tea, environmental conditions during growth, the timing of plucking, and the method of processing [Donlao & Ogawa, 2019; Tan *et al.*, 2017; Wei *et al.*, 2011; Ye *et al.*, 2018]. Additionally, the maturity of fresh tea leaves also influences catechin levels, and the tender tea leaves often contain higher concentrations of catechins [Xu *et al.*, 2021]. Higher levels of catechins not only contribute to the health benefits of the tea but also influence its flavor and overall sensory profile [Zhang *et al.*, 2020]. Notably, the EGCG (5.24–11.22 g/100 g) and ECG (1.95–3.87 g/100 g) levels quantified in Longnan green tea products substantially exceed those reported for Japanese green tea (EGCG content in the range of 0.09–6.75 g/100 g, ECG content in the range of 0.29–1.59 g/100 g) [Unno *et al.*, 2025].

Amino acids

The mean content of FAA in WX, WD, and KX green tea samples was 6.87, 7.07, and 5.81 g/100 g, respectively (**Table 1**). The quality of green tea is closely associated with its amino acid content, with higher amino acid levels typically indicating higher tea quality, as they contribute to a fresher and more umami-rich taste [Kazan *et al.*, 2019]. The relatively higher FAA content of the WX and WD green tea samples suggests that these products may possess superior sensory quality. The mean content of Glu was 0.43 g/100 g in WX, 0.38 g/100 g in WD, and 0.30 g/100 g in KX green tea. The content of Arg in all Longnan green teas ranged from 0.05 to 0.59 g/100 g. Such variations in amino acid content may result from differences in protein hydrolysis under distinct processing conditions [Ye *et al.*, 2018; Zhu *et al.*, 2021]. L-Theanine is known for its contribution to the umami flavor and broad spectrum of health benefits, such as regulating inflammation, protecting nerves, aiding gastrointestinal health, and potentially inhibiting tumors [Chen *et al.*, 2023]. Additionally, certain studies suggested that L-theanine might influence the aroma of tea [Guo *et al.*, 2019]. This compound was detected in all the studied samples with content ranging from 0.48 to 2.65 g/100 g (**Table 1**). In comparison, this range of L-theanine content, as well as the range of Arg content in Longnan green tea were within the ranges reported in the literature for Japanese green tea (0.03–3.06 and 0.03–0.97 g/100 g, respectively), although the Glu content (0.007–0.44 g/100 g) was lower in the cited study [Unno *et al.*, 2025]. These inter-regional differences likely reflect variations in tea cultivars, growing conditions, and processing techniques. It is important to note that processing techniques have a substantial influence on L-theanine content. For instance, the highest loss of L-theanine (nearly 50%) occurs during the withering stage, followed by the drying process [Sari & Velioglu, 2013]. This highlights the critical role of processing parameters in preserving L-theanine in green tea, which in turn reinforces the importance of L-theanine as a key determinant of tea quality.

Caffeine

WD green tea had the highest caffeine content among the three counties ranging from 3.68 to 4.62 g/100 g (**Table 1**). Given that the stimulating and invigorating effects of caffeine are positively correlated with its dosage [Choi *et al.*, 2025], this suggests that WD green tea may possess a stronger stimulatory potential. The mean caffeine content in the WX green tea was of 3.84 g/100 g (ranging from 3.28–4.31 g/100 g), whereas KX had a mean value of 3.76 g/100 g (ranging from 3.30–4.44 g/100 g). Caffeine, as the major alkaloid in tea, constitutes 3–5 g/100 g of the dry weight and is crucial for the bitterness of tea [Yu *et al.*, 2014]. Its content in tea is influenced by the age of the tea leaves, with younger, tender leaves generally having more caffeine [Xu *et al.*, 2021]. Deka *et al*. [2021] reported that the caffeine content of popular tea varieties from northeastern India ranged from 2.71 to 4.87 g/100 g, which is similar to the results achieved in this study.

Crude fiber

Longnan green tea showed a crude fiber content ranging from 6.42 to 9.94 g/100 g (**Table 1**). The crude fiber content tends to lower when younger tea leaves are used during processing [Aroyeun, 2013] and may serve as an indirect indicator of tea quality [Śmiechowska & Dmowski, 2006]. In contrast to our study, the crude fiber content of commercial green tea from Pakistan has been reported to be as high as 16.16 g/100 g [Adnan *et al.*, 2013], pointing to substantial differences in plucking standards and raw material selection criteria, with Longnan green tea being more tender compared to Pakistani commercial green tea.

Comprehensive evaluation of green tea quality using principal component analysis

PCA enabled the evaluation of the relative importance of each of the 14 indicators, thereby facilitating a comprehensive assessment of the quality of Longnan green tea. Results in **Table 2** show that 5 principal components with eigenvalues greater than 1 were identified, contributing to a cumulative explained variance of 82.25%. The individual contribution rates for these components were 38.31%, 16.65%, 10.45%, 8.63%, and 8.22%, respectively. A cumulative contribution rate between 70% and 85% (or higher) is typically regarded as adequate in PCA for capturing the majority of the information presented in the original dataset [Shlens, 2014]. Therefore, the five principal components identified in this study could effectively capture the major intrinsic quality information of Longnan green tea, and can be considered as the representative of the essential features and internal variability of the dataset. The Kaiser-Meyer-Olkin (KMO) index of 0.607 and the significance level of 0.001 indicated that it was possible to conduct PCA on the data set. The closer the KMO value to 1, the smaller the partial correlation among variables, and the more suitable the data for factor analysis. Generally, it is considered that when the KMO value is greater than 0.6, the data is moderately suitable for factor analysis. Although the KMO value was slightly lower (0.607) in the test, the significance level was highly significant (p=0.001, much less than 0.05), indicating that the data were still suitable for PCA analysis [Shi *et al*., 2021].

From the perspective of comprehensive score, it is known that PC_1 and PC_2 had the main role in the comprehensive quality evaluation, while PC_3, PC_4, and PC_5 did not account for a large proportion. As shown in **Table 2**, variables such as C (–0.704), GCG (0.879), ECG (0.802), and FAA (0.635), along with EGC (–0.951) and EC (–0.809), exhibited relatively large loadings on PC_1, which indicates that these variables contributed substantially to PC_1. Meanwhile, TPS (–0.628) and Arg (0.750) displayed large loadings on PC_2. The loading values reflected the degree to which each original variable influenced the principal component: the larger the absolute value of the loading, the greater the impact of the variable on the principal component. A positive loading signified a positive influence on the principal component, while a negative loading denoted a negative influence.

As shown in **Table 3**, the green tea samples with higher Y_1 values, such as WD-3 (2.84) and WD-6 (3.03), had notably elevated levels of GCG, ECG and FAA. In contrast, the green tea samples with lower Y_1 values, such as WX-2 (–5.09) and KX-4 (–3.77),

Table 2. Loading coefficients of physicochemical indicators of Longnan green tea from three counties on the five principal components (PC_1– PC_5) and parameters including eigenvalue, variance contribution rate, and cumulative contribution rate for each component.

Indicator/parameter	PC_1	PC_2	PC_3	PC_4	PC_5
Water extract	–0.458	–0.403	0.525	0.274	0.016
TPS	0.135	–0.628	0.469	–0.209	0.428
C	–0.704	0.463	–0.116	0.247	0.010
GCG	0.879	–0.239	0.041	–0.031	–0.032
EC	–0.809	0.380	0.057	–0.010	0.307
ECG	0.802	–0.111	0.132	0.247	0.260
EGC	–0.951	0.161	–0.045	0.050	0.025
EGCG	–0.437	–0.460	–0.403	0.495	0.025
FAA	0.635	0.573	–0.154	–0.018	0.159
L-Theanine	0.013	0.415	0.645	0.318	0.069
Glu	0.830	0.177	–0.232	0.043	–0.177
Arg	0.414	0.750	0.265	0.060	0.223
Caffeine	0.274	–0.122	–0.413	0.431	0.681
Crude fiber	–0.368	0.021	–0.180	–0.653	0.477
Eigenvalue	5.36	2.33	1.46	1.21	1.15
Contribution of variance (%)	38.31	16.65	10.45	8.63	8.22
Cumulative contribution (%)	38.31	54.96	65.41	74.04	82.25

TPS, tea polysaccharides; C, catechin; GCG, gallocatechin gallate; EC, epicatechin; ECG, epicatechin gallate; EGC, epigallocatechin; EGCG, epigallocatechin gallate; FAA, free amino acids; Glu, glutamic acid; Arg, arginine.

Table 3. Principal component analysis scores (Y_1–Y_5) and comprehensive score (Y) of Longnan green tea from different counties: Wenxian (WX), Wudu (WD), and Kangxian (KX).

Green tea	Y_1	Y_2	Y_3	Y_4	Y_5	Y
WX-3	2.52	1.34	1.59	0.11	0.16	1.68
WX-4	2.49	0.07	2.34	0.55	0.53	1.58
WX-5	1.70	2.58	−0.78	2.49	0.10	1.48
WX-6	1.70	2.58	−0.78	2.49	0.10	1.48
WD-3	2.84	−0.87	−0.27	−0.08	0.25	1.13
WD-1	2.55	−0.12	−0.99	0.42	−0.73	1.01
WD-6	3.03	−0.59	−1.88	−2.17	1.23	0.95
KX-2	1.90	−1.61	0.52	−0.14	0.89	0.70
WX-1	0.95	0.19	0.31	1.56	−0.08	0.68
WX-7	1.81	−0.18	−1.18	0.22	−0.73	0.61
KX-5	1.40	−1.63	1.62	0.22	−0.55	0.50
WD-5	−1.27	3.46	−0.19	−0.40	3.31	0.37
WX-8	−0.02	0.31	−0.28	1.10	−0.88	0.05
WD-4	−0.25	−0.19	−1.10	0.69	0.73	−0.15
KX-7	−0.30	−0.32	0.21	−1.03	−0.01	−0.29
KX-8	−0.13	−1.67	0.78	−0.88	−0.93	−0.49
KX-1	−0.80	0.20	−0.85	−1.07	0.49	−0.51
WD-2	−0.80	0.21	−1.42	0.09	−1.25	−0.62
WD-7	−1.60	−0.13	−0.72	1.15	−0.32	−0.77
KX-3	−1.27	−1.41	0.74	−1.15	0.65	−0.84
KX-9	−3.63	0.31	2.78	0.02	0.03	−1.27
KX-6	−3.52	−0.96	0.61	0.31	−0.73	−1.79
KX-4	−3.77	−1.16	0.57	−0.48	−0.43	−2.01
WX-2	−5.09	2.13	−1.27	−0.84	−1.20	−2.31

tended to have higher EGC and EC contents. Moreover, higher Y_2 values, such as in WX-5 (2.58), WX-6 (2.58), and WD-5 (3.46), suggested an elevated Arg content. The magnitude and sign of Y scores reflected the comprehensive characteristics of each tea sample. If certain indicators exhibited a strong negative correlation with a principal component, this might have resulted in a negative weighted composite Y value.

Volatile organic compound composition of green tea

The VOCs were analyzed by HS-GC-IMS to reveal the differences in Longnan green teas. A total of 121 signal peaks were detected across the 24 samples (**Table S2** in Supplementary Materials). Among these, 109 peaks were identified as corresponding to 72 different VOCs, comprising of 17 aldehydes, 17 alcohols, 18 ketones, 5 terpenes, 7 esters, 6 heterocyclic compounds, and 2 acids. The remaining 12 peaks could not be identified due to the limitations in the current commercial database.

As shown in **Table S2**, (Z)-2-penten-1-ol, 1-butanol, 1-propanol, ethanol, 1-penten-3-ol, and pentan-1-ol predominated among the 17 alcohols detected in green tea from three counties of Longnan. Ethanol, a key by-product of plant anaerobic respiration, is seldom regarded as an odor-active compound in tea. However, its presence in the tea infusion matrix might still affect the overall aroma profile of green tea [Huang *et al.*,

2023]. The relative contents of (*Z*)-2-penten-1-ol and its adduct (D), 2-hexen-1-ol and its adduct (D), and 1-butanol D in green tea from WX were significantly higher than those determined in the green tea from the other two counties. The relative contents of 1,8-cineole and its adduct (D), 1-propanol D, and linalool were notably higher in the WD green tea compared to WX and KX green teas. Linalool is a key volatile contributing to floral and citrus aroma [Liu *et al.*, 2023]. 1,8-Cineole has a camphoraceous scent and a cool herbal flavor, it is recognized as the major aromatic compound in ginger [Schaller & Schieberle, 2020], and has also been reported in tea aroma studies [Huang *et al.*, 2023]. 2-Methylbutanal, hexanal, pentanal, heptanal, and propanal exhibited a high content among the 17 aldehydes detected in green tea from the three counties. 2-Methylbutanal, which is an important aroma compound of green tea, was recognized as one of the primary compounds responsible for the malt flavor [Tatsu *et al.*, 2020]. 2,4-Heptadienal was significantly more abundant in the WX green tea compared to WD and KX green teas. It has a fatty floral aroma, while nonanal and heptanal are responsible for the green and fresh aroma of the tea infusion [Xiao *et al.*, 2022]. The main ketones identified in all of the tea samples analyzed were 2,3-butanedione, 1-hydroxy-2-propanone, 1-penten-3-one, 2-butanone, cyclopentanone, acetone, and 3-hydroxybutan-2-one. The relative contents of 2,3-butanedione, 1-hydroxy-2-propanone, 3-hydroxybutan-2-one, and acetone were significantly lower in WD and WX green teas compared to the KX green tea. 2,3-Butanedione significantly affects the aroma quality of green tea and can sometimes result in a 'cooked' flavor [Tao *et al.*, 2025; Yin *et al.*, 2022]. The relative contents of α-pinene, 3-carene, β-pinene, and limonene were higher in the WD green tea than in WX and KX green teas. Limonene in tea products may contribute to the formation of fruity aromas, and as an intermediate in the synthesis of many monoterpenes, plays a significant role in the formation of these compounds [Zhou *et al.*, 2024].

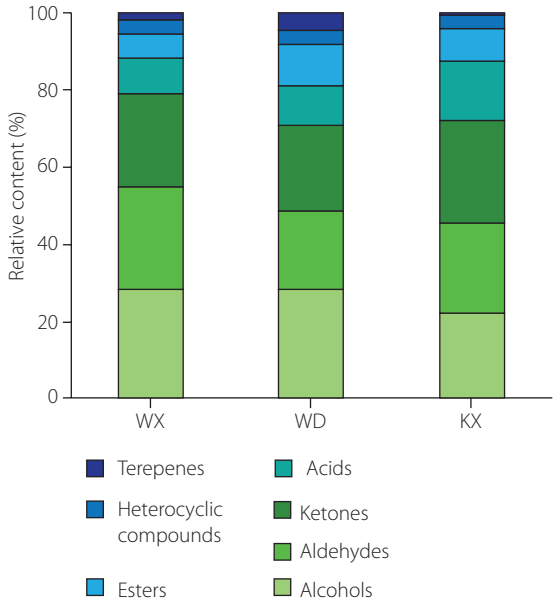

Figure 1. Relative content of different classes of volatile organic compounds in Longnan green tea from different counties: Wenxian (WX), Wudu (WD), and Kangxian (KX).

Figure 1 clearly illustrates significant differences in VOCs among green teas from different counties. Alcohols, aldehydes, and ketones accounted for the largest proportion of the total VOCs, corroborating the findings from studies on Guizhou green tea [Ge *et al.*, 2024]. Specifically, the WX green tea exhibited the highest alcohol content (28.30%), closely followed by WD samples (27.92%), whereas the KX green tea recorded the lowest alcohol level (22.21%). In terms of aldehydes, the levels in WX (26.81%) and KX (23.67%) samples were both higher than that in the WD green tea (20.85%). The KX green tea had the highest ketone content (26.22%), exceeding

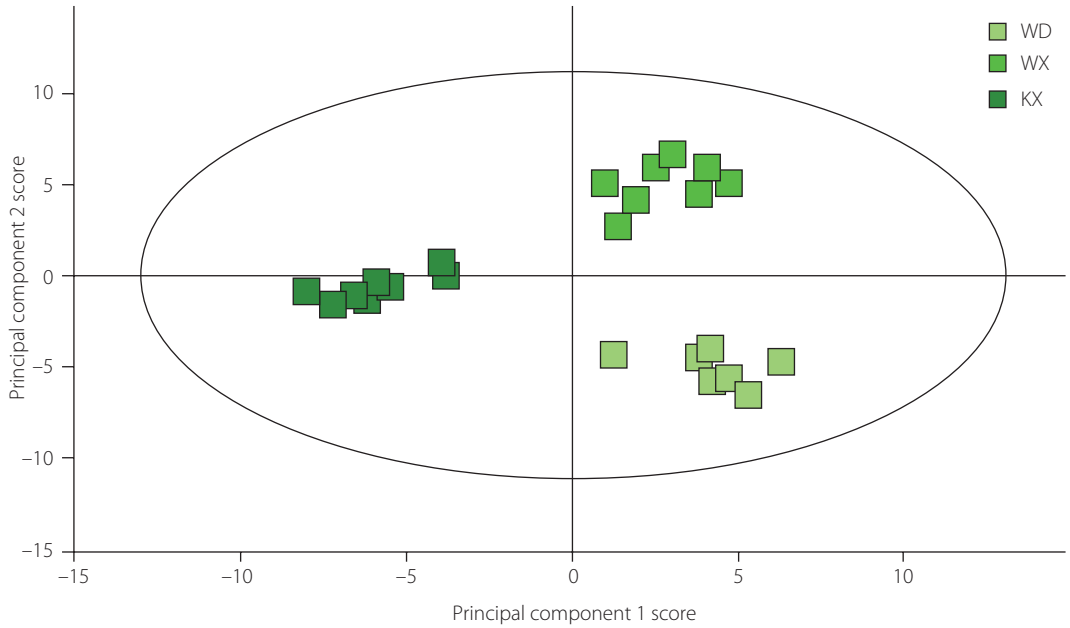

Figure 2. Orthogonal partial least squares-discriminant analysis plot of Longnan green teas from different counties: Wenxian (WX), Wudu (WD), and Kangxian (KX).

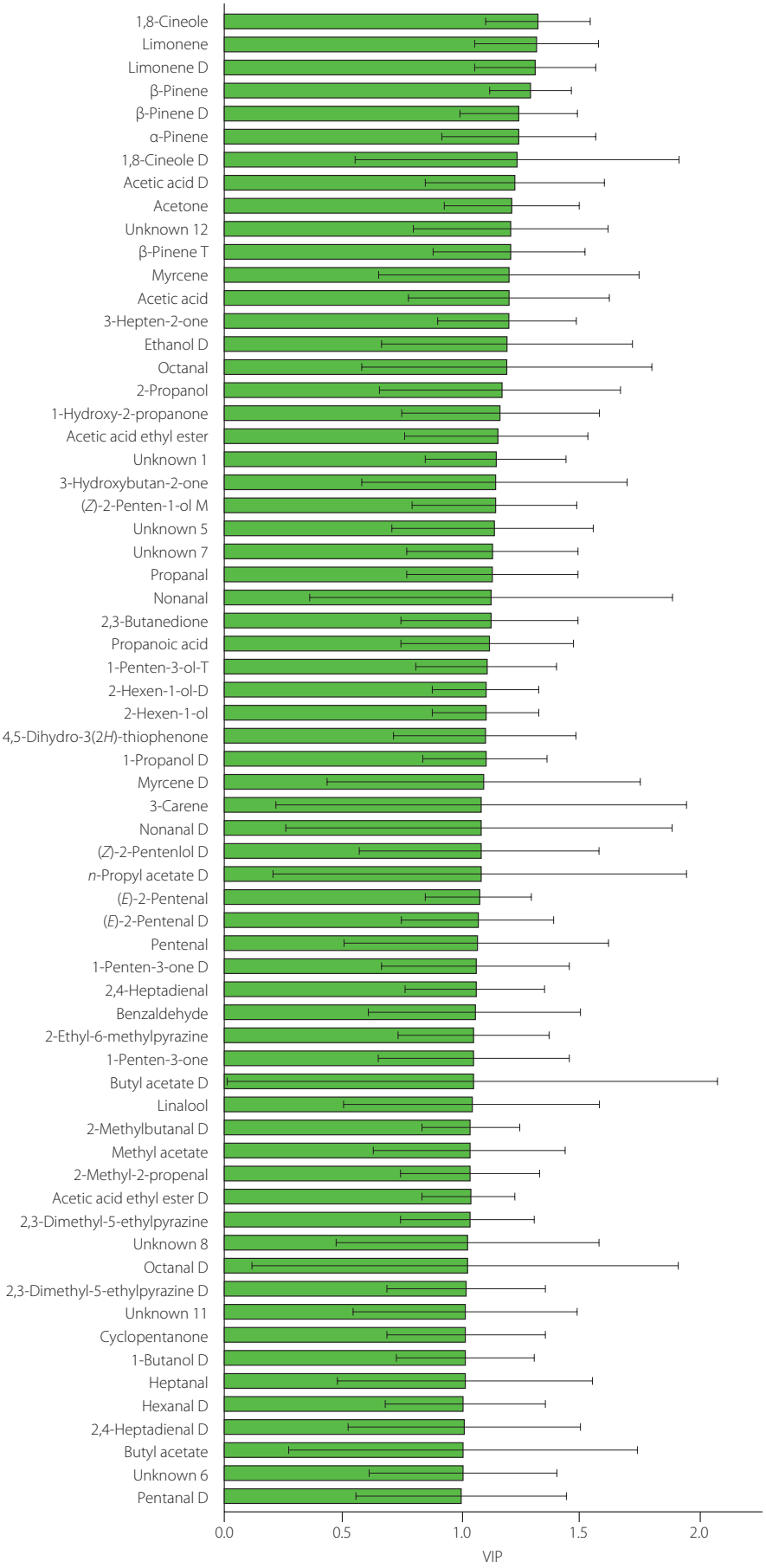

Figure 3. Variable importance in the projection (VIP) scores for volatile organic compounds (VOCs) of Longnan green tea, analyzed by orthogonal partial least squares-discriminant analysis VOCs with VIP>1 are shown. D and T in the compound names indicate ion mobility spectrometry (IMS)-formed adducts, dimers and trimers, respectively.

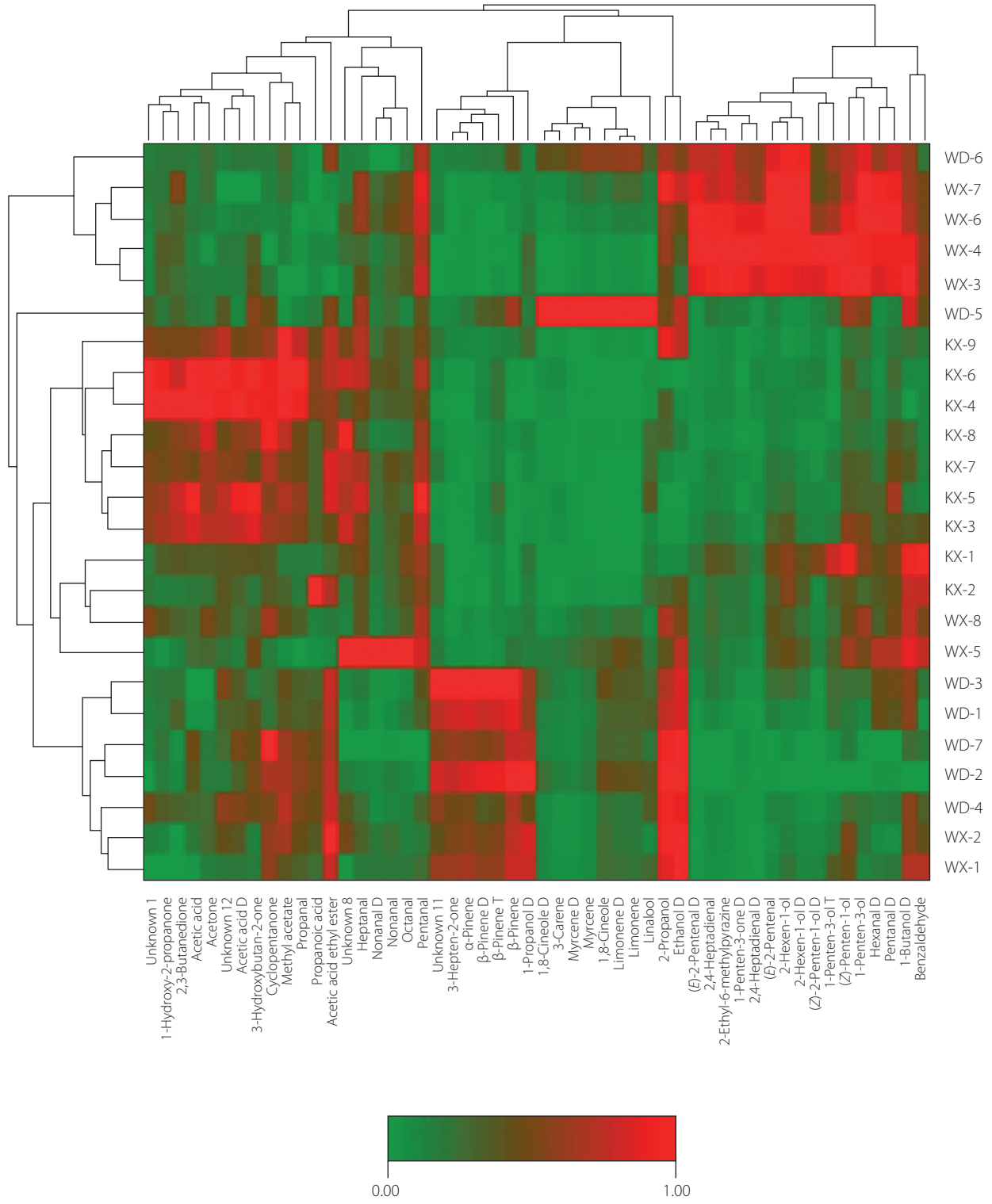

Figure 4. Cluster heatmap of key volatile organic compounds of Longnan green tea from different counties: Wenxian (WX), Wudu (WD), and Kangxian (KX). D and T in the compound names indicate ion mobility spectrometry (IMS)-formed adducts, dimers and trimers, respectively.

that of WX (24.06%) and WD (22.15%) samples. For acids, the KX green tea presented a significantly higher content (15.36%) compared to WX (9.07%) and WD (10.29%) samples. Regarding esters, the WD green tea contained the greatest amount (10.50%), followed by KX (8.13%) and WX (6.30%) samples. Meanwhile, the content of heterocyclic compounds was relatively consistent across teas from all three counties, ranging from 3.5% to 3.9% and indicating limited variation in this category. Previous research has shown that volatile terpenes in tea could safely and effectively enhance its aroma [Zeng *et al.*, 2019]. This study found that the WD green tea had the highest relative content of volatile terpenes at 4.43%, followed by the WX green tea at 1.94% and the KX green tea at 0.68%.

Results of multivariate statistical analysis

The differences in VOCs among Longnan green teas were analyzed using OPLS-DA based on the qualitative and quantitative results obtained from HS-GC-IMS. As shown in **Figure 2**, the KX green tea was distinctly located on the left side of the score plot, whereas WX and WD green tea samples were mainly clustered on the right, with WX samples positioned above and WD samples concentrated below. The dependent variable's fit index (R^2Y) was 0.937, the independent variable's fit index (R^2X) was 0.719, and the model's predictive ability index (Q^2) was 0.710. The R^2 and Q^2 values above 0.5 suggested that the model fitting results were acceptable.

The validated OPLS-DA model was suitable for distinguishing the geographical origins of green tea VOCs. VIP scores were used to evaluate the contribution of each VOC to the classification. Variables with a VIP score greater than 1 were deemed critical. A total of 65 key VOCs with VIP>1 were identified (**Figure 3**).

To systematically differentiate the VOCs in green tea from three counties in Longnan, stringent statistical criteria ($p<0.05$ and VIP>1) were used and ultimately enabled identifying 52 key VOCs. These identified VOCs included 9 alcohols, 9 aldehydes, 7 ketones, 5 terpenes, 2 acids, 2 esters, and 1 pyrazine. The distribution of these differential VOCs was visualized through a clustered heatmap (**Figure 4**) to facilitate a better understanding of the aroma variations among the three counties. The graphical representation effectively illustrated the quantitative and qualitative VOC variations across geographical origins, providing an intuitive framework for interpreting regional flavor characteristics.

As shown in **Figure 4**, Longnan green tea samples exhibited significant differences in the relative content of these VOCs. In the heatmap, red indicated a higher content, whereas green indicated a lower content. Although green tea samples from the same county were not entirely clustered together, this did not negate the presence of county-specific aroma patterns. Specifically, the WX green tea samples contained higher levels of (*E*)-2-pentenal D, 2,4-heptadienal D, 2-ethyl-6-methylpyrazine, 1-penten-3-one D, 2-hexen-1-ol and its adduct (D), (*Z*)-2-penten-1-ol and its adduct (D), hexanal D, pentanal D, and 1-butanol D, which are mainly aldehydes, alcohols, and ketones. These compounds are primarily associated with fruity, green, nutty, vegetable, fatty, almond, and bitter almond aroma notes (**Table S2**). In contrast, the WD green teas exhibited higher contents of 3-hepten-2-one, α-pinene, β-pinene and its adducts (D and T), 1,8-cineole and its adduct (D), limonene and its adduct (D), myrcene and its adduct (D), 3-carene, 1-propanol D, and linalool, these compounds are predominantly terpenoids and mainly imparted fruity, lemony, floral, pine-like, and minty aromas, resulting in a richer aromatic profile of the WD tea samples (**Table S2**). Meanwhile, the KX green tea samples had elevated levels of acetic acid and its adduct (D), 2,3-butanedione, acetone, 3-hydroxybutan-2-one, cyclopentanone, methyl acetate, and propanal, which belong mainly to ketones, acids, aldehydes, and esters. These compounds are mainly associated with sour, creamy, pungent, green, floral, minty, and nutty flavor attributes (**Table S2**).

CONCLUSIONS

This study comprehensively analyzed the physicochemical qualities and profile of VOCs of green tea samples from three counties in Longnan (Wenxian, Wudu, and Kangxian). The findings provide valuable insights into the quality differences and characteristic profiles of green tea from these counties.

The analysis of 14 physicochemical quality indices revealed significant differences in 5 key parameters of Glu, TPS, water extract, caffeine, and FAA among the three counties. Comprehensive evaluation analysis indicated that the primary distinctions among green tea samples from different counties are manifested in their catechin composition and amino acid characteristics. The majority of green tea samples from WX and WD exhibited higher contents of GCG, ECG, and FAA, whereas most KX green tea samples demonstrated higher levels of EGC, C, and EC.

The HS-GC-IMS analysis identified 72 VOCs in Longnan green tea samples, predominantly consisting of aldehydes, ketones, and alcohols. Significant differences in VOC profiles were observed among the three counties. The WX green tea exhibited higher proportions of alcohols and aldehydes, such as (*Z*)-2--penten-1-ol, 1-butanol, and 2,4-heptadienal. The WD green tea contained a greater abundance of terpene compounds, such as α-pinene, β-pinene, and linalool. Comparatively, the KX green tea demonstrated a higher relative content of ketones than the teas from the other two counties.

Our research provides valuable objective data and characterizes the physicochemical and volatile profiles of Longnan green tea from three counties. Future studies should expand upon these findings by incorporating larger sample sizes and adopting more comprehensive analytical strategies including sensory evaluation, metabolomics, and advanced chemometric modeling. Such a multidimensional analytical framework would enable a more holistic understanding of the tea quality determinants and regional characteristics of Longnan green tea, ultimately facilitating the development of geographic indication protection systems and quality standards tailored to this important tea-producing region.

RESEARCH FUNDING

This work was supported by the Gansu Province Characteristic Advantageous Agricultural Products Evaluation (TYNPZ2022-07), the Key Research and Development Project of Gansu Province (22YF7NA121), and the Central Government Guides Local Science and Technology Development Project of Shandong Province (YDZX2024036).

CONFLICT OF INTERESTS

The authors declare that they have no conflict of interest to influence the work reported in this paper.

ORCID IDs

X. Chen https://orcid.org/0009-0005-1022-677X
X. Li https://orcid.org/0009-0005-7552-9587
Y. Liu https://orcid.org/0009-0000-5314-0152
J. Ma https://orcid.org/0000-0003-3929-6040
H. Zhang https://orcid.org/0009-0003-3605-3104
S. Zhang https://orcid.org/0009-0007-5464-7781

SUPPLEMENTARY MATERIALS

The following are available online at **https://journal.pan.olsztyn.pl/Quality-Differences-of-Longnan-Green-Tea-Based-on-Physicochemical-Parameters-and,209006,0,2.html**; **Table S1**. Information about the Longnan green tea used in this study. **Table S2**. Headspace gas chromatography-ion mobility spectrometry (HS-GC-IMS) profiling of volatile organic compounds (VOCs) of Longnan green tea from different counties (Wenxian, WX; Wudu, WD; Kangxian, KX): Chromatographic and spectral data, relative content and aroma characteristics.

REFERENCES

1. Aaqil, M., Peng, C., Kamal, A., Nawaz, T., Zhang, F., Gong, J. (2023). Tea harvesting and processing techniques and its effect on phytochemical profile and final quality of black tea: a review. *Foods, 12*(24), art. no. 4467. **https://doi.org/10.3390/foods12244467**
2. Adnan, M., Ahmad, A., Ahmed, A., Khalid, N., Hayat, I., Ahmed, I. (2013). Chemical composition and sensory evaluation of tea (*Camellia sinensis*) commercialized in Pakistan. *Pakistan Journal of Botany, 45*(3), 901-907. **https://doi.org/10.29322/PJB.45.3.901-907**
3. Aroyeun, S.O. (2013). Crude fibre, water extracts, total ash, caffeine and moisture contents as diagnostic factors in evaluating green tea quality. *Italian Journal of Food Science, 25*(1), 70-75.
4. Chen, Q.H., Yang, X.B., Hong, P.Z., Liu, M.J., Li, Z.Y., Zhou, C.X., Zhong, S.Y., Liu, S. (2024). GC-MS, GC-IMS, and E-Nose analysis of volatile aroma compounds in wet-marinated fermented golden pomfret prepared using different cooking methods. *Foods, 13*(3), art. no. 390. **https://doi.org/10.3390/foods13030390**
5. Chen, S.N., Kang, J.X., Zhu, H.Q., Wang, K.X., Han, Z.Y., Wang, L.Y., Liu, J.S., Wu, Y., He, P., Yu, Y., Li, B. (2023). L-theanine and immunity: A review. *Molecules, 28*(9), art. no. 3846. **https://doi.org/10.3390/molecules28093846**
6. Choi, M.K., Ahn, H.S., Kim, D.E., Lee, D.S., Park, C.S., Kang, C.K. (2025). Effects of varying caffeine dosages and consumption timings on cerebral vascular and cognitive functions: A diagnostic ultrasound study. *Applied Sciences, 15*(4), art. no. 1703. **https://doi.org/10.3390/app15041703**
7. Deka, H., Barman, T., Dutta, J., Devi, A., Tamuly, P., Kumar Paul, R., Karak, T. (2021). Catechin and caffeine content of tea (*Camellia sinensis* L.) leaf significantly differ with seasonal variation: A study on popular cultivars in North East India. *Journal of Food Composition and Analysis, 96*, art. no. 103684. **https://doi.org/10.1016/j.jfca.2020.103684**
8. Deng, S., Zhang, G., Olayemi Aluko, O., Mo, Z., Mao, J., Zhang, H., Liu, X., Ma, M., Wang, Q., Liu, H. (2022). Bitter and astringent substances in green tea: composition, human perception mechanisms, evaluation methods and factors influencing their formation. *Food Research International, 157*, art. no. 111262. **https://doi.org/10.1016/j.foodres.2022.111262**
9. Donlao, N., Ogawa, Y. (2019). The influence of processing conditions on catechin, caffeine and chlorophyll contents of green tea (*Camelia sinensis*) leaves and infusions. *LWT – Food Science and Technology, 116*, art. no. 108567. **https://doi.org/10.1016/j.lwt.2019.108567**
10. GB/T 30987–2020 (2020). *Determination of Free Amino Acids in Plants.* State Administration for Market Regulation of China, National Standardization Administration Committee of China. **http://c.gb688.cn/bzgk/gb/showGb?type=online&hcno=4BF0E4CD3BD859FBC7DA3805D7A2F8A0**
11. GB/T 8314–2013 (2013). *Tea – Determination of Free Amino Acids Content.* State Administration for Market Regulation of China, National Standardization Administration Committee of China. **https://std.sacinfo.org.cn/home/query?stdCode=GB/T%208314-2013**
12. Ge, Y., Wang, L., Huang, Y., Jia, L., Wang, J. (2024). Characteristic flavor compounds in Guizhou green tea and the environmental factors influencing their formation: Investigation using stable isotopes, electronic nose, and headspace-gas chromatography ion migration spectrometry. *LWT – Food Science and Technology, 196*, art. no. 115887. **https://doi.org/10.1016/j.lwt.2024.115887**
13. Guo, X.Y., Ho, C.T., Schwab, W., Song, C.K., Wan, X.C. (2019). Aroma compositions of large-leaf yellow tea and potential effect of theanine on volatile formation in tea. *Food Chemistry, 280*, 73-82. **https://doi.org/10.1016/j.foodchem.2018.12.066**
14. Huang, D.Z., Li, M.R., Wang, H., Fu, M.Y., Hu, S.D., Wan, X.C., Wang, Z.C., Chen, Q. (2023). Combining gas chromatography-ion mobility spectrometry and olfactory analysis to reveal the effect of filled-N_2 anaerobic treatment duration on variation in the volatile profiles of gabaron green tea. *LWT – Food Science and Technology, 179*, art. no. 114630. **https://doi.org/10.1016/j.lwt.2023.114630**
15. ISO 10727:2002 (2002). *Tea and Instant Tea in Solid Form – Determination of Caffeine Content – Method Using High-Performance Liquid Chromatography.* International Organization for Standardization. **https://www.iso.org/standard/31494.html**
16. ISO 14502-2:2005 (2005). *Determination of Substances Characteristic of Green and Black Tea – Part 2: Content of Catechins in Green Tea – Method Using High-Performance Liquid Chromatography.* International Organization for Standardization. **https://www.iso.org/standard/31357.html**
17. ISO 15598:1999 (1999). *Tea – Determination of Crude Fibre Content*. International Organization for Standardization. **https://www.iso.org/standard/28336.html**
18. ISO 19563:2017 (2017). *Determination of Theanine in Tea and Instant Tea in Solid Form Using High-Performance Liquid Chromatography.* International Organization for Standardization. **https://www.iso.org/standard/65341.html**
19. ISO 9768: 1994 (1994). *Tea – Determination of Water Extract*. International Organization for Standardization. **https://www.iso.org/standard/21061.html**
20. Kazan, R.M., Seddik, H.A., Marstani, Z.M., Elsutohy, M.M., Yasri, N.G. (2019). Determination of amino acids content in tea species using liquid chromatography via pre-column fluorescence derivatization. *Microchemical Journal, 150*, art. no. 104103. **https://doi.org/10.1016/j.microc.2019.104103**
21. Koch, W., Kukula-Koch, W., Komsta, L., Marzec, Z., Szwerc, W., Glowniak, K. (2018). Green tea quality evaluation based on its catechins and metals composition in combination with chemometric analysis. *Molecules, 23*(7), art. no. 1689. **https://doi.org/10.3390/molecules23071689**
22. Kun, J., Yang, Y., Sun, J., Dai, H., Luo, Z., Tong, H. (2025). Characterization of potential aroma compounds in five aroma types of green tea using the sensomics approach. *LWT – Food Science and Technology, 215*, art. no. 117177. **https://doi.org/10.1016/j.lwt.2024.117177**
23. Li, M.M., Sun, M.Q., Ren, W., Man, L.M., Chai, W.Q., Liu, G.Q., Zhu, M.X., Wang, C. (2024). Characterization of volatile compounds in donkey meat by gas chromatography-ion mobility spectrometry (GC-IMS) combined with chemometrics. *Food Science of Animal Resources, 44*(1), 165-177. **https://doi.org/10.5851/kosfa.2023.e67**
24. Liu, N., Shen, S., Huang, L., Deng, G., Wei, Y., Ning, J., Wang, Y. (2023). Revelation of volatile contributions in green teas with different aroma types by GC–MS and GC–IMS. *Food Research International, 169*, art. no. 112845. **https://doi.org/10.1016/j.foodres.2023.112845**
25. Pan, S.Y., Nie, Q., Tai, H.C., Song, X.L., Tong, Y.F., Zhang, L.J.F., Wu, X.W., Lin, Z.H., Zhang, Y.Y., Ye, D.Y., Zhang, Y., Wang, X.Y., Zhu, P.L., Chu, Z.S., Yu, Z.L., Liang, C. (2022). Tea and tea drinking: China's outstanding contributions to the mankind. *Chinese Medicine, 17*(1), art. no. 27. **https://doi.org/10.1186/s13020-022-00571-1**
26. Parvez, S., Wani, I.A. (2024). Exploring the antioxidant realm of green tea: From extraction to fortification. *eFood, 5*(4), art. no. e172. **https://doi.org/10.1002/efd2.172**
27. Sari, F., Velioglu, Y.S. (2013). Changes in theanine and caffeine contents of black tea with different rolling methods and processing stages. *European Food Research and Technology, 237*(2), 229-236. **https://doi.org/10.1007/s00217-013-1984-z**
28. Schaller, T., Schieberle, P. (2020). Quantitation of key aroma compounds in fresh, raw ginger (*Zingiber officinale* Roscoe) from China and roasted ginger by stable isotope dilution assays and aroma profiling by recombination experiments. *Journal of Agricultural and Food Chemistry, 68*(51), 15284-15291. **https://doi.org/10.1021/acs.jafc.0c06733**
29. Shi, S.J., Wang, E.T., Li, C.X., Zhou, H., Cai, M.L., Cao, C.G., Jiang, Y. (2021). Comprehensive evaluation of 17 qualities of 84 types of rice based on principal component analysis. *Foods, 10*(11), art. no. 2883. **https://doi.org/10.3390/foods10112883**
30. Shlens, J. (2014). A tutorial on principal component analysis. *ArXiv preprint Arxiv, 1404*, art. no. 1100. **https://doi.org/10.48550/arXiv.1404.1100**
31. Śmiechowska, M., Dmowski, P. (2006). Crude fibre as a parameter in the quality evaluation of tea. *Food Chemistry, 94*(3), 366-368. **https://doi.org/10.1016/j.foodchem.2004.11.026**

32. SN/T 4260–2015 (2015). *Determination of Crude Polysaccharides in Plant Source Foods for Export – Phenol-sulfuric Acid Colorimetry.* General Administration of Quality Supervision, Inspection and Quarantine of China. **http://down.foodmate.net/standard/yulan.php?itemid=45196**
33. Tan, J., Engelhardt, U.H., Lin, Z., Kaiser, N., Maiwald, B. (2017). Flavonoids, phenolic acids, alkaloids and theanine in different types of authentic Chinese white tea samples. *Journal of Food Composition and Analysis, 57*, 8-15. **https://doi.org/10.1016/j.jfca.2016.12.011**
34. Tao, M., Guo, W., Liang, J., Liu, Z. (2025). Unraveling the key cooked off-flavor compounds in thermally sterilized green tea beverages, and masking effect of tea raw material baking. *Food Chemistry, 464*(Part 1), art. no. 141671. **https://doi.org/10.1016/j.foodchem.2024.141671**
35. Tatsu, S., Matsuo, Y., Nakahara, K., Hofmann, T., Steinhaus, M. (2020). Key odorants in Japanese roasted barley tea (Mugi-Cha) – differences between roasted barley tea prepared from naked barley and roasted barley tea prepared from hulled barley. *Journal of Agricultural and Food Chemistry, 68*(9), 2728-2737. **https://doi.org/10.1021/acs.jafc.9b08063**
36. Unno, K., Ikka, T., Yamashita, H., Kameoka, Y., Nakamura, Y. (2025). Stress-relieving effects of Japanese green tea: Evaluation using the molar ratio of caffeine and epigallocatechin gallate to theanine and arginine as an indicator. *Foods, 14*(1), art. no. 103. **https://doi.org/10.3390/foods14010103**
37. Vautz, W., Franzke, J., Zampolli, S., Elmi, I., Liedtke, S. (2018). On the potential of ion mobility spectrometry coupled to GC pre-separation – a tutorial. *Analytica Chimica Acta, 1024*, 52-64. **https://doi.org/10.1016/j.aca.2018.02.052**
38. Wang, L., Lin, X, Wang, L.X., Shao, JL., Chen, X.L., Liu, H.C., Mei, W.Q. (2019). Determination and analysis of multifunctional components in tea. *Journal of Food Safety and Quality 10*(22), 7779-7786. **https://doi.org/10.19812/j.cnki.jfsq11-5956/ts.2019.22.057**
39. Wang, Q., Yang, X., Zhu, C., Liu, G., Sun, Y., Qian, L. (2022). Advances in the utilization of tea polysaccharides: Preparation, physicochemical properties, and health benefits. *Polymers, 14*(14), art. no. 2775. **https://doi.org/10.3390/polym14142775**
40. Wang, S.Q., Chen, H.T., Sun, B.G. (2020). Recent progress in food flavor analysis using gas chromatography-ion mobility spectrometry (GC-IMS). *Food Chemistry, 315*, art. no. 126158. **https://doi.org/10.1016/j.foodchem.2019.126158**
41. Wei, K., Wang, L., Zhou, J., He, W., Zeng, J., Jiang, Y., Cheng, H. (2011). Catechin contents in tea (*Camellia sinensis*) as affected by cultivar and environment and their relation to chlorophyll contents. *Food Chemistry, 125*(1), 44-48. **https://doi.org/10.1016/j.foodchem.2010.08.029**
42. Wu, C.Y., Zhang, H., Zhang, H.M., Sun, J.B., Song, Z. (2024). Detection of *Ganoderma lucidum* spore oil adulteration using chemometrics based on a flavor fingerprint by HS-GC-IMS. *European Food Research and Technology, 250*(6), 1683-1693. **https://doi.org/10.1007/s00217-024-04497-w**
43. Xiao, K., Shi, Y., Liu, S., Chen, Y., Ni, D., Yu, Z. (2023). Compositions and antioxidant activity of tea polysaccharides extracted from different tea (*Camellia sinensis* L.) varieties. *Foods, 12*(19), art. no. 3584. **https://doi.org/10.3390/foods12193584**
44. Xiao, Y., Huang, Y.X., Chen, Y.L., Xiao, L.K., Zhang, X.L., Yang, C.H.W., Li, Z.J., Zhu, M., Liu, Z., Wang, Y. (2022). Discrimination and characterization of the volatile profiles of five Fu brick teas from different manufacturing regions by using HS-SPME/GC-MS and HS-GC-IMS. *Current Research in Food Science, 5*, 1788-1807. **https://doi.org/10.1016/j.crfs.2022.09.024**
45. Xu, C., Liang, L., Li, Y., Yang, T., Fan, Y., Mao, X., Wang, Y. (2021). Studies of quality development and major chemical composition of green tea processed from tea with different shoot maturity. *LWT – Food Science and Technology, 142*, art. no. 111055. **https://doi.org/10.1016/j.lwt.2021.111055**
46. Ye, Y.L., Yan, J.N., Cui, J.L., Mao, S.H., Li, M.F., Liao, X.L., Tong, H.R. (2018). Dynamic changes in amino acids, catechins, caffeine and gallic acid in green tea during withering. *Journal of Food Composition and Analysis, 66*, 98-108. **https://doi.org/10.1016/j.jfca.2017.12.008**
47. Yin, P., Kong, Y.-S., Liu, P.P., Wang, J.J., Zhu, Y., Wang, G.M., Sun, M.-F., Chen, Y., Guo, G.Y., Liu, Z.H. (2022). A critical review of key odorants in green tea: Identification and biochemical formation pathway. *Trends in Food Science & Technology, 129*, 221-232. **https://doi.org/10.1016/j.tifs.2022.09.013**
48. Yu, P., Yeo, A.S.L., Low, M.Y., Zhou, W. (2014). Identifying key non-volatile compounds in ready-to-drink green tea and their impact on taste profile. *Food Chemistry, 155*, 9-16. **https://doi.org/10.1016/j.foodchem.2014.01.046**
49. Yu, X.-L., Sun, D.-W., He, Y. (2020). Emerging techniques for determining the quality and safety of tea products: A review. *Comprehensive Reviews in Food Science and Food Safety, 19*(5), 2613–2638. **https://doi.org/10.1111/1541-4337.12611**
50. Zeng, L.T., Watanabe, N., Yang, Z.Y. (2019). Understanding the biosyntheses and stress response mechanisms of aroma compounds in tea (*Camellia sinensis*) to safely and effectively improve tea aroma. *Critical Reviews in Food Science and Nutrition, 59*(14), 2321-2334. **https://doi.org/10.1080/10408398.2018.1506907**
51. Zhang, L., Cao, Q.Q., Granato, D., Xu, Y.Q., Ho, C.T. (2020). Association between chemistry and taste of tea: A review. *Trends in Food Science & Technology, 101*, 139-149. **https://doi.org/10.1016/j.tifs.2020.05.015**
52. Zheng, K.W., Luo, X.Q., Song, S.J., Dong, R.J., Wang, P.M., Xu, B.B., Xu, J.Z. (2024). Qualitative and quantitative analysis for monitoring the fishy odor of anchovy oil. *International Journal of Food Engineering, 20*(4), 279-289. **https://doi.org/10.1515/ijfe-2023-0047**
53. Zheng, Z.X., Zhang, Y.P., Li, Y.X., Yang, X.Q., Du, J.R. (2021). Quality evaluation of Luzhou high-mountain green tea extract and optimization of its extraction process. *Contemporary Chemical Industry, 50*(4), 848-853+872.
54. Zhou, Q.Y., Liang, D.X., Ling, C.J., Gao, L.Y., Ling, Z. (2024). Characterization of the volatile components in the processing of *Citri Exocarpium Rubrum* black tea based on HS-SPME and GC/MS. *Food Science & Nutrition, 12*(10), 7913-7923. **https://doi.org/10.1002/fsn3.4374**
55. Zhu, B.Y., Zhang, J., Li, J.Y., Fang, S.M., Zhang, Z.Z., Wang, R.J., Deng, W.W. (2021). Aroma profile of Jinmudan tea produced using *Camellia sinensis*, cultivar Jinmudan using solid-phase microextraction, gas chromatography-mass spectrometry, and chemometrics. *European Food Research and Technology, 247*(5), 1061-1082. **https://doi.org/10.1007/s00217-021-03687-0**
56. Zhu, L.J., Ou, F.L., Xiang, Y., Wang, B., Mao, Y.C., Zhu, L.F., Zhang, Q., Lei, C. (2024). Detection and comparison of volatile organic compounds in four varieties of hawthorn using HS-GC-IMS. *Separations, 11*(4), art. no. 100. **https://doi.org/10.3390/separations11040100**

ORIGINAL ARTICLE
http://journal.pan.olsztyn.pl

Polish Journal of Food and Nutrition Sciences
2025, Vol. 75, No. 3, 274–282
DOI: 10.31883/pjfns/209007
ISSN 1230-0322, e-ISSN 2083-6007

Enhanced Bioaccumulation of Essential Minerals in Filamentous Fungal Biomass During Cultivation to Produce High Quality Vegan Food

Rachma Wikandari, Hasna Nisrina, Arima D. Setiowati, Ria Millati*

Department of Food and Agricultural Product Technology, Faculty of Agricultural Technology, Gadjah Mada University, Yogyakarta 55281, Indonesia

Filamentous fungi compounds have the ability to bind heavy metals; therefore, it is expected that supplementing cultivation media with essential minerals will lead to mineral accumulation in the fungal biomass. Such biomass can be considered as a food ingredient. This research aimed to investigate the effects of mineral supplementation on fungal growth and sensory properties of food products based on fungal biomass, as well as to determine the optimum supplementation concentration and harvest time. Essential minerals, including iron (Fe), zinc (Zn), and calcium (Ca), were added to the cultivation media of *Rhizopus oligosporus* at concentrations of 1.25–11.25, 0.50–5.25, and 50–125 mg/100 mL, respectively. The results showed that the addition of minerals at 3.75, 1.75, and 87.5 mg/100 mL for Fe, Zn, and Ca, respectively, did not significantly affect fungal growth in comparison with the control. Mineral supplementation with Fe, Zn, and Ca successfully increased the mineral content in the fungal biomass by 5, 5, and 13 times that of the biomass cultivated without supplementation, respectively. The mineral content of the biomass reached 28.26, 3.45, and 63.04 mg/100 g after 48 h of incubation for Fe, Zn, and Ca, respectively. The optimum harvesting times for Fe, Zn, and Ca were 48, 24, and 72 h, respectively. The addition of minerals did not affect the overall liking and taste of nugget made from the mineral-enriched fungal biomass. The Fourier transform infrared spectroscopy results showed that there was a new peak that represents new complexes between metal ions and functional group of the fungal biomass. This study revealed that cultivation media fortification with minerals offers a viable solution to enhance mineral content, which is often lacking in vegan diets.

Keywords: filamentous fungi, growth, mineral adsorption, sensory characteristics of fungal nugget

INTRODUCTION

The adoption of plant-based diets, driven by increasing health and environmental concerns associated with meat consumption, has been on the rise globally, including in Indonesia. Plant-based diets are often chosen for the potential benefits of reducing the incidence of chronic diseases and mitigating environmental impacts, such as greenhouse gas emissions and deforestation [Springmann *et al*., 2018; Willett *et al*., 2019]. Despite the benefits, plant-based diets face certain nutritional limitations. Specifically, they often lack complete essential amino acids, contain anti-nutritional factors and toxins, and are typically deficient in vital minerals, such as Fe, Zn, and Ca [Foster *et al*., 2013; Lynch *et al*., 2018; Neufingerl & Eilander, 2022].

To address mineral deficiencies in plant-based diets, various vegan products are fortified with essential minerals. Mineral fortification is typically carried out during the product formulation process. However, this fortification can lead to challenges, such as a detrimental effect on the product's sensory quality,

***Corresponding Author:**
e-mail: **ria_millati@ugm.ac.id** (Prof. R. Millati)

Submitted: 10 April 2025
Accepted: 5 August 2025
Published on-line: 22 August 2025

reduced bioavailability of the fortified minerals, and potential adverse interactions with other dietary components [Gibson *et al.*, 2020; Kanamarlapudi & Muddada, 2019; Mannar & Hurrell, 2018]. An alternative approach involves the use of filamentous fungi, which have remarkable ability to bind both essential and non-essential metal ions from their environment and increase the content of specific compounds within their biomass [Fomina & Gadd, 2014; Robinson *et al.*, 2021]. Chitin and other cell wall polysaccharides of filamentous fungi are rich in various metal-binding functional groups such as hydroxyl, carbonyl, amino, acetylamino, and carboxyl groups, which enable them to bind and accumulate metal ions [Ayangbenro & Babalola, 2017]. Previous studies have reported the use of *Bacillus subtilis* and *Saccharomyces cerevisiae* as carriers for iron and their application to chocolate fortification [Kanamarlapudi & Muddada, 2019]. Thus, mineral fortification during the cultivation of selected yeast and bacteria may be the superior method.

The most popular commercial fungal-based product is Quorn, produced from *Fusarium venenatum*. In addition, there are various other species of filamentous fungi deemed viable candidates for protein sources, such as *Aspergillus oryzae*, *Rhizopus delemar*, and *Neurospora intermedia* [Wang *et al.*, 2024]. Another potential filamentous fungus is *Rhizopus oligosporus*. It has an excellent nutritional profile and has been employed as a tempeh starter for centuries in Indonesia, demonstrating its safety and acceptability for consumers. This fungus is known for its high protein and fiber contents and absence of antinutritional factors [Wikandari *et al.*, 2023]. Several previous studies reported that some *Rhizopus* sp. have been explored for the ability to remove heavy metals, including cadmium (Cd), arsenic (As), copper (Cu), zinc (Zn), and iron (Fe) [Oladipo *et al.*, 2018; Tahir *et al.*, 2017]. Specifically, *R. oligosporus* has been reported to bind heavy metals, such as mercury (Hg) and copper (Cu) ions [Ozsoy, 2010; Ozsoy *et al.*, 2008]. Therefore, it is hypothesized that fungi can accumulate, within their biomass, minerals that are present in the growth medium. By enriching the growth medium with essential minerals, the resulting fungal biomass is expected to exhibit enhanced nutritional profiles with increased levels of minerals. Moreover, *R. oligosporus* can be cultivated on various substrates, including by-products from the food industry, thereby reducing production costs.

Information on the potential binding capacity of fungal biomass to minerals is scarce and the effects of mineral supplementation on fungal growth and the mineral adsorption efficiency of *R. oligosporus* have not been reported. Excessive metals may have toxic effects on filamentous fungal growth, depending on their metal tolerance [Ahmad *et al.*, 2005]. Shalaby *et al.* [2023] reported that elevated concentrations of minerals, including silver (Ag), zinc (Zn), and iron (Fe), could inhibit the growth of *Aspergillus* sp. In addition, some minerals have detrimental effects on the color and taste of the final product, which might affect consumer acceptance. This present study aimed to investigate the effects of mineral addition on the growth and sensory characteristics of the produced filamentous fungal biomass and to determine the optimum supplementation concentration and harvest time. This work highlights the potential of enriching cultivation media with essential minerals as a promising approach for enhancing the quality of filamentous fungal biomass.

MATERIAL AND METHODS

Microorganisms

The filamentous fungus used in this study was the commercial starter Raprima (Toko Hasil Bumi Langgan, DIY, Indonesia) which is produced from *Rhizopus microsporus* var. *oligosporus* [Hartanti *et al.*, 2015]. The molecular identification conducted by Yarlina *et al.* [2023] showed that the fungi were 100% similar to *R. microsporus* (CBS 631.82). The fungi were kept in the refrigerator at 4°C until use.

Cultivation of filamentous fungi

The cultivation of filamentous fungi was carried out according to a previously reported method [Wikandari *et al.*, 2023]. The filamentous fungi were cultivated using a concentration of 5 g/L glucose as the substrate. Fe, Zn, and Ca were added in the form of $FeSO_4 \times 7H_2O$, $ZnSO_4 \times 7H_2O$, and $CaSO_4 \times 2H_2O$, respectively. The mineral concentrations of the medium were selected to meet the recommended daily intake of minerals *per* consumption of 100 g of fungal biomass [National Academies of Sciences Engineering and Medicine, 2019]. $FeSO_4 \times 7H_2O$ was added at concentrations of 1.25, 3.75, and 11.25 mg/100 mL media. $ZnSO_4 \times 7H_2O$ was added at concentrations of 0.50, 1.75, and 5.25 mg/100 mL media, while $CaSO_4 \times 2H_2O$ was added at concentrations of 50.0, 87.5, and 125.0 mg/100 mL media. Thus, the media contained 0.25, 0.75, and 2.25 mg elemental Fe/100 mL media; 0.11, 0.38, and 1.14 mg elemental Zn/100 mL media; as well as 11.09, 19.39, and 27.71 mg elemental Ca/100 mL media. Medium without mineral addition was used as the control. The media was sterilized at 121°C for 15 min. One gram of starter was inoculated into a 250-mL Erlenmeyer shake-flask containing 100 mL of the media. The mixture was then incubated at room temperature and an agitation speed of 115 rpm for 48 h. Subsequently, the biomass was harvested and separated from the medium, and then washed with distilled water and pressed to remove excess water. The biomass was stored in a freezer at −18°C until use.

Estimation of mineral adsorption and optimal harvest time of filamentous fungal biomass

To evaluate adsorption of minerals during cultivation, the media and biomass samples were taken at 0, 24, and 48 h of incubation. To determine the optimal harvest time for the highest mineral content in filamentous fungal biomass, the incubation time was prolonged until 72 h. The mineral contents of the media and biomass were determined based on the method by Kalayci & Muhammet [2022] using inductively coupled plasma optical emission spectrometry (Agilent 700 Series ICP-OES, Santa Clara, CA, USA). Approximately 0.5 g of the sample was placed into a polytetrafluoroethylene digestion vessel to which 1.5 mL of HNO_3 and 2 mL of H_2O_2 were added. The sample was kept at room temperature for 6 h. The vessel was then closed

for digestion at 170°C for 18 min, then left to cool overnight. The sample was transferred to tubes and diluted to 10 mL with ultrapure water for ICP-OES analysis. The efficiency of mineral adsorption was calculated according to Akpomie *et al.* [2015] using Equation (1):

$$\text{Efficiency (\%)} = \frac{C_0 - C_e}{C_0} \times 100 \quad (1)$$

where: C_0 is the initial mineral concentration in the media (mg/100 mL) and C_e is the final mineral concentration in the media – after 48 h of incubation (mg/100 mL).

Sensory evaluation

The filamentous fungal biomass was served as vegan nuggets for sensory evaluation. The composition of the nuggets included fungal biomass (60%), white bread (6%), tapioca flour (6%), corn starch (1%), modified tapioca (10%), onion (8%), garlic (2%), mushroom seasoning (1%), salt (1%), sugar (3%), white pepper (0.4%), and nutmeg (0.1%), with all percentages calculated by weight. The frozen fungal biomass was first thawed and pressed to remove excess water. The binders and seasonings were minced using a food processor (Phillips HR7627, Amsterdam, The Netherlands) and incorporated with the fungal biomass. The nugget was formed in a tray (40×40 cm^2), steamed for 15 min, then coated with batter and breadcrumbs. Afterwards, it was fried (180°C) for 6 min and served to panelists with water and a cracker.

The sensory properties of the fungal nuggets were evaluated by 50 untrained panelists from the Gadjah Mada University, aged between 18–50 years. Individuals with any health problems (*e.g.*, anosmia, ageusia) or known allergic reactions to fungi were excluded. The sensory evaluation was conducted using a 7-point hedonic scale ranging from "extremely dislike" (score = 1) to "extremely like" (score = 7), with panelists assessing attributes including color, taste, and overall liking.

Color analysis

The fungal nuggets (2×2×1.5 cm^3) were cut into half to expose the internal color, which was subsequently analyzed using a chromameter (Konica Minolta Co. CR-400, Chiyoda, TYO, Japan). The color coordinated of CIELab space were determined as lightness (L^*), redness (a^*), and yellowness (b^*) [Pathera *et al.*, 2017].

Fourier transform infrared spectroscopy analysis

Fourier transform infrared spectroscopy (FTIR) analysis was carried out to discover the influence of mineral addition on functional groups of fungal biomass compounds. The fungal biomass was dried in the oven at 105°C for 24 h, then finely ground into powder. A total of 1 mg of the dried fungal biomass was measured and characterized using an attenuated total reflectance (ATR) FTIR spectrophotometer (Bruker Vertex80, Billerica, MA, USA) in the wavenumber range of 400–4,000 cm^{-1} with a scanning number of 32 and resolution of 4 cm^{-1}.

Statistical analysis

The filamentous fungal cultivation was performed in triplicate, and the analyses were conducted in duplicate. The results were presented as mean and standard deviation (SD). One-way analysis of variance (ANOVA) followed by Duncan's multiple range test (DMRT) was performed for multiple comparisons of the means ($p<0.05$) using IBM SPSS Statistics version 25.0 (International Business Machines Corporation, Armonk, NY, USA).

RESULTS AND DISCUSSION

Effect of mineral addition on the growth of filamentous fungi

This study focused on investigating the effects of mineral addition on fungal growth and determining the mineral concentrations that do not interfere with fungal growth. **Figure 1** shows that the addition of Fe and Zn at different concentrations did not significantly affect the growth of filamentous fungi compared to the control. A previous study reported similar results: the addition of various concentrations of Cd, Cu, lead (Pb), As, and Fe did not affect the growth of *R. microsporus* [Oladipo *et al.*, 2018]. This study also assessed the tolerance indices of *R. microsporus*, which exhibited high to very high tolerance in the media enriched with Cd (25–100 mg/kg), Cu (125–1,000 mg/kg), Pb (100–400 mg/kg), As (125–500 mg/kg), and Fe (200–800 mg/kg). *Rhizopus* species revealed high tolerance to several metals at various concentrations [Ahmad *et al.*, 2005; Sey & Belford, 2021; Zafar *et al.*, 2007]. The metal tolerance of filamentous fungi depends on the isolation site, toxicity, and concentration in the growth media [Zafar *et al.*, 2007].

However, the addition of Ca at 125 mg/100 mL media resulted in a significant decrease in the growth of filamentous fungi (**Figure 1**). Calcium is one of the essential nutrients for fungal growth, but it can be toxic and inhibit growth at excess concentration [Ye *et al.*, 2022]. The presence of calcium in appropriate concentration can promote the microbial growth and activity since it acts as an enzyme activator. However, excessive calcium can easily inhibit the microbial metabolism through the modification of cell membranes, thereby blocking the mass transfer between microbes and the substrate [Yang *et al.*, 2022]. Furthermore, Kumar & Dwivedi [2021] reported that the interaction between filamentous fungi and metals can be either positive or negative, depending on the fungi's tolerance to the metals in the cultivation media. The decrease in the growth rate could be due to metal toxicity, nutritional imbalance in the media, or enzyme inactivation. The present study results demonstrate that Fe, Zn, and Ca can be added in concentrations of 3.75 mg/100 mL, 1.75 mg/100 mL, and 87.5 mg/100 mL, respectively, without interfering with fungal growth.

Adsorption of minerals in filamentous fungi

To further investigate mineral adsorption by fungal biomass, the mineral content was analyzed in the cultivation media

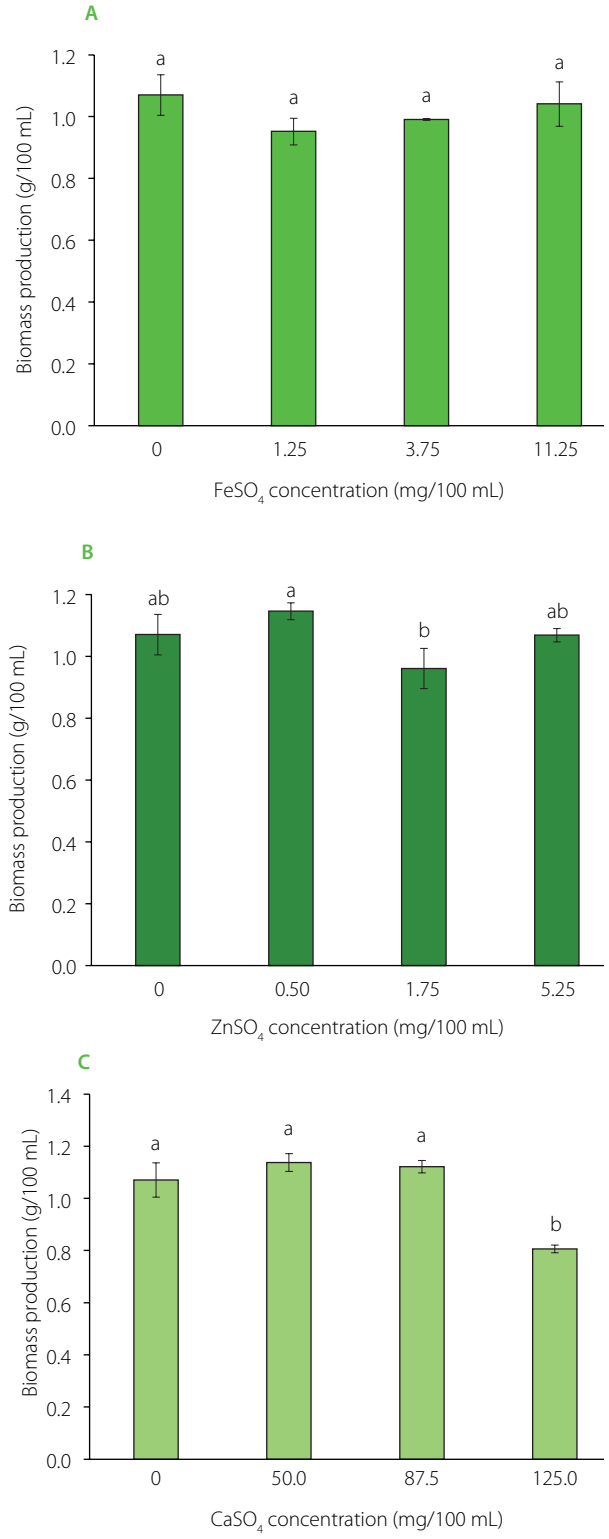

Figure 1. The effects of iron (**A**), zinc (**B**), and calcium (**C**) addition on the growth of filamentous fungal biomass of *Rhizopus oligosporus*. Different letters above bars represent significant differences ($p<0.05$).

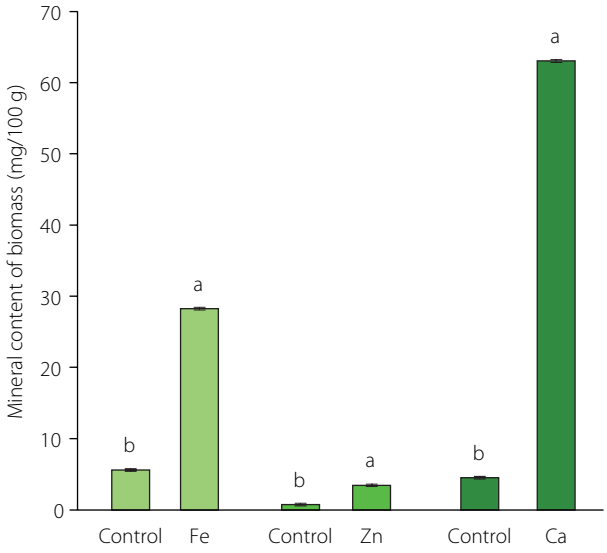

Figure 2. Mineral content of the filamentous fungal biomass of *Rhizopus oligosporus* with and without (control) mineral supplementation after 48 h of incubation. Different letters above bars, separately for each mineral, represent significant differences ($p<0.05$).

and in the fungal biomass. The amount of mineral added to the medium was the optimum mineral concentration obtained from the previous step. The mineral content of the fungal biomass cultivated on the media supplemented with minerals and on the media without supplementation (control) after 48 h of incubation is presented in **Figure 2**. The mineral content of the fortified-fungal biomass was 5–13 times higher than that of the control. These results indicate that *R. oligosporus* can bind and accumulate minerals, which is consistent with findings from several previous studies which demonstrated its ability to bind heavy metals, such as Hg and Cu [Ozsoy, 2010; Ozsoy *et al.*, 2008]. Filamentous fungi can bind and accumulate metal ions in two stages. In the first stage of the metal-fungi interaction, the cell wall binds the metal ions through a metabolically passive process. The compounds of cell walls of filamentous fungi are often negatively charged due to the presence of carboxyl and phosphate groups that allow the adsorption of positively charged metal ions through ion exchange, complexation, and physical adsorption. In the second stage, metal ions are transported into the cell through a metabolically active process [Kumar & Dwivedi, 2021; Zabochnicka-Świątek & Krzywonos, 2014].

The dietary requirements of Fe, Zn, and Ca are influenced by many factors, such as gender, age, and type of diet. The recommended daily allowance (RDA) of Fe, Zn, and Ca varies between 7–27, 3–13, and 700–1,300 mg/day, respectively [National Academies of Sciences, Engineering, and Medicine, 2019]. In the present study, the contents of Fe, Zn, and Ca in filamentous fungal biomass after 48 h of incubation were 28.26, 3.45, and 63.04 mg/100 g, respectively (**Figure 2**). This finding suggests that the consumption of 100 g of filamentous fungal biomass could meet the RDA of iron and fulfill the RDA of zinc for children 1–3 years old. However, the calcium content in filamentous fungal biomass would need to be increased to meet the RDA.

The mineral adsorption data for the filamentous fungal biomass are presented in **Table 1**. The results show that the iron

content in the cultivation media decreased during incubation and that the efficiency of Fe adsorption in fungal biomass was 73.57%. This could be due to the presence of iron in the soluble ferrous form, which is taken up more efficiently than the insoluble form. The Fe ions can then be absorbed through a ferrous iron transporter [Philpott, 2006].

The adsorption efficiencies of Zn and Ca, 4.74% and 9.55%, respectively, were lower than that of Fe (**Table 1**). This suggests that *R. oligosporus* may have less affinity for Zn and Ca. According to Tahir *et al.* [2017], the biosorption efficiency of zinc(II) by a group of fungi, including *A. oryzae*, *Penicillium chrysogenum*, and *Rhizopus oryzae*, ranges from 0.5% to 84.4% under various cultivation conditions. However, similar studies regarding the efficiency of calcium adsorption by filamentous fungi are lacking. Furthermore, the efficiency of mineral adsorption by filamentous fungi is associated with several environmental factors, such as pH, temperature, contact time, as well as concentration and age of the biomass [Zabochnicka-Świątek & Krzywonos, 2014].

Table 1. Mineral content in the media during cultivation of the filamentous fungal biomass of *Rhizopus oligosporus* and efficiency of mineral adsorption.

Mineral	Incubation time (h)	Mineral content in media (mg/100 mL media)	Efficiency (%)
Fe	0	0.6072±0.0083^{a}	73.57
	24	0.2170±0.0017^{b}	
	48	0.1605±0.0004^{c}	
Zn	0	0.2454±0.0003^{b}	4.74
	24	0.2611±0.0002^{a}	
	48	0.2338±0.0010^{c}	
Ca	0	5.9599±0.0012^{a}	9.55
	24	5.5833±0.0292^{b}	
	48	5.3909±0.0065^{c}	

Results are shown as mean ± standard deviation (SD). Different superscript letters within the same column, separately for each mineral, indicate significant differences (p<0.05).

Optimal harvest time of filamentous fungal biomass for a high mineral content

Metal uptake can be influenced by the age of the biomass, which affects the properties of the fungal cell wall and plays a vital role in adsorption mechanisms. To determine the optimal harvest time ensuring a high mineral content of the filamentous fungal biomass, the mineral content after 24, 48, and 72 h of incubation was monitored (**Figure 3**). The results show that the optimal harvest times for filamentous fungi with Fe, Zn, and Ca supplementation were 48, 72, and 24, respectively. The Fe and Ca contents of the filamentous fungal biomass decreased after 48 h of incubation. Fungal biomass age is one of the determinants of optimal adsorption conditions. In a study on metal biosorption, Shalaby *et al.* [2023] reported that extending the incubation time resulted in a lower removal efficiency of metal ions by *Aspergillus* sp. fungus. However, the Zn content of the filamentous fungal biomass increased between 48 and 72 h of incubation (**Figure 3**). The diverse trends among the minerals might be due to the different adsorption rates of the minerals in the fungal biomass. The mechanisms associated with mineral content changes and incubation time require further investigation.

Sensory scores and color coordinates of fungal nuggets

The product's sensory properties are the primary driving force behind purchase intention. Several minerals are dark in color, which might affect the color of the final product. Therefore, a sensory evaluation was conducted to investigate the effect of mineral supplementation of filamentous fungal biomass on consumer preferences for the fungal-based nugget product. The results are shown in **Figure 4**. The nuggets produced from the Ca-enriched fungal biomass received the lowest taste score compared with the control and the other samples. A slightly bitter, sour taste was expressed in the Ca sample. This suggests that the addition of calcium may cause a sensory change in taste, which is in accordance with a previous study reporting that calcium fortification at a concentration of more than 0.3% changed the taste and flavor of beef sausage [Prasetyo & Prayitno, 2021]. Furthermore, Palacios *et al.* [2021] mentioned that high amounts of calcium have been shown to increase acidity, chalkiness, and bitterness.

The study results reveal that the color scores given by the panelists to the Zn and Ca samples were not different from those of the control (**Figure 4**). However, the nuggets produced from the Fe-enriched fungal biomass received lower scores than the control. The color properties, including lightness, redness, and yellowness, of the fungal nuggets were further analyzed using a chromameter. The results show that the Fe sample had the lowest lightness value (**Table 2**), which suggested that iron might have a detrimental effect on the filamentous fungal nuggets. Iron fortification

Table 2. Color coordinates of nuggets produced from the mineral-enriched fungal biomass and non-enriched fungal biomass (control).

Fungal nugget	L^*	a^*	b^*
Control	49.36±0.58^{b}	−0.84±0.04^{a}	13.31±0.27^{a}
Fe-enriched	48.23±0.52^{c}	−0.76±0.08^{a}	13.09±0.11^{a}
Zn-enriched	51.00±0.62^{a}	−0.91±0.21^{ab}	13.57±0.40^{a}
Ca-enriched	51.42±0.06^{a}	−1.16±0.15^{b}	13.52±0.23^{a}

Results are shown as mean ± standard deviation (SD). Different superscript letters within the same column indicate significant differences (p<0.05). L^*, lightness; a^*, redness; b^*, yellowness.

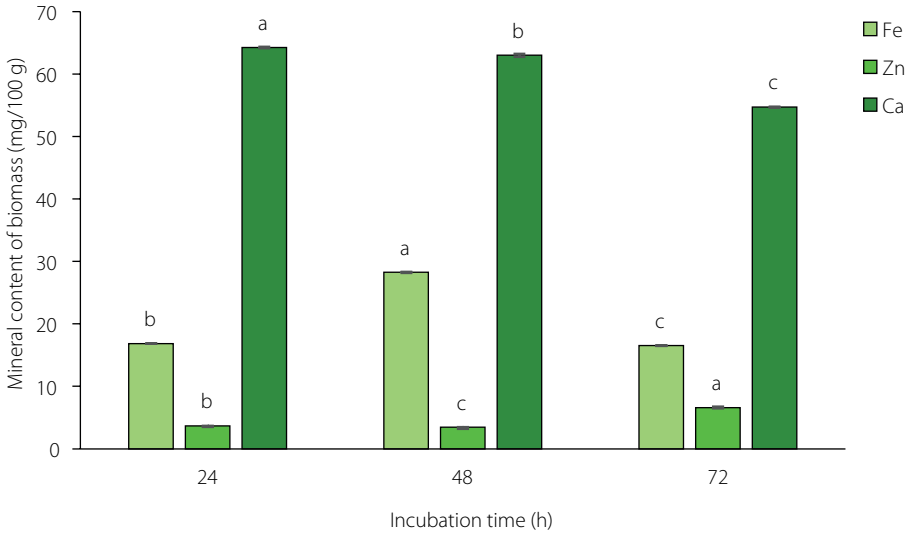

Figure 3. Changes in the mineral content of the filamentous fungal biomass of *Rhizopus oligosporus* in response to mineral supplementation during cultivation. Different letters above bars, separately for each mineral, represent significant differences ($p<0.05$).

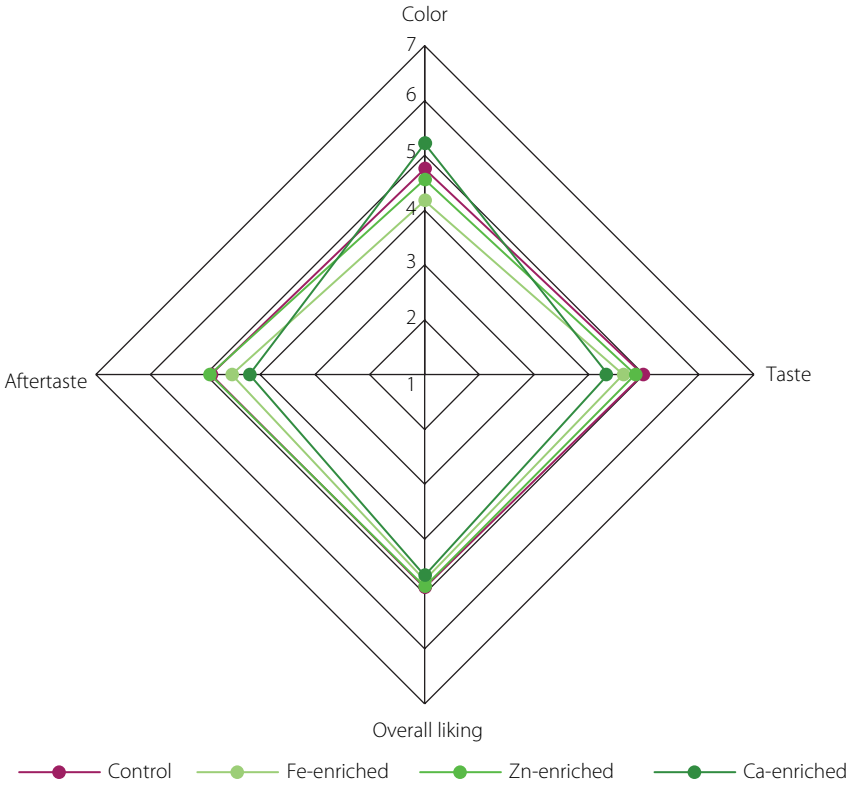

Figure 4. Sensory scores of nuggets produced from the mineral-enriched fungal biomass and non-enriched fungal biomass (control).

can cause unacceptable color changes in food [Hurrell, 2021]. Nuggets are expected to be white in color; therefore, the addition of excessive iron, which is a colored substance, might affect the color of the final product and consumer acceptance. Similar results were obtained from the iron fortification of chocolate [Kanamarlapudi & Muddada, 2019], yogurt [Santillán-Urquiza *et al.*, 2017], extruded snack [Bhat *et al.*, 2017], and cheese [Shoukat *et al.*, 2025]. The effects of Fe supplementation may be due to the characteristics of ferrous sulfate, which is water-soluble and has the potential to cause discoloration in food. The presence of Fe may also accelerate the Maillard reaction during heating, which may result in darker and more intense color [Kathuria *et al.*, 2023]. Various novel fortification techniques were studied to mitigate the discoloration, such as encapsulation and chelation. However, these techniques may affect the production cost and reduce the nutrient bioavailability [Manzoor *et al.*, 2024].

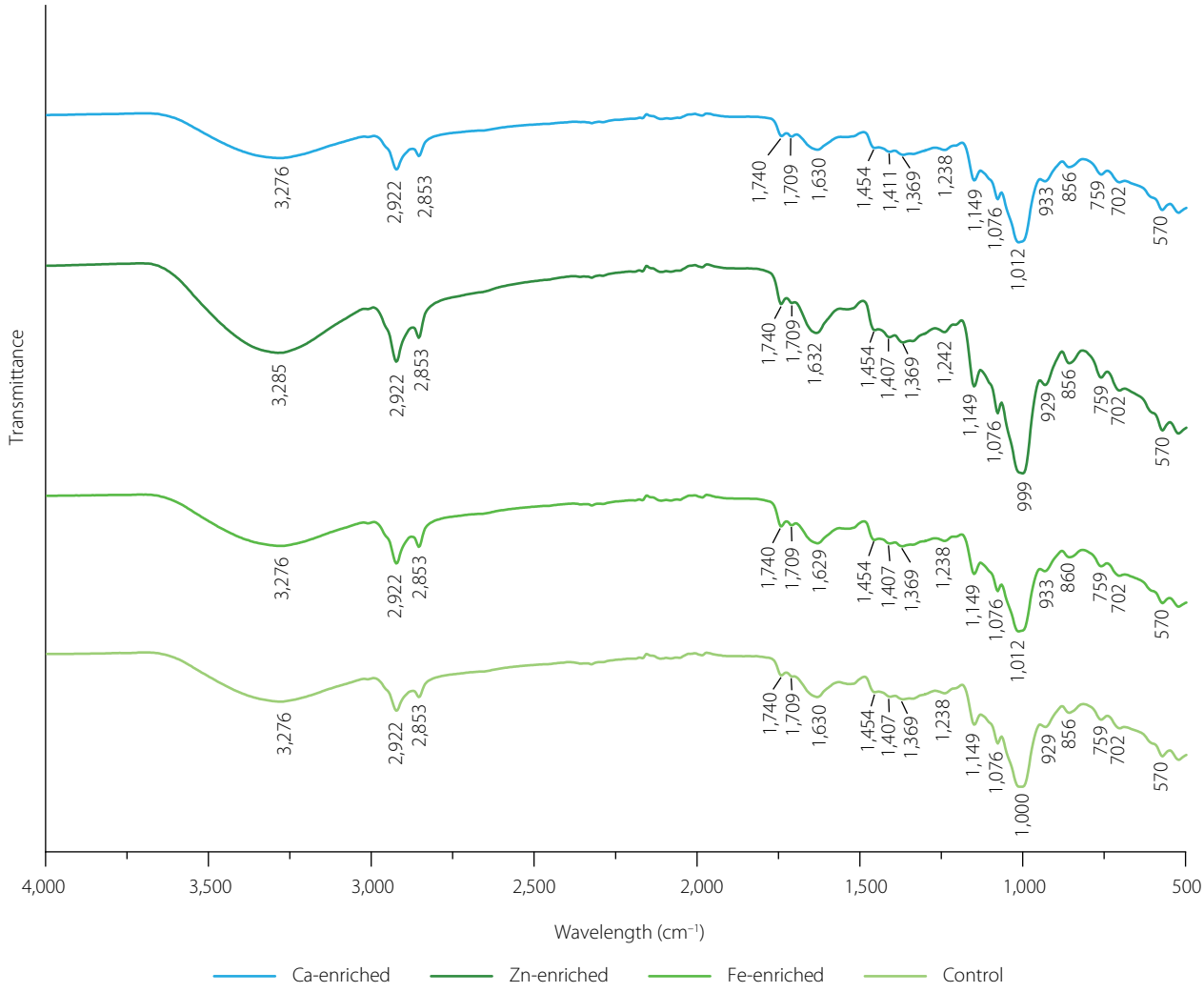

Figure 5. Fourier transform infrared spectra of the filamentous fungal biomass of *Rhizopus oligosporus* with mineral supplementation and without supplementation (control).

The addition of a single mineral did not affect significantly the overall liking of fungal nuggets (**Figure 4**). This indicates that the sensory characteristics of the fungal nuggets were still acceptable to consumers. Kanamarlapudi & Muddada [2019] conducted a study on iron fortification in chocolate using biosorbed biomass containing *B. subtilis* and *S. cerevisiae* and obtained similar results that the fortification with biosorbed biomass did not lead to any significant sensory changes.

Results of Fourier transform infrared spectroscopy analysis

Different studies reported the interaction of various ions with biomass such as *Arthrospira platensis* and *Chlorella vulgaris* [Ferreira *et al.*, 2011], *Padina tetrastromatica* [D'Souza *et al.*, 2008], *Trichoderma harzianum* [Shoaib *et al.*, 2013], *R. oligosporus* [Ozsoy *et al.*, 2008]. Overall, they indicated that the uptake of metal ions from the medium affected the carboxyl, carbonyl, phosphate or, amide groups. The absorption bands in the 3,700 to 3,200 cm^{-1} range are usually attributed to O–H and N–H stretching. The control and fungal biomass supplemented with Ca and Fe had a major peak at 3,276 cm^{-1}, with Ca having the lowest intensity (**Figure 5**). However, in the sample supplemented with Zn, the broad band appeared at a higher wavelength (3,285 cm^{-1}) and showed a significant increase in intensity. This could suggest that Zn^{2+} interfered with the hydrogen bonding network of hydroxyl and amine groups, which might have been due to the direct coordination between Zn^{2+} and biomolecular functional groups, leading to weaker hydrogen bonds and the NH group. A similar phenomenon was observed when *P. tetrastromatica* was grown in the medium with Cd which transformed the OH and NH groups from non-bounded to bounded ones [D'Souza *et al.*, 2008].

In general, changes in spectra intensity at 800–1,800 cm^{-1} could indicate changes in the protein and polysaccharide composition of the biomass in response to the presence of metal ions in the growth medium [D'Souza *et al.*, 2008]. The band at 999–1,012 cm^{-1} could indicate the C–C and C–O stretching of the carbohydrate fraction [Ferreira *et al.*, 2011]. However, Majumdar *et al.* [2008] mentioned that the bands in the region of 1,078–995 cm^{-1} were due to the presence of the phosphate

group in the biomass. Therefore, in our spectra, it was possible that this peak represented an overlap of those functional groups, as indicated by the visible shoulders on the band (**Figure 5**). Therefore, the changes in peak indicated that the presence of metal ions affected not only the carbohydrate composition but also the phosphate group of the biomass. Among all samples, the Zn-treated biomass exhibited the most noticeable spectral changes. In addition, peak positions at 1,407 cm^{-1} can be attributed to the COO– group present in the biomass [Majumdar *et al.*, 2008]. The change in the peak wavelength and intensity of the fungal biomasses (**Figure 5**) seemed to be caused by the binding of the metal ions. The amide I peak was observed at 1,630 cm^{-1} in the control and Ca-fortified sample and shifted to slightly lower and higher values in the sample with Fe and Zn, respectively. In addition, changes in the intensity were also observed, highlighting the effect of metal ions on the biomass protein content and properties. In this study, a band was observed at approximately 1,740 cm^{-1}, corresponding to the C=O stretching vibration of ester carbonyl groups. The presence of this peak in our spectra indicated the presence of lipid-related ester groups in the fungal biomass [D'Souza *et al.*, 2008]. The slight intensity change of this band across treatments may also suggest interactions with metal ions.

Kheeree *et al*. [2022] and Wang *et al.* [2018] mentioned that metal ions can form bonds with carboxyl, carbonyl, phosphate or amide groups, which is in line with our observations. Interaction between metal ions (positively charged) and functional groups (negatively charged) in the biomass could form new complexes. The result of the FTIR measurement confirmed the formation of new complexes between metal ions and functional groups in the fungal biomass. This is in accordance with the results of mineral analysis showing an increase in mineral content of the fungal biomass supplemented with essential minerals.

CONCLUSIONS

This study showed that *R. oligosporus* could adsorb essential metals, including Fe, Zn, and Ca, with optimal harvest times of 48, 72, and 24 h, respectively. The addition of minerals at concentrations of 3.75, 1.75, and 87.5 mg/100 mL for Fe, Zn, and Ca, respectively, did not affect the fungal growth in comparison with the control. It also did not affect the overall liking and taste of nuggets made from the mineral-enriched fungal biomass. This study revealed that the supplementation of the cultivation media with minerals offered a potential natural fortification method for the production of high-mineral vegan products. Future studies may focus on the evaluation of mineral bioavailability in filamentous fungal biomass.

RESEARCH FUNDING

The study was carried out under the Academic Excellence Improvement Program 2024, Universitas Gadjah Mada [grant number 6526/UN1.P1/PT.01.03/2024].

CONFLICT OF INTERESTS

The authors declare no competing interests in this publication.

ADDITIONAL INFORMATION

Ethical clearance approval for the involvement of human subjects in this study was granted by Medical and Health Research Ethics Committee (MHREC), Faculty of Medicine, Public Health and Nursing Universitas Gadjah Mada, reference number KE/FK/1517/EC/2024, dtd 09/30/2024.

ORCID IDs

R. Millati https://orcid.org/0000-0003-4367-1974
A.D. Setiowati https://orcid.org/0000-0003-0104-8068
R. Wikandari https://orcid.org/0000-0001-5650-6092

REFERENCES

1. Ahmad, I., Zafar, S., Ahmad, F. (2005). Heavy metal biosorption potential of *Aspergillus* and *Rhizopus* sp. isolated from wastewater treated soil. *Journal of Applied Sciences and Environment Management, 9*(1), 123–126.
2. Akpomie, K.G., Dawodu, F.A., Adebowale, K.O. (2015). Mechanism on the sorption of heavy metals from binary-solution by a low cost montmorillonite and its desorption potential. *Alexandria Engineering Journal*, *54*(3), 757–767. https://doi.org/10.1016/j.aej.2015.03.025
3. Ayangbenro, A.S., Babalola, O.O. (2017). A new strategy for heavy metal polluted environments: A review of microbial biosorbents. *International Journal of Environmental Research and Public Health, 14*(1), art. no. 94. https://doi.org/10.3390/ijerph14010094
4. Bhat, G.V., Kuna, A., Kavitha, C., Krishnaiah, N. (2017). Evaluation of *in-vitro* iron availability in iron fortified ready to eat extruded snack. *Biochemical and Cellular Archives*, *17*(2), 675–681.
5. D'Souza, L., Devi, P., Divya Shridhar, M.P., Naik, C.G. (2008). Use of Fourier Transform Infrared (FTIR) spectroscopy to study cadmium-induced changes in *Padina tetrastromatica* (Hauck). *Analytical Chemistry Insights*, *3*, 135–143. https://doi.org/10.4137/117739010800300001
6. Ferreira, L.S., Rodrigues, M.S., de Carvalho, J.C.M., Lodi, A., Finocchio, E., Perego, P., Converti, A. (2011). Adsorption of Ni^{2+}, Zn^{2+} and Pb^{2+} onto dry biomass of *Arthrospira (Spirulina) platensis* and *Chlorella vulgaris*. I. Single metal systems. *Chemical Engineering Journal*, *173*(2), 326–333. https://doi.org/10.1016/j.cej.2011.07.039
7. Fomina, M., Gadd, G. (2014). Biosorption: current perspectives on concept, definition and application. *Bioresource Technology*, *160*, 3–14. https://doi.org/10.1016/j.biortech.2013.12.102
8. Foster, M., Chu, A., Petocz, P., Samman, S. (2013). Effect of vegetarian diets on zinc status: A systematic review and meta-analysis of studies in humans. *Journal of the Science of Food and Agriculture*, *93*(10), 2362–2371. https://doi.org/10.1002/jsfa.6179
9. Gibson, R.S., Rahmannia, S., Diana, A., Leong, C., Haszard, J.J., Hampel, D., Reid, M., Erhardt, J., Suryanto, A.H., Sofiah, W.N., Fathonah, A., Shahab-Ferdows, S., Allen, L.H., Houghton, L.A. (2020). Association of maternal diet, micronutrient status, and milk volume with milk micronutrient concentrations in Indonesian mothers at 2 and 5 months postpartum. *American Journal of Clinical Nutrition*, *112*(4), 1039–1050. https://doi.org/10.1093/ajcn/nqaa200
10. Hartanti, A.T., Rahayu, G., Hidayat, I. (2015). *Rhizopus* Species from fresh tempeh collected from several regions in Indonesia. *HAYATI Journal of Biosciences*, *22*(3), 136–142. https://doi.org/10.1016/j.hjb.2015.10.004
11. Hurrell, R.F. (2021). Iron fortification practices and implications for iron addition to salt. *Journal of Nutrition*, *151*(Suppl. 1), 3S-14S. https://doi.org/10.1093/jn/nxaa175
12. Kalayci, S., Muhammet, S. (2022). Determination of some trace elements in dried red plum using inductively coupled plasma optical emission spectroscopy (ICP-OES). *Iranian Journal of Chemistry and Chemical Engineering*, *41*(11), 3742–3746. https://doi.org/10.30492/ijcce.2022.529125.4700
13. Kanamarlapudi, S.L.R.K., Muddada, S. (2019). Application of food-grade microorganisms for addressing deterioration associated with fortification of food with trace metals. *International Journal of Food Properties*, *22*(1), 1146–1155. https://doi.org/10.1080/10942912.2019.1628776
14. Kathuria, D., Hamid, Gautam, S., Thakur, A. (2023). Maillard reaction in different food products: Effect on product quality, human health and mitigation strategies. *Food Control*, *153*, art. no. 109911. https://doi.org/10.1016/j.foodcont.2023.109911

15. Kheeree, N., Kuptawach, K., Puthong, S., Sangtanoo, P., Srimongkol, P., Boonserm, P., Reamtong, O., Choowongkomon, K., Karnchanatat, A. (2022). Discovery of calcium-binding peptides derived from defatted lemon basil seeds with enhanced calcium uptake in human intestinal epithelial cells, Caco-2. *Scientific Reports*, *12*(1), art. no. 4659. **https://doi.org/10.1038/s41598-022-08380-0**
16. Kumar, V., Dwivedi, S.K. (2021). Mycoremediation of heavy metals: processes, mechanisms, and affecting factors. *Environmental Science and Pollution Research*, *28*(9), 10375–10412. **https://doi.org/10.1007/s11356-020-11491-8**
17. Lynch, H., Johnston, C., Wharton, C. (2018). Plant-based diets: Considerations for environmental impact, protein quality, and exercise performance. *Nutrients*, *10*(12), art. No. 1841. **https://doi.org/10.3390/nu10121841**
18. Majumdar, S.S., Das, S.K., Saha, T., Panda, G.C., Bandyopadhyoy, T., Guha, A.K. (2008). Adsorption behavior of copper ions on *Mucor rouxii* biomass through microscopic and FTIR analysis. *Colloids and Surfaces B: Biointerfaces*, *63*(1), 138–145. **https://doi.org/10.1016/j.colsurfb.2007.11.022**
19. Mannar, M.G.V., Hurrell, R.F. (2018). Chapter 1 – Food Fortification: Past Experience, Current Status, and Potential for Globalization. In M.G.V. Mannar, R.F. Hurrell (Eds). *Food Fortification in a Globalized World*, Academic Press, pp. 3-11. **https://doi.org/10.1016/C2014-0-03835-X**
20. Manzoor, M.F., Ali, A., Ain, H.B.U., Kausar, S., Khalil, A.A., Aadil, R.M., Zeng, X.A. (2024). Bioaccessibility mechanisms, fortification strategies, processing impact on bioavailability, and therapeutic potentials of minerals in cereals. *Future Foods*, *10*, art. no. 100425. **https://doi.org/10.1016/j.fufo.2024.100425**
21. National Academies of Sciences Engineering and Medicine. (2019). Dietary Reference Intakes for Sodium and Potassium. In V. A. Stallings, M. Harrison, M. Oria (Eds.), *Dietary Reference Intakes for Sodium and Potassium*. The National Academies Press. **https://doi.org/10.17226/25353**
22. Neufingerl, N., Eilander, A. (2022). Nutrient intake and status in adults consuming plant-based diets compared to meat-eaters: A systematic review. *Nutrients*, *14*(1), art. no. 29. **https://doi.org/10.3390/nu14010029**
23. Oladipo, O.G., Awotoye, O.O., Olayinka, A., Bezuidenhout, C.C., Maboeta, M.S. (2018). Heavy metal tolerance traits of filamentous fungi isolated from gold and gemstone mining sites. *Brazilian Journal of Microbiology*, *49*(1), 29–37. **https://doi.org/10.1016/j.bjm.2017.06.003**
24. Ozsoy, H.D. (2010). Biosorptive removal of Hg(II) ions by *Rhizopus oligosporus* produced from corn-processing wastewater. *African Journal of Biotechnology*, *9*(51), 8791–8799.
25. Ozsoy, H.D., Kumbur, H., Saha, B., van Leeuwen, J.H. (2008). Use of *Rhizopus oligosporus* produced from food processing wastewater as a biosorbent for Cu(II) ions removal from the aqueous solutions. *Bioresource Technology*, *99*(11), 4943–4948. **https://doi.org/10.1016/j.biortech.2007.09.017**
26. Palacios, C., Hofmeyr, G.J., Cormick, G., Garcia-Casal, M.N., Peña-Rosas, J.P., Betrán, A.P. (2021). Current calcium fortification experiences: a review. *Annals of the New York Academy of Sciences, 1484*(1), SI, 55-73. **https://doi.org/10.1111/nyas.14481**
27. Pathera, A.K., Riar, C.S., Yadav, S., Sharma, D.P. (2017). Effect of dietary fiber enrichment and different cooking methods on quality of chicken nuggets. *Korean Journal for Food Science of Animal Resources*, *37*(3), 410–417. **https://doi.org/10.5851/kosfa.2017.37.3.410**
28. Philpott, C.C. (2006). Iron uptake in fungi: A system for every source. *Biochimica et Biophysica Acta - Molecular Cell Research*, *1763*(7), 636–645. **https://doi.org/10.1016/j.bbamcr.2006.05.008**
29. Prasetyo, B., Prayitno, A.H. (2021). The sensory characteristics of fortified beef sausage with duck eggshell nano-calcium. *IOP Conference Series: Earth and Environmental Science*, *672*(1), art. no. 012042. **https://doi.org/10.1088/1755-1315/672/1/012042**
30. Robinson, J.R., Isikhuemhen, O.S., Anike, F.N. (2021). Fungal–metal interactions: A review of toxicity and homeostasis. *Journal of Fungi*, *7*(3), art. no. 225. **https://doi.org/10.3390/jof7030225**
31. Santillán-Urquiza, E., Méndez-Rojas, M.Á., Vélez-Ruiz, J.F. (2017). Fortification of yogurt with nano and micro sized calcium, iron and zinc, effect on the physicochemical and rheological properties. *LWT – Food Science and Technology*, *80*, 462–469. **https://doi.org/10.1016/j.lwt.2017.03.025**
32. Sey, E., Belford, E.J.D. (2021). Heavy metals tolerance potential of fungi species isolated from gold mine tailings in Ghana. *Journal of Environmental Health and Sustainable Development*, *6*(1), 1231–1242. **https://doi.org/10.18502/jehsd.v6i1.5765**
33. Shalaby, M.A., Matter, I.A., Gharieb, M.M., Darwesh, O.M. (2023). Biosorption performance of the multi-metal tolerant fungus *Aspergillus* sp. for removal of some metallic nanoparticles from aqueous solutions. *Heliyon*, *9*(5), art. no. e16125. **https://doi.org/10.1016/j.heliyon.2023.e16125**
34. Shoaib, A., Aslam, N., Aslam, N. (2013). *Trichoderma harzianum*: Adsorption, desorption, isotherm and FTIR studies. *Journal of Animal and Plant Sciences*, *23*(5), 1460–1465.
35. Shoukat, M., Hervé, V., Sarthou, A.S., Peron, A.C., Danel, A., Swennen, D., Bonnarme, P., Dugat-Bony, E. (2025). Iron fortification modifies the microbial community structure and metabolome of a model surface-ripened cheese. *International Journal of Food Microbiology*, *427*, art. no. 110971. **https://doi.org/10.1016/j.ijfoodmicro.2024.110971**
36. Springmann, M., Clark, M., Mason-D'Croz, D., Wiebe, K., Bodirsky, B.L., Lassaletta, L., de Vries, W., Vermeulen, S.J., Herrero, M., Carlson, K.M., Jonell, M., Troell, M., DeClerck, F., Gordon, L.J., Zurayk, R., Scarborough, P., Rayner, M., Loken, B., Fanzo, J., Godfray, H.C.J., Tilman, D., Rockström, J.,Willett, W. (2018). Options for keeping the food system within environmental limits. *Nature*, *562*, 519–525. **https://doi.org/10.1038/s41586-018-0594-0**
37. Tahir, A., Lateef, Z., Abdel-Megeed, A., Sholkamy, E.N., Mostafa, A.A. (2017). *In vitro* compatibility of fungi for the biosorption of zinc(II) and copper(II) from electroplating effluent. *Current Science*, *112*(4), 839–844. **https://doi.org/10.18520/cs/v112/i04/839-844**
38. Wang, L., Ding, Y., Zhang, X., Li, Y., Wang, R., Luo, X., Li, Y., Li, J., Chen, Z. (2018). Isolation of a novel calcium-binding peptide from wheat germ protein hydrolysates and the prediction for its mechanism of combination. *Food Chemistry*, *239*, 416–426. **https://doi.org/10.1016/j.foodchem.2017.06.090**
39. Wang, R., Rousta, N., Mahboubi, A., Fristedt, R., Undeland, I., Sandberg, A.S., Taherzadeh, M.J. (2024). *In vitro* protein digestibility and mineral accessibility of edible filamentous fungi cultivated in oat flour. *NFS Journal*, *36*, art. no. 100189. **https://doi.org/10.1016/j.nfs.2024.100189**
40. Wikandari, R., Tanugraha, D.R., Yastanto, A.J., Manikharda, Gmoser, R., Teixeira, J.A. (2023). Development of meat substitutes from filamentous fungi cultivated on residual water of tempeh factories. *Molecules*, *28*(3), art. no. 997. **https://doi.org/10.3390/molecules28030997**
41. Willett, W., Rockström, J., Loken, B., Springmann, M., Lang, T., Vermeulen, S., Garnett, T., Tilman, D., DeClerck, F., Wood, A., Jonell, M., Clark, M., Gordon, L.J., Fanzo, J., Hawkes, C., Zurayk, R., Rivera, J.A., De Vries, W., Majele Sibanda, L., Afshin, A., Chaudhary, A., Herrero, M., Agustina, R., Branca, F., Lartey, A., Fan, S., Crona, B., Fox, E., Bignet, V., Troell, M., Lindahl, T., Singh, S., Cornell, S.E., Reddy, S.K., Narain, S., Nishtar, S., Murray, C.J.L. (2019). Food in the *Anthropocene*: The EAT–Lancet Commission on healthy diets from sustainable food systems. *The Lancet*, *393*(10170), 447–492. **https://doi.org/10.1016/S0140-6736(18)31788-4**
42. Yang, S., Luo, J., Li, Y.Y., Liu, J. (2022). Contradictory effects of calcium on biological and membrane treatment of municipal solid waste leachate: A review and process optimization *via* biogas recirculation. *Journal of Cleaner Production*, *338*, art. no. 130568. **https://doi.org/10.1016/j.jclepro.2022.130568**
43. Yarlina, V.P., Nabilah, F., Djali, M., Andoyo, R., Lani, M.N. (2023). Mold characterization in "RAPRIMA" tempeh yeast from LIPI and over-fermented Koro Pedang (Jack Beans) tempeh. *Food Research*, *7*(Suppl. 1), 125–132. **https://doi.org/10.26656/fr.2017.7(S1).27**
44. Ye, J., Wang, Y., Li, X., Wan, Q., Zhang, Y., Lu, L. (2022). Synergistic antifungal effect of a combination of iron deficiency and calcium supplementation. *Microbiology Spectrum*, *10*(3), art. no. e01121-22. **https://doi.org/10.1128/spectrum.01121-22**
45. Zabochnicka-Świątek, M., Krzywonos, M. (2014). Potentials of biosorption and bioaccumulation processes for heavy metal removal. *Polish Journal of Environmental Studies*, *23*(2), 551–561.
46. Zafar, S., Aqil, F., Ahmad, I. (2007). Metal tolerance and biosorption potential of filamentous fungi isolated from metal contaminated agricultural soil. *Bioresource Technology*, *98*(13), 2557–2561. **https://doi.org/10.1016/j.biortech.2006.09.051**

ORIGINAL ARTICLE
http://journal.pan.olsztyn.pl

Polish Journal of Food and Nutrition Sciences
2025, Vol. 75, No. 3, 283–302
DOI: 10.31883/pjfns/209424
ISSN 1230-0322, e-ISSN 2083-6007

Vacuum and Ultrasound-Assisted Impregnation of Gala Apples with Sea Buckthorn Juice and Calcium Lactate: Functional Properties, Antioxidant Profile, and Activity of Polyphenol Oxidase and Peroxidase of Freeze-Dried Products

Marcellus Arnold[1], Urszula Tylewicz[2,3], Joanna Suliburska[4], Michał Świeca[5], Aneta Wojdyło[6], Anna Gramza-Michałowska[1]*

[1]Department of Gastronomy Science and Functional Foods, Faculty of Food Science and Nutrition, Poznań University of Life Sciences, Wojska Polskiego 31, 60-624 Poznań, Poland
[2]Department of Agricultural and Food Sciences, University of Bologna, Piazza Goidanich 60, 47521 Cesena, Italy
[3]Interdepartmental Centre for Agri-Food Industrial Research, University of Bologna, Via Quinto Bucci 336, 47521 Cesena, Italy
[4]Department of Human Nutrition and Dietetics, Faculty of Food Science and Nutrition, Poznań University of Life Sciences, Wojska Polskiego 31, 60-624 Poznań, Poland
[5]Department of Biochemistry and Food Chemistry, University of Life Sciences, Skromna 8, 20-704 Lublin, Poland
[6]Department of Fruit, Vegetable and Plant Nutraceutical Technology, Faculty of Biotechnology and Food Science, Wrocław University of Environmental and Life Sciences, Chełmońskiego 37, 51-630 Wrocław, Poland

Vacuum impregnation (VI) and ultrasound-assisted impregnation (US) were applied to Gala apples with the aim of improving the antioxidant capacity and calcium content of freeze-dried apples. An impregnation solution was composed of 93.8% sea buckthorn (SB) juice with 0 and 4% (*w/w*) calcium lactate (CaL). Gala apples conventionally impregnated (CON) at 30°C for 120 min were also prepared for comparison. The VI was performed at 200, 400, and 600 mbar with 10 min of each holding and relaxation time. US treatment was performed for 10, 20, and 30 min and was continued with CON for 110, 100, and 90 min, respectively. The VI at 200 mbar and US for 30 min at 0% CaL produced freeze-dried samples with the highest antioxidant capacity, higher than that of the CON and the non-impregnated samples: fresh apple (FA) and those after dipping in 1% ascorbic acid (FA+AA). The addition of 4% CaL optimally improved the calcium content when VI at 200 mbar and US for 20 min were applied. Generally, the freeze-dried apples impregnated under these conditions had lower antioxidant capacity compared to those treated without CaL. The impregnation process (CON, VI, and US) affected the mass transfer and composition of phenolics and carotenoids in the freeze-dried apples. Additionally, polyphenol oxidase (PPO) and peroxidase (POD) activities were completely inhibited upon CON and US treatment for 30 min at 0% CaL. While at 4% CaL, US for 20 min reduced PPO activity by 19.4% as compared to FA+AA. The end products, particularly those obtained at 4% CaL, could serve as potential functional snacks for consumers with osteoporosis and calcium issues, considering their calcium content and antioxidant properties.

Keywords: bioactive compounds, calcium enrichment, enzymatic browning, functional snack, non-conventional technology

INTRODUCTION

The development of functional food products has been a recent trend aimed at minimizing the risk of non-communicable diseases (NCD), including osteoporosis and calcium deficiency. It was previously observed that consumers aged 36–50 years consider functional foods as an essential means to prevent

***Corresponding Author:**
e-mail: **anna.gramza@up.poznan.pl** (Prof. A. Gramza-Michałowska)

Submitted: 17 May 2025
Accepted: 12 August 2025
Published on-line: 26 August 2025

osteoporosis and other NCD [Plasek *et al.*, 2020]. Among many bioactive compounds, calcium and antioxidants (*e.g.*, carotenoids and phenolics) are the key ones in preventing those issues [Kulczyński *et al.*, 2024; Martiniakova *et al.*, 2022]. In addition, the manufacture of functional food products utilizing locally sourced raw materials is encouraged to support sustainability, particularly by minimizing the carbon footprint.

Apple is known as a fruit with high productivity in Europe and across the world. According to the Food and Agriculture Organization (FAO), 18% of worldwide apple production was accounted for by Europe in 2023, amounting to more than 17.5 million tons [FAO, 2025]. Apple is widely consumed, either fresh (60–75%) or processed (20–40%) into various products including juice, cider, jam, and dried products, *etc.* [De la Peña-Armada & Mateos-Aparicio, 2022]. Furthermore, consuming dried fruit instead of unhealthy snacks may be a viable way to meet the World Health Organization's (WHO) daily fruit intake recommendations and promote the adoption of a sustainable diet [Testa *et al.*, 2023]. In our preliminary study, we developed a locally sourced apple-based healthy snack conventionally impregnated (at an atmospheric pressure) using local sea buckthorn (SB) juice. The optimized impregnation conditions were as follows: 93.8% (*w/w*) SB juice in water, 4% (*w/w*) calcium lactate (CaL) addition, 120 min, and 30°C [Arnold *et al.*, 2025]. The application of these conditions resulted in freeze-dried products with improved calcium content and minimal loss of antioxidant activities, compared to those impregnated with inulin only and the untreated samples.

Non-conventional technologies, particularly vacuum impregnation (VI) and ultrasound-assisted impregnation (US), were studied to promote mass transfer during the impregnation process to a greater extent than the conventional (CON) or atmospheric impregnation, thus improving the functional properties of plant-based products, including apples [Panayampadan *et al.*, 2022; Santarelli *et al.*, 2020; Vasile *et al.*, 2022]. The VI can promote the mass transfer process between the impregnating solution and solid porous food by intensifying the capillary flow in the cells due to the pressure gradients during the process. When vacuum pressure is applied, the internal cell pore volume becomes larger than under atmospheric pressure and thereby increases internal volume. The hydrodynamic mechanism (HDM) is initiated simultaneously, and the impregnating solution starts flowing into the capillaries until mass transfer equilibrium is reached. Subsequent restoration to atmospheric pressure is then applied, and the food is allowed to remain immersed during the relaxation time. During this phase, HDM and compression-induced deformation of the solid matrix take place, with external pressure acting as the driving forces. The cell pores of food eventually become filled with the impregnating solution, altering the physicochemical and functional properties of the product [Panayampadan *et al.*, 2022]. Following the application of high-power US (high intensity, >1 W/cm^2; low frequency, 18–100 kHz), the phenomena, such as sponge effect and cavitation, occur in liquids or solids containing moisture [Nowacka *et al.*, 2021]. These phenomena cause the formation of microbubbles in the material and improve mass transfer during the impregnation process.

The application of VI to improve the functional properties of apple-based products has been recently reported using blueberry juice and CaL at 200 mbar [Castagnini *et al.*, 2021], apple-peer juice at 40–80 mbar [Pasławska *et al.*, 2019], grape juice concentrate at 133–667 mbar [González-Pérez *et al.*, 2022], and lemon juice at 738 mbar [Santarelli *et al.*, 2020]. In turn, applications in apple-based products using vitamin B_{12} (24 kHz, 400 W) [Vasile *et al.*, 2022] and chokeberry juice concentrate (40 kHz, 0.1 W/g) [Masztalerz *et al.*, 2021] have been reported for the US treatment. Some studies also demonstrated synergistic effects of US and VI using a hibiscus extract solution [Dinçer, 2022], a mixture of black carrot phenolics and CaL [Yılmaz & Ersus Bilek, 2018], aloe vera juice [Trusinska *et al.*, 2024], and chokeberry juice concentrate [Masztalerz *et al.*, 2021].

To the best of our knowledge, to date, the application of VI and US to improve the functional properties of plant matrices has not been carried out using SB juice, without or with CaL. It is worth noting that SB is abundant in Europe and Asia, and is rich in lipo- and hydrophilic antioxidants, as well as other health-promoting compounds, such as vitamins and minerals, that can promote the general health of consumers [Ciesarová *et al.*, 2020]. Therefore, this study aimed to investigate the antioxidant activities and calcium content of freeze-dried Gala apples after the application of VI and US using SB juice without and with CaL, in comparison to CON treatment, highlighting the novelty of VI and US with SB juice to enhance the functional properties of apples based on our previous study [Arnold *et al.*, 2025]. The mass-transfer phenomena after impregnation (before freeze-drying), color, enzyme activities (including polyphenol oxidase (PPO) and peroxidase (POD)), and composition of antioxidants of freeze-dried products were analyzed as well.

MATERIALS AND METHODS

Raw materials and chemicals

Apples (*Malus domestica* Borkh. cv. Gala) were purchased from a local market in Cesena, originating from VOG s.a.c. in Terlan, South Tyrol, Italy. A homogeneous batch of apples (20 kg) was transported to the laboratory of the Department of Agricultural and Food Sciences (DISTAL) of the University of Bologna in Cesena, and randomly divided into 16 treatment groups: 2 controls – FA and FA+AA; and 14 impregnated samples – CON, VI (200, 400, 600 mbar), US (10, 20, 30 min), each prepared without and with CaL. An equal weight of apples was allocated to each group. All the samples were stored at 4°C and processed within a week. The apples were washed, peeled, cored, and sliced to a thickness of 5 mm to obtain the C-shaped slices. The slices were then dipped for 2 min in a 1% (*w/v*) ascorbic acid (Sigma Aldrich, St. Louis, MO, USA) solution, at a sample to solution ratio of 1:4 (*w/v*) to delay enzymatic browning. The raw fresh apple flesh (FA) and those dipped in a 1% (*w/v*) ascorbic acid solution (FA+AA) were used as the controls, each in triplicate. The organic sea buckthorn (SB) (*Hippophae rhamnoides* L.) juice was purchased from KoRo (Berlin, Germany), with SB fruits

grown in an organic farm in Brandenburg, Germany. The calcium L-lactate hydrate was purchased from Sigma Aldrich. Prior to impregnation treatment, the total soluble solid content of raw FA, raw FA+AA, SB juice, and the final impregnating solution was measured using a DBR 95 digital refractometer (XS Instruments, Carpi, Italy).

All chemicals were purchased from Sigma Aldrich, including 2,2′-azino-bis(3-ethylbenzothiazoline-6-sulfonic acid) diammonium salt (ABTS), 2,2-diphenyl-1-picrylhydrazyl (DPPH), 2,2′-azobis(2-methylpropionamidine) dihydrochloride (AAPH), fluorescein sodium salt, sodium acetate trihydrate, 2,4,6-tris(2-pyridyl)-*s*-triazine (TPTZ), iron(III) chloride hexahydrate, iron(II) sulfate heptahydrate, (±)-6-hydroxy-2,5,7,8-tetramethylchromane-2-carboxylic acid (Trolox), Folin-Ciocalteu's phenol reagent, acetic acid, gallic acid, hydrochloric acid, 65% nitric acid, methanol, potassium persulfate, sodium carbonate, lanthanum(III) chloride, monopotassium phosphate, disodium phosphate, polyvinylpolypyrrolidone (PVPP), catechol, and guaiacol. ACL (lipid-soluble substances) and ACW (water-soluble substances) reagent kits were purchased from Analytik Jena (Jena, Germany). The solvents for ultra-performance liquid chromatography (UPLC) method were bought from Sigma Aldrich. The standards of phenolic compounds included phenolic acids (chlorogenic acid), flavan-3-ols ((±)-(epi)catechin, procyanidin B_1), dihydrochalcones (phloretin 2-*O*-xyloglucoside), flavonols (quercetin 3-*O*-glucoside and isorhamnetin 3-*O*-glucoside) and carotenoids (lutein, zeaxanthin, β-carotene) were obtained from Extrasynthese (Genay, France).

Impregnation of apples using sea buckthorn juice and calcium lactate

The impregnation process was divided into three types: conventional (CON) and non-conventional which included vacuum (VI) and ultrasound-assisted impregnation (US). The impregnating solution and process were designed based on the optimization from a preliminary study [Arnold *et al.*, 2025]. The impregnating solution consisted of 93.8% (*w/w*) SB juice in water, with 0 and 4% (*w/w*) calcium lactate (CaL); these conditions were chosen as they ensured the optimum antioxidant capacity and calcium content of freeze-dried Gala slices when impregnated under CON conditions at 30°C for 120 min. The sample to solution ratio of 1:5 (*w/w*) was chosen to prevent concentration changes during the treatment. Each CON, VI, and US treatment was carried out in triplicate using independent samples of Gala apples (raw FA+AA) before freeze-drying, and the samples were analyzed accordingly.

In the CON treatment, the raw FA+AA was impregnated in the solution in a parafilm-wrapped beaker at an atmospheric pressure. The samples were continuously shaken at 100 rpm, 30°C, for 120 min (Shaker 709, ASAL, Milan, Italy). For the VI treatment, the solution was conditioned at 30°C for 5 min prior to the treatment. The raw FA+AA was then immersed in the beaker containing the solution and the VI was carried out in a closed chamber connected to a vacuum pump and an automatic controller system (AVCS, S.I.A., Bologna, Italy). The VI treatments were performed at three different absolute pressures 200, 400, and 600 mbar. The total duration of each VI treatment was 28 min, consisting of 4 min to decrease the pressure to 200, 400, or 600 mbar; 10 min of holding time at those pressures; 4 min to recover the pressure to the atmospheric pressure; and 10 min of relaxation at the atmospheric pressure at 30°C [Kidoń *et al.*, 2023]. For the US treatment, the raw FA+AA was immersed in the beaker containing the solution, and the US treatment was conducted for 10, 20, and 30 min (25 kHz, 1,000 W, 30°C) in an ultrasonic bath (Xtra ST 600H, Elmasonic, Singen, Germany). During the US treatment, the temperature was kept constant at 30°C by a recirculating cooler (FL601, Julabo, Seelbach, Germany) with a coil exchanger inserted in the treatment tank. The water temperature was controlled by a probe thermometer throughout the treatment. A negligible increase in temperature (up to 1°C depending on the treatment time) was observed during the treatment. Afterwards, the conventional impregnation process was conducted for additional 110, 100, and 90 min for US treatments of 10, 20, and 30 min, respectively to reach the total impregnation time of 120 min.

After the CON, VI, and US treatments, the samples were removed from the solutions, drained, and blotted using absorbing paper, and their weight was recorded for mass transfer analysis. Moreover, water activity was also measured on the whole samples, while color and chemical analyses were performed on freeze-dried samples. For the freeze-dried samples, the control and treated samples were frozen at –40°C for 24 h, and freeze-dried for 48 h (Lio2000, CinquePascal S.r.l., Milan, Italy). All samples with related abbreviations are described in **Table 1**.

Table 1. Codes of apple flesh control samples without (FA) and with dipping in an ascorbic acid solution (FA+AA), and apple flesh samples subjected to conventional (CON), and non-conventional impregnation (vacuum impregnation, VI, and ultrasound-assisted impregnation, US).

Sample codes	Dipping time (min)	VI pressure (mbar)	US time (min)	CON time (min)
FA	–	–	–	–
FA+AA	2	–	–	–
CON	2	–	–	120
VI_200	2	200	–	10*
VI_400	2	400	–	10*
VI_600	2	600	–	10*
US_10	2	–	10	110**
US_20	2	–	20	100**
US_30	2	–	30	90**

*For vacuum impregnation, the relaxation time was conducted adapting the conventional impregnation conditions (30°C, atmospheric pressure). **After ultrasound-assisted impregnation, the conventional impregnation was conducted subsequently to reach 120 min of total impregnation process.

Analysis of mass transfer phenomena and water activity

After the impregnation treatment, the weight gain/loss, water gain/loss, and solid gain/loss of the samples were calculated according to Equations (1), (2) and (3), respectively, with the note that positive and negative calculated values refer to the gain and loss, respectively:

$$\text{Weight gain/loss (\%)} = \frac{m_t - m_0}{m_0} \times 100 \quad (1)$$

$$\text{Water gain/loss (\%)} = \frac{m_t x_{wt} - m_0 x_{w0}}{m_0} \times 100 \quad (2)$$

$$\text{Solid gain/loss (\%)} = \frac{m_t x_{STt} - m_0 x_{ST0}}{m_0} \times 100 \quad (3)$$

where: m_0 is initial weight before the impregnation process (kg), m_t is weight after impregnation process at time t (kg), x_{w0} is initial water mass fraction (kg/kg), x_{wt} is water mass fraction after the impregnation process at time t (kg/kg), x_{ST0} is initial total solids (dry matter) mass fraction (kg/kg), and x_{STt} is total solids (dry matter) mass fraction after the impregnation process at time t (kg/kg).

The moisture and dry matter contents were determined by drying the samples at 70°C until the weight was constant [AOAC, 2002]. The water activity (a_w) was measured by an aWLife meter (WaterLab, Steroglass S.r.l., Perugia, Italy) at 25°C. All analyses were conducted in triplicate.

Color analysis

The color measurement of SB juice and the surface of freeze-dried samples before grinding was performed in ten repetitions using a ColorFlex EZ colorimeter (HunterLab, Reston, VA, USA) in the CIE $L^*a^*b^*$ scale. Prior to measurement, the colorimeter was calibrated using a black and white tile (L^* 93.47, a^* 0.83, b^* 1.33). The L^* (lightness), a^* (greenness/redness), and b^* (blueness/yellowness) of the sample were measured, and total color difference (ΔE), browning index (BI) [Buera *et al.*, 1985], whiteness index (WI) [Judd & Wyszecki, 1963], and yellowness index (YI) [Francis & Clydesdale, 1975] were calculated using Equations (4), (5), (6), and (7), respectively:

$$\Delta E = \sqrt{(\Delta L^*)^2 + (\Delta a^*)^2 + (\Delta b^*)^2} \quad (4)$$

where: ΔL^*, Δa^*, and Δb^* are the differences of L^*, a^*, and b^*, respectively, between FA+AA and other analyzed samples.

$$\text{BI} = 100 \times \frac{x - 0.31}{0.172} \quad (5)$$

$$\text{where: } x = \frac{a^* + 1.75L^*}{5.645L^* + a^* - 3.012b^*}$$

$$\text{WI} = 100 - \sqrt{(100 - L^*)^2 + a^{*2} + b^{*2}} \quad (6)$$

$$\text{YI} = 142.86 \times \frac{b^*}{L^*} \quad (7)$$

Determination of total phenolic content and antioxidant capacity

The freeze-dried powder was extracted using 80% methanol (*v/v*) at a sample-to-solvent ratio of 1:20 (*w/v*). The SB juice (filtered through a 0.45 µm membrane, Membrane Solutions, Auburn, WA, USA) was diluted in 80% methanol (*v/v*) at a sample-to-solvent ratio of 1:10 (*w/v*). The samples were shaken in a water bath at 150 rpm, and 50°C for 120 min. After cooling to room temperature, the samples were centrifuged (4°C, 12,000×*g*, 10 min) and filtered to obtain the supernatant. The extraction was conducted in duplicate, and the obtained extracts were used to determine the total phenolic content and antioxidant capacity.

The total phenolic content (TPC) was determined in triplicate by the Folin-Ciocalteu assay following a previous report [Singleton & Rossi, 1965], in which the absorbance of the extracts was measured at λ=725 nm using an SP-880 spectrophotometer (Metertech, Taipei, Taiwan). The TPC was expressed as mg gallic acid equivalent (GAE) *per* 100 g of product.

The ABTS, DPPH, ferric-reducing antioxidant power (FRAP), oxygen radical absorbance capacity (ORAC), and photochemiluminescence (PCL) assays were carried out in triplicate to determine the antioxidant capacity of the products. The ability of the samples to reduce the ABTS cation radical was measured spectrophotometrically using an SP-880 spectrophotometer (Metertech) set at λ=734 nm after 6 min of incubation of the reaction mixture containing the extract and ABTS cation radicals generated with potassium persulfate, according to a previous report [Re *et al.*, 1999]. The results were expressed as mg Trolox equivalent (TE) *per* 100 g of product.

The DPPH radical scavenging activity was determined as described previously [Sánchez-Moreno *et al.*, 1998]. The absorbance of the reaction mixture containing the extract and DPPH radicals was measured at λ=515 nm after incubation in the dark for 20 min. The results were expressed as mg TE *per* 100 g of product.

FRAP of the samples was determined according to the Benzie & Strain [1999] method. The FRAP reagent was prepared by mixing the acetate buffer (pH 3.6), 10 mM TPTZ solution in 40 mM HCl, and 20 mM of $FeCl_3 \times H_2O$ solution at the ratio of 10:1:1 (*v/v/v*). The extract was added to the prepared reagent and incubated at 37°C for 4 min. The reduction of TPTZ-Fe^{3+} to TPTZ-Fe^{2+} with the presence of antioxidants was assessed at λ=593 nm. The results were presented as mmol Fe(II) *per* 100 g of product.

The ORAC assay measured the AAPH-generated peroxyl radicals scavenging ability of the antioxidants in the sample extracts, using a fluorescein solution [Ou *et al.*, 2001]. The readings were taken at a given excitation (λ=493 nm) and emission wavelength (λ=515 nm) on an F-2700 fluorescence spectrophotometer (Hitachi, Kyoto, Japan). The results were presented as mg TE/100 g of product.

The PCL assay was performed using a Photochem apparatus (Analytik Jena, Germany). In this assay, the superoxide anion radicals ($O_2^{\bullet -}$) were produced by optical excitation

of a photosensitizer. The antioxidant capacity of the samples against the radicals was detected with the presence of chemiluminogenous compound – luminol. The antioxidant capacity of lipid-soluble (ACL) and water-soluble (ACW) substances of the extract was measured according to the protocol and using the reagent kits from the manufacturer. Additionally, the integral antioxidant capacity (IAC) was calculated as the sum of ACL and ACW [Besco *et al.*, 2007]. The results were presented as mg TE *per* 100 g of product.

Determination of calcium content

The calcium content of SB juice, raw FA, raw FA+AA, and freeze-dried samples was determined in triplicate by atomic absorption spectrometry (Hitachi Z2000, Tokyo, Japan) using the air-acetylene flame, following a previous study [Sulibursk & Krejpcio, 2014]. The complete mineralization of 1 g of the sample was performed in a muffle furnace at 450°C for 72 h. The obtained ash was then dissolved in 1 M nitric acid and diluted in 0.5% $LaCl_3$ solution. The methods were validated by simultaneous analysis of the reference material (Soya Bean Flour, INCT-SBF-4) with 95.7% accuracy for calcium. Deionized water and acid-washed glassware were used in this study. The results were presented as mg Ca *per* 100 g of product.

Quantification of phenolics and carotenoids

The extraction of phenolics and carotenoids of the selected freeze-dried samples, followed by their quantification using ultra-performance liquid chromatography with photodiode array detection (UPLC-PDA; ACQUITY UPLC system, Waters Corporation, Milford, MA, USA) was performed following a previous study [Tkacz *et al*., 2020]. To extract phenolics, 0.5 g of powdered samples was mixed with 5 mL of 70% methanol (*v/v*, in water) with 2% (*w/v*) ascorbic acid and 1% (*v/v*) acetic acid, followed by 15 min of sonication (35 kHz; Sonorex RK514H, Bandelin, Berlin, Germany). The mixtures were stored at 4° for 24 h C, and sonication was repeated once afterwards. The supernatants from centrifugation at 14,000×*g*, 4°C for 10 min performed using an MPW-352R centrifuge (MPW MED. Instruments, Warsaw, Poland) were collected and filtered through a syringe filter with a polytetrafluoroethylene (PTFE) membrane, 0.20 µm (Millex Samplicity Filter, Merck, Darmstadt, Germany). The filtrate phenolic compound separation was carried out using an ACQUITY UPLC BEH C18 column (1.7 µm, 2.1×100 mm, Waters Corporation), which temperature was maintained at 30°C. The injection volume was 5 µL and the elution, using a mobile phase consisting of 2% (*v/v*) formic acid (solvent A) and 100% acetonitrile (solvent B) applied in a gradient system, was completed in 15 min with a flow rate of 0.42 mL/min. The gradient program started with 98–65% solvent A (to 12 min), and then to 0% (to 14 min), the gradient returned to the initial composition (98% A) until 15 min for held constant to re-equilibrate the column. Identification of compounds was conducted based on retention times and PDA spectra of standards and using literature data [Tkacz *et al.*, 2020]. For quantification, the absorbance was measured at 280 nm for flavan-3-ols expressed as (±)-(epi)catechin equivalents (calibration curve in a concentration range of 5–10 mg/L; R^2=0.9978), procyanidin B_1 (5–10 mg/L; R^2=0.9995) and dihydrochalcones expressed as phloretin 2-*O*-xyloglucoside equivalents (10–20 mg/L; R^2=0.9992); at 320 nm for phenolic acids expressed as chlorogenic acid equivalents (10–25 mg/L; R^2=0.9989); and at 360 nm for flavonols expressed as quercetin 3-*O*-glucoside and isorhamnetin 3-*O*-glucoside equivalents (10–25 mg/L; R^2=0.9995 and 0.9957, respectively).

For carotenoid extraction, in dark conditions, 0.4 g of the powdered samples and 10% $MgCO_3$ solution were shaken with 4 mL of a mixture of hexane, acetone and methanol (2:1:1, *v/v/v*) with 1% butylated hydroxytoluene (*w/v*) (300 rpm, 15 min; DOS-10L Digital Orbital Shaker, ELMI, Riga, Latvia). Supernatants were collected after centrifugation (same as phenolics extraction). The extraction was repeated two (for FA and FA+AA) to three times (for CON, VI, and US). The combined supernatants underwent evaporation (XcelVap, Biotage, Uppsala, Sweden), and the residues were diluted in a mixture of methanol and tetrahydrofuran (4:1, *v/v*). Solutions were filtered through PTFE syringe filters before injection. UPLC-PDA separation of carotenoids was performed at 32°C using the ACQUITY UPLC BEH Shield RP C18 column (2.1×100 mm, 1.7 µm; Waters Corporation) with a C18 guard column. A volume of 10 µL was injected, and the flow rate of the mobile phase was 0.5 mL/min. The mobile phase was used in a gradient system of 0.1% (*v/v*) formic acid, (solvent A) and a mixture of acetonitrile and methanol (7:3, *v/v*) (solvent B). The elution started with 25% A (to 0.60 min); 4.9% A (to 6.50 min); 0% A (to 13.60 min); 25% A (to 16.60 min). The analysis was monitored at wavelength of 450 nm, and the spectra were measured. Carotenoids were identified by comparing their retention times and spectra with those of standards and using literature data [Tkacz *et al.*, 2020]. Quantification was performed based on standard curves for lutein (5–10 mg/L; R^2= 0.9994), zeaxhantin (5–15 mg/L; R^2= 0.9979), and β-carotene (10–25 mg/L; R^2= 0.9999).

The results of UPLC-PDA analyses were calculated as the mean of two replicates and expressed as mg *per* 100 g of freeze-dried product.

Determination of polyphenol oxidase and peroxidase activity

Polyphenol oxidase (PPO) and peroxidase (POD) activities in selected freeze-dried samples were measured according to the method described previously [Sikora *et al.*, 2020]. The product extraction for enzyme activity measurements was performed at 4°C. About 0.3 g of the powdered freeze-dried sample was mixed vigorously with 2 mL of 0.067 M Sorensen's phosphate buffer solution (SPBS, pH 7.0, determined previously as the optimal pH in freeze-dried apple for both PPO and POD activities) and 0.02 g of PVPP. The mixtures were shaken at 1,400 rpm for 30 min (thermo-shaker TS-100C, Biosan, Riga, Latvia). The supernatant was collected for further analysis, after centrifugation at 12,000×*g*.

The final reaction mixture for PPO activity measurement consisted of 50 µL of extract, 900 µL of 0.067 M SPBS (pH 7.0), and 50 µL of 0.5 M catechol as the substrate. For the POD activity measurement, the final reaction mixture contained 100 µL of extract, 800 µL of 0.067 M SPBS (pH 7.0), 50 µL of 0.04 M H_2O_2, and 50 µL of 0.04 M guaiacol as the substrate. The absorbance changes (ΔA) with the time at 420 and 470 nm for PPO and POD activity, respectively, were monitored at 25°C using a UV-Vis spectrophotometer (UV-1280, Shimadzu, Kyoto, Japan). The absorbance was linear with the time at the first 3 min. The amount of enzyme that changes an absorbance 0.001 *per* min under the specified conditions was defined as one unit (U) of enzyme activity. The PPO and POD activities were determined in triplicate for each product, and results were expressed in unit of enzyme activity *per* g of product (U/g product).

Statistical analysis

The differences between treatments with 0 and 4% CaL were analyzed by a T-test. One-way analysis of variance (ANOVA) followed by Tukey's post hoc test was used to compare FA, FA+AA, CON, US, and VI at the same CaL concentration (before and after freeze-drying) and also to compare SB juice, raw FA, and raw FA+AA. Analyses ware performed using the Statistica 13.1 software (StatSoft Inc., Krakow, Poland). Principal component analysis (PCA) was carried out to explore the distribution of antioxidant capacity, calcium, dry matter, and ash content, as impacted by impregnation processes. Visualization of PCA was conducted using OriginPro 10.1 (OriginLab Corporation, Northampton, MA, USA). The significance level of 95% was considered in this study.

RESULTS AND DISCUSSION

Physicochemical and functional properties of raw materials

This research used SB juice as the main ingredient of the impregnating solution of Gala apple flesh. The physicochemical parameters and antioxidant capacity of the SB juice, as well as raw apple flesh (FA), and FA after dipping in 1% (*w/v*) ascorbic acid solution (raw FA+AA) are shown in **Table 2**. The content of total soluble solids of SB juice reached 5.03°Brix, and was lower than those of the raw FA and FA+AA. This SB juice from fruits grown in an organic farm in Germany had a slightly lower content of total soluble solids than Polish (5.7–7.2°Brix) [Tkacz *et al.*, 2019] or Chinese (6.97–13.50°Brix) SB juice [Zhang *et al.*, 2024]. The impregnating solution consisting of 93.8% (*w/w*) SB juice in water with 0% CaL had 4.53±0.15°Brix, and that with 4% CaL had 7.47±0.06°Brix of total soluble solids, which was slightly hypotonic compared to raw FA+AA (8.80°Brix).

SB juice contained 11.83 mg Ca/100 g, which was more than twice the amount found in apples (**Table 2**). This value was comparable to the calcium content of SB juice from Poland (12.7 mg Ca/100 g) or other countries (2.1–10.9 mg Ca/100 g) [Ciesarová *et al.*, 2020]. In terms of TPC and antioxidant capacity, SB juice generally showed significantly higher values than raw FA and FA+AA. We hypothesize that, with better chemical composition than apple, SB juice, with or without 4% CaL, could be beneficial in improving the functional properties of apple in the form of freeze-dried chips through conventional and non-conventional impregnation processes.

Table 2. Physicochemical properties and antioxidant capacity of sea buckthorn (SB) juice, raw fresh apple flesh, without (FA) and with dipping process in an ascorbic acid solution (FA+AA).

Parameter	SB juice	Raw FA	Raw FA+AA
Total soluble solids (°Brix)	5.03±0.06^c	11.90±1.22^a	8.80±0.10^b
Dry matter (g/100 g)	7.84±0.02^c	15.11±0.19^a	12.80±0.29^b
Calcium content (mg/100 g)	11.83±0.44^a	3.51±0.16^c	5.58±0.38^b
TPC (mg GAE/100 g)	280.14±3.38^a	58.22±1.30^c	92.96±0.84^b
ABTS (mg TE/100 g)	103.52±4.93^a	69.71±2.20^b	66.95±0.39^b
DPPH (mg TE/100 g)	186.62±2.28^a	61.01±0.75^c	68.12±0.94^b
FRAP (mmol Fe(II)/100 g)	1.76±0.05^a	0.39±0.01^c	0.51±0.01^b
ORAC (mg TE/100 g)	915.7±72.7^a	416.7±5.3^b	408.7±23.3^b
PCL-ACL (mg TE/100 g)	150.77±0.70^a	90.13±3.49^b	90.28±0.47^b
PCL-ACW (mg TE/100 g)	68.33±0.33^a	55.41±0.41^b	67.33±1.44^a
PCL-IAC (mg TE/100 g)	219.10±0.38^a	145.54±3.90^c	157.61±1.56^b

The results are presented as mean ± standard deviation. Different lowercases mean significant differences ($p<0.05$) between samples within the same row. TPC, total phenolic content; ABTS, ABTS radical cation scavenging activity; DPPH, DPPH radical scavenging activity; FRAP, ferric-reducing antioxidant power; ORAC, oxygen radical absorbance capacity; PCL-ACL and PCL-ACW, photochemiluminescence assay – antioxidant capacity of lipid- and water-soluble substances, respectively; PCL-IAC, integral antioxidant capacity in PCL assay; GAE, gallic acid equivalent; TE, Trolox equivalent.

Mass transfer phenomena and water activity

The mass transfer results of the impregnated FA+AA prior to freeze-drying are presented in **Table 3**. Regardless of the pressure and the CaL concentration used, the VI caused a significant weight and water gain of ascorbic acid-treated apple flesh. The lower the VI absolute pressure, the higher the weight and water gain. The highest ($p<0.05$) weight gain and water gain were determined in VI_200 with 0% CaL and reached 18.72% and 17.49%, respectively. The weight and water gain in fresh-cut apples after VI were reported in a previous study. Various Polish cultivars of apple cubes showed weight gain of 15–32% after the VI treatment (150 mbar) using a solution containing 0.5% ascorbic acid, 0.5% citric acid, and 10% sucrose (*w/w*) [Kidoń *et al.*, 2023]. The authors also found that the weight gain was negatively correlated (r=–0.85) with firmness of apples before VI. In another study, VI performed at 738 mbar on Golden Delicious cubes (13.25–13.50°Brix) using hypotonic lemon juice (6.25°Brix) showed significantly higher weight

and water gain compared to those prepared by the dipping process [Neri *et al.*, 2019].

The water gain/loss of CON and US-treated FA+AA under the same CaL concentration was similar ($p \geq 0.05$) (**Table 3**). The values ranged from –3.46% (US_30, 4% CaL) to 1.41% (US_20, 0% CaL). About 1% weight loss was observed in FA+AA impregnated in 0% CaL, while 4% CaL resulted in about 2–4% weight loss, especially in the US-treated samples. There was no significant ($p \geq 0.05$) weight loss difference between FA+AA prepared with 0 and 4% CaL in CON and all US treatments, except for US_20, where 4% CaL caused significantly ($p < 0.05$) higher weight loss than 0% CaL. According to literature, the US treatment (probe, 24 kHz, 400 W) of Granny Smith apple, impregnated with hypotonic vitamin B_{12} solution, showed minor water gain/loss, depending on the US power and treatment time (5–15 min) applied [Vasile *et al.*, 2022]. The same authors also observed that the treatment at 400 W with two different amplitudes of 20% and 100% resulted in up to 2% water loss and 5.1% water gain, respectively.

The total solid gain/loss in all treatments was close to zero, however slight but significant ($p < 0.05$) differences were found between the samples (**Table 3**). The highest solid loss was observed in US_10 with 0% CaL, and the highest solid gain in VI_200 and VI_400 with 4% CaL. In comparison to 0% CaL, the 4% CaL treatment caused significantly ($p < 0.05$) higher solid gain in VI and CON, and solid loss in US_10 and US_20. For US_30, there was no significant difference ($p \geq 0.05$) between the samples treated with and without CaL. A solid loss of apple was also highlighted in US-assisted impregnation using a hypotonic vitamin B_{12} solution [Vasile *et al.*, 2022] and VI in a hypotonic lemon juice solution [Neri *et al.*, 2019].

In terms of a_w, the value determined for the treated FA+AA (CON, VI, and US) ranged from 0.989 to 0.998 for 0% CaL, and from 0.989 to 0.996 for 4% CaL (**Table 3**), whereas the a_w of raw FA and FA+AA were 0.994 and 0.998, respectively.

The results of this research indicated that the mass transfer phenomena and the a_w of the impregnated apples were affected by the composition of the solution, impregnation types, and process parameters. In the CON treatment, as the used solutions were rather hypotonic, the mass transfer, especially water transfer, may have occurred toward apple tissue by simple diffusion [Vasile *et al.*, 2022]. US and VI could cause cellular damage, allowing fluid to flow within the plant matrix [Yılmaz & Ersus Bilek, 2018]. The VI removes intercellular air and native liquid in the apple, and subsequently the emptied intercellular spaces and pores can be easily filled with the impregnating solution [Pasławska *et al.*, 2019], in this case, SB juice and CaL solution. Vacuum also intensifies capillary flows and favors mass transfer during impregnation, which occurs due to surface tension at the solid-solution interface [Vinod *et al.*, 2024]. The US treatment could also promote mass transfer during the impregnation process due to the cavitation phenomenon and continuous sponge effect of the apple tissue [Nowacka *et al.*, 2021]. Other factors, such as cultivars [Kidoń *et al.*, 2023], maturity of apples [Casim *et al.*, 2023], or even their cultivation method (organic and conventional apples) [Neri *et al.*, 2019], could also affect the mass transfer phenomena during impregnation, as different apples showed different physicochemical characteristics.

Color of freeze-dried apples

Next to functional properties, color also is one of the important factors that can attract consumer to buy and consume

Table 3. Mass transfer results and water activity of raw fresh apple flesh (FA), FA dipped in ascorbic acid solution (FA+AA), and FA+AA samples subjected to conventional (CON), and non-conventional impregnation (vacuum impregnation, VI, and ultrasound-assisted impregnation, US) in sea buckthorn juice without and with calcium lactate (CaL).

Treatment	Weight gain/loss (%)		Water gain/loss (%)		Solid gain/loss (%)		Water activity	
	0% CaL	4% CaL	0% CaL	4% CaL	0% CaL	4% CaL	0% CaL	4% CaL
Raw FA	–	–	–	–	–	–	0.994 ± 0.001^{abc}	0.994 ± 0.001^{abc}
Raw FA+AA	–	–	–	–	–	–	0.998 ± 0.001^{a}	0.998 ± 0.001^{a}
CON	-1.02 ± 0.04^{dA}	-0.72 ± 0.13^{cA}	0.36 ± 0.04^{deA}	-1.08 ± 0.11^{cB}	-1.38 ± 0.01^{eB}	0.35 ± 0.02^{cA}	0.995 ± 0.003^{abcA}	0.996 ± 0.002^{abA}
VI_200	18.72 ± 1.67^{aA}	16.74 ± 1.44^{aA}	17.49 ± 1.47^{aA}	14.16 ± 1.25^{aA}	1.23 ± 0.20^{aB}	2.58 ± 0.19^{aA}	0.989 ± 0.001^{cA}	0.989 ± 0.003^{cA}
VI_400	14.85 ± 0.34^{bA}	13.89 ± 0.81^{aA}	14.26 ± 0.30^{bA}	11.47 ± 0.70^{aB}	0.59 ± 0.04^{bB}	2.42 ± 0.11^{abA}	0.991 ± 0.005^{bcA}	0.989 ± 0.002^{cA}
VI_600	9.07 ± 0.91^{cA}	8.96 ± 0.86^{bA}	9.94 ± 0.81^{cA}	6.93 ± 0.74^{bA}	-0.87 ± 0.10^{dB}	2.03 ± 0.12^{bA}	0.996 ± 0.002^{abA}	0.991 ± 0.005^{bcA}
US_10	-1.05 ± 0.17^{dA}	-2.39 ± 0.58^{cA}	1.41 ± 0.15^{dA}	-0.81 ± 0.52^{cB}	-2.46 ± 0.02^{fB}	-1.58 ± 0.07^{eA}	0.998 ± 0.001^{aA}	0.988 ± 0.001^{cB}
US_20	-1.03 ± 0.12^{dA}	-3.13 ± 0.59^{cB}	0.39 ± 0.10^{deA}	-1.96 ± 0.52^{cB}	-1.41 ± 0.01^{eB}	-1.16 ± 0.07^{eA}	0.996 ± 0.001^{abA}	0.988 ± 0.001^{cB}
US_30	-1.91 ± 1.15^{dA}	-4.07 ± 1.26^{cA}	-1.71 ± 1.00^{eA}	-3.46 ± 1.10^{cA}	-0.21 ± 0.15^{cA}	-0.62 ± 0.16^{dA}	0.991 ± 0.002^{bcA}	0.989 ± 0.003^{cA}

The results are presented as mean ± standard deviation. Different lowercases mean significant differences ($p < 0.05$) between samples within the same column. Different uppercases mean significant differences ($p < 0.05$) between 0 and 4% CaL within the same impregnation treatment and parameter. Sample codes refer to Table 1.

Table 4. Color parameters of freeze-dried products: fresh apple flesh (FA), FA dipped in ascorbic acid solution (FA+AA), and FA+AA samples subjected to conventional (CON), and non-conventional impregnation (vacuum impregnation, VI, and ultrasound-assisted impregnation, US) in sea buckthorn juice without and with calcium lactate (CaL).

Color parameter	CaL concentration	FA	FA+AA	CON	VI_200	VI_400	VI_600	US_10	US_20	US_30
*L**	0%	79.3±1.7^{b}	82.9±1.0^{a}	72.0±2.8^{cA}	68.4±1.4^{dB}	69.8±1.2^{cdB}	71.9±1.3^{cB}	71.7±2.0^{cA}	70.8±2.2^{cdA}	70.4±2.1^{cdA}
	4%	79.3±1.7^{b}	82.9±1.0^{a}	68.6±1.9^{deB}	69.7±0.9^{dA}	72.9±1.1^{cA}	74.7±1.2^{cA}	68.0±2.6^{deB}	67.1±1.0^{eB}	66.9±1.4^{eB}
*a**	0%	3.4±1.3^{c}	−0.2±0.4^{d}	12.3±2.7^{abA}	13.8±0.6^{abA}	12.4±1.4^{abA}	11.2±1.2^{bA}	12.5±2.8^{abA}	13.4±2.3^{abA}	14.9±2.6^{aA}
	4%	3.4±1.3^{e}	−0.2±0.4^{f}	12.8±1.8^{abA}	11.4±0.7^{bcB}	9.9±1.1^{cdB}	8.1±1.0^{dB}	13.2±1.9^{aA}	13.6±1.0^{aA}	13.7±1.4^{aA}
*b**	0%	25.3±1.6^{e}	18.0±2.6^{f}	57.5±4.3^{abA}	53.1±1.4^{bcdA}	52.1±4.0^{cdA}	51.4±2.8^{dA}	57.0±4.2^{abcA}	57.8±3.7^{abA}	60.9±5.6^{aA}
	4%	25.3±1.6^{c}	18.0±2.6^{d}	48.4±5.7^{bcB}	47.3±3.2^{bB}	47.2±2.3^{bB}	47.0±2.9^{bB}	48.6±3.5^{abB}	52.3±3.7^{aB}	52.8±3.4^{aB}
Δ*E*	0%	9.0±2.2^{d}	–	42.9±5.1^{abA}	40.5±1.4^{bcA}	38.7±3.6^{bcA}	37.0±2.8^{cA}	42.5±5.1^{abcA}	43.8±4.2^{abA}	47.2±6.2^{aA}
	4%	9.0±2.2^{d}	–	36.1±5.6^{abcB}	34.2±2.8^{bcB}	32.4±2.5^{bcB}	31.3±2.8^{cB}	36.6±4.6^{abB}	40.2±3.7^{aA}	40.8±3.1^{aB}
BI	0%	41±4^{d}	24±4^{d}	151±27^{abcA}	145±7^{bcA}	135±14^{bcA}	125±12^{cA}	150±26^{abcA}	157±22^{abA}	175±33^{aA}
	4%	41±4^{f}	24±4^{f}	127±25^{bcdA}	117±11^{cdeB}	107±10^{deB}	101±10^{eB}	130±22^{abcA}	147±19^{abA}	149±15^{aB}
WI	0%	67.0±2.1^{b}	75.1±2.2^{a}	34.9±5.1^{deB}	36.6±1.3^{cdB}	38.5±3.2^{cdB}	40.4±2.7^{cB}	35.1±4.9^{cdeB}	33.9±4.2^{deA}	30.6±5.9^{eB}
	4%	67.0±2.1^{b}	75.1±2.2^{a}	40.8±5.3^{deA}	42.7±2.6^{cdA}	44.7±2.4^{cdA}	46.0±2.7^{cA}	40.3±4.5^{deA}	36.7±3.6^{eA}	36.2±2.9^{eA}
YI	0%	45.7±3.4^{d}	31.0±4.6^{e}	114.4±11.6^{abA}	111.0±3.0^{bcA}	106.5±6.4^{bcA}	102.1±5.9^{cA}	113.8±11.1^{bcA}	116.7±9.7^{abA}	123.7±13.3^{aA}
	4%	45.7±3.4^{e}	31.0±4.6^{f}	101.0±12.6^{bcB}	96.9±6.2^{cdB}	92.5±5.3^{cdB}	89.8±5.8^{dB}	102.5±10.9^{abcB}	111.5±9.3^{abA}	112.7±7.1^{aB}

The results are presented as mean ± standard deviation. Different lowercases mean significant differences ($p<0.05$) between samples within the same row. Different uppercases mean significant differences ($p<0.05$) between 0 and 4% CaL within the same impregnation treatment and color parameter. Δ*E*, total color difference compared to FA+AA sample; BI, browning index; WI, whiteness index; YI, yellowness index. Sample codes refer to Table 1.

the functional food products. The color of the freeze-dried control and impregnated apple flesh was described by several parameters (**Table 4**). Regarding controls, FA+AA exhibited higher L^*, lower a^* and b^*, as well as higher WI and lower YI compared to FA ($p<0.05$). This might be explained by the role of ascorbic acid that could prevent melanin formation through intermediate products binding, *e.g.*, *o*-quinone, thus increasing the lightness of the apple [Moon *et al.*, 2020].

The color parameters of freeze-dried impregnated apples (CON, VI, and US) were influenced by the SB juice in the impregnation solution, and more specifically by the carotenoids present in it. For SB juice, L^*, a^*, and b^* were 52.9±0.1, 22.0±0.1, and 63.5±0.3, respectively. The treated samples had lower L^* and WI, and higher a^*, b^*, BI, and YI than the controls ($p<0.05$) (**Table 4**). The ΔE of the impregnated samples ranged from 37.0 to 47.2 in 0% CaL, and 31.3 to 40.8 in 4% CaL, indicating that the color difference between FA+AA and all impregnated apple products could be clearly noticed by observers. The color changes of apple chips or fresh apple pieces caused by the use of a colored impregnation solution or an osmotic dehydration solution were observed in other studies, *e.g.*, apples with cranberry and grape juices [Wang *et al.*, 2022], beetroot juice [Aguirre-García *et al.*, 2020], and chokeberry juice [Lech *et al.*, 2018].

The enzymatic browning, which determines color, may occur in apple products, due to the presence of polyphenol oxidase (POD) and peroxidase (POD). Although the color parameters of apple products, especially L^*, ΔE, BI, WI, and YI, were used in some studies to observe the enzymatic browning, those parameters are not always in accordance with PPO and POD activities as the color of the impregnating or dipping solution may also affect those parameters [Arnold & Gramza-Michałowska, 2022]. The activity of PPO and POD was determined in our study and discussed below to confirm whether the enzymatic browning occurred in the freeze-dried products.

Regarding the application of non-conventional impregnations (VI and US), only freeze-dried samples prepared under certain treatment conditions showed significant differences in BI, WI, and YI compared to CON (**Table 4**). However, ΔE did not show any significant differences between CON and non-conventional treatments in either 0% or 4% CaL solution. This might be due to the intense color from SB juice in the samples, noting that for products with intense color, even the ΔE values of 6–7 may still be subtle to the eye [Tylewicz *et al.*, 2020]. In another report, the VI with isotonic CaL solutions caused a significant darkening of melon, which might be due to changes in the structural properties of the tissue as a consequence of vacuum application and/or gas-liquid exchange that can alter the refraction index [Tappi *et al.*, 2016]. The application of ultrasound in combination with VI using a solution containing 9% sucrose, 0.5% citric acid, and 0.5% ascorbic acid (*w/w*) also affected the ΔE of cranberry, showing that cranberries impregnated at 50 mbar had lower ΔE than those treated at 300 mbar [Mierzwa *et al.*, 2022].

Generally, the addition of 4% CaL tended to cause significant changes in the color parameters of the products, regardless of the impregnation method (CON, VI, or US). The VI of fresh-cut melon using up to 5% of CaL also showed significant changes in L^* and hue angle, depending on the pressure levels [Tappi *et al.*, 2016]. In another study, similar chroma values were found for pineapples osmotically dehydrated in sugar solution with 2 and 4% CaL [Silva *et al.*, 2014].

Total phenolic content and antioxidant capacity of freeze-dried apples

The TPC and antioxidant capacity (determined by ABTS, DPPH, FRAP, ORAC, PCL-ACL, PCL-ACW, and PCL-IAC assays assays) of freeze-dried controls and impregnated samples is shown in **Figure 1**. In controls, FA+AA in general showed higher TPC and antioxidant capacity than FA, due to the presence of ascorbic acid. However, an insignificant increase was found in ABTS and ORAC assays ($p\geq0.05$).

Among the impregnated samples (CON, VI, and US), the addition of 4% CaL in the solution significantly ($p<0.05$) decreased the TPC and antioxidant capacity of the samples, except for the TPC and ORAC values in US_10 and US_20, and ABTS in CON, where the values were similar ($p\geq0.05$) between CaL concentrations. This phenomenon could be explained by the presence of calcium in the samples, which increased the weight of the freeze-dried samples and subsequently reduced the TPC and antioxidant capacity *per* 100 g of the sample with 4% CaL [Arnold *et al.*, 2025]. Another possible mechanism could also be the total soluble solid change of the impregnating solution from 4.53°Brix in 0% CaL to 7.47°Brix in 4% CaL solution, which subsequently affected the mass transfer phenomenon and influenced the TPC and antioxidant capacity of freeze-dried products. Although both solutions were still mildly hypotonic than raw FA+AA (8.80°Brix), the higher total soluble solid difference between 0% CaL solution and raw FA+AA could have caused a higher increase in the TPC and antioxidant capacity of the samples than 4% CaL solution. In mango, adding sucrose to the grape-residue solution (raising total soluble solids) during osmosonication-assisted vacuum impregnation (US and VI combined) did not significantly increase the TPC, while US and VI alone without sucrose increased TPC [Batista de Medeiros *et al.*, 2019].

In **Figure 1**, it was observed that mainly the CON samples showed higher TPC and antioxidant capacity than FA+AA and FA. However, the significance of these differencesvaried depending on the type of antioxidant assay and CaL concentration. Although other studies reported increased antioxidant activity of apple products impregnated in hypertonic solutions, *e.g.*, concentrated chokeberry juice without [Masztalerz *et al.*, 2021] or with sucrose [Kowalska *et al.*, 2020] and beetroot juice with sucrose [Aguirre-García *et al.*, 2020], the impregnation using hypotonic SB juice solution in this study could also increase the TPC and antioxidant activity of the end product, especially in the treatment with 0% CaL. Another study also observed faster migration of phenolic compounds into cucumber slices after impregnation in a hypotonic gallic acid solution than in a hypertonic gallic acid-glycerol solution, and further used various

Figure 1. Total phenolic content, TPC (**A**), ABTS radical cation scavenging activity (**B**), DPPH radical scavenging activity (**C**), ferric-reducing antioxidant power, FRAP (**D**), oxygen radical absorbance capacity, ORAC (**E**), and results of photochemiluminescence assay including antioxidant capacity of lipid-soluble substances, PCL-ACL (**F**) water-soluble substances, PCL-ACW (**G**), and integral antioxidant capacity, PCL-IAC (**H**) of freeze-dried products: fresh apple flesh (FA), FA dipped in ascorbic acid solution (FA+AA), and FA+AA samples subjected to conventional (CON) and non-conventional impregnation (vacuum impregnation, VI, and ultrasound-assisted impregnation, US) in sea buckthorn juice without and with calcium lactate (CaL). Different lowercase letters indicate significant differences ($p<0.05$) between samples within the same CaL concentration. Different uppercase letters indicate significant differences ($p<0.05$) between 0 and 4% CaL within the same impregnation treatment. GAE, gallic acid equivalent; TE, Trolox equivalent. Sample codes refer to Table 1.

hypotonic herbal solutions to improve the TPC and antioxidant activities (ABTS and FRAP assays) of cucumber slices [Giannakourou *et al.*, 2019].

In contrast to this study, our previous research found lower or similar TPC and antioxidant capacity of freeze-dried Polish Gala apples conventionally impregnated with hypotonic Polish SB juice, even without CaL addition, as compared to FA+AA and FA [Arnold *et al.*, 2025]. The variation in raw material origin may explain the differences in results, as apples and SB juice from different regions can exhibit distinct physicochemical compositions [Ciesarová *et al.*, 2020; Raj *et al.*, 2021]. The differences in physicochemical compositions of apples and SB juice may further influence the mass transfer during the impregnation process and subsequently the chemical composition and antioxidant properties of the end products.

In this study, the application of non-conventional techniques (VI and US) under certain treatment conditions improved the TPC and antioxidant capacity of freeze-dried samples in comparison to CON treatments under the same CaL concentration (**Figure 1**). For the VI treatment, samples prepared with VI_200 exhibited the highest TPC and antioxidant capacity in both 0% and 4% CaL. This indicated that the lower the pressure applied, the more empty intercellular spaces in apple tissue, and the better the mass transfer as more antioxidants from SB juice filled those spaces and eventually increased the antioxidant capacity of the freeze-dried product. This was in accordance with the weight gain (**Table 3**), where VI_200 exhibited the highest weight gain in 0% CaL (18.72%) and 4% CaL (16.74%).

In another study using hypotonic lemon juice (6.25°Brix), it was observed that the VI of organic and conventional Golden Delicious (13.25–13.50°Brix), even at 738 mbar and 10 s of holding time, could increase TPC by 8–11% and antioxidant activity by 10–13% (ABTS assay) [Santarelli *et al.*, 2020]. In the present study, in comparison to CON at the same CaL concentration, the TPC of samples after VI_200 increased 14.8% and 19.5% for 0 and 4% CaL, respectively. Among antioxidant assays, the highest increases after VI_200 were observed in PCL-ACW, which were 26.8% and 29.9% for 0 and 4% CaL, respectively. However, it is noteworthy that the type of impregnating solution, treatment time, and vacuum level in the VI treatment may influence the antioxidant capacity of end products. Pasławska *et al.* [2019] observed both negative and positive impacts of VI (40–80 mbar, 10–80 s) of Ligol apple in apple-pear juice or citric acid solution on the TPC and antioxidant activities (ABTS and FRAP assays) [Pasławska *et al.*, 2019]. In contrast, Trusinska *et al.* [2024], who used an isotonic aloe vera-trehalose solution (13 °Brix) during VI of Italian Golden Delicious slices, observed that VI (200 mbar, 10 min) significantly decreased vitamin C content by 34% and TPC by 32%, while similar antioxidant activity was observed in the ABTS assay. Nevertheless, based on the present study, VI especially at 200 mbar, could be an effective way not only to increase the TPC and antioxidant capacity of freeze-dried apples, but also to save more time as the treatment lasted shorter (28 min) than US or CON (120 min).

In the US treatment, the longer the treatment time, the higher the TPC and antioxidant capacity of the samples, especially in the 0% CaL solution. The US treatment (45 kHz, 900 W, 10–30 min) prior to VI was also reported to minimize the loss of TPC and vitamin C caused by VI alone [Trusinska *et al.*, 2024]. The US treatment may loosen the apple matrix, facilitating the impregnating solution to penetrate into the matrix [Indriani *et al.*, 2023], thus improving the antioxidant properties of the end freeze-dried products.

As the highest TPC and antioxidant capacity among the samples treated with 0% CaL were observed for US_30, the optimum US treatment with 4% CaL was US_20. In comparison to US_20 (in 4% CaL), the US_30 sample had significantly ($p<0.05$) lower antioxidant capacity in all assays, while TPC did not differ significantly($p\geq0.05$). After the application of those optimum US conditions (US_30 for 0% CaL and US_20 for 4% CaL), the TPC of samples increased 11.7% and 13.8% for 0 and 4% CaL, respectively, compared to CON samples. Among antioxidant capacity assays, the highest increase was observed in PCL-ACW (29.7%) for 0% CaL and ORAC (35.5%) for 4% CaL.

During the US-assisted impregnation, the mass transfer in the samples was faciliated by cavitation, which is the formation, growth, and collapse of bubbles in the impregnating solution or solids (which contain moisture), produced by the pressure fluctuations generated by the ultrasound waves [Nowacka *et al.*, 2021]. The implosion of these microbubbles could promote mass transfer rates and further influence various mechanical properties [Batista de Medeiros *et al.*, 2019]. The pores of the apple flesh in this study could expand more with the action of collapsed bubble, resulting in more intercellular spaces inside the flesh, and further allowing more antioxidants from the impregnating solution (in this case, SB juice) would infuse through the pores; this was similarly explained in the influence of US on vacuum impregnated apple flesh using black carrot concentrate [Yılmaz & Ersus Bilek, 2018]. However, in the 4% CaL solution, the decline in antioxidant capacity after 30 min of the US treatment might be due to US-induced aggregation of the compounds of impregnating solution within the apple matrix, leading to an increased total soluble solid content with prolonged US treatment. This might cause irreversible excessive cell ruptures, so that during relaxation time, the excessively ruptured cells could not optimally retain the infused antioxidants from SB juice solution. Also, in some cases, viscous solutions make penetration of solutes more difficult compared to less viscous solutions [Tappi *et al.*, 2016]. Furthermore, a study observed that the application of US (33 kHz, 60 W) to cherry in water for up to 40 min increased the TPC and antioxidant activities (ABTS and DPPH assays) of cherry, due to cell disruption and more effective extraction of phenolics. However, after 60 min, the cell disruption might be excessive, resulting in detrimental effects, such as phenolics degradation [Muzaffar *et al.*, 2016]. Apples impregnated with black carrot concentrate also showed higher ion leakage when US treatment (33 kHz) was applied at 198 W, compared to those at 0–158 W, indicating a higher rate of cellular damage in plant tissue [Yılmaz & Ersus Bilek, 2018].

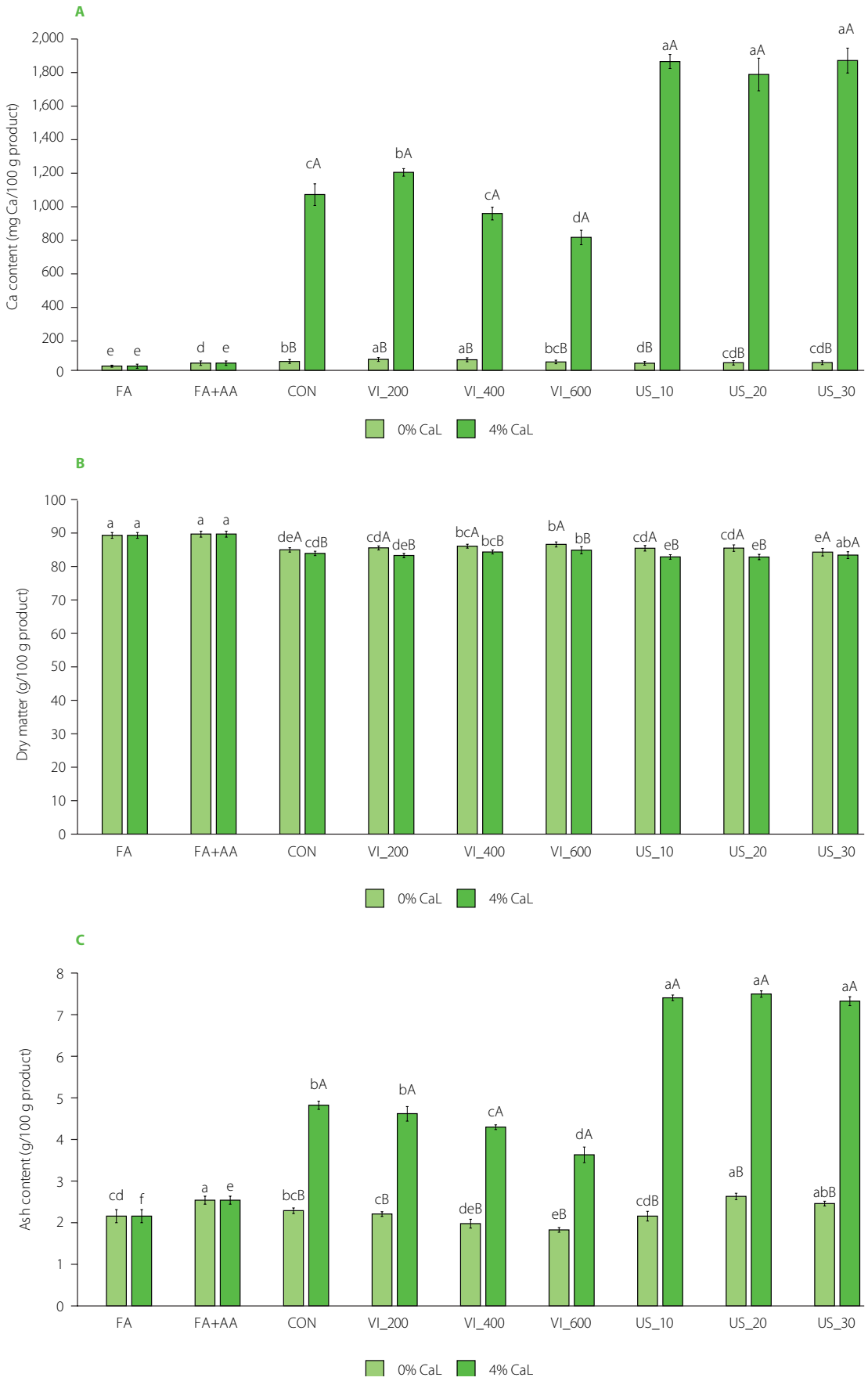

Figure 2. Content of calcium (**A**), dry matter (**B**), and ash (**C**) of freeze-dried products: fresh apple flesh (FA), FA dipped in ascorbic acid solution (FA+AA), and FA+AA samples subjected to conventional (CON) and non-conventional impregnation (vacuum impregnation, VI, and ultrasound-assisted impregnation, US) in sea buckthorn juice without and with calcium lactate (CaL). Different lowercase letters indicate significant differences ($p<0.05$) between samples within the same CaL concentration. Different uppercase letters indicate significant differences ($p<0.05$) between 0 and 4% CaL within the same impregnation treatment. Sample codes refer to Table 1.

Calcium content of freeze-dried apples

The calcium content of freeze-dried apples before and after the impregnation treatment is shown in **Figure 2**. The FA had a calcium content of 25.78 mg Ca/100 g, while FA+AA showed a higher calcium content of 43.65 mg Ca/100 g. The dipping process with ascorbic acid may have changed the calcium content of FA through mass transfer. In 0% CaL solution, all impregnated samples (CON, VI, and US) showed a higher calcium content than FA. However, when compared to FA+AA, only CON (54.22 mg Ca/100 g) and VI (51.09–66.65 mg Ca/100 g) freeze-dried apples had significantly (p<0.05) higher values, while US samples (43.45-46.71 mg Ca/100 g) had similar (p≥0.05) values. In our previous study, using SB juice and Gala apples from other sources (fruits originating from Poland), a calcium content of 79.44 mg Ca/100 g was determined in a conventionally-impregnated sample without CaL addition [Arnold *et al.*, 2025]. The higher calcium content of SB juice than raw FA and FA+AA (**Table 2**) might explain the increasing calcium content in the impregnated samples without CaL.

The samples prepared at 4% CaL in the solution, as expected, showed a significantly (p<0.05) higher calcium content than those treated at 0% CaL (**Figure 2**). Interestingly, among the VI treatments, only VI_200 effectively (p<0.05) increased the calcium content of the freeze-dried apples compared to CON (from 1,194 to 1,060 mg Ca/100 g), while the VI_400 sample showed similar (p≥0.05) values and VI_600 showed 24.3% lower calcium content than CON. When comparing CON with VI_600 in the 4% CaL solution, the pressure used in VI_600 was not sufficient to enhance impregnation. Instead, it may have caused the impregnating solution, along with the calcium, to be drawn out of the apple tissue. This could explain the reduced calcium content observed in the sample, a phenomenon also reported in a previous study using Fuji apples [Assis *et al.*, 2019]. Casim *et al.* [2023] determined calcium contents of 3,600 and 5,200 mg Ca/kg in Granny Smith dried apples treated by atmospheric (4.5 h, 20°C) and vacuum impregnation (50 mm Hg, 10 min) using an isotonic solution containing 3% calcium gluconate and 2.24% CaL, which were higher than those of the untreated apples (39 mg Ca/kg).

US treatments (4% CaL) resulted in a higher calcium content of the freeze-dried apples, *i.e.*, 49.3–56.4% higher compared to VI_200 and 68.3–76.1% higher compared to CON (**Figure 2**). However, the duration of the US treatment did not significantly (p≥0.05) affect the calcium content. Therefore, US_20 (4% CaL), with 1,783 mg Ca/100 g, was suggested as optimal, considering it increased both calcium content and antioxidant capacity. The simultaneous application of US (130 W, 35 kHz) during VI (211 mmHg), using a solution containing 3% CaL and 0.8% black carrot concentrate, led to a 13.8% calcium content increase in Starking Delicious apple discs, compared to VI without US [Yılmaz & Ersus Bilek, 2018]. The authors also stated that the addition of Ca could inhibit microbial activity in the product by improving the resistance of cellular structures to microbial infection, and also due to the presence of lactate ions derived from Ca-lactate.

As additional information, considering 25% calcium absorption in adults, consuming 100 g of freeze-dried apples prepared at VI_200 and US_20 in 4% CaL solution may fulfill 29.8% and 44.6% of the recommended daily allowance for adults aged 19–50 [National Institutes of Health, 2022].

Relationship between total phenolic content, antioxidant capacity, and physicochemical parameters of freeze-dried apples

PCA was applied to better understand the relationship between TPC, antioxidant capacity, calcium, dry matter, and ash content of freeze-dried apples. The first two principal components accounted for 92.45% of the total variance (PC1 – 64.79%; PC2 – 27.66%). In the PCA biplot, three groups were noticeable, including a cluster with control samples (FA and FA+AA), a cluster with apples impregnated with 4% CaL, and a group with samples impregnated with 0% CaL (**Figure 3**). Distinctive subgroups of CON, VI, and US were also observed in the cluster with the apples impregnated with 4% CaL. Variables that distinguished freeze-dried apples treated at 0% CaL were TPC and antioxidant capacity determined by different antioxidant assays, while calcium and ash content characterized samples at 4% CaL. The calcium content of the products was affected not only by the concentration of CaL in the solution, but also by the technology applied during the impregnation process. The calcium content of the product was correlated with ash content, while TPC was associated with antioxidant capacity, especially when it was determined by ORAC, FRAP, ABTS, and DPPH assays.

Content of individual phenolics and carotenoids of freeze-dried apples

The composition of phenolics and carotenoids of the freeze-dried apple controls and samples with selected treatments from 0% CaL (CON, VI_200, and US_30) and 4% CaL (CON, VI_200, and US_20) is shown in **Table 5**. The total phenolics of the impregnated samples (226.18–328.02 mg/100 g product) determined by UPLC-PDA were more than twice as high as those of FA and FA+AA (95.03–99.53 mg/100 g product). The application of VI and US generally improved the total phenolics compared to CON, regardless of the CaL concentration, although increases for US_30 without CaL and VI_200 with CaL were insignificant (p≥0.05). Furthermore, CON and VI at 0% CaL showed significantly higher total phenolics than those treated at 4% CaL (p<0.05), while US showed similar values. This trend of results was in accordance with the antioxidant capacity and TPC (**Figure 1**).

However, the increase was not found in all phenolic subgroups. The impregnated samples regardless of the CaL addition had lower sums of phenolic acids compared to controls, except VI_200 without CaL which showed a similar value to controls (**Table 5**). Controls also had more dihydrochalcones (6.56–6.88 mg/100 g product) than the treated apples. Although the application of VI and US could enhance the impregnation of a bioactive-containing solution into the apple, it could also lead to microstructural changes in the tissue, possibly degrading

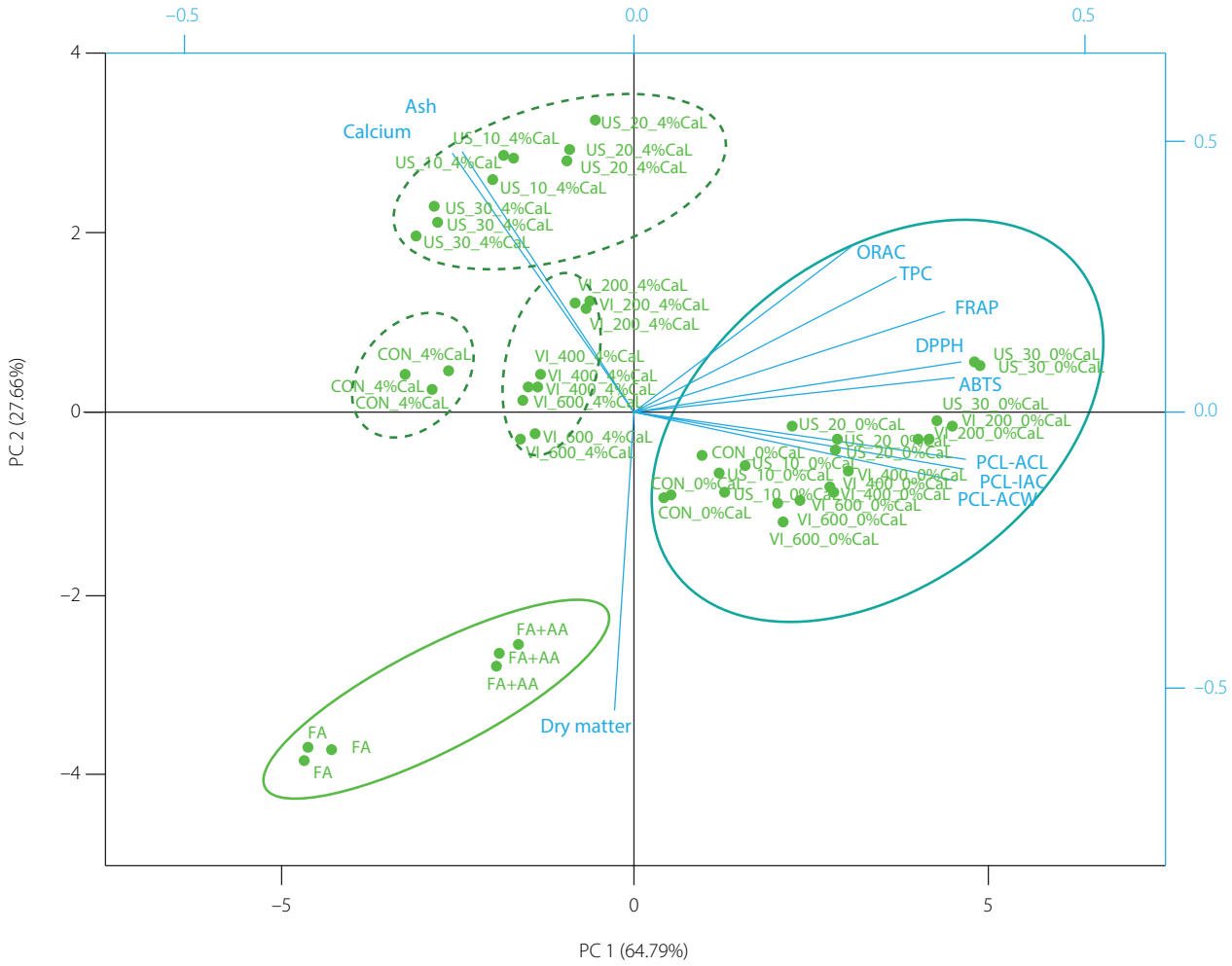

Figure 3. Biplot of principal component analysis of total phenolic content, antioxidant capacity, and physicochemical parameters of freeze-dried products: fresh apple flesh (FA), FA dipped in ascorbic acid solution (FA+AA), and FA+AA samples subjected to conventional (CON) and non-conventional impregnation (vacuum impregnation, VI, and ultrasound-assisted impregnation, US) in sea buckthorn juice without and with calcium lactate (CaL). Sample codes refer to Table 1.

or enhancing the migration of some native antioxidants, in this case lower molecular weight phenolics like phenolic acids and dihydrochalcones, out of the apple matrix [Vinod *et al.*, 2024; Yılmaz & Ersus Bilek, 2018]. Therefore, it is necessary for industries to control the processing parameters of VI and US to improve the functional properties of food products, noting that the sample matrix and process parameters will profoundly affect specific compound behavior.

Furthermore, the impregnated samples with 0% CaL showed the highest range of flavan-3-ols content, followed by 4% CaL and controls (**Table 5**). Catechin was generally the predominant compound among flavan-3-ols in the impregnated samples, due to the involvement of SB juice; sea buckthorn fruits are rich in this compound [Guo *et al.*, 2017] Among phenolics, flavonols were the most abundant subgroup in the impregnated samples also due to SB juice, while only quercetin 3-*O*-rhamnoside was found in FA and FA+AA. The profile of SB fruit comprises mainly diverse simple glycosides of isorhamnetin and quercetin with less frequent occurrence of kaempferol [Ciesarová *et al.*, 2020]. Isorhamnetin 3-*O*-rutinoside (about 36%) and isorhamnetin 3-*O*-glucoside (about 22%) were the major flavonols, which were also dominant in the end product of our previous study, using Polish Gala and SB juice from the Polish retail market [Arnold *et al.*, 2025], as well as agreed with the flavonol composition determined in various SB juices [Tkacz *et al.*, 2020]. The flavonol content of SB differs due to maturity, climate, cultivars, and geographical sites. It is worth noting that flavonoids play important roles in osteogenesis [Yuca *et al.*, 2024] and the prevention of chronic diseases, such as diabetes, cardiovascular diseases, and cancer, due to their antioxidant activity [Ciesarová *et al.*, 2020].

For carotenoids, just like with the phenolic compounds, the impregnated freeze-dried apples with SB juice showed higher total carotenoids (16.47–38.88 mg/100 g) than the controls (2.70–-3.02 mg/100 g) (**Table 5**). Among carotenoids, carotenes dominated with the highest content in VI_200 at 0% CaL accounting for 21.62 mg/100 g product. When comparing between 0 and 4% CaL in each treatment (CON, VI, US), the CON and VI samples prepared at 0% CaL showed higher total carotenoids, while US had similar values. Carotenoids have been studied not only for their contribution to antioxidant activity, but also for their role in bone metabolism, such as bone mineral density and bone

Table 5. Phenolic and carotenoid compositions of freeze-dried products (mg/100 g): fresh apple flesh (FA), FA dipped in ascorbic acid solution (FA+AA) and FA+AA samples subjected to conventional (CON), and non-conventional impregnation (vacuum impregnation, VI, and ultrasound-assisted impregnation, US) in sea buckthorn juice without and with calcium lactate (CaL).

Compound	Control		0% CaL			4% CaL		
	FA	FA+AA	CON	VI_200	US_30	CON	VI_200	US_20
Phenolics								
p-Coumaric acid *O*-hexoside	30.44±1.85^{ab}	32.24±0.42^{a}	25.34±0.04^{cd}	33.07±0.33^{a}	21.78±1.51^{e}	26.91±0.35^{bc}	27.45±0.24^{bc}	22.72±0.49^{de}
Ferulic acid *O*-hexoside	3.52±0.27^{a}	2.97±0.04^{a}	2.77±0.07^{a}	3.4±0.22^{a}	4.06±1.76^{a}	2.51±0.20^{a}	2.04±0.04^{a}	2.24±0.07^{a}
Sum of phenolic acids	**33.96±2.13^{ab}**	**35.22±0.46^{a}**	**28.10±0.03^{c}**	**36.48±0.55^{a}**	**25.84±3.26^{c}**	**29.42±0.55^{bc}**	**29.50±0.20^{bc}**	**24.96±0.42^{c}**
(+)-Catechin	2.26±0.18^{d}	3.02±0.09^{d}	44.90±1.85^{a}	35.41±0.49^{b}	36.93±3.50^{b}	34.24±2.02^{b}	25.00±0.18^{c}	37.58±0.06^{b}
Procyanidin B_1	nd	nd	34.58±0.96^{ab}	42.72±0.53^{a}	32.86±8.01^{ab}	23.47±0.46^{b}	27.14±0.25^{b}	31.98±0.41^{ab}
(–)-Epicatechin	13.37±0.90^{a}	12.21±0.37^{ab}	8.38±0.99^{c}	11.88±0.36^{ab}	9.20±0.75^{c}	12.41±0.10^{ab}	10.23±0.52^{bc}	9.07±0.33^{c}
Procyanidin C_1	42.20±0.70^{a}	36.94±0.49^{b}	20.35±0.15^{cd}	23.90±2.49^{c}	18.32±0.53^{d}	22.07±0.04^{cd}	22.01±0.33^{cd}	18.22±0.52^{d}
Sum of flavan-3-ols	**57.84±1.43^{d}**	**52.16±0.21^{d}**	**108.2±0.25^{ab}**	**113.9±1.82^{a}**	**97.32±11.29^{abc}**	**92.18±2.34^{bc}**	**84.39±1.29^{c}**	**96.86±1.20^{bc}**
Phloretin 2-*O*-xyloglucoside	2.51±0.09^{bc}	2.28±0.08^{c}	0.50±0.09^{d}	0.74±0.12^{d}	0.98±0.06^{d}	2.40±0.21^{bc}	3.03±0.05^{b}	4.27±0.39^{a}
Derivative of dihydrochalcones	2.87±0.52^{a}	2.80±0.11^{a}	nd	nd	nd	nd	nd	nd
Phloretin 2-*O*-glucoside	1.50±0.41^{a}	1.48±0.06^{a}	nd	nd	nd	nd	nd	nd
Sum of dihydrochalcones	**6.88±1.02^{a}**	**6.56±0.03^{a}**	**0.50±0.09^{e}**	**0.74±0.12^{e}**	**0.98±0.06^{de}**	**2.40±0.21^{cd}**	**3.03±0.05^{bc}**	**4.27±0.39^{b}**
Isorhamnetin 3,7-*O*-dihexoside	nd	nd	6.94±0.24^{b}	8.56±0.36^{a}	8.16±0.06^{a}	4.61±0.12^{c}	6.96±0.07^{b}	8.77±0.02^{a}
Isorhamnetin 3-*O*-sophoroside-7-*O*-rhamnoside	nd	nd	5.29±0.11^{bc}	6.36±0.33^{a}	6.03±0.28^{ab}	3.62±0.29^{d}	4.95±0.04^{c}	6.45±0.12^{a}
Quercetin 3-*O*-(dirhamnosyl)hexoside	nd	nd	1.81±0.28^{bc}	2.25±0.36^{ab}	2.26±0.07^{ab}	1.32±0.02^{c}	1.87±0.12^{bc}	2.56±0.03^{a}
Quercetin 3-galactoside-7-*O*-rhamnoside	nd	nd	3.21±0.04^{ab}	3.84 ± 0.19^{a}	3.48±0.58^{ab}	1.70±0.13^{c}	2.80±0.11^{b}	3.79±0.06^{a}
Quercetin 3-*O*-rutinoside	nd	nd	3.50±0.00^{b}	4.51 ± 0.18^{a}	4.13±0.43^{ab}	2.35±0.26^{c}	3.33±0.31^{b}	4.39±0.03^{a}
Isorhamnetin 3-*O*-glucoside-7-*O*-rhamnoside	nd	nd	28.46±0.88^{b}	34.11±0.53^{a}	33.77±0.22^{a}	19.33±0.98^{c}	28.45±0.59^{b}	35.15±0.24^{a}
Quercetin 3-*O*-glucoside	nd	nd	4.71±0.83^{ab}	5.30±0.72^{a}	6.16±0.07^{a}	3.57±0.24^{b}	4.99±0.31^{ab}	6.26±0.22^{a}

Table 5 continued. Phenolic and carotenoid compositions of freeze-dried products (mg/100 g): fresh apple flesh (FA), FA dipped in ascorbic acid solution (FA+AA) and FA+AA samples subjected to conventional (CON), and non-conventional impregnation (vacuum impregnation, VI, and ultrasound-assisted impregnation, US) in sea buckthorn juice without and with calcium lactate (CaL).

Compound	Control		0% CaL			4% CaL		
	FA	FA+AA	CON	VI_200	US_30	CON	VI_200	US_20
Kaempferol 3-*O*-hexoside-7-*O*-rhamnoside	nd	nd	3.77±0.02^{ab}	4.28±0.13^{a}	4.04±1.02^{ab}	2.65±0.07^{b}	3.92±0.30^{ab}	4.80±0.02^{a}
Isorhamnetin 3-*O*-(rhamnosyl)hexoside	nd	nd	1.28±0.02^{b}	1.52±0.01^{a}	1.51±0.06^{a}	0.99±0.06^{c}	1.28±0.06^{b}	1.58±0.00^{a}
Isorhamnetin 3-*O*-rutinoside	nd	nd	53.35±0.37^{b}	64.23±0.37^{a}	63.57±0.78^{a}	36.70±1.42^{c}	52.77±0.67^{b}	67.65±0.51^{a}
Quercetin 3-*O*-rhamnoside	0.85±0.04^{e}	1.09±0.11^{de}	1.69±0.12^{abc}	1.70±0.18^{ab}	1.88±0.09^{ab}	1.16±0.00^{cde}	1.42±0.20^{bcd}	1.96±0.21^{a}
Isorhamnetin 3-*O*-glucoside	nd	nd	30.98±0.47^{c}	37.80±0.99^{b}	38.28±0.38^{ab}	22.79±1.22^{d}	31.18±1.43^{c}	41.15±0.86^{a}
Kaempferol 3-*O*-rutinoside	nd	nd	1.12±0.06^{a}	1.31±0.17^{a}	1.13±0.02^{a}	0.74±0.09^{b}	1.05±0.07^{ab}	1.22±0.09^{a}
Isorhamnetin 3-*O*-rhamnoside	nd	nd	1.02±0.17^{a}	1.13±0.13^{a}	1.19±0.09^{a}	0.66±0.04^{b}	1.07±0.03^{a}	1.28±0.04^{a}
Sum of flavonols	**0.85±0.04^{e}**	**1.09±0.11^{e}**	**147.13±1.00^{c}**	**176.91±0.41^{b}**	**175.59±0.61^{b}**	**102.18±4.56^{d}**	**146.02±2.36^{c}**	**187.00±1.27^{a}**
Total phenolics	**99.53±2.50^{f}**	**95.03±0.12^{f}**	**283.93±1.13^{cd}**	**328.02±0.98^{a}**	**299.72±15.23^{bc}**	**226.18±7.25^{e}**	**262.93±3.79^{d}**	**313.09±3.28^{ab}**
Carotenoids								
Lutein isomer	0.49±0.03^{a}	0.36±0.04^{b}	nd	nd	nd	nd	nd	nd
All-*trans*-lutein	0.21±0.03^{a}	0.17±0.03^{a}	nd	nd	nd	nd	nd	nd
Zeaxanthin isomer	nd	nd	5.51±1.14^{b}	12.93±0.49^{a}	10.79±0.00^{a}	3.98±0.81^{b}	4.43±1.37^{b}	11.49±0.04^{a}
Sum of carotenes	1.86±0.10^{d}	2.36±0.61^{d}	18.34±2.23^{ab}	21.62±0.00^{a}	12.54±0.00^{c}	12.26±0.16^{c}	16.48±0.93^{abc}	14.45±3.03^{bc}
Phytofluene	0.14±0.01^{c}	0.13±0.01^{c}	0.30±0.05^{ab}	0.34 ±0.02^{ab}	0.31±0.03^{ab}	0.23±0.02^{bc}	0.36±0.02^{a}	0.28±0.06^{ab}
Total carotenoids	**2.70±0.08^{d}**	**3.02±0.55^{d}**	**24.15±3.42^{b}**	**34.88±0.47^{a}**	**23.64±0.03^{bc}**	**16.47±0.99^{c}**	**21.27±2.33^{bc}**	**26.22±3.13^{b}**

The results are presented as mean ± standard deviation. Different lowercases mean significant differences ($p<0.05$) between samples within the same row. nd, Not detected. Sample codes refer to Table 1.

mineral content in various *in vitro* and *in vivo* studies, which may be beneficial for people with osteoporosis [Kulczyński *et al.*, 2024].

In this study, the impregnation process of Gala flesh using SB juice, without or with 4% CaL, either through conventional or non-conventional impregnation (VI and US) affected the composition of phenolics and carotenoids, which may in turn impact the functional properties of the end products.

Polyphenol oxidase and peroxidase activity of freeze-dried apples

PPO and POD are the enzymes responsible for browning in apple products, which causes discoloration and degradation of phenolics [Moon *et al.*, 2020]. Their inhibition is important for maintaining the quality of apple products. The PPO and POD activity of freeze-dried apple controls and samples with selected treatments from 0% CaL (CON, VI_200, and US_30) and 4% CaL (CON, VI_200, and US_20) are shown in **Figure 4**. For PPO activity, the highest value was found in FA (3,795 U/g). In comparison to FA, the FA+AA reduced the PPO activity by 11.2%, which was comparable to our previous results (13.7%) [Arnold *et al.*, 2025]. Another study observed higher PPO and POD activity in freeze-dried apple (Jonagold, without blanching) than in hot air-dried apple, where the enzymes were almost inactivated due to high temperature [Ahmad-Qasem *et al.*, 2017]. The authors explained that the enzymes may be preserved in a latent state at low temperature during freeze-drying, yet their activities can be recovered when they come into contact with an aqueous medium.

The PPO activity was not observed in CON and US_30 at 0% CaL (**Figure 4**), which might be caused by complete inhibition from the antioxidants in the samples treated at 0% CaL, confirmed by their high antioxidant capacity. Ultrasound treatment may also inactivate browning enzymes (*i.e.*, PPO) by changing their secondary and tertiary structures [Iqbal *et al.*, 2020]. However, VI_200 at 0% CaL still showed PPO activity (3,486 U/g), a value similar to FA and FA+AA. In this case, despite the high antioxidant capacity found in VI_200, the applied high vacuum (pressure of 200 mbar) might deteriorate the texture of apple flesh [Kidoń *et al.*, 2023], and thus release more PPO during impregnation. Additionally, the sum of phenolic acids of VI_200 at 0% CaL was high, yet still similar to controls (**Table 5**), which may have acted as substrates of PPO.

In 4% CaL, US_20 reduced PPO activity by 19.4% compared with FA+AA, while CON and VI_200 showed similar values to FA+AA (**Figure 4**). Neri *et al.* [2019] applied lower vacuum pressure (738 mbar) during VI of organic and conventional Golden Delicious cubes using a lemon juice solution; this treatment successfully inhibited PPO activity by 32 and 16% in respective treated apple cubes. Additionally, the composition of organic acid contained in the impregnating solution may also influence the inhibition of PPO activity in treated apples [Santarelli *et al.*, 2020]. Another non-conventional technology, high-pressure processing of peaches in a CaL solution (0-2%), was applied and also increased the PPO activity of Clingstone peach, while caused no effect on Freestone peach [Techakanon & Barrett, 2017].

The POD activity of FA+AA was more than three times higher than of FA (**Figure 4**). The POD activity was completely inhibited in all selected treatments at 0% CaL, which might be linked to the high antioxidant activity and reducing agents that masked the POD activity by reacting with H_2O_2 as one of the POD substrates [Rojas-Graü *et al.*, 2008]. In contrast, at 4% CaL, POD activity was completely inhibited in CON but increased to 3,444 and 4,002 U/g for VI_200 and US_20, respectively. This might be caused by the combination of non-conventional technologies and the higher total soluble solid content in the solution

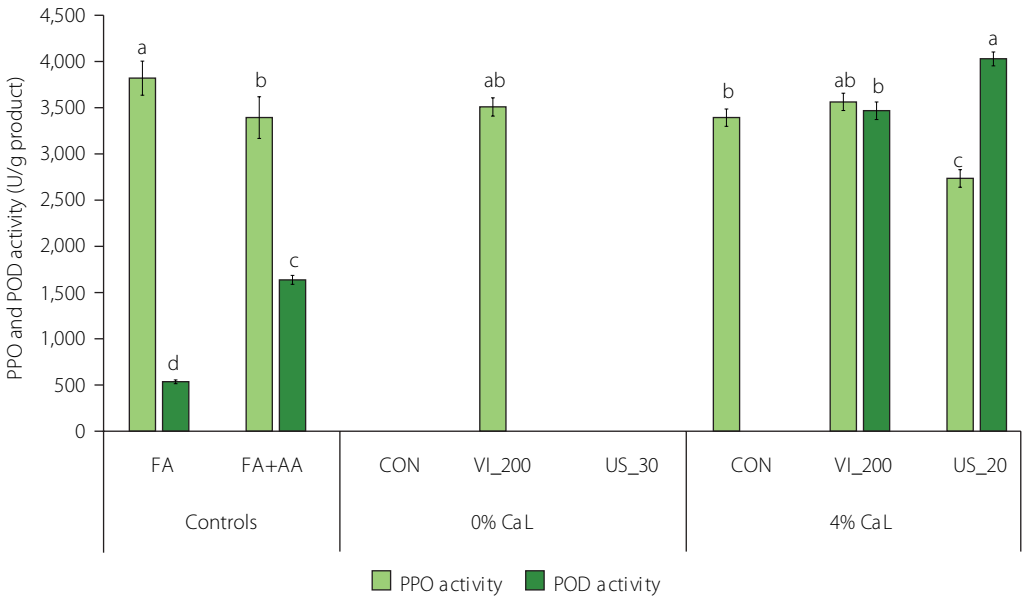

Figure 4. Polyphenol oxidase (PPO) and peroxidase (POD) activities of freeze-dried products: fresh apple flesh (FA), FA dipped in ascorbic acid solution (FA+AA), and FA+AA samples subjected to conventional (CON) and non-conventional impregnation (vacuum impregnation, VI, and ultrasound-assisted impregnation, US) in sea buckthorn juice without and with calcium lactate (CaL). Different lowercase letters indicate significant differences ($p<0.05$) between samples within the same enzyme. Sample codes refer to Table 1.

containing 4% CaL (7.47 °Brix) than in 0% CaL (4.53 °Brix) that could affect the cell structure and thus promote the release of POD. Nevertheless, the antioxidants could not effectively inhibit the POD activity in those treatments. Additionally, a study explained that ultrasound could activate POD by partially unfolding the protein structure, exposing more of the catalytic center and increasing the affinity for the substrate without fully denaturing the protein [Li & Tang, 2021].

Furthermore, although ascorbic acid was reported by previous studies to prevent PPO and POD activities [Arnold & Gramza-Michałowska, 2022; Moon *et al.*, 2020], in some cases it could act as a pro-oxidant that increased PPO and POD activity in apples [Rojas-Graü *et al*., 2008]. Nevertheless, despite the presence of POD activity observed in some treatments in this study, the POD contribution to enzymatic browning is lower than that of PPO because of the low concentration of H_2O_2 in apples [Rodríguez-Arzuaga *et al.*, 2019].

CONCLUSIONS

The impregnation of apple flesh using 93.8% SB juice in water (*w/w*), without or with 4% CaL was carried out conventionally and non-conventionally. Compared with CON, the application of VI and US affected the mass transfer phenomenon and thus resulted in freeze-dried apple products with higher antioxidant capacity and calcium content. The application of VI_200 enabled the development of freeze-dried apple samples with the highest antioxidant capacity (at 0% CaL) and calcium content (at 4% CaL), while the application of US_30 at 0% CaL and US_20 at 4% CaL also effectively improved the antioxidant capacity and calcium content, respectively. In comparison to CON, VI was also beneficial in terms of time-saving and improvement of functional properties, while US could improve the functional properties despite requiring the same treatment time as CON. The output of this study provides a suggestion to consumers and the food industry to consume or produce new alternative locally sourced healthy snacks that may potentially reduce the risk of osteoporosis and calcium deficiency, especially by applying non-conventional technologies. The demonstrated antioxidant properties, calcium content, and enzyme activities of the products suggest that VI and US have potential for application in the development of dried fruit snacks aimed at people with osteoporosis and calcium deficiency. However, it is worth noting that the industrial application of VI and US involves challenges that need to be considered, such as process scale-up, cost, uniformity, regulatory requirements, and the product's sensory properties and quality. Furthermore, as this study focused on *in vitro* analysis, further research is needed to evaluate the bioaccessibility and bioavailability of antioxidants and calcium, particularly through *in vitro* digestion, *in vivo* experiments, and human studies.

RESEARCH FUNDING

This research was funded by the National Science Centre, Poland, grant number: 2023/49/N/NZ9/00862 and Poznan University of Life Sciences, Poland, Department of Gastronomy Science and Functional Foods (statutory grant no 506.751.03.00).

CONFLICT OF INTERESTS

The authors declare that they have no known competing financial interests or personal relationships that could have appeared to influence the work reported in this paper.

ORICD IDs

M. Arnold **https://orcid.org/0000-0002-1749-8592**
A. Gramza-Michałowska **https://orcid.org/0000-0002-0744-9033**
U. Tylewicz **https://orcid.org/0000-0002-8192-6803**
J. Suliburska **https://orcid.org/0000-0002-0937-8427**
M. Świeca **https://orcid.org/0000-0002-6513-8399**
A. Wojdyło **https://orcid.org/0000-0002-0067-0691**

REFERENCES

1. Aguirre-García, M., Hernández-Carranza, P., Cortés-Zavaleta, O., Ruiz-Espinosa, H., Ochoa-Velasco, C.E., Ruiz-López, I.I. (2020). Mass transfer analysis of bioactive compounds in apple wedges impregnated with beetroot juice: A 3D modelling approach. *Journal of Food Engineering*, *282*, art. no. 110003. **https://doi.org/10.1016/j.jfoodeng.2020.110003**
2. Ahmad-Qasem, M.H., Nijsse, J., García-Pérez, J.V., Khalloufi, S. (2017). The role of drying methods on enzymatic activity and phenolics content of impregnated dried apple. *Drying Technology*, *35*(10), 1204–1213. **https://doi.org/10.1080/07373937.2016.1236344**
3. AOAC (2002). *Official Methods of Analysis* (17th ed.). *Method number: 920.15*. The Association of Official Analytical Chemists International, Gaithersburg, MD, USA.
4. Arnold, M., Białas, W., Kulczyński, B., Multisona, R.R., Suliburska, J., Świeca, M., Wojdyło, A., Gramza-Michałowska, A. (2025). Product development study of freeze-dried apples enriched with sea buckthorn juice and calcium lactate. *Molecules*, *30*(7), art. no. 1504. **https://doi.org/10.3390/molecules30071504**
5. Arnold, M., Gramza-Michałowska, A. (2022). Enzymatic browning in apple products and its inhibition treatments: A comprehensive review. *Comprehensive Reviews in Food Science and Food Safety*, *21*(6), 5038–5076. **https://doi.org/10.1111/1541-4337.13059**
6. Assis, F.R., Rodrigues, L.G.G., Tribuzi, G., de Souza, P.G., Carciofi, B.A.M., Laurindo, J.B. (2019). Fortified apple (*Malus* spp., var. Fuji) snacks by vacuum impregnation of calcium lactate and convective drying. *LWT – Food Science and Technology*, *113*, art. no. 108298. **https://doi.org/10.1016/j.lwt.2019.108298**
7. Batista de Medeiros, R.A., Vieira da Silva Júnior, E., Fernandes da Silva, J.H., da Cunha Ferreira Neto, O., Rupert Brandão, S.C., Pimenta Barros, Z.M., Sá da Rocha, O.R., Azoubel, P.M. (2019). Effect of different grape residues polyphenols impregnation techniques in mango. *Journal of Food Engineering*, *262*, 1–8. **https://doi.org/10.1016/j.jfoodeng.2019.05.011**
8. Benzie, I.F.F., Strain, J.J. (1999). Ferric reducing/antioxidant power assay: Direct measure of total antioxidant activity of biological fluids and modified version for simultaneous measurement of total antioxidant power and ascorbic acid concentration. *Methods in Enzymology*, *299*, 15–27. **https://doi.org/10.1016/S0076-6879(99)99005-5**
9. Besco, E., Braccioli, E., Vertuani, S., Ziosi, P., Brazzo, F., Bruni, R., Sacchetti, G., Manfredini, S. (2007). The use of photochemiluminescence for the measurement of the integral antioxidant capacity of baobab products. *Food Chemistry*, *102*(4), 1352–1356. **https://doi.org/10.1016/j.foodchem.2006.05.067**
10. Buera, M.P., Petriella, C., Lozano, R.D. (1985). Definition of color in the non-enzymatic browning process. *Die Farbe*, *32/33*(2), 316–326.
11. Casim, S., Romero-Bernal, A.R., Contigiani, E., Mazzobre, F., Gómez, P.L., Alzamora, S.M. (2023). Design of apple snacks – A study of the impact of calcium impregnation method on physicochemical properties and structure of apple tissues during convective drying. *Innovative Food Science and Emerging Technologies*, *85*, art. no. 103342. **https://doi.org/10.1016/j.ifset.2023.103342**
12. Castagnini, J.M., Tappi, S., Tylewicz, U., Romani, S., Rocculi, P., Rosa, M.D. (2021). Sustainable development of apple snack formulated with blueberry juice and trehalose. *Sustainability*, *13*(16), art. no. 9204. **https://doi.org/10.3390/su13169204**
13. Ciesarová, Z., Murkovic, M., Cejpek, K., Kreps, F., Tobolková, B., Koplík, R., Belajová, E., Kukurová, K., Daško, Ľ., Panovská, Z., Revenco, D., Burčová, Z. (2020). Why is sea buckthorn (*Hippophae rhamnoides* L.) so exceptional? A review. *Food Research International*, *133*, art. no. 109170. **https://doi.org/10.1016/j.foodres.2020.109170**

14. De la Peña-Armada, R., Mateos-Aparicio, I. (2022). Sustainable approaches using green technologies for apple by-product valorisation as a new perspective into the history of the apple. *Molecules*, *27*(20), art. no. 6937. **https://doi.org/10.3390/molecules27206937**
15. Dinçer, C. (2022). Modeling of hibiscus anthocyanins transport to apple tissue during ultrasound-assisted vacuum impregnation. *Journal of Food Processing and Preservation*, *46*(6), 1–10. **https://doi.org/10.1111/jfpp.15886**
16. FAO. (2025). *Crops and Livestock Products*. **https://www.fao.org/faostat/en/#data/QCL**
17. Francis, F.J., Clydesdale, F.M. (1975). *Food Colorimetry: Theory and Applications*. AVI Publishing Co. Inc.
18. Giannakourou, M., Strati, I.F., Kriebardis, A.G., Mantanika, V., Poulis, S., Zoumpoulakis, P., Sinanoglou, V.J. (2019). Shelf life extension and quality improvement of cucumber slices impregnated in infusions of edible herbs. *Analytical Letters*, *52*(17), 2677–2691. **https://doi.org/10.1080/00032719.2019.1589476**
19. González-Pérez, J.E., Jiménez-González, O., Ramírez-Corona, N., Guerrero-Beltrán, J.A., López-Malo, A. (2022). Vacuum impregnation on apples with grape juice concentrate: Effects of pressure, processing time, and juice concentration. *Innovative Food Science and Emerging Technologies*, *77*, art. no. 102981. **https://doi.org/10.1016/j.ifset.2022.102981**
20. Guo, R., Guo, X., Li, T., Fu, X., Liu, R.H. (2017). Comparative assessment of phytochemical profiles, antioxidant and antiproliferative activities of Sea buckthorn (*Hippophaë rhamnoides* L.) berries. *Food Chemistry*, *221*, 997–1003. **https://doi.org/10.1016/j.foodchem.2016.11.063**
21. Indriani, S., Benjakul, S., Quan, T.H., Sitanggang, A.B., Chaijan, M., Kaewthong, P., Petcharat, T., Karnjanapratum, S. (2023). Effect of different ultrasound-assisted process modes on extraction yield and molecular characteristics of pepsin-soluble collagen from Asian bullfrog skin. *Food and Bioprocess Technology*, *16*(12), 3019–3032. **https://doi.org/10.1007/s11947-023-03118-w**
22. Iqbal, A., Murtaza, A., Marszałek, K., Iqbal, M.A., Chughtai, M.F.J., Hu, W., Barba, F.J., Bi, J., Liu, X., Xu, X. (2020). Inactivation and structural changes of polyphenol oxidase in quince (*Cydonia oblonga* Miller) juice subjected to ultrasonic treatment. *Journal of the Science of Food and Agriculture*, *100*(5), 2065–2073. **https://doi.org/10.1002/jsfa.10229**
23. Judd, D.B., Wyszecki, G. (1963). *Color in Business, Science and Industry*. 2nd edition. John Wiley Sons, pp. 1-500.
24. Kidoń, M., Radziejewska-Kubzdela, E., Biegańska-Marecik, R., Kowalczewski, P.Ł. (2023). Suitability of apples flesh from different cultivars for vacuum impregnation process. *Applied Sciences*, *13*(3), art. no. 1528. **https://doi.org/10.3390/app13031528**
25. Kowalska, J., Marzec, A., Domian, E., Galus, S., Ciurzyńska, A., Lenart, A., Kowalska, H. (2020). The use of antioxidant potential of chokeberry juice in creating pro-healthy dried apples by hybrid (Convection-microwave-vacuum) method. *Molecules*, *25*(23), art. no. 5680. **https://doi.org/10.3390/molecules25235680**
26. Kulczyński, B., Sidor, A., Brzozowska, A., Gramza-Michałowska, A. (2024). The role of carotenoids in bone health – A narrative review. *Nutrition*, *119*, art. no. 112306. **https://doi.org/10.1016/j.nut.2023.112306**
27. Lech, K., Michalska, A., Wojdyło, A., Nowicka, P., Figiel, A. (2018). The influence of physical properties of selected plant materials on the process of osmotic dehydration. *LWT – Food Science and Technology*, *91*, 588–594. **https://doi.org/10.1016/j.lwt.2018.02.012**
28. Li, F., Tang, Y. (2021). The activation mechanism of peroxidase by ultrasound. *Ultrasonics Sonochemistry*, *71*, art. no. 105362. **https://doi.org/10.1016/j.ultsonch.2020.105362**
29. Martiniakova, M., Babikova, M., Mondockova, V., Blahova, J., Kovacova, V., Omelka, R. (2022). The role of macronutrients, micronutrients and flavonoid polyphenols in the prevention and treatment of osteoporosis. *Nutrients*, *14*(3), art. no. 523. **https://doi.org/10.3390/nu14030523**
30. Masztalerz, K., Lech, K., Wojdyło, A., Nowicka, P., Michalska-Ciechanowska, A., Figiel, A. (2021). The impact of the osmotic dehydration process and its parameters on the mass transfer and quality of dried apples. *Drying Technology*, *39*(8), 1074–1086. **https://doi.org/10.1080/07373937.2020.1741607**
31. Mierzwa, D., Szadzińska, J., Gapiński, B., Radziejewska-Kubzdela, E., Biegańska-Marecik, R. (2022). Assessment of ultrasound-assisted vacuum impregnation as a method for modifying cranberries' quality. *Ultrasonics Sonochemistry*, *89*, art. no. 106117. **https://doi.org/10.1016/j.ultsonch.2022.106117**
32. Moon, K.M., Kwon, E.B., Lee, B., Kim, C.Y. (2020). Recent trends in controlling the enzymatic browning of fruit and vegetable products. *Molecules*, *25*(12), art. no. 2754. **https://doi.org/10.3390/molecules25122754**
33. Muzaffar, S., Ahmad, M., Wani, S.M., Gani, A., Baba, W.N., Shah, U., Khan, A.A., Masoodi, F.A., Gani, A., Wani, T.A. (2016). Ultrasound treatment: effect on physicochemical, microbial and antioxidant properties of cherry (*Prunus avium*). *Journal of Food Science and Technology*, *53*(6), 2752–2759. **https://doi.org/10.1007/s13197-016-2247-3**
34. National Institutes of Health (2022). *Calcium: Fact sheet for health professionals*. **https://ods.od.nih.gov/factsheets/Calcium-HealthProfessional/#en1**
35. Neri, L., Santarelli, V., Di Mattia, C.D., Sacchetti, G., Faieta, M., Mastrocola, D., Pittia, P. (2019). Effect of dipping and vacuum impregnation pretreatments on the quality of frozen apples: A comparative study on organic and conventional fruits. *Journal of Food Science*, *84*(4), 798–806. **https://doi.org/10.1111/1750-3841.14489**
36. Nowacka, M., Dadan, M., Tylewicz, U. (2021). Current applications of ultrasound in fruit and vegetables osmotic dehydration processes. *Applied Sciences*, *11*(3), art. no. 1269. **https://doi.org/10.3390/app11031269**
37. Ou, B., Hampsch-Woodill, M., Prior, R.L. (2001). Development and validation of an improved oxygen radical absorbance capacity assay using fluorescein as the fluorescent probe. *Journal of Agricultural and Food Chemistry*, *49*(10), 4619–4626. **https://doi.org/10.1021/jf010586o**
38. Panayampadan, A.S., Alam, M.S., Aslam, R., Kaur, J. (2022). Vacuum impregnation process and its potential in modifying sensory, physicochemical and nutritive characteristics of food products. *Food Engineering Reviews*, *14*(2), 229–256. **https://doi.org/10.1007/s12393-022-09312-4**
39. Pasławska, M., Stepien, B., Nawirska-Olszanska, A., Sala, K. (2019). Studies on the effect of mass transfer in vacuum impregnation on the bioactive potential of apples. *Molecules*, *24*(19), art. n. 3533. **https://doi.org/10.3390/molecules24193533**
40. Plasek, B., Lakner, Z., Kasza, G., Temesi, Á. (2020). Consumer evaluation of the role of functional food products in disease prevention and the characteristics of target groups. *Nutrients*, *12*(1), art. no. 69. **https://doi.org/10.3390/nu12010069**
41. Raj, Y., Kumar, A., Das, S., Srivatsan, V., Kumar, D., Kumar, R. (2021). A comparative analysis of compositional and phytochemical attributes in fruits of low chilling apple varieties cultivated in the eastern and western Himalaya. *Scientia Horticulturae*, *286*(6), art. no. 110221. **https://doi.org/10.1016/j.scienta.2021.110221**
42. Re, R., Pellegrini, N., Proteggente, A., Pannala, A., Yang, M., Rice-Evans, C. (1999). Antioxidant activity applying an improved ABTS radical cation decolorization assay. *Free Radical Biology Medicine*, *26*(9-10), 1231–1237. **https://doi.org/10.1016/S0891-5849(98)00315-3**
43. Rodríguez-Arzuaga, M., Ríos, G., Piagentini, A.M. (2019). Mild heat treatments before minimal processing reduce browning susceptibility and increase total phenolic content of low-chill apple cultivars. *Journal of Food Processing and Preservation*, *43*(11), art. no. e14209. **https://doi.org/10.1111/jfpp.14209**
44. Rojas-Graü, M.A., Soliva-Fortuny, R., Martín-Belloso, O. (2008). Effect of natural antibrowning agents on color and related enzymes in fresh-cut fuji apples as an alternative to the use of ascorbic acid. *Journal of Food Science*, *73*(6), S267–S272. **https://doi.org/10.1111/j.1750-3841.2008.00794.x**
45. Sánchez-Moreno, C., Larrauri, J.A., Saura-Calixto, F. (1998). A procedure to measure the antiradical efficiency of polyphenols. *Journal of the Science of Food and Agriculture*, *76*(2), 270–276. **https://doi.org/10.1002/(SICI)1097-0010(199802)76:2<270::AID-JSFA945>3.0.CO;2-9**
46. Santarelli, V., Neri, L., Sacchetti, G., Di Mattia, C.D., Mastrocola, D., Pittia, P. (2020). Response of organic and conventional apples to freezing and freezing pre-treatments: Focus on polyphenols content and antioxidant activity. *Food Chemistry*, *308*, art. no. 125570. **https://doi.org/10.1016/j.foodchem.2019.125570**
47. Sikora, M., Złotek, U., Świeca, M. (2020). Effect of basil leaves and wheat bran water extracts on enzymatic browning of lettuce. *International Journal of Food Science and Technology*, *55*(3), 1318–1325. **https://doi.org/10.1111/ijfs.14406**
48. Silva, K.S., Fernandes, M.A., Mauro, M.A. (2014). Effect of calcium on the osmotic dehydration kinetics and quality of pineapple. *Journal of Food Engineering*, *134*, 37–44. **https://doi.org/10.1016/j.jfoodeng.2014.02.020**
49. Singleton, V.L., Rossi, J.A. (1965). Colorimetry of total phenolics with phosphomolybdic-phosphotungstic acid reagents. *American Journal of Enology and Viticulture*, *16*(3), 144–158. **https://doi.org/10.5344/ajev.1965.16.3.144**
50. Suliburska, J., Krejpcio, Z. (2014). Evaluation of the content and bioaccessibility of iron, zinc, calcium and magnesium from groats, rice, leguminous grains and nuts. *Journal of Food Science and Technology*, *51*(3), 589–594. **https://doi.org/10.1007/s13197-011-0535-5**

51. Tappi, S., Tylewicz, U., Romani, S., Siroli, L., Patrignani, F., Dalla Rosa, M., Rocculi, P. (2016). Optimization of vacuum impregnation with calcium lactate of minimally processed melon and shelf-life study in real storage conditions. *Journal of Food Science*, *81*(11), E2734–E2742. **https://doi.org/10.1111/1750-3841.13513**
52. Techakanon, C., Barrett, D.M. (2017). The effect of calcium chloride and calcium lactate pretreatment concentration on peach cell integrity after high-pressure processing. *International Journal of Food Science and Technology*, *52*(3), 635–643. **https://doi.org/10.1111/ijfs.13316**
53. Testa, R., Rizzo, G., Schifani, G., Tinebra, I., Farina, V., Vella, F., Migliore, G. (2023). Can dried fruits replace unhealthy snacking among millennials? An empirical study on dried fruit consumption in Italy. *Sustainability)*, *15*(9), art. no. 7083. **https://doi.org/10.3390/su15097083**
54. Tkacz, K., Wojdyło, A., Turkiewicz, I.P., Bobak, Ł., Nowicka, P. (2019). Anti-oxidant and anti-enzymatic activities of sea buckthorn (*Hippophaë rhamnoides* L.) fruits modulated by chemical components. *Antioxidants*, *8*(12), art. no. 618. **https://doi.org/10.3390/antiox8120618**
55. Tkacz, K., Wojdyło, A., Turkiewicz, I.P., Ferreres, F., Moreno, D.A., Nowicka, P. (2020). UPLC-PDA-Q/TOF-MS profiling of phenolic and carotenoid compounds and their influence on anticholinergic potential for AChE and BuChE inhibition and on-line antioxidant activity of selected *Hippophaë rhamnoides* L. cultivars. *Food Chemistry*, *309*, art. no. 125766. **https://doi.org/10.1016/j.foodchem.2019.125766**
56. Trusinska, M., Rybak, K., Drudi, F., Tylewicz, U., Nowacka, M. (2024). Combined effect of ultrasound and vacuum impregnation for the modification of apple tissue enriched with aloe vera juice. *Ultrasonics Sonochemistry*, *104*, art. no. 106812. **https://doi.org/10.1016/j.ultsonch.2024.106812**
57. Tylewicz, U., Oliveira, G., Alminger, M., Nohynek, L., Dalla Rosa, M., Romani, S. (2020). Antioxidant and antimicrobial properties of organic fruits subjected to PEF-assisted osmotic dehydration. *Innovative Food Science and Emerging Technologies*, *62*, art. no. 102341. **https://doi.org/10.1016/j.ifset.2020.102341**
58. Vasile, F.E., Simal, S., Rosselló, C., Eim, V.S. (2022). Power ultrasound-assisted impregnation of apple cubes with vitamin B12. *Food and Bioprocess Technology*, *15*(1), 219–229. **https://doi.org/10.1007/s11947-021-02752-6**
59. Vinod, B.R., Asrey, R., Sethi, S., Menaka, M., Meena, N.K., Shivaswamy, G. (2024). Recent advances in vacuum impregnation of fruits and vegetables processing: A concise review. *Heliyon*, *10*(7), art. no. e28023. **https://doi.org/10.1016/j.heliyon.2024.e28023**
60. Wang, X., Kahraman, O., Feng, H. (2022). Impact of osmotic dehydration with/without vacuum pretreatment on apple slices fortified with hypertonic fruit juices. *Food and Bioprocess Technology*, *15*(7), 1588–1602. **https://doi.org/10.1007/s11947-022-02834-z**
61. Yılmaz, F.M., Ersus Bilek, S. (2018). Ultrasound-assisted vacuum impregnation on the fortification of fresh-cut apple with calcium and black carrot phenolics. *Ultrasonics Sonochemistry*, *48*, 509–516. **https://doi.org/10.1016/j.ultsonch.2018.07.007**
62. Yuca, H., Şenocak, T.Ç., Yiğit, O., Albayrak, M.G., Güvenalp, Z. (2024). Semi-quantitative analysis on sea buckthorn phenolic-rich extract coating bone-like open porous NiTi-based alloy. *Heliyon*, *10*(14), art. no. e34594. **https://doi.org/10.1016/j.heliyon.2024.e34594**
63. Zhang, Z., Chen, Y., Chen, Z., Gao, Z., Cheng, Y., Qu, K. (2024). Quality analysis and assessment of representative sea buckthorn fruits in northern China. *Food Chemistry: X*, *24*, art. no. 101828. **https://doi.org/10.1016/j.fochx.2024.101828**

ORIGINAL ARTICLE
http://journal.pan.olsztyn.pl

Polish Journal of Food and Nutrition Sciences
2025, Vol. 75, No. 3, 303–313
DOI: 10.31883/pjfns/205003
ISSN 1230-0322, e-ISSN 2083-6007

Moisture Desorption and Thermodynamic Characteristics of Nixtamalized Maize and Fermented Cassava Flour Blends

Ndi B. Bongjo[1,2*], Charles C. Ariahu[1,3], Barnabas A. Ikyenge[1,2]

[1]Centre for Food Technology and Research, Benue State University, PMB 102119 Makurdi, Nigeria
[2]Department of Chemistry, Benue State University, PMB 102119 Makurdi, Nigeria
[3]Department of Food Science and Technology, College of Food Technology and Human Ecology, Joseph Sarwuan Tarka University, Makurdi, Nigeria

This study examined the moisture desorption and thermodynamic characteristics of four blends from nixtamalized/non-nixtamalized maize flour and fermented/non-fermented cassava flour. Maize grains were nixtamalized by their cooking in 1% $Ca(OH)_2$ solution and 18 h steeping. Cassava flour was fermented by the backslopping method. The flour blends were constituted in the ratio of 2:1 (*w/w*) of maize to cassava flour. Desorption isotherms were determined at temperatures ranging from 10°C to 40°C using a gravimetric method. The experimental data were fitted to the Guggenheim–Anderson–de Boer (GAB), Brunauer–Emmett–Teller (BET) and Oswin models to characterize the moisture desorption behavior. Results revealed that the use of nixtamalized and fermented flours in blends significantly influenced the desorption isotherms yielding type II isotherms. BET and GAB models exhibited percent root mean square of error at <10%, with the GAB equation showing the best fit for the desorption data. The monolayer moisture content (M_0) decreased with increasing temperature for all blends, and those with fermented cassava flours had lower M_0. The net isosteric heat of desorption decreased as equilibrium moisture content increased, reflecting the progressive saturation of high-energy binding sites. The blends with nixtamalized flour exhibited reduced isosteric heat compared to the sample with untreated flours. The differential entropy of desorption increased as the equilibrium moisture content increased and, thus, indicated thermodynamic compensation. The study demonstrates that nixtamalization and fermentation influence the water-binding characteristics of maize and cassava flour blends, with implications for improved drying efficiency and extended shelf-life.

Keywords: blended flour, desorption isotherm, isosteric heat, nixtamalization, sorption models

INTRODUCTION

A crucial humanitarian issue is to ensure food security for groups suffering from malnutrition. According to the Food and Agricultural Organization (FAO), deficiency of nutrients in the diet is responsible for more than half of infant mortality worldwide [FAO, 2022]. The burden of nutritional deficiency is excruciating for persons with lower incomes, including mostly those from the developing countries [Erokhin *et al*., 2021].

Maize and cassava are staple crops for over 800 million people; however, a diet dominated by flour from these plants causes nutritional deficiencies (*e.g*., niacin, calcium). Sustainable processing techniques, like nixtamalization and fermentation, can address these gaps, as shown by FAO data linking calcium-supplemented diets to reduced child mortality [FAO, 2022]. Nixtamalization and fermentation are traditional processing techniques that significantly influence the physicochemical properties of these flours; enhancing their nutritional quality

***Corresponding Author:**
e-mail: **betrandbongjo@gmail.com** (N.B. Bongjo)

Submitted: 19 February 2025
Accepted: 12 May 2025
Published on-line: 22 August 2025

[Sefa-Dedeh *et al*., 2004; Widowati *et al*., 2025]. Nixtamalization, being a thermo-alkaline process, improves starch gelatinization and retrogradation by altering its structure and rendering it improved physical properties, as shown in black bean and maize flours [Gutiérrez-Cortez *et al*., 2022; Santiago-Ramos *et al*., 2018]. This process also enhances the content of minerals, such as calcium and iron, and reduces resistant starch content, which can improve the nutritional profile of foods [Gutiérrez-Cortez *et al*., 2022; Santiago-Ramos *et al*., 2018]. Furthermore, it reduces antinutrient levels, such as phytates, which can inhibit mineral absorption, thereby increasing the bioavailability of essential nutrients like iron and zinc [Hassan *et al*., 2024; Matendo *et al*., 2023]. Sefa-Dedeh *et al*. [2003] reported that lactic acid fermentation of nixtamalized maize, further enhances these benefits by lowering pH and increasing titratable acidity. Such changes in pH can additionally improve the microbial safety and sensory properties of fermented foods. Similarly, fermentation impacts the nutritional and functional properties of cassava flour [Mohidin *et al*., 2023; Widowati *et al*., 2025]. Fayemi & Ojokoh [2014] reported that different fermentation methods, such as traditional, brine, and backslopping, affect the physical properties of a cassava flour product – fufu. For instance, brine and backslopping fermentation techniques result in lighter fufu with lower swelling indices and bulk densities compared to traditional method. These fermentation processes also enhance the protein content and mineral levels, making them valuable for nutritional enrichment of cassava flour [Fayemi & Ojokoh, 2014]. Blending nixtamalized maize and fermented cassava flours creates a superior food product with multiple advantages. This combination enhances the nutritional profile by increasing calcium, niacin, and protein availability from the maize while reducing cyanogenic compounds and adding B-group vitamins from the cassava fermentation process [Bongjo *et al*., 2025a,b]. The blend offers improved functional properties with better viscoelasticity and texture, extended shelf-life through reduced microbial and enzymatic activity (as a result of reduced moisture content), and complementary amino acid profiles that provide a more complete protein source. The processing methods decrease contents of antinutrients, like phytates, while developing complex flavors, with the slight alkalinity of nixtamalized maize complementing the subtle acidity of fermented cassava. Beyond the nutritional and culinary benefits, this blend preserves traditional food processing techniques and modern applications, promoting local food security.

Nixtamalization, a process involving the cooking and steeping of maize in an alkaline solution, alters the integral structure of the maize starch molecules [Gutiérrez-Cortez *et al*., 2022] which could have implications on the thermodynamic properties and moisture sorption isotherms of nixtamalized products. The study of moisture desorption and thermodynamic characteristics of maize and cassava-based flours is crucial for optimizing their processing and storage conditions. Research has shown that nixtamalized maize flour exhibits type II sorption isotherms, which are effectively described by Guggenheim–Anderson–de Boer (GAB) and Henderson models [Ramírez-Miranda *et al*., 2014]. The isosteric heat and entropy of nixtamalized maize flour decreased with increasing moisture content, indicating changes in energy requirements during processing and storage [Ramírez-Miranda *et al*., 2014]. Understanding the thermodynamic properties, such as the isosteric heat of desorption, is also essential for evaluating the energy performance of drying processes for cassava products. Studies have demonstrated that fermentation has minimal impact on the desorption characteristics of cassava products, with the modified Chung–Pfost equation effectively capturing the temperature dependency of the isosteric heat of desorption [Sarnavi *et al*., 2023].

It has been shown that mathematical models describing moisture sorption isotherms allow for effective prediction of water activity in the product during dehydration [Hssaini *et al*., 2022; Labuza & Altunakar, 2020]. Moisture sorption isotherms provide critical insights into how water moves and interacts within different food materials, particularly during dehydration processes [Tejada-Ortigoza *et al*., 2020; Zhang *et al*., 2016]. By analyzing sorption isotherm data, key thermodynamic properties, including net isosteric heat, differential enthalpy, and entropy, are obtained [Sengev *et al*., 2016, 2018]. These parameters not only reveal critical information about water behavior within food products but also enable precise estimation of energy requirements for drying processes. Moreover, recent research has highlighted the significance of desorption enthalpies in optimizing drying operations [Biswal *et al*., 2017], further underscoring the importance of these thermodynamic analyses in food processing research.

Despite the wide application of nixtamalization and fermentation to improve the nutritional value of maize and cassava flours, respectively, few studies have so far explored the thermodynamic properties of these traditionally processed flours. To the best of our knowledge, blends of these flours have not been studied in this respect. Therefore, the aim of our study was to evaluate how nixtamalization of maize flour and fermentation of cassava flour affect moisture desorption isotherms and thermodynamic properties of maize and cassava flour blends.

MATERIALS AND METHODS

Raw materials and preparation of flours

Maize grains of white variety (15 kg) and cassava tubers of sweet variety (50 kg) were purchased on the Wurukum and Wannune markets, respectively, located in Makurdi (Nigeria).

Non-nixtamalized maize flour was obtained by grinding maize grains in an electric power grinder (DE-2000g; Golden Bull, Kuala Lumpur, Malaysia) after cleaning them from extraneous materials. The flour was sieved through a 40 mm mesh and packaged in low-density polyethylene bags until further analysis.

Nixtamalized maize flour was prepared according to the procedure described by Milán-Carrillo *et al*. [2004] with slight modifications. The maize grains (3 batches of 5 kg each) were immersed in a 1% $Ca(OH)_2$ solution at a ratio of 1:3 (*w/v*) and cooked for 40 min. Cooked grains were left in the $Ca(OH)_2$ solution for 18 h to steep and then drained. The excess of unabsorbed $Ca(OH)_2$

and the pericarp were removed from the soaked grains by washing them three times with water. The nixtamal thus obtained was dried in a BioChef dehydrator (KT-DE-BC-9T, Vitality4 Life UK Ltd, Peterborough, UK) at 65°C for 24 h and ground in an electric power grinder (Golden Bull). The nixtamalized maize flour that was passed through the 40 mm sieve was sealed in low-density polyethylene bags and stored at ambient temperature until further experiments.

The cassava tubers, after removing their peel and washing in water, were cut into pieces, which were then dried at 65°C for 48 h in the BioChef dehydrator (Vitality4 Life UK Ltd) to obtain non-fermented cassava flour. Fermentation of cassava flour was performed using the back-slopping method. Briefly, flour (50 g) was suspended in distilled water at a ratio of 1:3 (*w/v*) and left for 24 h at ambient temperature. Half of each fermented mixture was used as a starter for subsequent fermentation cycles. There were four fermentation cycles (*i.e.*, fermentation lasted up to the 96th h). Fermentation was controlled by pH measurements and continued until the pH values stabilized. After fermentation, the flour was dried at 50°C for 24 h using BioChef dehydrator (Vitality4 Life UK Ltd) and sieved through a 40 mm mesh. The non-fermented cassava flour and fermented cassava flour were stored in low-density polyethylene bags until analyses.

Formulation of flour blends

Maize and cassava flours were mixed in a ratio of 2:1 (*w/w*) using a food mixer (Model: B5; Jiangmen Shengli Food Machinery Co., Ltd., Jiangmen, GD, China) to obtain four blends including a blend of non-nixtamalized corn flour and non-fermented cassava flour (NNNF), a blend of non-nixtamalized corn flour and fermented cassava flour (NNF), a blend of nixtamalized corn flour and non-fermented cassava flour (NXNF), and a blend of nixtamalized corn flour and fermented cassava flour (NXF). The ratio of maize to cassava flour in blends was established based on preliminary studies in which blends (NNNF, NNF, NXNF and NXF) were formulated in 3 different ratios (1:1, 1:2 and 2:1, *w/w*), and sensory evaluation of the fufu produced from all these blends was carried out. Blends in the 2:1 (*w/w*) ratio provided the fufu with higher overall acceptability. These blends were stored until analysis in the same conditions as flours, after placing them in polyethylene bags.

Determination of equilibrium moisture content

The equilibrium moisture content was determined using a gravimetric method according to the procedure described by Ariahu *et al.* [2005]. The varying humidity conditions were created using sulfuric acid solutions of 10, 20, 30, 40, 50 and 60% concentrations providing water activity (a_w) between 0.15 and 0.96. A volume of 200 mL of each sulfuric acid solution was measured into plastic containers (500 mL) over which the flour blends weighed into crown corks (in duplicates of 0.5 g each) were placed on wire gauze. Before this placement, the flour blends were moistened with distilled water and kept at 30°C and 98% relative humidity (RH) until they reached equilibrium. The sealed containers with samples were kept at different temperatures of 10, 20, 30 and 40°C using an SPX-80-II incubator (Searchtech Instruments, UK). The samples maintained at RH above 50% were treated with 0.25% sodium azide solution to prevent microorganism growth [Sengev *et al.*, 2016]. The sample weights were measured every 48 h using an AE Adam 160 balance (Adam Equipment Co, Milton Keynes, UK). This weighing process continued until the difference between successive measurements was 0.5% or less. The entire procedure of removing each of the flour blends for weighing and returning them to their airtight containers took between 2 and 5 min, following the guidelines established by the Cooperative Project Cost 90 [Sengev *et al.*, 2018].

The equilibrium moisture content (EMC) was calculated using Equation (1) and moisture desorption isotherms, *e.g.*, a_w *vs.* ECM were plotted for each temperature:

$$EMC = \frac{M \times W_1 + 100 \times (W_3 - W_2)}{W_1 + (W_3 - W_2)} \quad (1)$$

where: M is the initial moisture content of the sample, W_1 is the weight of sample during sorption, W_2 is the initial weight of the sample and crown cork, and W_3 is the final weight of the sample and crown cork at equilibrium.

Modeling and analysis of sorption data

The experimental data of EMC and a_w of the flour blends were fitted using the Brunauer–Emmett–Teller (BET), GAB and Oswin models, which are described by Equations 2, 3 and 4, respectively. These models were chosen for their reported fit for starchy foods over various water activities [Ocheme *et al.*, 2013]:

$$\frac{a_w}{(1 - a_w) \times M} = \frac{1}{M_0 \times C} + \frac{(C - 1) \times a_w}{M_0 \times C} \quad (2)$$

$$M = \frac{M_0 \times G \times k \times a_w}{(1 - k \times a_w)(1 - k \times a_w + G \times k \times a_w)} \quad (3)$$

$$M = A \times \left[\frac{a_w}{1 - a_w} \right]^B \quad (4)$$

where: M is the equilibrium moisture content, M_0 is the monolayer moisture content, while A, B, G, k and C are constants related to the heat of sorption.

Parameters of the BET and Oswin models were determined through linear regression analysis, while the quadratic parameters for the GAB model were computed using the Origin 2024b (OriginLab Corporation, Northampton, MA, USA). The monolayer moisture contents (M_0) in BET and GAB models were determined from the regression equations of their respective plots, using the moisture desorption data as the basis for calculation.

The surface area of sorption (S_0) is related to the monolayer moisture content and was computed using Equation 5:

$$S_0 = 3{,}513.42 \times M_0 \quad (5)$$

where: 3,513.42 is a constant derived from Avogadro's number and the cross-sectional area of a water molecule.

To evaluate how well the various models performed, the percent root mean square of error (%RMSE) was calculated by comparing experimental moisture content values (M_{obs}) with predicted moisture content values (M_{est}) as in Equation 6 [Sengev *et al*., 2016]:

$$\%RMSE = \frac{\sqrt{\sum\left[\frac{M_{obs} - M_{est}}{M_{obs}}\right]^2}}{n} \times 100 \quad (6)$$

where: n is the number of experimental data.

Analysis of thermodynamic properties

The Clausius-Clapeyron Equation (7) was used to determine the net isosteric heat of desorption (ΔH_{st}) and indirectly, differential entropy of sorption (ΔS^0). This equation described isosteres obtained by plotting $\ln(a_w)$ *vs*. the inverse of temperature in absolute scale (1/T) for a given equilibrium moisture content [Ariahu *et al*., 2005]. ΔH_{st} was calculated from the slope ($-\Delta H_{st}/R$) and ΔS^0 was derived from the intercept (C_{st}), corresponding to the coefficient ($\Delta S^0/R$):

$$\ln a_w = C_{st} - \frac{\Delta H_{st}}{R} \times \frac{1}{T} \quad (7)$$

where: ΔH_{st} is the net isosteric heat, C_{st} is a constant related to the entropy of sorption, T is temperature at absolute scale and R is a molar gas constant (0.008314 kJ/mol×K).

RESULTS AND DISCUSSION

Effect of temperature on the moisture desorption isotherm

The moisture desorption isotherms of NXNF, NXF, NNF, and NNNF blends at different temperatures are presented in **Figure 1**. The blends exhibited S-shaped (type II) isotherms. It was due to the high starch content of the flours, which was determined in our previous study [Bongjo *et al*., 2025b]. Type II isotherms are common for carbohydrate-rich products as shown, for example, by the results presented for sorghum-based [Sengev *et al*., 2016] and soybean-plantain-based [Agbor *et al*., 2024] food products. A high carbohydrate content (>70%) causes multilayer sorption with progressive gelatinization of starch, exposing hydrophilic sites, during nixtamalization [Santiago-Ramos *et al*., 2018].

The equilibrium moisture content of the blends decreased as the temperature increased from 10 to 40°C (**Figure 1**). Such a relationship is often reported in sorption studies and is explained by the fact that with increasing temperature the excited state of molecules of water vapor changes and their kinetic energy increases, which results in less binding to active sorption sites [Zeymer *et al*., 2022]. It was also observed, for instance, for different varieties of milled rice [Chen *et al*., 2019] and for a mixture of corn silage and fermentation residue from animal breeding [Poós & Szabó, 2019]. Additionally, an increase in temperature lowered the isotherm curves, resulting in higher a_w at a constant equilibrium moisture content (**Figure 1**). This means that the product is more susceptible to microbial spoilage. An increase in temperature at constant a_w leads to a decrease in moisture content, which is much safer for the product and ensures its better stability, as reported by Ocheme *et al*. [2013]. Gichau *et al*. [2020] also observed a similar scenario for complementary food from amaranth-sorghum grain blends. Studies have also reported that at low moisture content, water molecules are adsorbed to the active sites on the surface of the solids. However, as moisture content increases, the swelling of the solid increases, creating additional binding sites, allowing more water to be retained [Shih *et al*., 2011].

Effect of treatments on the moisture desorption isotherms

The NNNF blend was observed to have the highest sorptive capacity at all temperatures (**Figure 1**). However, the samples that were treated with nixtamalization and fermentation had relatively lower EMCs. The varying water desorption characteristics of NXF and NXNF blends compared to NNNF blend can be understood by considering the complex interactions between water and the food matrix compounds. Nixtamalization modifies the structural components of foods, particularly starch and protein, significantly influencing moisture dynamics. Water initially penetrates more rapidly into processed samples with partially gelatinized starch or altered protein structures due to the more accessible molecular architecture. However, as sorption progresses, these samples tend to release unbound water more readily, ultimately resulting in lower EMC because of a reduced number of tightly bound water sites. This phenomenon highlights the complex relationship between food processing techniques and moisture sorption at the molecular level [Santiago-Ramos *et al*., 2018]. The observed differences between the NNNF blend and the NXF and NXNF blends could also be due to the different contents of hydroscopic compounds like sugars and amorphous compound. The NNNF blend may have higher levels of soluble sugars or amorphous compounds that are highly hygroscopic and bind water strongly at equilibrium, increasing EMC, while the NXF and NXNF samples may have fewer such components, resulting in their lower EMC.

The effect of fermentation on the sorptive capacity of the flour blends could also be significant. Similarly to nixtamalization, fermentation altered food properties by modifying the starch and protein structures, which can impact moisture sorption characteristics. Research has shown that fermented foods often demonstrate enhanced thermal stability and reduced water uptake, particularly at lower RH levels [Sun-Waterhouse *et al*., 2014]. Studies have also shown that non-treated food samples tend to exhibit a higher equilibrium moisture content compared to fermented alternatives. For instance,

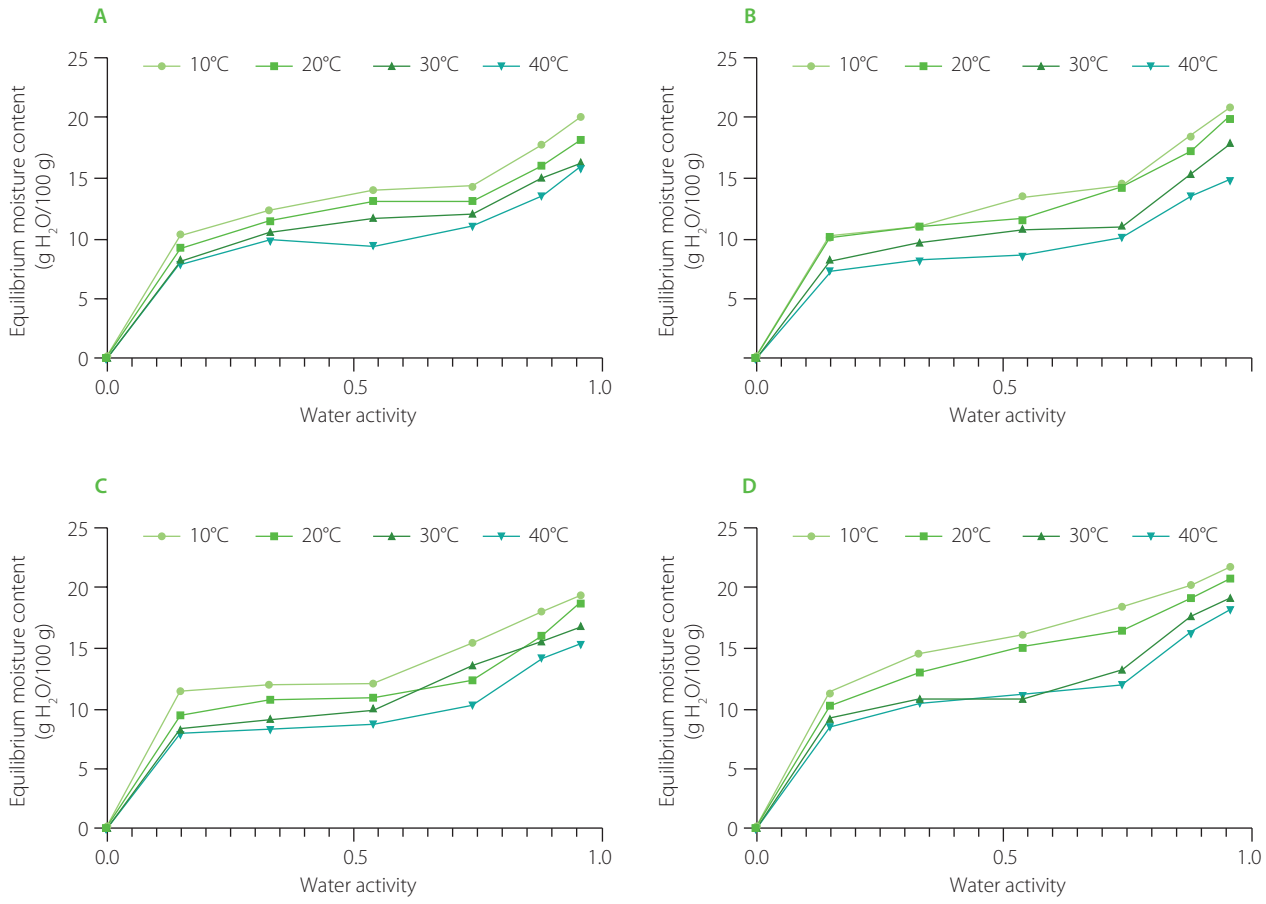

Figure 1. Moisture desorption isotherms of blends of nixtamalized maize flour and non-fermented cassava flour (NXNF) (**A**), nixtamalized maize flour and fermented cassava flour (NXF) (**B**), non-nixtamalized maize flour and fermented cassava flour (NNF) (**C**), and non-nixtamalized maize flour and non-fermented cassava flour (NNNF) (**D**) at different temperatures.

Igbabul *et al*. [2012] found that non-blanched, non-fermented arrowroot lily tubers absorbed more moisture than their blanched and fermented counterparts. They concluded that heat treatment might have damaged active binding sites, while fermentation could modify tissue structures, consequently reducing the number of water-binding sites available to water molecules. Similar findings were reported in studies of complementary foods made from fermented pre-gelatinized plantain and soybean flours [Agbor *et al*., 2024], further supporting the hypothesis that food processing techniques significantly influence moisture interactions at the molecular level.

Fit of the sorption models

The adequacy of experimental data for moisture desorption was evaluated using the BET, GAB and Oswin equations, and their fit expressed as the percentage of root mean square of error (%RMSE) is presented in **Table 1**. The BET model is the most commonly used for modeling sorption isotherms of various foods and is considered appropriate when the a_w <0.50. The GAB model is also widely used for analyzing the sorption properties of food products and provides a good fit to data for porous materials. On the other hand, the Oswin model conveniently describes the sorption of food products in the a_w range of 0.05 to 0.95 [Ariahu *et al*., 2005; Igbabul *et al*., 2012]. In our study, the GAB equation fitted better than the BET and Oswin equations having mean RMSE values <5%. For example, for the NXF blend, RMSE of the GAB model ranged from 3.39 to 6.80% depending on the desorption temperature, while the ranges for BET and Oswin models were 5.64–7.30% and 15.78–16.96%, respectively. Although the RMSEs of the BET model were higher than those of the GAP model for most flour blends (except the NXF blend at 30°C and NXNF and NNNF at 40°C), the former should also be considered as showing very good predictive performance, with mean RMSE below 7.1%. In statistical modelling, RMSE exceeding 10% suggests poor model performance, while values of 10% or less indicate a fairly good model fit, providing confidence that the model is able to accurately describe the moisture sorption [Wang & Brennan, 1991]. López-Vidaña *et al*. [2021] also reported that the GAB model fitted the moisture sorption isotherms of stevia leaves significantly better than the other models tested. Some researchers have also reported the GAB model being the best fit model for pulp and seed of *Syzygium cumini* [Araújo & Pena, 2022] as well as for fresh *S. cumini* fruit [Biswal *et al*., 2017]. In contrast, Arslan-Tontul [2020] reported that the BET model described moisture sorption isotherm of whole chia seed better than the GAB model did.

Table 1. Percent root mean square error (%RMSE) of moisture sorption models for blends of maize and cassava flours at different temperatures.

Blend	Model	10°C	20°C	30°C	40°C	Mean
NXNF	BET	4.49	4.47	4.71	5.28	4.74
	GAB	3.80	4.11	4.11	5.83	4.46
	Oswin	16.92	17.25	17.41	17.11	17.17
NXF	BET	5.66	5.64	6.28	7.30	6.22
	GAB	3.39	3.65	6.80	5.44	4.82
	Oswin	15.96	16.03	16.96	15.78	16.18
NNF	BET	5.41	5.53	8.33	8.92	7.05
	GAB	3.26	5.08	4.28	6.40	4.76
	Oswin	16.22	16.13	17.61	17.02	16.75
NNNF	BET	2.90	3.84	5.52	5.28	4.39
	GAB	1.40	2.09	4.64	5.53	3.42
	Oswin	16.93	17.25	16.42	16.92	16.88

BET, Brunauer–Emmett–Teller model; GAB, Guggenheim–Anderson–de Boer model; NXF, nixtamalized maize flour and fermented cassava flour; NXNF, nixtamalized maize flour and non-fermented cassava flour; NNF, non-nixtamalized maize flour and fermented cassava flour; NNNF, non-nixtamalized maize flour and non-fermented cassava flour.

Table 2. Brunauer–Emmett–Teller (BET) model parameters for desorption isotherms of maize and cassava flour blends.

Blend	Temperature (°C)	r^2	Slope coefficient	Intercept coefficient	C	M_0 (g H_2O/100 g solids)	S_0 (m^2/g)
NXNF	10	0.952	0.099	0.006	18.06	9.50	335.51
	20	0.956	0.104	0.007	15.67	8.99	317.57
	30	0.958	0.112	0.008	14.39	8.28	292.64
	40	0.949	0.114	0.008	15.19	8.21	290.11
NXF	10	0.946	0.118	0.004	27.77	8.18	289.19
	20	0.944	0.116	0.005	26.58	8.33	294.15
	30	0.941	0.124	0.008	16.42	7.55	266.70
	40	0.949	0.157	0.006	26.53	6.13	216.54
NNF	10	0.944	0.111	0.003	33.82	8.77	309.97
	20	0.949	0.119	0.005	22.98	8.04	284.19
	30	0.914	0.135	0.008	18.56	6.99	246.93
	40	0.922	0.152	0.007	24.23	6.29	222.29
NNNF	10	0.971	0.084	0.006	16.25	11.19	395.31
	20	0.96	0.093	0.007	15.27	10.04	354.86
	30	0.946	0.116	0.006	19.05	8.20	289.76
	40	0.949	0.114	0.008	15.19	8.21	290.11

r^2, Determination coefficient; M_0, monolayer moisture content; S_0, surface area of sorption; C, BET constant; NXF, nixtamalized maize flour and fermented cassava flour; NXNF, nixtamalized maize flour and non-fermented cassava flour; NNF, non-nixtamalized maize flour and fermented cassava flour; NNNF, non-nixtamalized maize flour and non-fermented cassava flour.

Table 3. Guggenheim–Anderson–de Boer (GAB) model parameters for desorption isotherms of maize and cassava flour blends.

Blend	Temperature (°C)	r^2	G	K	M_0 (g H_2O/100 g solids)	S_0 (m^2/g)
NXNF	10	0.965	37.78	0.46	11.07	391.01
	20	0.966	33.86	0.41	10.89	384.79
	30	0.971	31.13	0.40	10.14	358.14
	40	0.953	48.54	0.53	7.51	265.27
NXF	10	0.969	38.30	0.55	9.79	345.77
	20	0.970	59.19	0.57	8.75	309.15
	30	0.922	42.39	0.57	7.61	268.79
	40	0.962	63.64	0.60	6.28	222.04
NNF	10	0.976	65.13	0.52	9.71	343.03
	20	0.954	79.41	0.58	7.82	276.36
	30	0.962	26.55	0.55	8.30	293.31
	40	0.947	64.38	0.61	6.26	221.13
NNNF	10	0.994	31.76	0.33	15.44	545.44
	20	0.987	27.25	0.38	13.57	479.43
	30	0.954	49.28	0.60	8.11	286.72
	40	0.942	39.67	0.55	8.30	293.21

r^2, Determination coefficient; M_0, monolayer moisture content; G and K, GAB constants; S_0, surface area of sorption; NXF, nixtamalized maize flour and fermented cassava flour; NXNF, nixtamalized maize flour and non-fermented cassava flour; NNF, non-nixtamalized maize flour and fermented cassava flour; NNNF, non-nixtamalized maize flour and non-fermented cassava flour.

Monolayer moisture contents and derivative parameters

The parameters of BET and GAB models for desorption isotherm of flour blends are shown in **Tables 2** and **3**, respectively. The models allowed for the estimation of the monolayer moisture content (M_0) representing the moisture level at which the surface of the material is fully covered by a single layer of water molecules [Ariahu *et al*., 2005]. M_0 is a critical parameter in food preservation studies because it determines the optimal moisture state at which food products maintain maximum stability during storage – microbial growth and chemical degradation are limited. By precisely determining the M_0, more effective strategies for food processing, storage, and preservation can be developed [Lahsasni *et al*., 2003]. The M_0 reported in this study decreased with an increase in temperature for each flour blend (**Table 2** and **3**). This agrees with the findings reported by Sengev *et al*. [2018] who studied the moisture sorption behavior of sorghum-based complementary foods. A similar observation was made by Gichau *et al*. [2020] for amaranth-sorghum-based complementary foods. Rakshit *et al*. [2014] also observed a similar situation with monolayer moisture content decreasing from 1.29 g/100 g solids at 15°C to 1.03 g/100 g solids at 45°C for *wadi* – a legume-based traditional condiment. Sormoli & Langrish [2015] while investigating the moisture characteristics of spray-dried orange juice powder and Biswal *et al*. [2017] while studying the moisture sorption behavior of *S. cumini* fruit both observed this behavior; *i.e.*, a decrease in M_0 with an increase in temperature. They further suggested that the decrease in monolayer moisture content may be attributed to a reduction in the total number of active sites available for water binding. This reduction could result from physical and/or chemical changes in the product caused by temperature variations. This could be the case in this study as a result of the treatments; nixtamalization and fermentation, which lead to the modification of the food compound structure. Research have further shown that the decrease in M_0 occurs because, as temperature increases, some water molecules gain enough energy to break away from their sorption sites [Ariahu *et al*., 2005; Igbabul *et al*., 2012]. These findings suggest that the expected storage temperature of the flour samples will play a crucial role in determining the optimal moisture content for maximum shelf stability.

The M_0 of foods varies with the composition of the food as well as the treatments or processes applied in the production of the food material. The values obtained in this study (6.26–15.44 g H_2O/100 g solids in the GAB model and 6.13–11.19 g H_2O/100 g solids in the BET model, **Tables 2** and **3**) were higher than those

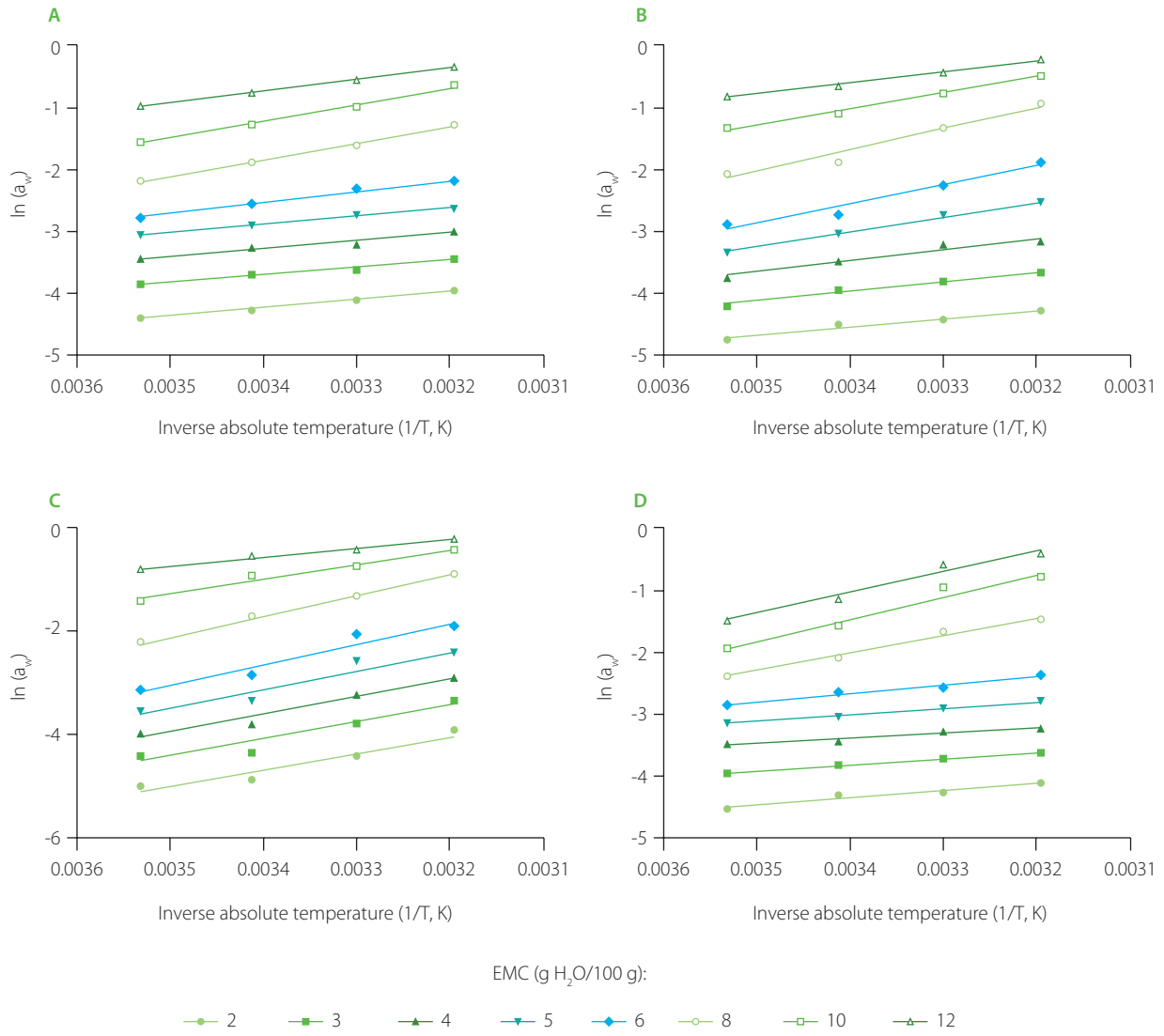

Figure 2. Clausius–Clapeyron relationship between water activity (a_w) and temperature in absolute scale (T) for moisture desorption isotherms of blends of nixtamalized maize flour and non-fermented cassava flour (NXNF) (**A**), nixtamalized maize flour and fermented cassava flour (NXF) (**B**), non-nixtamalized maize flour and fermented cassava flour (NNF) (**C**), and non-nixtamalized maize flour and non-fermented cassava flour (NNNF) (**D**). ECM, equilibrium moisture content.

reported by Gichau *et al.* [2020] who found M_0 ranging from 2.86 to 3.26 g/100 g solids for amaranth-sorghum-based complementary foods. This was also the case with tropical freshwater crayfish (2.27–5.48 g/100 g solids), as reported by Ariahu *et al.* [2005]. The results were, however, similar to those reported by Igbabul *et al.* [2012] for African arrowroot lily tuber mash. The results in this study were also consistent with observations made by other researchers who reported that for both adsorption and desorption, the M_0 values obtained by the GAB model were considerably higher than those obtained by the BET model [Ariahu *et al.*, 2005; Gichau *et al.*, 2020; Igbabul *et al.*, 2012]. Moreover, the blends with fermented cassava flours (NXF and NNF) had lower M_0 than those with non-fermented cassava flour (NXNF and NNNF) at each temperature (**Tables 2** and **3**), indicating the need for more rigorous control of the latter during storage.

Similarly as in the case of M_0, the blends with nixtamalized flour (NXF and NXNF) had lower S_0 than the NNNF blend; having higher values in both sorption models. This could be because during nixtamalization (which causes gelatinization), starch molecules absorb water, swell and rupture. When these molecules rupture, there is loss of water leading to shrinkage. Hence, there is a lesser surface area than in the non-nixtamalized samples.

Thermodynamic properties

To determine thermodynamic properties of the flour blends, the curves of $\ln(a_w)$ *vs.* inverse of temperature in absolute scale were plotted and they are shown in **Figure 2**. The parameters of the Clausius–Clapeyron equation, which described these curves, and calculated values of net isosteric heat and differential entropy of desorption are presented in **Table 4**. The ΔH_{st} decreased from 21.97 to 10.04 for the NXNF blend, from 29.15 to 11.33 for the NXF blend, from 34.06 to 13.43 for the NNF blend, and from 28.92 to 6.76 for the NNNF blend. The NNF sample had the highest ΔH_{st} as opposed to the NXNF blend exhibiting

Table 4. Parameters of Clausius–Clapeyron equation and differential entropy of desorption for blends of maize and cassava flours.

Blend	Parameter	Equilibrium moisture content (g H_2O/100 g solids)							
		2	3	4	5	6	8	10	12
NXNF	N	4	4	4	4	4	4	4	4
	A	–2,643	–2,570	–1,908	–1,745	–1,383	–1,242	–1,224	–1,207
	B	7.53	7.16	5.78	3.41	1.82	0.89	0.41	0.01
	r^2	0.974	0.971	0.992	0.979	0.953	0.966	0.942	0.960
	ΔH_{st} (kJ/mol)	21.97	21.37	15.86	14.51	11.50	10.33	10.18	10.04
	ΔS^0 (kJ/mol×K)	–0.063	–0.060	–0.048	–0.028	–0.015	–0.007	–0.003	–0.000
NXF	N	4	4	4	4	4	4	4	4
	A	–3,506	–3,103	–2,660	–2,360	–1,799	–1,780	–1,534	–1,363
	B	10.25	8.05	8.01	5.53	5.024	2.60	1.28	0.12
	r^2	0.974	0.971	0.974	0.977	0.988	0.919	0.942	0.876
	ΔH_{st} (kJ/mol)	29.15	25.80	22.12	19.62	14.96	14.80	12.75	11.33
	ΔS^0 (kJ/mol×K)	–0.085	–0.067	–0.067	–0.046	–0.042	–0.022	–0.011	–0.001
NNF	N	4	4	4	4	4	4	4	4
	A	–4,097	–4,027	–3,574	–3,382	–3,235	–3,180	–2,715	–1,615
	B	12.23	11.07	9.05	8.24	7.92	6.93	6.17	4.94
	r^2	0.987	0.942	0.911	0.922	0.885	0.868	0.927	0.923
	ΔH_{st} (kJ/mol)	34.06	33.48	29.71	28.12	26.90	26.44	22.57	13.43
	ΔS^0 (kJ/mol×K)	–0.102	–0.092	–0.075	–0.069	–0.066	–0.058	–0.051	–0.041
NNNF	N	4	4	4	4	4	4	4	4
	A	–3,478	–3,249	–2,750	–1,383	–1,113	–966.6	–962.1	–813.6
	B	10.35	10.00	7.34	2.05	0.60	0.54	0.51	0.27
	r^2	0.920	0.928	0.952	0.977	0.901	0.979	0.987	0.902
	ΔH_{st} (kJ/mol)	28.92	27.01	22.86	11.50	9.25	8.04	8.00	6.76
	ΔS^0 (kJ/mol×K)	–0.086	–0.083	–0.061	–0.017	–0.005	–0.005	–0.004	–0.002

ΔS^0, Differential entropy of desorption; ΔH_{st}, net isosteric heat; n, no. of entries; r^2, determination coefficient; B, intercept coefficient; A, slope; NXF, nixtamalized maize flour and fermented cassava flour; NXNF, nixtamalized maize flour and non-fermented cassava flour; NNF, non-nixtamalized maize flour and fermented cassava flour; NNNF, non-nixtamalized maize flour and non-fermented cassava flour.

the lowest net isosteric heat within the equilibrium moisture content range of 2 to 4 g H_2O/100 g solids. The ΔH_{st} is a difference in isosteric heat and the latent heat of vaporization of pure water at a particular system temperature [Arslan-Tontul, 2020]. In this study, it was notably greater at low levels of equilibrium moisture content, but it progressively diminished with rising moisture content, approaching the latent heat of vaporization of pure water. As the equilibrium moisture content approached 5–6 g H_2O/100 g solids, the ΔH_{st} continued to decrease, but much more slowly, or leveled off to become nearly constant with further increases in moisture content. The decrease in ΔH_{st} with increasing amounts of sorbed water can be explained by the initial sorption process, which occurs on the most active and available sites, leading to high interaction energy [Li X. *et al.*, 2011; Li Y. *et al.*, 2016; Sengev *et al.*, 2018]. As these high-energy sites become occupied, sorption shifts to less active sites, resulting in lower heats of sorption due to the formation of multilayers. At high equilibrium moisture content, the heat of sorption

gradually approaches the heat of condensation of pure water [Araújo & Pena, 2022; Sengev *et al*., 2018]. Additionally, the variation in heat of sorption with moisture content provides essential data for estimating energy consumption and optimizing the design of drying equipment. It also offers insights into the balance between water–solid and water–water interactions, which influence the sorption behavior of the material [Al-Muhtaseb *et al*., 2002]. For industrial application, lower isosteric heat (~12 kJ/mol) in the NXNF blend suggests energy-efficient drying for fufu production, reducing costs compared to traditional methods.

The ΔS^0 values ranged from −0.063 to −0.000 for the NXNF blend, from −0.085 to −0.001 for the NXF blend, from −0.102 to −0.041 for the NNF blend, and from −0.086 to −0.002 for the NNNF blend (**Table 4**). The increase in ΔS^0 was observed as the equilibrium moisture content of NXNF, NXF, NNF and NNNF increased with high disorderliness at lower moisture contents. The disorderliness disappeared (low degree of disorderliness) as the curve approached the equilibrium moisture content of 6 g H_2O/100 g solids. The low degrees of disorderliness indicate that water molecules are strongly bound to the adsorbent, they are more ordered and less available to participate in deteriorative reactions [Sengev *et al*., 2018]. The ΔS^0 of the flour blends increased up to the equilibrium moisture content of 6 g H_2O/100 g solids and became close to constant as the moisture content increased (**Table 4**). One possible explanation is that the rising moisture content counterbalanced the increased availability of hydrophilic sites, preventing any significant entropy changes in either direction. Similar asymptotic trends have been documented in previous research [Araújo & Pena, 2022; Sarnavi *et al*., 2023]. The negative ΔS^0 values determined in our study may be attributed to either chemical desorption processes or structural modifications of the desorbent, as suggested by Ayala-Aponte [2016] and Sengev *et al*. [2018].

CONCLUSIONS

The moisture desorption analysis of nixtamalized/non-nixtamalized maize and fermented/non-fermented cassava flour blends showed type II sorption isotherms. The equilibrium moisture content decreased as water activity declined and as temperature increased. When assessing how well different models fit the data, the GAB equation proved to be the most effective for modeling the moisture desorption behavior of these flour blends. The isosteric heat of desorption decreased as equilibrium moisture content increased, while differential entropy of desorption showed the opposite trend, increasing with higher equilibrium moisture contents. For most blends, these respective decreases in isosteric heat and increases in entropy slowed down at an equilibrium moisture content of 5–6 g H_2O/100 g solids, after which they exhibited asymptotic behavior. The blends containing nixtamalized maize flour (NXF, NXNF) exhibited lower EMC and reduced isosteric heat *vs*. the blend of untreated flours (NNNF), suggesting their higher storage stability. To sum up, nixtamalization and fermentation influence the water-binding characteristics of maize and cassava flour blends, with implications for improved drying efficiency and extended shelf-life.

RESEARCH FUNDING

The study received no external funding.

CONFLICT OF INTERESTS

The authors declare that they have no conflicts of interest.

ORCID IDs

C.C. Ariahu https://orcid.org/0009-0003-6307-2933
N.B. Bongjo https://orcid.org/0000-0002-0717-6119

REFERENCES

1. Agbor, A.E., Ariahu, C.C., Adie, P.A., Ariahu, E.C. (2024). Moisture transfer characteristics and microbiological stability of fermented pre-gelatinized plantain and soybean based complementary food flours. *Asian Food Science Journal*, *23*(4), 44–53. https://doi.org/10.9734/afsj/2024/v23i4710
2. Al-Muhtaseb, A.H., McMinn, W.A.M., Magee, T.R.A. (2002). Moisture sorption isotherm characteristics of food products: A review. *Food and Bioproducts Processing: Transactions of the Institution of Chemical Engineers, Part C*, *80*(2), 118–128. https://doi.org/10.1205/09603080252938753
3. Araújo, A.L. de, Pena, R. da S. (2022). Moisture desorption behavior and thermodynamic properties of pulp and seed of jambolan *(Syzygium cumini*). *Heliyon*, *8*(5), art. no. e09443. https://doi.org/10.1016/j.heliyon.2022.e09443
4. Ariahu, C.C., Kaze, S.A., Achem, C.D. (2005). Moisture sorption characteristics of tropical fresh water crayfish (*Procambarus clarkii*). *Journal of Food Engineering*, *75*(3), 355–363. https://doi.org/10.1016/j.jfoodeng.2005.03.062
5. Arslan-Tontul, S. (2020). Moisture sorption isotherm, isosteric heat and adsorption surface area of whole chia seeds. *LWT – Food Science and Technology*, *119*, art. no. 108859. https://doi.org/10.1016/j.lwt.2019.108859
6. Ayala-Aponte, A.A. (2016). Thermodynamic properties of moisture sorption in cassava flour. *DYNA revista de la Facultad de Minas*, *83*(197), 139-145. https://doi.org/10.15446/dyna.v83n197.51543
7. Biswal, S., Mohapatra, M., Panda, M.K., Dash, S.K. (2017). Moisture desorption isotherms of fresh Jamun (*Syzygium cumini*) fruit. *Indian Journal of Agricultural Research*, *51*(3), 267–271. https://doi.org/10.18805/ijare.v51i03.7917
8. Bongjo, N.B., Ariahu, C.C., Ikyenge, B.A. (2025a). Nixtamalization and fermentation as treatments for enhancing the functional and nutritional properties of foods. *American Journal of Food Science and Technology*, *4*(1), 50–59. https://doi.org/10.54536/ajfst.v4i1.3916
9. Bongjo, N.B., Ariahu, C.C., Ikyenge, B.A. (2025b). Nixtamalization and fermentation enhance the nutritional and sensory attributes of maize and cassava-based fufu. *Journal of Advances in Food Science and Technology*, *12*(1), 21–37. https://doi.org/10.56557/jafsat/2025/v12i19100
10. Chen, Z., Wang, R., Li, X., Zhu, J., Xu, Y., Liu, J. (2019). Sorption equilibrium moisture and isosteric heat of cold plasma treated milled rice. *Innovative Food Science and Emerging Technologies*, *55*(11), 35–47. https://doi.org/10.1016/j.ifset.2019.05.012
11. Erokhin, V., Diao, L., Gao, T., Andrei, J.V., Ivolga, A., Zong, Y. (2021). The supply of calories, proteins, and fats in low-income countries: A four-decade retrospective study. *International Journal of Environmental Research and Public Health*, *18*(14), art. no. 7356. https://doi.org/10.3390/ijerph18147356
12. FAO (2022). The state of food security and nutrition in the world 2022. In *Repurposing Food and Agricultural Policies to Make Healthy Diets More Affordable*.
13. Fayemi, O.E., Ojokoh, A.O. (2014). The effect of different fermentation techniques on the nutritional quality of the cassava product (Fufu). *Journal of Food Processing and Preservation*, *38*(1), 183–192. https://doi.org/10.1111/j.1745-4549.2012.00763.x
14. Gichau, A.W., Okoth, J.K., Makokha, A. (2020). Moisture sorption isotherm and shelf life prediction of complementary food based on amaranth–sorghum grains. *Journal of Food Science and Technology*, *57*(3), 962–970. https://doi.org/10.1007/s13197-019-04129-2
15. Gutiérrez-Cortez, E., Hernández-Becerra, E., Londoño-Restrepo, S.M., Millán-Malo, B.M., Morales-Sánchez, E., Gaytán-Martínez, M., Rodriguez-Garcia, M.E. (2022). Changes in the physicochemical properties of maize endosperm, endosperm fractions, and isolated starches because of nixtamalization. *Journal of Cereal Science, 108*, art. no. 103583. https://doi.org/10.1016/j.jcs.2022.103583
16. Hassan, S.M., Forsido, S.F., Tola, Y.B., Bikila, A.M. (2024). Physicochemical, nutritional, and sensory properties of tortillas prepared from nixtamalized

quality protein maize enriched with soybean. *Applied Food Research, 4*(1), art. no. 100383.
https://doi.org/10.1016/j.afres.2023.100383

17. Hssaini, L., Ouaabou, R., Charafi, J., Idlimam, A., Lamharrar, A., Razouk, R., Hanine, H. (2022). Hygroscopic proprieties of fig (*Ficus carica* L.): Mathematical modelling of moisture sorption isotherms and isosteric heat kinetics. *South African Journal of Botany*, *145*, 265–274.
https://doi.org/10.1016/J.SAJB.2020.11.026
18. Igbabul, B.D., Ariahu, C.C., Umeh, E.U. (2012). Moisture desorption isotherms of african arrowroot lily (*Tacca involucrata*) tuber mash as influenced by blanching and natural fermentation. *Journal of Food Technology*, *10*(1), 8–16.
https://doi.org/10.3923/jftech.2012.8.16
19. Labuza, T.P., Altunakar, B. (2020). Chapter 7 – Water activity prediction and moisture sorption isotherms. In G.V. Barbos-Cánovas, A.J. Fontana Jr., S.J. Schmidt, T.P. Labuza (Eds.), *Water Activity in Foods: Fundamentals and Applications*, John Wiley & Sons Inc., pp. 161–205.
https://doi.org/10.1002/9781118765982.ch7
20. Lahsasni, S., Kouhila, M., Mahrouz, M., Fliyou, M. (2003). Moisture adsorption-desorption isotherms of prickly pear cladode (*Opuntia ficus* indica) at different temperatures. *Energy Conversion and Management*, *44*(6), 923–936.
https://doi.org/10.1016/S0196-8904(02)00094-8
21. Li, X., Cao, Z., Wei, Z., Feng, Q., Wang, J. (2011). Equilibrium moisture content and sorption isosteric heats of five wheat varieties in China. *Journal of Stored Products Research*, *47*(1), 39–47.
https://doi.org/10.1016/j.jspr.2010.10.001
22. Li, Y., Wang, X., Jiang, P., Li, X.J. (2016). Sorption equilibrium moisture and isosteric heat of adsorption of Chinese dried wheat noodles. *Journal of Stored Products Research*, *67*, 19–27.
https://doi.org/10.1016/j.jspr.2016.01.007
23. López-Vidaña, E.C., Téllez, M.C., Figueroa, I.P., Espinosa, L.F.S., Castillo-Téllez, B. (2021). Moisture sorption isotherms, isosteric heat, and Gibbs free energy of stevia leaves. *Journal of Food Processing and Preservation*, *45*(1), art. no. e15016.
https://doi.org/10.1111/jfpp.15016
24. Matendo, R.E., Imathiu, S., Udomkun, P., Owino, W.O. (2023). Effect of nixtamalization of maize and heat treatment of soybean on the nutrient, antinutrient, and mycotoxin levels of maize-soybean-based composite flour. *Frontiers in Sustainable Food Systems*, *7*, art. no. 1057123.
https://doi.org/10.3389/fsufs.2023.1057123
25. Milán-Carrillo, J., Gutiérrez-Dorado, R., Cuevas-Rodríguez, E.O., Garzón-Tiznado, J.A., Reyes-Moreno, C. (2004). Nixtamalized flour from quality protein maize (*Zea mays* L.). Optimization of alkaline processing. *Plant Foods for Human Nutrition*, *59*(1), 35–44.
https://doi.org/10.1007/s11130-004-4306-6
26. Mohidin, S.R.N.S.P., Moshawih, S., Hermansyah, A., Asmuni, M.I., Shafqat, N., Ming, L.C. (2023). Cassava (*Manihot esculenta* Crantz): A systematic review for the pharmacological activities, traditional uses, nutritional values, and phytochemistry. *Journal of Evidence-Based Integrative Medicine*, *28*.
https://doi.org/10.1177/2515690X231206227
27. Ocheme, O.B., Ariahu, C.C., Ingbian, E.K. (2013). Moisture sorption characteristics of dakuwa (Nigerian cereal/groundnut snack). *International Journal of Food Engineering*, *9*(4), 499–504.
https://doi.org/10.1515/ijfe-2012-0242
28. Poós, T., Szabó, V. (2019). Desorption isotherms and isosteric heat of anaerobic fermentation residues. *Chinese Journal of Chemical Engineering*, *27*(10), 2510–2517.
https://doi.org/10.1016/j.cjche.2019.01.013
29. Rakshit, M., Moktan, B., Hossain, S.A., Sarkar, P.K. (2014). Moisture sorption characteristics of wadi, a legume-based traditional condiment. *Journal of Food Science and Technology*, *51*(2), 301–307.
https://doi.org/10.1007/s13197-011-0491-0
30. Ramírez-Miranda, M., Cruz y Victoria, M., Vizcarra, M., Anaya-Sosa, I. (2014). Determination of moisture sorption isotherms and their thermodynamics properties of nixtamalized maize flour. *Revista Mexicana de Ingenieria Quimica*, *13*(1), 165–178.
31. Santiago-Ramos, D., Figueroa-Cárdenas, J. de D., Véles-Medina, J.J., Salazar, R. (2018). Physicochemical properties of nixtamalized black bean (*Phaseolus vulgaris* L.) flours. *Food Chemistry*, *240*, 456–462.
https://doi.org/10.1016/j.foodchem.2017.07.156
32. Sarnavi, H.J., Precoppe, M., García-Triñanes, P., Chapuis, A., Tran, T., Bradley, M.S.A., Müller, J. (2023). Determining the heat of desorption for cassava products based on data measured by an automated gravimetric moisture sorption system. *Journal of the Science of Food and Agriculture*, *103*(1), 389–399.
https://doi.org/10.1002/jsfa.12153
33. Sefa-Dedeh, S., Cornelius, B., Afoakwa, E.O. (2003). Effect of fermentation on the quality characteristics of nixtamalized corn. *Food Research International*, *36*(1), 57–64.
https://doi.org/10.1016/S0963-9969(02)00108-4
34. Sefa-Dedeh, S., Cornelius, B., Sakyi-Dawson, E., Afoakwa, E.O. (2004). Effect of nixtamalization on the chemical and functional properties of maize. *Food Chemistry*, *86*(3), 317–324.
https://doi.org/10.1016/j.foodchem.2003.08.033
35. Sengev, I.A., Ariahu, C.C., Abu, J.O., Gernah, D.I. (2016). Moisture adsorption and thermodynamic properties of sorghum-based complementary foods. *International Journal of Food Engineering and Technology*, *1*(1), 26–33.
https://doi.org/10.11648/j.ijfet.20170101.11
36. Sengev, I.A., Ariahu, C.C., Abu, J.O., Gernah, D.I. (2018). Moisture desorption isotherms and thermodynamic properties of sorghum-based complementary foods. *European Journal of Biophysics*, *6*(2), 23–31.
https://doi.org/10.11648/j.ejb.20180602.11
37. Shih, F.F., Daigle, K.W., Champagne, E.T. (2011). Effect of rice wax on water vapour permeability and sorption properties of edible pullulan films. *Food Chemistry*, *127*(1), 118–121.
https://doi.org/10.1016/J.FOODCHEM.2010.12.096
38. Sormoli, M.E., Langrish, T.A.G. (2015). Moisture sorption isotherms and net isosteric heat of sorption for spray-dried pure orange juice powder. *LWT – Food Science and Technology*, *62*(1, Part 2), 875–882.
https://doi.org/10.1016/j.lwt.2014.09.064
39. Sun-Waterhouse, D., Zhao, M., Waterhouse, G.I.N. (2014). Protein modification during ingredient preparation and food processing: Approaches to improve food processability and nutrition. *Food and Bioprocess Technology*, *7*(7), 1853–1893.
https://doi.org/10.1007/s11947-014-1326-6
40. Tejada-Ortigoza, V., Welti-Chanes, J., Campanella, O.H., Peleg, M. (2020). Estimating equilibrium moisture content from relatively short sorption experiments. *LWT – Food Science and Technology*, *132*, art. no. 109832.
https://doi.org/10.1016/j.lwt.2020.109832
41. Wang, N., Brennan, J.G. (1991). Moisture sorption isotherm characteristics of potatoes at four temperatures. *Journal of Food Engineering*, *14*(4), 269–287.
https://doi.org/10.1016/0260-8774(91)90018-N
42. Widowati, S., Misgiyarta, Setyawan, N., Herawati, H., Widaningrum, Suhirman, S., Noerwijati, K., Budiono, R., Astuti, S.D., Tjahjohutomo, R., Unadi, A., Budiharti, U. (2025). Physicochemical and functional properties of cassava flour produced by controlled fermentation using mixed culture from various bacteria and yeast. *Journal of Agriculture and Food Research*, *19*, art. no. 101684.
https://doi.org/10.1016/J.JAFR.2025.101684
43. Zeymer, J.S., Corrêa, P.C., de Oliveira, G.H.H., de Araujo, M.E.V., Guzzo, F., Baptestini, F.M. (2022). Moisture sorption isotherms and hysteresis of soybean grains. *Acta Scientiarum - Agronomy*, *45*(1), art. no. 56615.
https://doi.org/10.4025/actasciagron.v45i1.56615
44. Zhang, H., Bai, Y., Zhao, X., Duan, R. (2016). Water desorption isotherm and its thermodynamic analysis of glutinous rice flour. *American Journal of Food Technology*, *11*(4), 115–124.
https://doi.org/10.3923/ajft.2016.115.124

INSTRUCTIONS FOR AUTHORS

SUBMISSION. Original contributions relevant to food and nutrition sciences are accepted on the understanding that the material has not been, nor is being, considered for publication elsewhere. All papers should be submitted and will be processed electronically via Editorial Manager system (available from PJFNS web site: http://journal.pan.olsztyn.pl). On submission, a corresponding author will be asked to provide: Cover letter; Files with Manuscripts, Tables, Figures/Photos; and Names of two potential reviewers (one from the author's homeland – but outside author's Institution, and the other from abroad). All papers which have been qualified as relevant with the scope of our Journal are reviewed. All contributions, except the invited reviews are charged. Proofs will be sent to the corresponding author and should be returned within one week since receipt. No new material may be inserted in the text at proof stage. It is the author's duty to proofread proofs for errors.

Authors should very carefully consider the preparation of papers to ensure that they communicate efficiently, because it permits the reader to gain the greatest return for the time invested in reading. Thus, we are more likely to accept those that are carefully designed and conform the instruction. Otherwise, papers will be rejected and removed from the online submission system.

SCOPE. The Polish Journal of Food and Nutrition Sciences publishes original, basic and applied papers, and reviews on fundamental and applied food research, preferably these based on a research hypothesis, in the following Sections:

Food Technology:
- Innovative technology of food development including biotechnological and microbiological aspects
- Effects of processing on food composition and nutritional value

Food Chemistry:
- Bioactive constituents of foods
- Chemistry relating to major and minor components of food
- Analytical methods

Food Quality and Functionality:
- Sensory methodologies
- Functional properties of food
- Food physics
- Quality, storage and safety of food

Nutritional Research:
- Nutritional studies relating to major and minor components of food (excluding works related to questionnaire surveys)

"News" section:
- Announcements of congresses
- Miscellanea

OUT OF THE SCOPE OF THE JOURNAL ARE:
- Works which do not have a substantial impact on food and nutrition sciences
- Works which are of only local significance i.e. concern indigenous foods, without wider applicability or exceptional nutritional or health related properties
- Works which comprise merely data collections, based on the use of routine analytical or bacteriological methods (i.e. standard methods, determination of mineral content or proximate analysis)
- Works concerning biological activities of foods but not providing the chemical characteristics of compounds responsible for these properties
- Nutritional questionnaire surveys
- Works related to the characteristics of foods purchased at local markets
- Works related to food law
- Works emphasizing effects of farming / agricultural conditions / weather conditions on the quality of food constituents
- Works which address plants for non-food uses (i.e. plants exhibiting therapeutic and/or medicinal effects)

TYPES OF CONTRIBUTIONS. *Reviews*: (at least: 30 pages and 70 references) these are critical and conclusive accounts on trends in food and nutrition sciences; *Original papers*: (maximally: 30 pages and 40 references) these are reports of substantial research; *Reports on post and forthcoming scientific events, and letters to the Editor* (all up to three pages) are also invited (free of charge).

REVIEW PROCESS. All scientific contributions will be peer-reviewed on the criteria of originality and quality. Submitted manuscripts will be preevaluated by Editor-in-Chief and Statistical Editor (except for review articles), and when meeting PJFNS' scope and formal

requirements, they will be sent to a Section Editor who upon positive preevaluation will assign at least two reviewers from Advisory Board Members, reviewers suggested by the author or other experts in the field. Based on the reviews achieved, Section Editor and Editor-in--Chief will make a decision on whether a manuscript will be accepted for publication, sent back to the corresponding author for revision, or rejected. Once a manuscript is sent back to the corresponding author for revision, all points of the reviews should be answered or rebuttal should be provided in the Explanation letter. The revised manuscripts will be checked by Section Editor and by the original reviewers (if necessary), and a final decision will be made on acceptance or rejection by both Section Editor and Editor-in-Chief.

Polish Journal of Food and Nutrition Sciences uses CrossCheck's iThenticate software to detect instances of similarity in submitted manuscripts. In publishing only original research, PJFNS is committed to deterring plagiarism, including self-plagiarism.

COPYRIGHT LICENSE AGREEMENT referring to Authorship Responsibility and Acknowledgement, Conflict of Interest and Financial Disclosure, Copyright Transfer, are required for all authors, i.e. *Authorship Responsibility and Acknowledgement*: Everyone who has made substantial intellectual contributions to the study on which the article is based (for example, to the research question, design, analysis, interpretation, and written description) should be an author. It is dishonest to omit mention of someone who has participated in writing the manuscript ("ghost authorship") and unfair to omit investigator who have had important engagement with other aspects of the work. All contributors who do not meet the criteria for authorship should be listed in an Acknowledgments section. Examples of those who might be acknowledged include a person who provided purely technical help, writing assistance, or a department chairperson who provided only general support. Any financial and material support should also be acknowledged. *Conflict of Interest and Financial Disclosure*: Authors are responsible for disclosing financial support from the industry or other conflicts of interest that might bias the interpretation of results. *License to Publish*: All articles published on the website of Polish Journal of Food and Nutrition Sciences are available in the Open Access format, meaning they are freely accessible online without charge to anyone, anywhere.

Since volume 75, Authors publish their works under the Creative Commons Attribution 4.0 License (CC BY 4.0). Pursuant to the License terms, Authors retain the copyright and full publishing rights without restrictions. The License permits unrestricted use, distribution and reproduction, provided that the original work is cited. The specific license terms of use are available on https://creativecommons.org/licenses/by/4.0/

In volumes 64–74, Authors published their works under the Creative Commons Attribution-NonCommercial-NoDerivs Licenses (CC BY-NC-ND) 3.0 and 4.0, pursuant to which they retained the copyright, and other proprietary rights relating to the article, such as patent rights, to use the substance of the article in future own works, including lectures and books, to reproduce the article for own purposes, provided the copies are not intended for commercial re-use or for share of the adapted and derivative versions. The specific license terms of use are available on http://creativecommons.org/licenses/by-nc-nd/3.0 and http://creativecommons.org/licenses/by-nc-nd/4.0.

In earlier volumes (47–63), Authors published their works under Copyright Transfer License, pursuant to which they retained the right to revise, adapt, prepare derivative works, present orally, or distribute the work provided that all such use was for the personal noncommercial benefit of the author(s) and was consistent with any prior contractual agreement between the publisher and authors.

A manuscript will not be published once the signed form has not been submitted to the Editor with the manuscript revised after positive reviews.

CHANGES TO AUTHORHIP. Authors are expected to consider carefully the list and order of authors before submitting their manuscript and provide the definitive list of authors at the time of the original submission. Any addition, deletion or rearrangement of author names in the authorship list should be made only before the manuscript has been accepted and only if approved by the journal Editor. To request such a change, the Editor must receive the following from the corresponding author: (a) the reason for the change in author list and (b) written confirmation (e-mail, letter) from all authors that they agree with the addition, removal or rearrangement. In the case of addition or removal of authors, this includes confirmation from the author being added or removed.

ETHICAL APPROVAL OF STUDIES AND INFORMED CONSENT. For all manuscripts reporting data from studies involving human participants or animals, formal approval by an appropriate institutional review board or ethics committee is required and should be described in the Methods section. For those investigators who do not have formal approval from ethics review committees, the principles outlined in the Declaration of Helsinki should be followed. For investigations of humans, state in the Methods section the manner in which informed consent was obtained from the study participants (i.e., oral or written). Editors may request that authors provide documentation of the formal review and recommendation from the institutional review board or ethics committee responsible for oversight of the study.

UNAUTHORIZED USE. Unauthorized use of the PJFNS name, logo, or any content for commercial purposes or to promote commercial goods and services (in any format, including print, video, audio, and digital) is not permitted by IAR&FR PAS.

MANUSCRIPTS. A manuscript in English must be singlesided, preferably in Times New Roman (12) with 1.5-point spacing, without numbers of lines. The Editor reserves the right to make literary corrections and to make suggestions to improve brevity. English is the official language. The English version of the paper will be checked by Language Editor. Unclear and unintelligible version will be returned for correction.

Every paper should be divided under the following headings in this order: a **Title** (possibly below 150 spaces); the **Name(s)** of the author(s) in full. In paper with more than one author, the asterisk indicates the name of the author to whom correspondence and inquiries should be addressed, otherwise the first author is considered for the corre-spondence. Current full postal address of the indicated corresponding author or the first author must be given in a footnote on the title page; the **Place(s)** where the work was done including the institution name, city, country if not Poland. In papers originated from several institu-tions the names of the authors should be marked with respective superscripts; the **Key words** (up to 6 words or phrases) for the main topics of the paper; an **Abstract** (up to 250 words for regular papers and reviews) summarizing briefly main results of the paper, no literature references; an **Introduction** giving essential background by saying why the research is important, how it relates to previous works and stating clearly the objectives at the end; **Materials and Methods** with

sufficient experimental details permitting to repeat or extend the experiments. Literature references to the methods, sources of material, company names and location (city, country) for specific instruments must be given. Describe how the data were evaluated, including selection criteria used; **Results and Discussion** presented together (in one chapter). Results should be presented concisely and organized to supplement, but not repeat, data in tables and figures. Do not display the data in both tabular and graphic form. Use narrative form to present the data for which tables or figures are unnecessary. Discussion should cover the implications and consequences, not merely recapitulating the results, and it must be accomplished with concise **Conclusions**; **Acknowledgements** should be made to persons who do not fill the authorship criteria (see: Authorship forms); **Research funding** should include financial and material support; **Conflict of Interests**: Authors should reveal any conflicts of interest that might bias the interpretation of results; and **References** as shown below.

REFERENCES each must be listed alphabetically at the end of the paper (each should have an Arabic number in the list) in the form as follows: **Periodicals** – names and initials of all the authors, year of publication, title of the paper, journal title as in Chemical Abstracts, year of publication, volume, issue, inclusive page numbers, or article id.; **Books** – names and initials of all the authors, names of editors, chapter title, year of publication, publishing company, place of publication, inclusive page numbers; **Patents** – the name of the application, the title, the country, patent number or application number, the year of publication.

For papers published in language other than English, manuscript title should be provided in English, whereas a note on the original language and English abstract should be given in parentheses at the end.

The reference list should only include peer-reviewed full-text works that have been published or accepted for publication. Citations of MSc/PhD theses and works unavailable to international Editors, Reviewers, and Readers should be limited as much as possible.

References in the text must be cited by name and year in square parentheses (e.g.: one author – [Tokarz, 1994]; two authors – [Słonimski & Campbell, 1987]; more than two authors – [Amarowicz *et al*., 1994]). If more than one paper is published in the same year by the same author or group of authors use [Tokarz, 1994a, b]. Unpublished work must only be cited where necessary and only in the text by giving the person's name.

Examples:

Article in a journal:

Słonimski, B.A., Campbell, L.D., Batista, E., Howard B. (2008). Gas chromatographic determination of indole glucosinolates. Journal of Science and Food Agriculture, 40(5), 131–143.

Asher, A., Tintle, N.L., Myers, M., Lockshon, L., Bacareza, H., Harris, W.S. (2021). Blood omega-3 fatty acids and death from COVID-19: A pilot study. *Prostaglandins, Leukotrienes and Essential Fatty Acids, 166*, art. no. 102250.

Book:

Weber, W., Ashton, L., Milton, C. (2012). Antioxidants – Friends or Foes? 2nd edition. PBD Publishing, Birmingham, UK. pp. 218–223.

Chapter in a book:

Uden, C., Gambino, A., Lamar, K. (2016). Gas chromatography. In M. Queresi, W. Bolton (Eds.), CRC Handbook of Chromatography, CRC Press Inc., Boca Raton, Florida, USA, pp. 44–46.

ABBREVIATIONS AND UNITS. Abbreviations should only be used when long or unwieldy names occur frequently, and never in the title; they should be given at the first mention of the name. Metric SI units should be used. The capital letter L should be used for liters. Avoid the use of percentages (% g/g,% w/w; Mol%; vol%), ppm, ppb. Instead, the expression such as g/kg, g/L, mg/kg, mg/mL should be used. A space must be left between a number and a symbol (e.g. 50 mL not 50mL). A small x must be used as multiplication sign between numeric values (e.g. 5 × 102 g/mL). Statistics and measurements should be given in figures, except when the number begins a sentence. Chemical formulae and solutions must specify the form used. Chemical abbreviations, unless they are internationally known, Greek symbols and unusual symbols for the first time should be defined by name. Common species names should be followed by the Latin at the first mention, with contracting it to a single letter or word for subsequent use.

FIGURES should be submitted in separate files. Each must have an Arabic number and a caption. Captions of all Figures should be provided on a separate page "Figure Captions". Figures should be comprehensible without reference to the text. Self-explanatory legend to all figures should be provided under the heading "Legends to figures"; all abbreviations appearing on figures should be explained in figure footnotes. Three-dimensional graphs should only be used to illustrate real 3D relationships. Start the scale of axes and bars or columns at zero, do not interrupt them or omit missing data on them. Figures must be cited in Arabic numbers in the text.

TABLES should be submitted in separate files. They should be as few in number and as simple as possible (like figures, they are expensive and space consuming), and include only essential data with appropriate statistical values. Each must have an Arabic number and a caption. Captions of all Tables should be provided on a separate page "Table Captions". Tables should be self-explanatory; all abbreviations appearing in tables should be explained in table footnotes. Tables must be cited in Arabic numbers in the text.

PUBLICATION FEE. Since 16th December 2024, a standard publication fee has been established at the rate of 500 EUR (plus VAT if applicable, e.g. for private persons). For Polish Authors an equivalent fee was set at 1950 PLN +23%VAT. The fee applies irrespective of the number of pages and tables/figures in the manuscript. Payment instructions will be sent to Authors via e-mail with acceptance letter.

Information on publishing and subscription is available from:

Ms. Joanna Molga
Editorial Office of Pol. J. Food Nutr. Sci.
Institute of Animal Reproduction and Food Research Trylińskiego 18, 10-683 Olsztyn, Poland
phone (48 89) 500 32 45
e-mail: pjfns@pan.olsztyn.pl; http://journal.pan.olsztyn.pl

Nutrition